Ambivalence of Drug Metabolism: Exploration of Cilazapril and Candesartan Prodrugs for Transdermal Delivery and Search for Toxic Reactive Intermediates of N^G-Acylated Hetarylpropylguanidines

Dissertation

zur Erlangung des Doktorgrades der Naturwissenschaften (Dr. rer. nat.) der
Naturwissenschaftlichen Fakultät IV – Chemie und Pharmazie –
der Universität Regensburg

vorgelegt von

Miriam Ertel

aus Lüneburg

2011

Die vorliegende Arbeit entstand in der Zeit von Februar 2007 bis Juni 2011 unter der Leitung von Herrn Prof. Dr. A. Buschauer am Institut für Pharmazie der Naturwissenschaftlichen Fakultät IV - Chemie und Pharmazie - der Universität Regensburg.

Das Promotionsgesuch wurde eingereicht im Juni 2011.

Tag der mündlichen Prüfung: 15. Juli 2011

Prüfungsausschuss:	Prof. Dr. J. Heilmann	(Vorsitzender)
	Prof. Dr. A. Buschauer	(Erstgutachter)
	Prof. Dr. G. Bernhardt	(Zweitgutachter)
	Prof. Dr. J. Wegener	(Prüfer)

Danksagung

An dieser Stelle möchte ich mich bedanken bei:

Herrn Prof. Dr. A. Buschauer für die Möglichkeit zur Durchführung dieses vielseitigen Projekts, seine wissenschaftlichen Anregungen und seine konstruktive Kritik bei der Durchsicht dieser Arbeit,

Herrn Prof. G. Bernhardt für seine wissenschaftlichen Hilfestellungen, sein stetes Interesse am Fortgang der Experimente, seine konstruktive Kritik bei der Durchsicht dieser Arbeit, die Erstellung des Zweitgutachtens und für sein hervorragendes Kesselgulasch,

der Hexal AG für die finanzielle Unterstützung, insbesondere Herrn J. Nink und seinen Mitarbeitern /-innen Frau T. Pries, Herrn M. Sedlmayr, Frau V. Sonntag und Herrn J. Lange für die fachliche Unterstützung, die Bereitstellung von Hautproben und Equipment, die Herstellung von TTS-Chargen und die Bereitstellung von Permeations-daten,

Herrn PD Dr. T. Weiß und Mitarbeitern /-innen für die Bereitstellung von humanen Hepatocyten,

der gemeinnützigen und staatlich kontrollierten Stiftung HTCR (Human Tissue and Cell Research) für die Bereitstellung von humanen Gewebeproben,

Frau Dr. A. Rottmann und Frau Dr. M. Bairlein von der Bayer Schering Pharma AG für die Durchführung von Metabolismusstudien,

Herrn Dr. T. Spruß und Frau P. Pistor für die Anfertigung der histologischen Präparate und deren Färbung,

Herrn J. Kiermaier für seine engagierte Hilfe bei der LC-MS/MS-Analytik,

Frau E. Schreiber für die Durchführung der Ca^{2+}-Assays,

Frau B. Wenzl für die Durchführung der Kristallviolettassays und die Kultivierung der HT-29 Zellen

Herrn O. Baumann und Herrn F. Wiesenmayer für die Präparation von Nacktmaushaut und von Rattenlebern,

Herrn R. Kutta für das Fitten von Daten einiger enzymatischer Hydrolysen,

Herrn S. Pilsl für die Unterstützung bei der Durchführung von bioanalytischen Untersuchungen,

meinen Forschungs- und Schwerpunktpraktikanten sowie studentischen Hilfskräften für ihre engagierte Mitarbeit im Labor,

allen Mitarbeitern der analytischen Abteilungen der Fakultät für die Aufnahme von NMR- und Massenspektren, sowie der Durchführung der Elementaranalysen,

meinen Laborkollegen Herrn Dr. M. Spickenreither, Herrn F. Binder, Herrn R. Geyer und Frau M. Kaske für eine schöne Zeit im Labor,

Frau M. Wechler, Frau S. Heinrich, Frau K. Reindl, Frau U. Hasselmann und Herrn P. Richthammer für die Unterstützung bei technischen und organisatorischen Problemen,

allen Mitgliedern des Lehrstuhls für ihre Kollegialität, Hilfsbereitschaft und ein gutes Arbeitsklima

und denjenigen, die mehr als nur Dank verdienen: meiner Familie und meinem Freund Nikola.

Contents

Chapter 1
General Introduction

1.1 Drug metabolism

Drug metabolism i.e. biotransformation of xenobiotics (exogenous compounds entering the body) describes the process of converting lipophilic, easily absorbable substances into more hydrophilic substances, which are readily excreted from the body in order to prevent accumulation of the xenobiotic.[1] Drug metabolism is catalyzed by various enzyme systems and can be divided into four reaction categories: hydrolysis, reduction, oxidation and conjugation. Since the first three introduce a functional group, they are often called functionalization reactions and are summarized under the term phase I reactions, whereas conjugation reactions are referred to as phase II reactions. Some major phase I and phase II enzymes are summarized in Table 1.1. Although functionalization often facilitates subsequent conjugation, phase I and phase II reactions do not necessarily occur sequentially but independently of each other.

Table 1.1. Major enzymes involved in phase I and phase II metabolism.[1]

Phase I enzymes	Phase II enzymes
Hydrolases (esterases, amidases)	UDP-Glucuronosyltransferases (UGTs)
Cytochrome P450	Sulfotransferase
Flavin-monooxygenases	Glutathione S-transferases (GSTs)
Monoamine oxidase	Acetyltransferase
Oxidoreductases	Amino acid transferase

Mainly, drug metabolism takes place in the liver, but also intestine, kidney, skeletal muscle, skin or plasma can contribute to biotransformation.[2] Concerning intracellular distribution of drug metabolizing enzymes, the highest activities are located in the endoplasmic reticulum and in the cytosol.[2] The most crucial role in drug metabolism is associated with the cytochrome P450 (CYP) enzyme system.[1] All CYP enzymes are heme (protoporphyrin IX)-containing proteins that catalyze a monooxygenation of a broad variety of substrates. The reaction involves the transfer of one atom of oxygen into the substrate, while the other is reduced to water. Necessary reducing equivalents are furnished by the closely associated NADPH cytochrome P450 reductase.[1] It is reported that in humans more than 50 % of the orally effective drugs in current use are metabolized by two CYP enzymes, namely CYP3A4 and CYP2D6.[3]

Drug metabolism does not only influence the physicochemical properties of a drug but can also alter the pharmacodynamic features. Most commonly, the pharmacological

activity of an active drug is terminated. However, drug metabolism can also result in the formation of pharmacologically active metabolites.[4] Therefore, it can be utilized to overcome various problems associated with a drug´s pharmacokinetic or pharmacodynamic properties, by the sophisticated design of drugs, comprising distinct soft "spots" for intentional biotransformation reactions. The development of prodrugs follows this approach (cf. section 1.2.1).

A further crucial aspect of drug metabolism is the metabolic conversion of certain xenobiotics, leading to the formation of reactive metabolites/intermediates (cf. section 1.3.1). Although less common, this activation process plays an important role in chemical toxicity and chemical mutagenicity/carcinogenicity.[1]

Figuratively speaking, drug metabolism can be considered as two sides of the same coin; one leading to desired, beneficial effects, whereas the other one results in adverse side effects due to toxification.

1.2 Beneficial effects of drug metabolism: Using prodrug biotransformation as a key strategy towards antihypertensive transdermal therapeutic systems

1.2.1 The prodrug approach

The term "pro-drug" was first introduced by Albert in 1958 to describe any compound that needs biotransformation prior to exhibiting its pharmacological effect.[5-6] This broad definition can be refined to signify "the transformation of a drug in an inactive transport form that releases the drug either at or near the site of action *in vivo* through chemical or enzymatic reaction.[6] On one hand a further differentiation leads to the classification of carrier prodrugs, bearing a temporary, usually covalent and non-toxic transport moiety (promoiety), which is cleaved *in vivo* by a hydrolytic reaction to release the active principle (Figure 1.1). On the other hand bioprecursors can be designed by a molecular modification of the active principle, generating a new compound, which is metabolized to regain the active principle *in vivo*.[7] In general, the prodrug approach is taken into account, when an improvement of physicochemical, biopharmaceutical or pharmacokinetic properties of a potent pharmacologically active compound is desired. Thus, by prodrugs, problems related to for example drug formulation and delivery such as poor aqueous solubility, chemical instability, insufficient oral absorption or skin permeability, high first-pass metabolism and

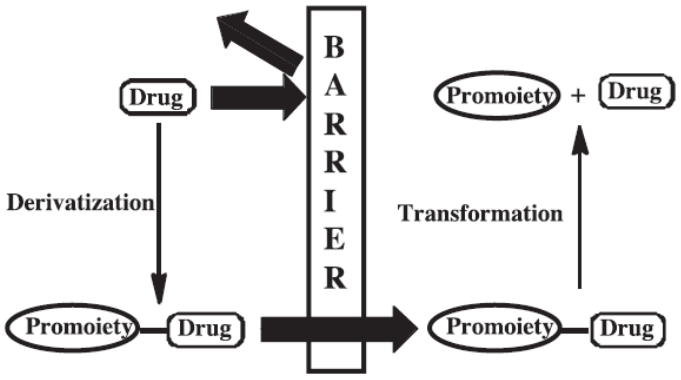

Figure 1.1. A simplified illustration of the carrier prodrug concept. Adopted from Stella.[5]

toxicity can be solved.[8-9] In addition, with respect to improved patient compliance, elimination of unacceptable taste or odor and avoidance of irritation or pain upon drug administration become possible.[9-10] Another interesting objective of prodrug strategies is tissue-selective delivery including, e.g., enzyme-prodrug cancer therapy.[10] The current percentage of the drugs approved worldwide is estimated to approx. 5-7 %, and from 2000-2008 about 20 % of all worldwide approved new small molecules have been prodrugs, indicating that the prodrug concept has become an integral part of the drug design and delivery process.[8, 11]

1.2.2 Transdermal drug delivery

In order to overcome problems associated with traditional modes of drug administration, in the last decades great effort was made to explore the transdermal route for delivery of drugs into the systemic circulation.[12] Consequentially, besides oral therapy the transdermal administration was stated the most innovative research area for drug delivery.[13] Compared to the oral route transdermal drug delivery is associated with a variety of advantages including avoidance of gastrointestinal side effects and hepatic first-pass metabolism, sustained delivery to provide a steady plasma profile without plasma concentration peaks typical for oral administration. Thereby, systemic side effects are reduced and patient compliance by convenient, patient-friendly and flexible administration as well as a potentially reduced frequency of dosing is improved. Furthermore, the drug input can be promptly interrupted on intoxication, thus increasing safety.[14-16] However, disadvantages of transdermal application are possible skin irritations and sensitizations and the fact that it is not suitable for drugs that require high blood levels.[15] Despite extensive research efforts, since the launch of the first transdermal patch against motion sickness by the end of 1979, the transdermal drug delivery market is currently based on only a few low molecular weight drugs for a limited number of therapeutic areas (cf. Table 1.2). The main problem associated with passive transdermal delivery arises from the highly efficient barrier properties of the skin, which can be overcome only by molecules with specific physicochemical properties.[17] Due to their potential for providing constant and sustained drug plasma levels and reduced application frequency, transdermal therapeutic systems are particularly advantageous for the treatment of diseases requiring long-term pharmacotherapy as, e.g., cardiovascular diseases.[15]

Table 1.2. Examples of currently available transdermal therapeutic systems approved by the US Food and Drug Administration (Mar 2011).[17-18]

Drug	Trade name	Indication	Company	Approval date
Buprenorphine	Butrans	Analgesia	Purdue Pharma LP	2010
Clonidine	Catapres-TTS	Hypertension	Boehringer Ingelheim	1984
Estradiol	Alora	HRT[a]	Watson Labs	1996
	Climara	HRT[a]	Bayer HLTHcare	1994
	Estraderm	HRT[a]	Novartis	1986
	Estradiol	HRT[a]	Mylan Technologies	2000
	Menostar	HRT[a]	Bayer HLTHcare	2004
	Vivelle	HRT[a]	Novartis	1994
	Vivelle-Dot	HRT[a]	Novartis	1996
Ethinyl estradiol/ levonorgestrol	Climara pro	HRT[a]	Bayer HLTHcare	2003
Ethinyl estradiol/ norelgestromin	Ortho Evra	Contraception	Ortho-McNeil	2001
Ethinyl estradiol/ norethindrone	Combipatch	HRT[a]	Novartis	1998
Fentanyl	Duragesic	Analgesia	Alza	1990
	Fentanyl	Analgesia	Mylan Technologies	2005
	Fentanyl	Analgesia	Lavipharm Labs	2006
	Fentanyl	Analgesia	Watson Labs	2007
Lidocaine	Lidoderm	Analgesia	Teikoku Pharma	1999
Lidocaine/ tetracaine	Synera	Analgesia	Zars Pharm	2005
Methylphenidate	Daytrana	ADHD[b]	Noven Pharms Inc	2006
Nicotine	Habitrol	Smoking cessation	Novartis	1999
	Nicoderm CQ	Smoking cessation	Sanofi Aventis US	1991
	Nicotine	Smoking cessation	Aveva	1997
Nitroglycerin	Minitran	Angina	Graceway	1996
	Nitroglycerin	Angina	Mylan	1996
	Nitroglycerin	Angina	Hercon Labs	1998
	Nitroglycerin	Angina	Kremers Urban Pharms	2004
Oxybutynin	Oxytrol	Overactive bladder	Watson	2003
Rivastigmine	Exelon	Alzheimer's disease	Novartis	2007
Rotigotine	Neupro[c]	Parkinson's disease	Schwarz Pharma	2007
Selegiline	EMSAM	Depression	Somerset	2006
Scopolamine	Transderm Scop	Motion sickness	Novartis	1979
Testosterone	Androdrem	Hypogonadism	Watson Labs	1995

[a] HRT = hormone replacement therapy, [b] ADHD = attention deficit hyperactivity disorder, [c] discontinued

1.2.3 Renin-angiotensin-aldosterone system

The renin-angiotensin-aldosterone system (RAAS) plays a key role in the regulation of blood volume and blood pressure.[19] In response to decreases in blood volume and renal perfusion, the aspartyl protease renin is secreted by juxtaglomerular cells of the kidney and cleaves angiotensinogen, produced in the liver, to form the inactive decapeptide angiotensin I (Ang I). Ang I is further converted into the biologically active octapeptide angiotensin II (Ang II) by angiotensin-converting enzyme (ACE) and non-ACE enzymes such as cathepsin G and chymase. Ang II is a potent vasoconstrictor and promotes secretion of the mineralocorticoid aldosterone from the adrenal gland, which causes enhanced sodium reabsorption, thereby increasing blood pressure. Furthermore, Ang II inhibits renin release *via* a negative feedback mechanism.[20]

1.2.3.1 Angiotensin-converting enzyme

The angiotensin-converting enzyme (ACE), a type-I membrane-anchored dipeptidyl carboxypeptidase, serves as a key component in the RAAS by cleaving the carboxy terminal His-Leu dipeptide from Ang I to produce Ang II. Moreover, ACE inactivates the vasodilatory peptide bradykinin.[21] ACE exists in two isoforms. The somatic form (sACE) is almost ubiquitously expressed, especially in endothelial cells of arterioles, lung, kidney, small intestine and in a variety of neuronal cells in the brain.[22] The second isoform, testicular ACE (tACE), is found in male germinal cells and has a single active site, whereas the somatic form is a two-domain protein, each containing a conserved His-GluXXHis zinc metallopeptidase binding motif.[22] The active site zinc ion is coordinated by the two histidines in the conserved binding motif, a glutamate 24 residues downstream and an activated water molecule.[23]

1.2.3.2 Angiotensin II receptors

Most of the physiological effects of angiotensin II (Ang II) are mediated by the angiotensin type 1 receptor (AT_1R) and the angiotensin type 2 receptor (AT_2R), both belonging to the seven-transmembrane superfamily of G protein-coupled receptors. The AT_1R is widely distributed in all organs, including liver, adrenals, brain, lung, kidney, heart and vasculature.[24] The AT_2R is ubiquitously expressed at high density in developing fetal tissue, but is much less abundant in adult tissues.[24-25]

The signaling pathway of Ang II turned out to be very complex, since a series of signaling cascades is activated by Ang II on binding to the AT_1R. Evidentially, one of the major biological functions of Ang II, vasoconstriction, is mediated *via* activation of the classic G protein-mediated pathways by coupling to $G_{q/11}$, $G_{12/13}$, and $G_{\beta\gamma}$ complexes. In addition, Ang II cross-talks with several kinases, including MAP kinases, receptor tyrosine kinases (e.g. EGFR) and nonreceptor tyrosine kinases (e.g. Janus kinases (JAK)) *via* AT_1Rs. Furthermore, the AT_1R-mediated activation of NAD(P)H oxidase leads to the generation of reactive oxygen species. These signaling cascades lead to physiological and pathophysiological effects such as vasoconstriction, smooth muscle cell growth, hypertrophy and cell migration.[24]

Regarding the signaling pathways of AT_2R, coupling to $G_{i\alpha2}$ and $G_{i\alpha3}$ proteins is discussed[26] leading to the activation of pathways including tyrosine or serine/threonine phosphatases[24], phospholipase A_2, nitric oxide and cyclic guanosine monophosphate[25]. Studies have shown that AT_1R and AT_2R have counter regulatory effects on the cardiovascular and renal system.[27]

1.2.4 Hypertension

Hypertension is recognized as one of the leading risk factors for cardiovascular morbidity and mortality.[28] In 2000 the worldwide number of adults suffering from hypertension was estimated to 972 million, two thirds living in developing countries. By 2025, the total number is expected to reach 1.56 billion.[29] According to the European Society of Hypertension (ESH) and the European Society of Cardiology (ESC) hypertension is

diagnosed at a systolic blood pressure of ≥ 140 mmHg or a diastolic blood pressure of ≥ 90 mmHg.[30] Lifestyle factors, such as physical inactivity, a salt-rich, fatty diet or alcohol and tobacco use are assumed to promote the disease.[29] Furthermore, hypertension is known to be a major risk factor for concomitant and secondary diseases such as myocardial infarction, congestive heart failure, stroke and end-stage renal disease, all of which are associated with significant morbidity and mortality.[31]

1.2.5 Antihypertensives

For the pharmacological treatment of hypertension following classes of antihypertensive drugs are recommended in mono- or combination therapy: ACE inhibitors, angiotensin receptor antagonists (ARBs), diuretics, β-blockers and calcium channel blockers.[30] Furthermore, aldosterone receptor antagonists (e.g. spironolactone, eplerone) or α_2 adrenergic agonists like clonidine are used as add-on therapy.[32] In the last decade new potential therapeutic targets for antihypertensive therapy beyond the classical RAAS pathway were discovered (cf. Figure 1.2). In 2007, the first direct renin inhibitor, aliskiren, was approved by the US FDA.[33]

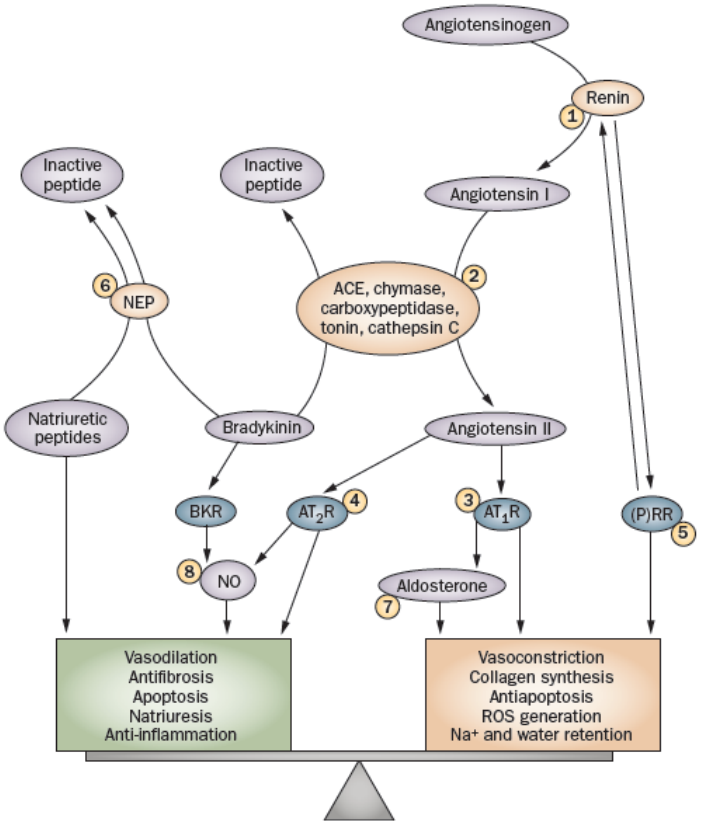

Figure 1.2. Vasoactive balance of the renin-angiotensin-aldosterone system. Established and possible therapeutic targets for antihypertensive therapy include (1) Renin inhibition; (2) ACE inhibition; (3) AT_1R blockade; (4) AT_2R stimulation; (5) (P)RR blockade; (6) NEP inhibition; (7) aldosterone-receptor blockade or aldosterone-synthase inhibition; (8) NO-cGMP stimulation. Abbreviations: BKR = bradykinin receptor; cGMP = cyclic guanosine monophosphate; NEP = neutral endopeptidase; NO = nitric oxide; (P)RR = (pro)renin receptor; ROS = reactive oxygen species.
Reprinted by permission from Macmillan Publishers Ltd: Nat. Rev. Cardiol.[28], copyright 2010.

In the following, special emphasis is laid on a closer discussion of ACE inhibitors and angiotensin receptor antagonists, as these drug classes are of particular relevance for this thesis.

1.2.5.1 ACE inhibitors

In the nineteen-sixties the ACE-inhibiting properties of peptides present in *Bothrops jararaca* snake venom were discovered by serendipity.[34] Consequentially, in 1977 the first orally available ACE inhibitor (ACEi), captopril, was designed based on the sequence of the nonapeptide SQ 20,881 (Glu-Trp-Pro-Arg-Pro-Gln-Ile-Pro-Pro) and the structure of bovine pancreatic carboxypeptidase A, a zinc-dependent carboxypeptidase assumed to have a catalytic mechanism and an active site comparable to ACE.[35-36] Furthermore, a similar approach, based on the inhibition of the zinc-dependent proteinase thermolysin, led to the development of enalapril and lisinopril. Until today a variety of ACE inhibitors was designed (cf. Figure 1.4), nearly all of them containing a Zn^{2+} binding group (sulfhydryl, carboxylate or phosphinate), a free carboxylate group interacting with a positively charged protein amino acid and a hydrophobic residue (mostly a phenylpropyl moiety) that undergoes van der Waals interactions with amino acid side chains in the S_1 pocket. Details about substrate binding were provided by crystal structures in complex with captopril[37], enalaprilat[37] and lisinopril[21] (Figure 1.3). Except for captopril and lisinopril, all ACE inhibitors depicted in Figure 1.4 are prodrugs. By esterification of one of the carboxylic acid groups the lipophilicity is increased resulting in a considerable increase in absorption after administration.[38] Following absorption from the GI-tract, the prodrug esters require enzymatic hydrolysis by esterases to liberate the corresponding active principle, which is able to coordinate the active site zinc ion and to efficiently inhibit ACE.

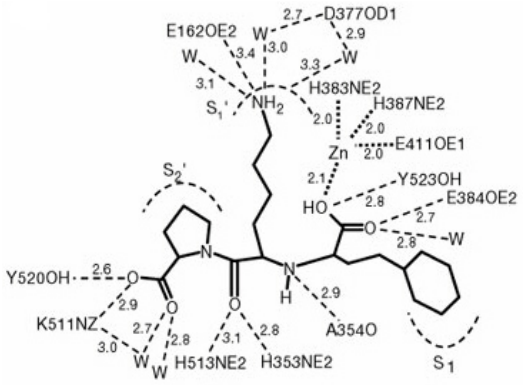

Figure 1.3. Schematic view of lisinopril binding in the active site of tACE with distances marked in A°. The different binding subsites are labelled. Adapted by permission from Macmillan Publishers Ltd: Nature[21], copyright 2003.

ACE inhibition directly reduces the amount of circulating Ang II, thus promoting vasodilation and decreasing systemic vascular resistance resulting in reduced blood pressure. In addition to their established use as antihypertensives and for treatment and prevention of heart failure, patients with left ventricular dysfunction, post-myocardial infarction, peripheral vascular disease, diabetes, stroke, transient ischaemic attack or chronic kidney disease have also been proven to benefit from ACEis. Moreover, ACEis show significant cardio- and vasculoprotective effects.[39] The most common adverse effect experienced with ACEis is cough, which is assumed to be caused by accumulation of bradykinin, often requiring cessation of the therapy. Additionally, as a rare but potentially life-threatening side effect angioedema is described.[40]

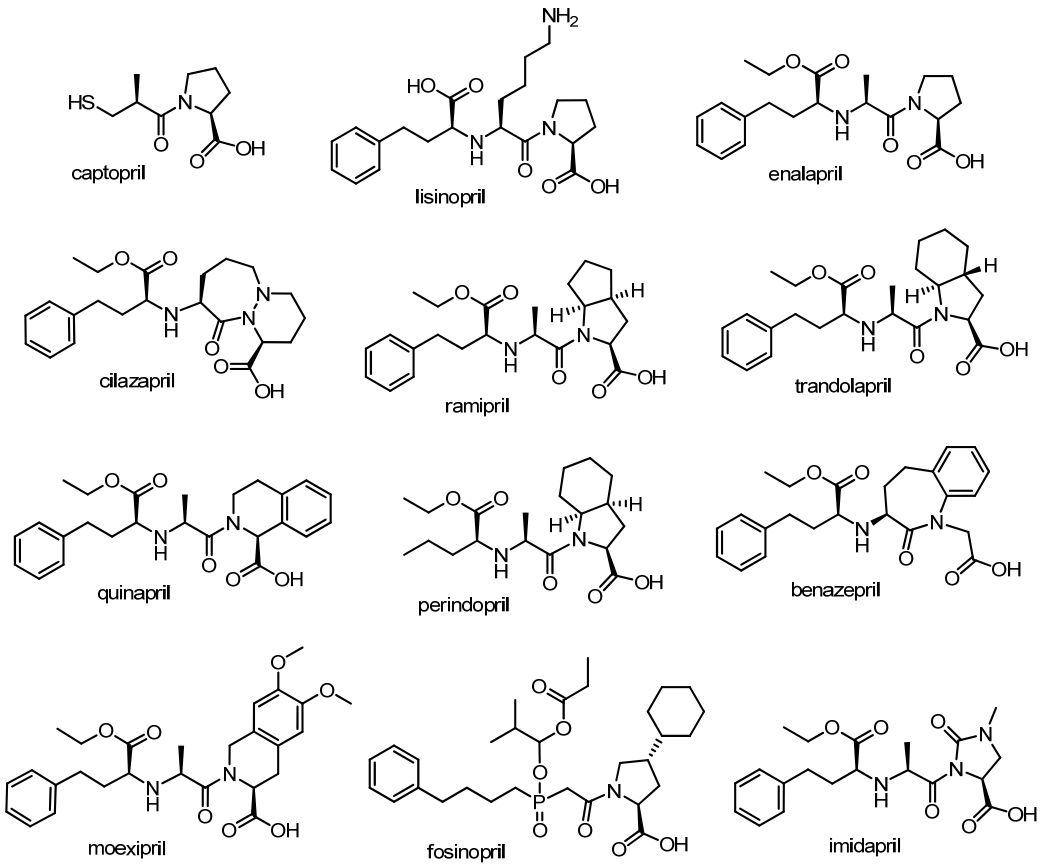

Figure 1.4. Inhibitors of the angiotensin-converting enzyme approved by the US FDA.[18] Cilazapril is not available in the United States, but in Europe. Imidapril is only approved in Japan.

1.2.5.2 Angiotensin II AT_1 receptor antagonists

The development of potent nonpeptide Ang II receptor antagonists (ARBs) with high AT_1 selectivity was initiated by the discovery of 1-benzylimidazol-5-acetic acid derivatives like S-8307 and S-8308 (Figure 1.5) derived from a screening program by Takeda Chemical Industries in 1982. Two different design strategies followed by DuPont and SmithKline Beecham, respectively, based on molecular modeling and knowledge of the structure-activity relationships of the peptide were used to align the selective but weak antagonists S-8307 and S-8308 to the C-terminal region of putative active conformations of Ang II. These approaches resulted in the identification of the highly potent ARBs losartan and eprosartan (Figure 1.5).[41] By modifying or replacing the imidazole ring of losartan a variety of different ARBs was obtained including imidazole, dihydroimidazol-4-one, benzimidazole and other heterocycles containing antagonists as well as acyclic analogues. Particular enhancement of binding activity was achieved by introduction of the privileged 2'-tetrazole-biphenylmethyl structure.[42] In general, the presence of an acidic group (either a tetrazole or carboxylic acid) seems to be favorable for the interaction with a basic amino acid group, presumably, the highly conserved arginine-167 (Arg167) in transmembrane region IV of the AT_1R.[43] Similarly, an acidic moiety at the 5-position of the imidazole ring and the 7-position of the benzimidazole ring, respectively, is proposed

to interact with a positively charged lysine (Lys199) residue in transmembrane region V of the AT_1R.[44]

At present, eight ARBs are approved by the US FDA (Figure 1.5), four of them representing prodrugs. Candesartan cilexetil, olmesartan medoxomil and azilsartan medoxomil show improved oral bioavailability compared to the corresponding diacids and release their active principles on enzymatic hydrolysis of the carrier promoieties. Losartan can be regarded as a bioprecursor, as it is oxidized *in vitro* to the metabolite EXP3174 that is about 20 times[31] more potent than losartan itself. In Germany, all ARBs shown in Figure 1.5 except for azilsartan medoxomil are currently on the market.

By selectively blocking the AT_1R, ARBs effectively antagonize AT_1R-mediated effects of Ang II. Furthermore, the blockade leads to a shift of the vasoactive balance (cf. Figure 1.2), due to an enhanced activation of the AT_2R. Resulting effects are a decrease in blood pressure as well as a protection of tissues from oxidative stress and resultant chronic vascular disease.[45]

ARBs were found to exhibit a very favorable safety profile with low incidence of adverse effects. Cough, a frequent side effect of ACEi, is much less common with ARBs and only rare cases of angioedema have been noted.[45] Consequentially, a discontinuation of ARBs is rare. In fact, it was shown that ARBs had the highest 1-year compliance among five major classes of antihypertensive drugs.[46]

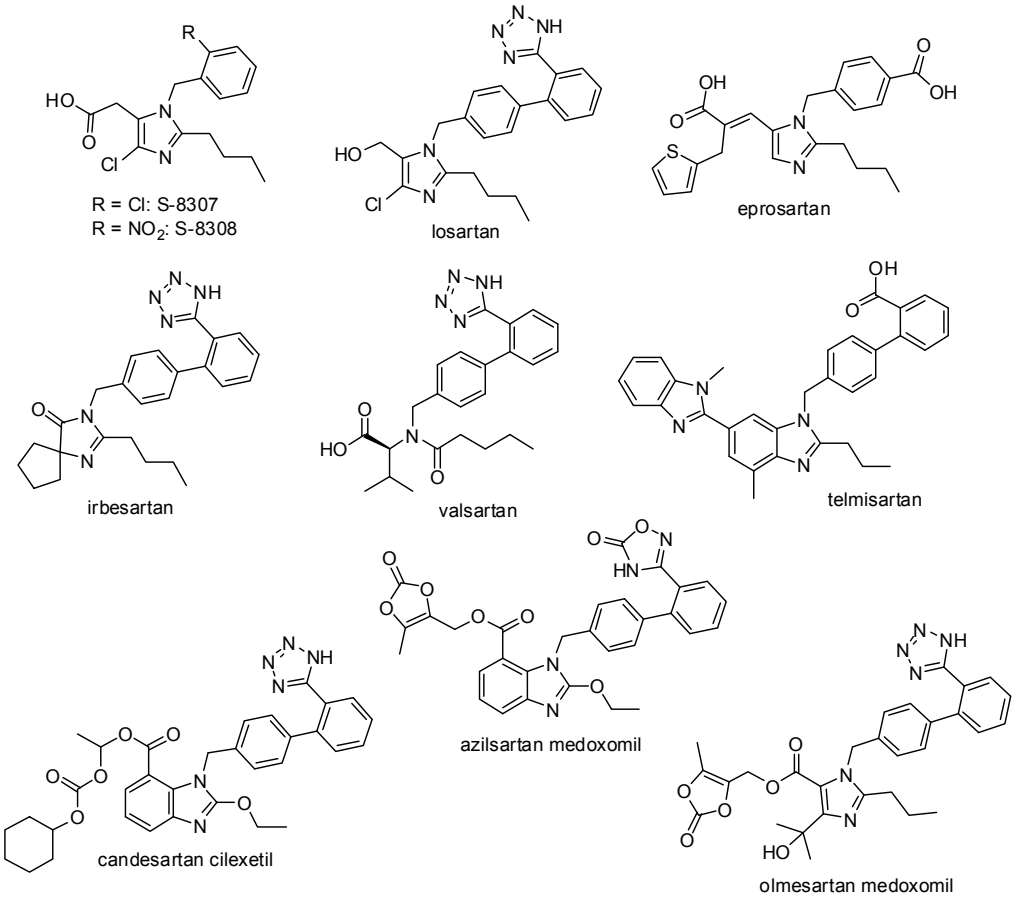

Figure 1.5. Lead structures S-8307 and S-8308 discovered by Takeda Chemical Industries and subsequently developed angiotensin II AT_1 receptor antagonists approved by the US FDA[18].

1.3 Adverse effects of drug metabolism: Formation of reactive metabolites by bioactivation

1.3.1 Reactive metabolites and adverse drug reactions

In contrast to metabolic detoxification, in certain cases bioactivation of xenobiotics can result in the formation of chemically reactive metabolites/intermediates. Due to their high reactivity such metabolites exhibit short half-lives of generally less than one minute and are usually not detectable in plasma.[47] Their existence can only be indirectly proven, e.g. by *in vitro* trapping reactions (cf. Chapter 6) or investigation of covalent binding using a radiolabeled parent compound.[48] Since the formation of reactive metabolites is usually catalyzed by cytochrome P450 enzymes, involving oxidation, the nature of such species is mostly electrophilic.[47] In general, the tendency of a compound to form reactive metabolites is a function of its chemical structure.[47] Today a variety of organic functional groups is known to be associated with bioactivation, such as aromatic amines, *p*-aminophenols, benzene rings or heterocycles like furan or thiophene.[49]

The most prominent and widely studied compound that generates reactive metabolites of P450-mediated bioactivation is acetaminophen. Besides phase II glucuronidation or sulfonation, acetaminophen undergoes P450-mediated two-electron oxidation resulting in the formation of the reactive *N*-acetyl-*p*-benzoquinone imine (NAPQI) (Scheme 1.1). This species is readily trapped and detoxified by glutathione (GSH) addition. However, when hepatic GSH levels are depleted, NAPQI can form adducts with proteins, oxidize cysteine residues of proteins, covalently bind to liver and renal DNA and eventually disrupt cellular homeostasis.[49]

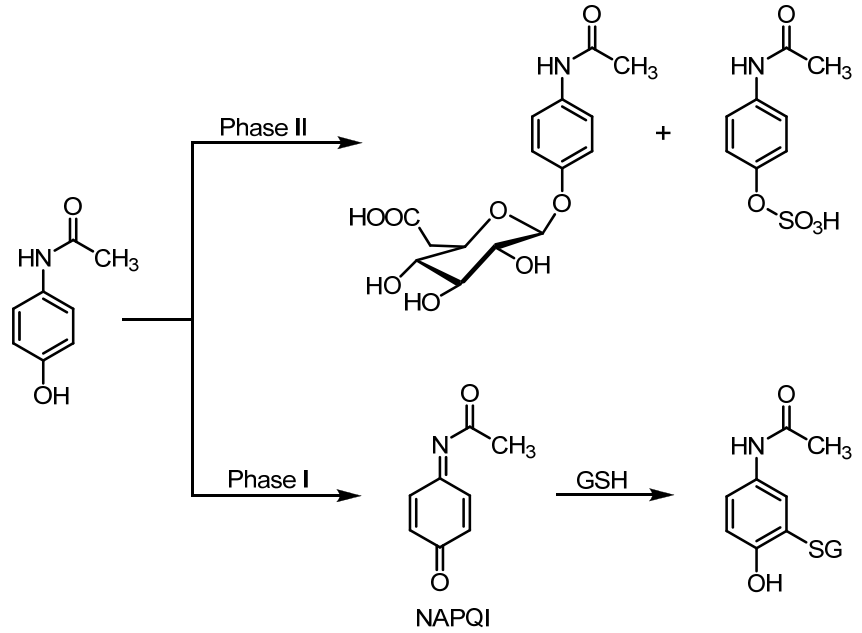

Scheme 1.1. Metabolism and bioactivation of acetaminophen.

Based on a multitude of examples, it is now widely accepted that there is a strong link between bioactivation and drug-induced toxicity as well as adverse drug reactions (ADR) such as hepatotoxicity or hypersensitivity (Scheme 1.2).[49]

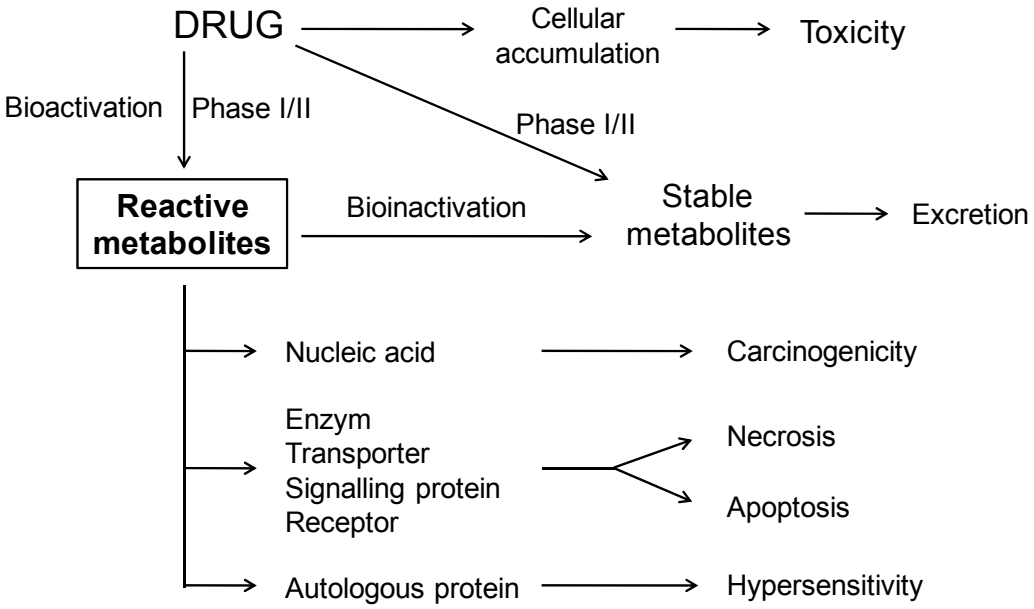

Scheme 1.2. Pathways of drug metabolism highlighting the link between formation of reactive metabolites and adverse toxic effect deriving from reaction of reactive metabolites with cellular macromolecules. Modified from Park et al.[47]

However, it should be noted that not all the drugs that possess organic functional groups being prone to bioactivation are actually bioactivated, and that bioactivation does not inevitably result in toxicity.[49] In fact, the balance between bioactivation, detoxification and defense mechanisms appears to be the key-determinant of chemical toxicity.[1, 50]
Recently, it was suggested from published data that, besides lack of efficacy, preclinical toxicity was the primary cause for the high attrition rate in drug development.[51] Furthermore, ADRs were stated to be the major reason for patient morbidity and a significant cause of patient mortality.[52-53] They often appear to be unpredictable from the knowledge of the basic pharmacology of the drug and show no simple dose-response relationship (idiosyncratic ADRs).[54] Moreover, ADRs usually have a low incidence, which makes them very difficult to detect in phase three clinical trials, especially when the number of patients in those trials is small.[55] Therefore, detection of reactive metabolites is considered a topic of serious concern in early stages of drug development to help avoid safety issues that could lead to compound failure at a later stage.[56]

1.3.2 N^G-acylated hetarylpropylguanidines

Based on the imidazolylpropylguanidine derivatives impromidine and arpromidine (Scheme 1.3), which were found to be highly potent histamine H_2 receptor (H_2R) agonists with an approximately 50 and 100-fold higher potency, respectively, than histamine on the spontaneously beating guinea pig right atrium,[57-59] a novel class of N^G-acylated analogues with improved pharmacokinetic properties was developed in our workgroup.[60]

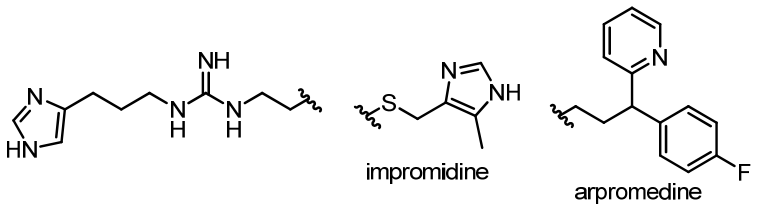

Scheme 1.3. Structures of the H_2R agonists impromidine and arpromidine.

Due to the strongly basic guanidine moiety (pK_a ~ 13) guanidine-type H_2R agonists are nearly quantitatively protonated at physiological pH. By introduction of a carbonyl function adjacent to the guanidine moiety basicity is decreased by 4-5 orders of magnitude (pK_a ~ 8). Thus, the resulting N^G-acylated guanidines (Scheme 1.4) are absorbed from the gastrointestinal tract and are capable of penetrating across the blood-brain barrier.[60]

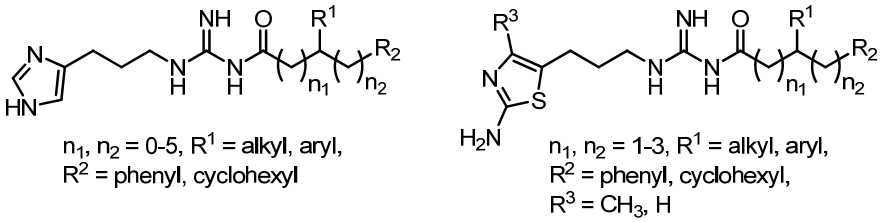

Scheme 1.4. General structures of N^G-acylated imidazolylpropylguanidines and N^G-acylated 2-aminothiazolylpropylguanidines.

Furthermore, bioisosteric replacement of the imidazole ring by a 2-aminothiazole or a 2-amino-4-methylthiazole group led to equipotent or even more potent H_2R (partial) agonists with remarkably improved selectivity over the H_3R and H_4R.[61]

However, there is increasing evidence that cytochrome P450-catalyzed bioactivation of heterocycles like the imidazole and aminothiazole ring is associated with the formation of reactive intermediates or toxic metabolites.[62]

1.4 References

1. Parkinson, A.; Ogilvie, B. W. Biotransformation of Xenobiotics. In *Casarett and Doull's toxicology : the basic science of poisons*, 7. ed.; Casarett, L. J.; Doull, J.; Klaassen, C. D., Eds., McGraw-Hill: New York, NY [u.a.], 2008; pp XV, 1310 S.
2. Ionescu, C.; Caira, M. R. *Drug metabolism : current concepts*. Springer: Dordrecht, 2005; p X, 420 S.
3. Gonzalez, F. J.; Tukey, R. H. Drug metabolism. In *Goodman & Gilman's the pharmacological basis of therapeutics*, 11. ed.; Brunton, L. L.; Goodman, L. S.; Gilman, A., Eds., McGraw-Hill: New York [u.a.], 2006; pp XXIII, 2021 S.
4. Fura, A.; Shu, Y. Z.; Zhu, M.; Hanson, R. L.; Roongta, V.; Humphreys, W. G. Discovering drugs through biological transformation: role of pharmacologically active metabolites in drug discovery. *J. Med. Chem.* **2004**, 47, 4339-4351.
5. Stella, V. J. A Case for Prodrugs. In *Prodrugs*, Stella, V. J.; Borchardt, R. T.; Hageman, M. J.; Oliyai, R.; Maag, H.; Tilley, J. W., Eds., Springer New York: 2007; Vol. V, pp 3-33.
6. Silva, A. T.; Chung, M. C.; Castro, L. F.; Guido, R. V.; Ferreira, E. I. Advances in prodrug design. *Mini-Rev. Med. Chem.* **2005**, 5, 893-914.
7. Wermuth, C. G. Designing prodrugs and bioprecursors. In *The practice of medicinal chemistry*, 2. ed.; Wermuth, C. G., Ed. Academic Press: Amsterdam [u.a.], 2003; pp XIV, 768 S.
8. Rautio, J.; Kumpulainen, H.; Heimbach, T.; Oliyai, R.; Oh, D.; Jarvinen, T.; Savolainen, J. Prodrugs: design and clinical applications. *Nat. Rev. Drug. Discov.* **2008**, 7, 255-270.
9. Rautio, J.; Taipale, H.; Gynther, J.; Vepsalainen, J.; Nevalainen, T.; Jarvinen, T. In vitro evaluation of acyloxyalkyl esters as dermal prodrugs of ketoprofen and naproxen. *J. Pharm. Sci.* **1998**, 87, 1622-1628.
10. Ettmayer, P.; Amidon, G. L.; Clement, B.; Testa, B. Lessons learned from marketed and investigational prodrugs. *J. Med. Chem.* **2004**, 47, 2393-2404.
11. Stella, V. J. Prodrugs: Some thoughts and current issues. *J. Pharm. Sci.* **2010**, 99, 4755-4765.
12. Touitou, E. Drug delivery across the skin. *Expert Opin. Biol. Ther.* **2002**, 2, 723-733.
13. Barry, B. W. Breaching the skin's barrier to drugs. *Nat. Biotechnol.* **2004**, 22, 165-167.
14. Guy, R. H.; Hadgraft, J.; Bucks, D. A. Transdermal drug delivery and cutaneous metabolism. *Xenobiotica* **1987**, 17, 325-343.
15. Ranade, V. V. Drug delivery systems. 6. Transdermal drug delivery. *J. Clin. Pharmacol.* **1991**, 31, 401-418.
16. Thomas, B. J.; Finnin, B. C. The transdermal revolution. *Drug Discov. Today* **2004**, 9, 697-703.
17. Farahmand, S.; Maibach, H. I. Transdermal drug pharmacokinetics in man: Interindividual variability and partial prediction. *Int. J. Pharm.* **2009**, 367, 1-15.
18. www.fda.gov
19. Muller, D. N.; Luft, F. C. Direct renin inhibition with aliskiren in hypertension and target organ damage. *Clin. J. Am. Soc. Nephrol.* **2006**, 1, 221-228.
20. Hsueh, W. A.; Wyne, K. Renin-Angiotensin-aldosterone system in diabetes and hypertension. *J. Clin. Hypertens. (Greenwich)* **2011**, 13, 224-237.
21. Natesh, R.; Schwager, S. L.; Sturrock, E. D.; Acharya, K. R. Crystal structure of the human angiotensin-converting enzyme-lisinopril complex. *Nature* **2003**, 421, 551-554.
22. Coates, D. The angiotensin converting enzyme (ACE). *Int. J. Biochem. Cell Biol.* **2003**, 35, 769-773.
23. Williams, T. A.; Corvol, P.; Soubrier, F. Identification of two active site residues in human angiotensin I-converting enzyme. *J. Biol. Chem.* **1994**, 269, 29430-29434.
24. Mehta, P. K.; Griendling, K. K. Angiotensin II cell signaling: physiological and pathological effects in the cardiovascular system. *Am. J. Physiol. Cell Physiol.* **2007**, 292, C82-97.
25. de Gasparo, M.; Catt, K. J.; Inagami, T.; Wright, J. W.; Unger, T. International union of pharmacology. XXIII. The angiotensin II receptors. *Pharmacol. Rev.* **2000**, 52, 415-472.
26. Zhang, J.; Pratt, R. E. The AT2 receptor selectively associates with Gialpha2 and Gialpha3 in the rat fetus. *J. Biol. Chem.* **1996**, 271, 15026-15033.
27. Schulman, I. H.; Raij, L. The angiotensin II type 2 receptor: what is its clinical significance? *Curr. Hypertens. Rep.* **2008**, 10, 188-193.
28. Paulis, L.; Unger, T. Novel therapeutic targets for hypertension. *Nat. Rev. Cardiol.* **2010**, 7, 431-441.
29. Hypertension: uncontrolled and conquering the world. *Lancet* **2007**, 370, 539.

30. Mancia, G.; De Backer, G.; Dominiczak, A.; Cifkova, R.; Fagard, R.; Germano, G.; Grassi, G.; Heagerty, A. M.; Kjeldsen, S. E.; Laurent, S.; Narkiewicz, K.; Ruilope, L.; Rynkiewicz, A.; Schmieder, R. E.; Boudier, H. A.; Zanchetti, A.; Vahanian, A.; Camm, J.; De Caterina, R.; Dean, V.; Dickstein, K.; Filippatos, G.; Funck-Brentano, C.; Hellemans, I.; Kristensen, S. D.; McGregor, K.; Sechtem, U.; Silber, S.; Tendera, M.; Widimsky, P.; Zamorano, J. L.; Erdine, S.; Kiowski, W.; Agabiti-Rosei, E.; Ambrosioni, E.; Lindholm, L. H.; Viigimaa, M.; Adamopoulos, S.; Bertomeu, V.; Clement, D.; Farsang, C.; Gaita, D.; Lip, G.; Mallion, J. M.; Manolis, A. J.; Nilsson, P. M.; O'Brien, E.; Ponikowski, P.; Redon, J.; Ruschitzka, F.; Tamargo, J.; van Zwieten, P.; Waeber, B.; Williams, B. 2007 Guidelines for the Management of Arterial Hypertension: The Task Force for the Management of Arterial Hypertension of the European Society of Hypertension (ESH) and of the European Society of Cardiology (ESC). *J. Hypertens.* **2007**, 25, 1105-1187.
31. Naik, P.; Murumkar, P.; Giridhar, R.; Yadav, M. R. Angiotensin II receptor type 1 (AT_1) selective nonpeptidic antagonists--a perspective. *Bioorg. Med. Chem.* **2010**, 18, 8418-8456.
32. DeQuattro, V.; Li, D. Sympatholytic therapy in primary hypertension: a user friendly role for the future. *J. Hum. Hypertens.* **2002**, 16 Suppl 1, S118-123.
33. Wu, K. C.; Gerstenblith, G. Update on newer antihypertensive medicines and interventions. *J. Cardiovasc. Pharmacol. Ther.* **2010**, 15, 257-267.
34. Ferreira, S. H. A Bradykinin-Potentiating Factor (Bpf) Present in the Venom of Bothrops Jararca. *Br. J. Pharmacol.* **1965**, 24, 163-169.
35. Cushman, D. W.; Pluscec, J.; Williams, N. J.; Weaver, E. R.; Sabo, E. F.; Kocy, O.; Cheung, H. S.; Ondetti, M. A. Inhibition of angiotensin-coverting enzyme by analogs of peptides from Bothrops jararaca venom. *Experientia* **1973**, 29, 1032-1035.
36. Ondetti, M. A.; Rubin, B.; Cushman, D. W. Design of specific inhibitors of angiotensin-converting enzyme: new class of orally active antihypertensive agents. *Science* **1977**, 196, 441-444.
37. Natesh, R.; Schwager, S. L.; Evans, H. R.; Sturrock, E. D.; Acharya, K. R. Structural details on the binding of antihypertensive drugs captopril and enalaprilat to human testicular angiotensin I-converting enzyme. *Biochemistry (Mosc).* **2004**, 43, 8718-8724.
38. Beaumont, K.; Webster, R.; Gardner, I.; Dack, K. Design of ester prodrugs to enhance oral absorption of poorly permeable compounds: challenges to the discovery scientist. *Curr. Drug Metab.* **2003**, 4, 461-485.
39. Bertrand, M. E. Provision of cardiovascular protection by ACE inhibitors: a review of recent trials. *Curr. Med. Res. Opin.* **2004**, 20, 1559-1569.
40. Brown, N. J.; Vaughan, D. E. Angiotensin-converting enzyme inhibitors. *Circulation* **1998**, 97, 1411-1420.
41. Wexler, R. R.; Greenlee, W. J.; Irvin, J. D.; Goldberg, M. R.; Prendergast, K.; Smith, R. D.; Timmermans, P. B. Nonpeptide angiotensin II receptor antagonists: the next generation in antihypertensive therapy. *J. Med. Chem.* **1996**, 39, 625-656.
42. Mire, D. E.; Silfani, T. N.; Pugsley, M. K. A review of the structural and functional features of olmesartan medoxomil, an angiotensin receptor blocker. *J. Cardiovasc. Pharmacol.* **2005**, 46, 585-593.
43. Yamano, Y.; Ohyama, K.; Kikyo, M.; Sano, T.; Nakagomi, Y.; Inoue, Y.; Nakamura, N.; Morishima, I.; Guo, D. F.; Hamakubo, T.; et al. Mutagenesis and the molecular modeling of the rat angiotensin II receptor (AT1). *J. Biol. Chem.* **1995**, 270, 14024-14030.
44. Fierens, F. L.; Vanderheyden, P. M.; Gaborik, Z.; Minh, T. L.; Backer, J. P.; Hunyady, L.; Ijzerman, A.; Vauquelin, G. Lys(199) mutation of the human angiotensin type 1 receptor differentially affects the binding of surmountable and insurmountable non-peptide antagonists. *J. Renin Angiotensin Aldosterone Syst.* **2000**, 1, 283-288.
45. Zaman, M. A.; Oparil, S.; Calhoun, D. A. Drugs targeting the renin-angiotensin-aldosterone system. *Nat. Rev. Drug. Discov.* **2002**, 1, 621-636.
46. Hernandez-Hernandez, R.; Sosa-Canache, B.; Velasco, M.; Armas-Hernandez, M. J.; Armas-Padilla, M. C.; Cammarata, R. Angiotensin II receptor antagonists role in arterial hypertension. *J. Hum. Hypertens.* **2002**, 16 Suppl 1, S93-99.
47. Park, B. K.; Kitteringham, N. R.; Maggs, J. L.; Pirmohamed, M.; Williams, D. P. The role of metabolic activation in drug-induced hepatotoxicity. *Annu. Rev. Pharmacool. Toxicol.* **2005**, 45, 177-202.
48. Evans, D. C.; Watt, A. P.; Nicoll-Griffith, D. A.; Baillie, T. A. Drug-protein adducts: an industry perspective on minimizing the potential for drug bioactivation in drug discovery and development. *Chem. Res. Toxicol.* **2004**, 17, 3-16.

49. Kalgutkar, A. S.; Gardner, I.; Obach, R. S.; Shaffer, C. L.; Callegari, E.; Henne, K. R.; Mutlib, A. E.; Dalvie, D. K.; Lee, J. S.; Nakai, Y.; O'Donnell, J. P.; Boer, J.; Harriman, S. P. A comprehensive listing of bioactivation pathways of organic functional groups. *Curr. Drug Metab.* **2005**, 6, 161-225.
50. Castell, J. V.; Gomez-Lechon, M. J.; Ponsoda, X.; Bort, R. The use of cultured hepatocytes to investigate the mechanisms of drug hepatotoxicity. *Cell Biol. Toxicol.* **1997**, 13, 331-338.
51. Kola, I.; Landis, J. Can the pharmaceutical industry reduce attrition rates? *Nat. Rev. Drug Discovery* **2004**, 3, 711-715.
52. Lazarou, J.; Pomeranz, B. H.; Corey, P. N. Incidence of adverse drug reactions in hospitalized patients: a meta-analysis of prospective studies. *JAMA* **1998**, 279, 1200-1205.
53. Pirmohamed, M.; Breckenridge, A. M.; Kitteringham, N. R.; Park, B. K. Adverse drug reactions. *BMJ* **1998**, 316, 1295-1298.
54. Park, B. K.; Kitteringham, N. R.; Powell, H.; Pirmohamed, M. Advances in molecular toxicology-towards understanding idiosyncratic drug toxicity. *Toxicology* **2000**, 153, 39-60.
55. Uetrecht, J. Idiosyncratic drug reactions: past, present, and future. *Chem Res Toxicol* **2008**, 21, 84-92.
56. Argoti, D.; Liang, L.; Conteh, A.; Chen, L.; Bershas, D.; Yu, C. P.; Vouros, P.; Yang, E. Cyanide trapping of iminium ion reactive intermediates followed by detection and structure identification using liquid chromatography-tandem mass spectrometry (LC-MS/MS). *Chem. Res. Toxicol.* **2005**, 18, 1537-1544.
57. Buschauer, A. Synthesis and in vitro pharmacology of arpromidine and related phenyl(pyridylalkyl)guanidines, a potential new class of positive inotropic drugs. *J. Med. Chem.* **1989**, 32, 1963-1970.
58. Durant, G. J.; Duncan, W. A.; Ganellin, C. R.; Parsons, M. E.; Blakemore, R. C.; Rasmussen, A. C. Impromidine (SK&F 92676) is a very potent and specific agonist for histamine H2 receptors. *Nature* **1978**, 276, 403-405.
59. Leurs, R.; Smit, M. J.; Timmerman, H. Molecular pharmacological aspects of histamine receptors. *Pharmacol. Ther.* **1995**, 66, 413-463.
60. Ghorai, P.; Kraus, A.; Keller, M.; Gotte, C.; Igel, P.; Schneider, E.; Schnell, D.; Bernhardt, G.; Dove, S.; Zabel, M.; Elz, S.; Seifert, R.; Buschauer, A. Acylguanidines as bioisosteres of guanidines: NG-acylated imidazolylpropylguanidines, a new class of histamine H2 receptor agonists. *J. Med. Chem.* **2008**, 51, 7193-7204.
61. Kraus, A.; Ghorai, P.; Birnkammer, T.; Schnell, D.; Elz, S.; Seifert, R.; Dove, S.; Bernhardt, G.; Buschauer, A. N(G)-acylated aminothiazolylpropylguanidines as potent and selective histamine H(2) receptor agonists. *ChemMedChem* **2009**, 4, 232-240.
62. Dalvie, D. K.; Kalgutkar, A. S.; Khojasteh-Bakht, S. C.; Obach, R. S.; O'Donnell, J. P. Biotransformation reactions of five-membered aromatic heterocyclic rings. *Chem. Res. Toxicol.* **2002**, 15, 269-299.

Chapter 2
Scope and Objectives

The primary function of drug metabolism is the conversion of lipophilic, easily absorbable xenobiotics into more hydrophilic xenobiotics to facilitate excretion from the body to prevent accumulation. However, drug metabolism can also result in the activation of pharmacologically inactive drugs or in the formation of reactive metabolites/intermediates, i.e. electrophilic compounds capable of reacting with cellular macromolecules. The former process can be exploited, mostly for the activation of prodrugs to overcome problems associated with a drug´s pharmacokinetic or pharmacodynamic properties, whereas the latter is often undesirable, as it can lead to adverse drug reactions and toxicity. Examples for both scenarios are highlighted in this work.

The advantages associated with drug application *via* a transdermal therapeutic system (TTS) are well accepted. Particularly due to the potential for providing constant and sustained drug plasma levels and reduced application frequency, TTS are advantageous for the treatment of diseases requiring long-term pharmacotherapy as, e.g., cardiovascular diseases. Up to now, only the α_2-adrenoreceptor agonist clonidine is approved in the USA as TTS for the treatment of hypertension. Thus, there is a strong discrepancy between the high incidence of hypertension and the practically non-existing supply of transdermally applicable antihypertensive drugs. Thus, the development of novel TTS for the treatment of hypertension is highly desirable. A prerequisite for transdermal application is a sufficiently high systemic bioavailability of the drug, which requires appropriate physicochemical properties to overcome the barrier function of the skin. The subject of previous work was to find suitable prodrugs of the angiotensin II AT_1 receptor antagonist candesartan and the angiotensin-converting enzyme (ACE) inhibitor trandolapril, which can be administered *via* a TTS.[1] Therein, trandolapril was found to be inappropriate for this purpose, since its prodrugs have a strong tendency to decompose, giving diketopiperazines during synthesis and storage by intramolecular cyclization reactions. As those ACE inhibitors, which have a conformationally constrained structure like cilazapril, show no distinct tendency to diketopiperazine formation, cilazapril was considered a promising drug for TTS development.
The aim of this work was the design, synthesis and bioanalytical as well as biopharmaceutical characterization of candesartan and cilazapril prodrugs with respect to suitability for application *via* a TTS. Carrier-prodrug structures were chosen by analogy with the orally administered prodrug candesartan cilexetil taking into consideration promoieties of various approved and successfully marketed prodrugs. The new potential prodrugs

should be investigated with respect to solid-state stability, susceptibility for enzymatic hydrolysis, i.e. half-lives in the presence of porcine liver esterase, porcine skin homogenate, human plasma and cultured human hepatocytes, and stability against spontaneous, non-enzymatic hydrolysis in buffer. In addition, investigation of the potential candesartan prodrugs for angiotensin II AT_1 antagonism was envisaged by means of a spectrofluorimetric Ca^{2+}-assay using AT_1 receptor-expressing rat glomerular mesangial cells.

To further elucidate the potential for transdermal application, selected candesartan and cilazapril prodrugs comprising the most promising properties in terms of physicochemistry, stability and enzymatic hydrolyzability should be explored with respect to TTS manufacturing, quality, stability and transdermal permeation through animal and human skin using Franz diffusion cells.

A further project focused on the adverse side of drug metabolism, namely on the detection and identification of reactive metabolites/intermediates. Based on the histamine H_2 receptor (H_2R) ligands impromidine and arpromidine, N^G-acylated hetarylpropylguanidines were developed in our workgroup, which turned out to be highly potent H_2R agonists[2-3] and could serve as valuable pharmacological tools for *in vitro* and future *in vivo* studies. Two compound sub-classes were developed either comprising an imidazole ring or a 2-aminothiazole group. There is strong evidence that the 2-aminothiazole moiety is associated with adverse drug reactions by cytochrome P450-mediated formation of reactive metabolites.[4] The aim of this project was the elucidation of the toxic potential of N^G-acylated 2-aminothiazolylpropylguanidines derived from the bioactivation of the heterocycle. To investigate the formation of reactive metabolites/intermediates, representative N^G-acylated 2-aminothiazolylpropylguanidines were selected to explore the applicability of trapping by glutathione (GSH) on incubation with liver microsomes and to identify potential GSH adducts and putative reactive molecular species, respectively, by means of liquid chromatography/tandem mass spectrometry (LC-MS/MS). Furthermore, the impact of the substitution pattern at the 2-aminothiazole moiety concerning the formation of reactive metabolites should be investigated. Additionally, in view of further *in vitro* and *in vivo* investigations possible unspecific chemical toxicity of selected N^G-acylated hetarylpropylguanidines should be taken into consideration by testing for hemolysis and cytotoxicity.

References

1. Ertel, M. Potentielle Prodrugs von ACE-Hemmern und Angiotensin II AT_1-Rezeptorantagonisten: Synthese und analytische Untersuchungen. Diploma, Regensburg, Regensburg, 2006.
2. Ghorai, P.; Kraus, A.; Keller, M.; Götte, C.; Igel, P.; Schneider, E.; Schnell, D.; Bernhardt, G.; Dove, S.; Zabel, M.; Elz, S.; Seifert, R.; Buschauer, A. Acylguanidines as bioisosteres of guanidines: NG-acylated imidazolylpropylguanidines, a new class of histamine H2 receptor agonists. *J. Med. Chem.* **2008,** 51, 7193-204.
3. Kraus, A.; Ghorai, P.; Birnkammer, T.; Schnell, D.; Elz, S.; Seifert, R.; Dove, S.; Bernhardt, G.; Buschauer, A. N(G)-acylated aminothiazolylpropylguanidines as potent and selective histamine H(2) receptor agonists. *ChemMedChem* **2009,** 4, 232-40.
4. Kalgutkar, A. S.; Driscoll, J.; Zhao, S. X.; Walker, G. S.; Shepard, R. M.; Soglia, J. R.; Atherton, J.; Yu, L.; Mutlib, A. E.; Munchhof, M. J.; Reiter, L. A.; Jones, C. S.; Doty, J. L.; Trevena, K. A.; Shaffer, C. L.; Ripp, S. L. A rational chemical intervention strategy to circumvent bioactivation liabilities associated with a nonpeptidyl thrombopoietin receptor agonist containing a 2-amino-4-arylthiazole motif. *Chem. Res. Toxicol.* **2007,** 20, 1954-65.

Chapter 3
Prodrugs of Candesartan and Cilazapril

3.1 Introduction

The term prodrug describes an inactive transport form of a drug that releases the active drug *in vivo* after chemical or enzymatic conversion.[1] Approximately 49 % of all prodrugs marketed in 2002[2] were classified as being activated by hydrolysis.[3] Since esterases are widely distributed throughout the body rendering the ester bond quite labile *in vivo*, the development of ester-based carrier prodrugs became a popular strategy to improve certain drug properties as e.g. oral bioavailability.[4] The choice of an appropriate pro-moiety, which influences the physicochemical profile as well as the pharmacokinetic and metabolic behavior should be carefully considered.[5]

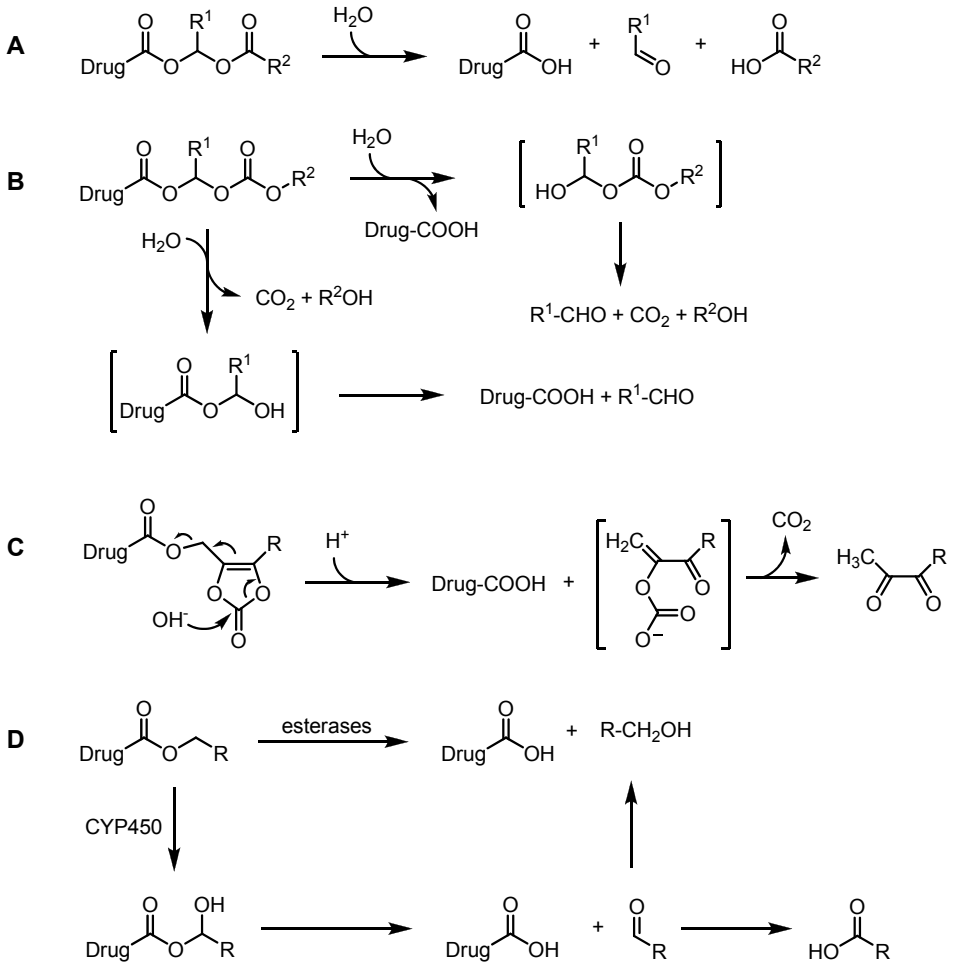

Scheme 3.1. Hydrolytic activation of prodrugs containing an (acyloxy)alkyl group (**A**), an [(alkoxycarbonyl)oxy]-alkyl group (**B**) or a (2-oxo-1,3-dioxol-4-yl)methyl ester pro-moiety (**C**).[5] **D**: Pathways for ester bond cleavage catalyzed by esterases or cytochrome P450 enzymes.[4]

Double esters, also referred to as cascade prodrugs, cyclic carbonates and simple esters are counted among well established ester-based pro-moieties that become hydrolyzed by different types of esterases or get activated by oxidation through cytochrome P450 enzymes (Scheme 3.1). An important property of a prodrug is the rate of biotransformation, commonly indicated by the half-life. The rate of biotransformation is influenced, e.g., by the stereochemistry of the prodrug or molecular properties such as steric bulk as well as interindividual variations and species differences.[4] Major enzymes involved in the bioconversion of ester-based prodrugs are carboxylesterases, cholinesterases as butyrylcholinesterase (BChE), paraoxonase and cytochrome P450 enzymes. In addition, acetylcholinesterase (AChE) was shown to take part in prodrug activation.[4] Carboxylesterase, AChE and BChE belong to the group of type B-esterases and are also referred to as serine esterases due to a conserved serine residue in their catalytic triad (Ser-Glu-His). They are known to be involved in the activation of a variety of prodrugs.[6-8] Carboxylesterases show extremely wide and overlapping substrate specificities, presumably due to a large and flexible binding pocket, and are virtually present throughout the body. Besides high activity in the liver, kidney and small intestine, they are also present in the skin.[4] In contrast to carboxylesterases, AChE has a much higher substrate-specificity with acetylcholine being its characteristic substrate, whereas BChE, besides preferential cleavage of butyrylcholine, also hydrolyzes a variety of other esters.[4] AChE and BChE are mainly localized in brain and plasma, but human skin[9] has also been shown to have cholinesterase activity.[4] Paraoxonase is a calcium-dependent type A-esterase known to catalyze the hydrolysis of a broad spectrum of compounds including aromatic esters, organophosphates, lactones and cyclic carbonate esters.[10] High paraoxonase activity is particularly found in plasma.[4] Although carboxylic acid esters are typically cleaved by esterases, oxidative hydrolysis by cytochrome P450 enzymes represents an alternative route of ester-based prodrug activation.[11]

Based on a model of ACE interacting with inhibitors such as captopril, optimization of binding energies by introduction of a 7,6-bicyclic ring system with *S,S*-configuration resulted in the discovery of the highly potent angiotensin-converting enzyme inhibitor (ACEi) cilazaprilat.[12] Cilazapril (Figure 3.1) is the monoethyl ester prodrug of the corresponding dicarboxylic acid cilazaprilat, designed for better oral bioavailability. After absorption it is hydrolyzed by esterases *in vivo* to yield the active principle cilazaprilat. In the following, compounds, which contain the partial structure of cilazapril and are additionally esterified at the heterocyclic carboxylic acid, are referred to as “cilazapril prodrugs” or “prodrugs of cilazapril”, although cilazaprilat of course is the active principle.

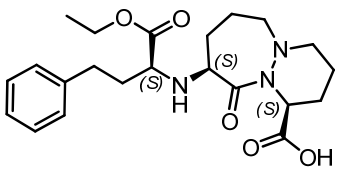

Figure 3.1. Structure of the ACEi cilazapril.

Flexible compounds like enalapril or moexipril have a more or less pronounced tendency to form a cyclic degradation product, a so-called diketopiperazine or piperazine-2,5-dione.[13] By increasing the rigidity of the ACEi the tendency to undergo an intramolecular ring-closure reaction becomes negligible.

Cilazapril causes an increase in plasma renin activity and a decrease in plasma angiotensin II and aldosterone concentrations resulting in long-term reduction of arterial blood pressure by dilatation of peripheral vessels and decreased vascular resistance.[14]

Candesartan (Figure 3.2) is a nonpeptide angiotensin II receptor antagonist (ARB) that selectively inhibits the binding of Ang II to the AT_1 receptor. At clinically relevant concentrations, candesartan behaves like an insurmountable antagonist at the AT_1R and produces a long-lasting blockade (*in vitro* and *in vivo*) of the vascular contractile effects of Ang II, resulting in an effective decrease of blood pressure.[15] It is administered orally as the double ester prodrug candesartan cilexetil (Figure 3.2), which is rapidly and completely hydrolyzed by carboxylesterases during absorption from the gastrointestinal tract to release the active principle.[16]

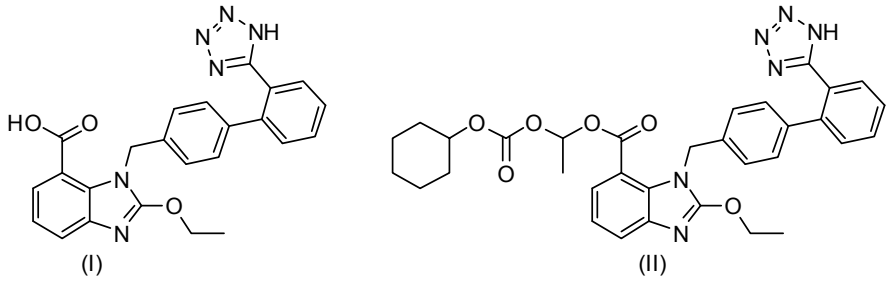

Figure 3.2. Structures of the ARBs candesartan (I) and candesartan cilexetil (II).

3.2 Selection of appropriate prodrug candidates

Due to inappropriate physicochemical properties candesartan and cilazapril are not suitable for transdermal application. However, it can be speculated that masking of acidic functional groups results in improved permeation. Based on this working hypothesis, the synthesis of different carrier prodrugs by esterification of the free carboxylic acid moiety in candesartan and cilazapril, respectively, was considered.

Ideally, these prodrugs should be pharmacologically inactive and sufficiently stable during synthesis, purification, formulation and in the TTS-matrix, whereas after transdermal absorption, i. e. under physiological conditions, a rapid and complete conversion to the active drug is desired. The liberated fragments of the carrier group must have at best no or tolerable toxicity and no unwanted pharmacology.[17] Furthermore, certain requirements in terms of lipophilicity and water solubility should be fulfilled.

By analogy of the structure of candesartan cilexetil the synthesis of appropriate prodrug candidates should focus on double ester prodrugs as 1-(alkoxycarbonyloxy)alkyl and 1-(acyloxy)alkyl esters, which represent well established and approved carrier-prodrug structures and can be found in various successfully marketed drugs, e.g. β-lactam antibiotics, nucleotide analogue reverse transcriptase inhibitors or in the ACE inhibitor fosinopril. Thereby, the introduction of a 1-ethyl bridge is preferred to a methylene-bridged double ester, as the latter generates toxic formaldehyde upon biotransformation and is chemically less stable. Likewise, pivalate-generating prodrugs appeared to be associated with some degree of toxicity, since pivalic acid influences carnitine homeostasis. Thus, carnitine levels of patients receiving chronic treatment should be clinically controlled.[18]

Inspired by the immunosuppressive drug mycophenolate mofetil, morpholinoethyl esters of candesartan and cilazapril were taken into consideration as water solubility can be increased by salt formation. Since double ester prodrugs such as 1-(acyloxy)ethyl and 1-(alkoxycarbonyloxy)ethyl esters are assumed to be hydrolyzed faster than simple esters due to the better accessibility of the site of hydrolysis, a combination of a basic substituent with a double ester moiety (1-((alkylamino)oxycarbonyloxy)ethyl, 1-(morpholinylalkyloxycarbonyloxy)ethyl or 1-(2-morpholinoacetoxy)ethyl), was considered.

By analogy with marketed prodrugs such as olmesartan medoxomil, azilsartan medoxomil or lenampicillin, a cyclic carbonate prodrug structure ((oxodioxolyl)methyl moiety) should be synthesized and the effect of a bulky substituent in C-5 position should be explored.

Recently, Majumdar and Sloan reported on *N*-alkyl-*N*-alkyloxycarbonylaminomethyl (NANAOCAM) and *N*-aryl-*N*-alkyloxycarbonylaminomethyl (NArNAOCAM) prodrugs of carboxylic acid containing drugs for topical delivery. These pro-moieties were found to be hydrolyzed chemically instead of enzymatically *via* an S_N1 type pathway. In contrast to NANAOCAM esters NArNAOCAM derivatives are reported to be reasonably stable.[19]

Therefore, a small set of NArNAOCAM prodrugs was included in the list of appropriate prodrug candidates.

The preparation of simple alkyl esters should be self-evident due to ease of synthesis. However, previous investigations of our working group on the hydrolysis of trandolapril ethyl ester revealed that the esterified heterocyclic carboxylic acid is too stable (unpublished results). Therefore, an ethyl ester of cilazapril was synthesized to corroborate this finding using another ACEi core structure.

Table 3.1 summarizes the respective prodrug candidates of cilazapril and candesartan.

Table 3.1. Prodrug candidates of cilazapril and candesartan.

prodrug moiety	R	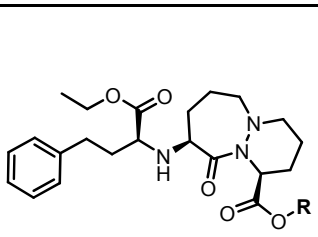	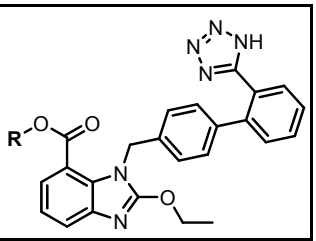
1-(alkoxycarbonyloxy)ethyl	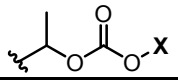	**X** = CH_2CH_3, Cy, ^{i}Pr	**X** = ^{i}Pr
1-(acyloxy)ethyl	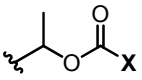	**X** = CH_3, ^{t}Bu	**X** = ^{t}Bu
(oxodioxolyl)methyl	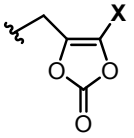	**X** = CH_3, ^{t}Bu	**X** = CH_3, ^{t}Bu
morpholinoalkyl		**X** = CH_2–N⟨O⟩	**X** = CH_2–N⟨O⟩
alkyl		**X** = CH_3	-
N-aryl-*N*-alkyloxy-carbonylaminomethyl	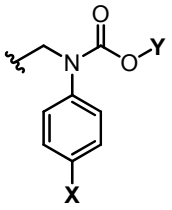	**X** = H, **Y** = CH_2CH_3 **X** = $COOCH_2CH_3$, **Y** = CH_2CH_3 **X** = $COOCH_2CH_3$, **Y** = CH_3	-
"basic double esters"	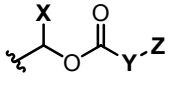	**X** = CH_3, **Y** = CH_2, **Z** = ⟨N⟩–O	**X** = CH_3, **Y** = O, **Z** = CH_2CH_2–N⟨O⟩ **X** = CH_3, **Y** = O, **Z** = CH_2CH_2–NEt_2

3.3 Chemistry

3.3.1 Cilazapril derivatives

Towards the synthesis of cilazapril ester prodrugs the free carboxylic acid moiety of cilazapril was coupled to various prodrug building blocks (cf. Table 3.1) by common esterification pathways. One should keep in mind that due to the conserved (*S*)-configuration of the existing three stereocenters in cilazapril the introduction of another stereocenter in the pro-moiety leads to the generation of two diastereomers, which can be separated by chromatography.

According to Scheme 3.2 the cilazapril 1-(alkyloxycarbonyloxy)ethyl esters **3.1**-**3.3** were synthesized by a substitution reaction of cilazapril with commercially available 1-(alkyloxycarbonyloxy)ethyl chlorides in DMF under basic conditions.

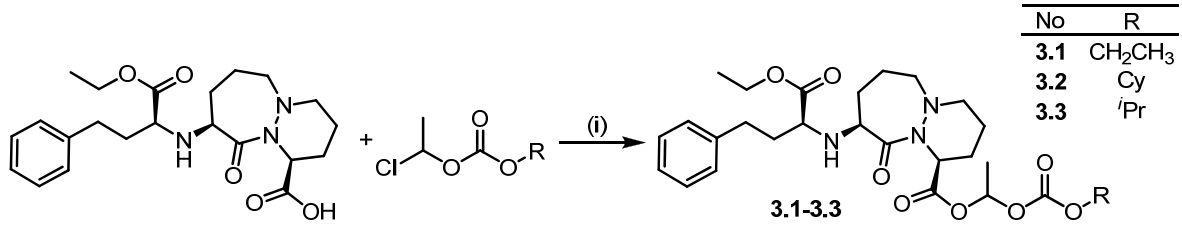

No	R
3.1	CH_2CH_3
3.2	Cy
3.3	^{i}Pr

Scheme 3.2. Synthesis of cilazapril 1-(alkyloxycarbonyloxy)ethyl esters **3.1-3.3**. Reagents and conditions: (i) $ClCHCH_3OCOOR$ (1.3 eq), K_2CO_3 (1.2 eq), DMF, 0 °C to rt, overnight.

The 1-chloroethyl alkanoate building blocks **3.4** and **3.5** were prepared by a solvent-free reaction of acetaldehyde with the pertinent acid chloride under lewis acid catalysis[20]. Subsequent coupling to cilazapril using the same conditions as employed for the synthesis of **3.1**-**3.3** yielded the cilazapril 1-(acyloxy)ethyl esters **3.6** and **3.7** (Scheme 3.3).

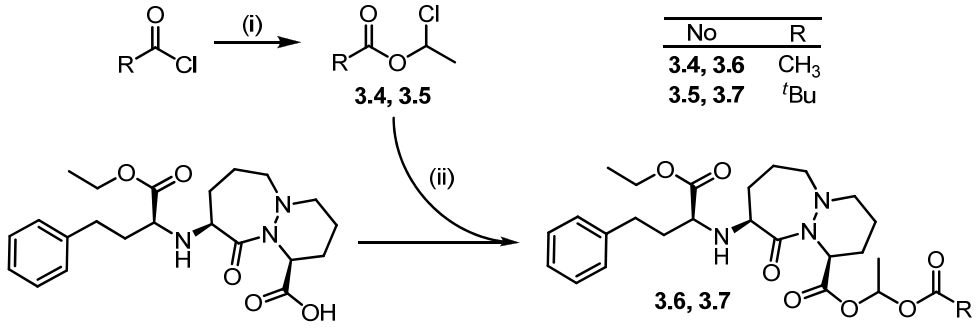

No	R
3.4, 3.6	CH_3
3.5, 3.7	^{t}Bu

Scheme 3.3. Synthesis of cilazapril 1-(acyloxy)ethyl esters **3.6** and **3.7**. Reagents and conditions: (i) acetaldehyde (1.04 eq), $ZnCl_2$, -20 °C to rt, 1-3 h; (ii) **3.4**, **3.5** (1.3 eq), K_2CO_3 (1.2 eq), DMF, 0 °C to rt, overnight.

Scheme 3.4 summarizes the synthesis of 4-*tert*-butyl-5-methyl-1,3-dioxol-2-one (**3.9**) using an umpolung strategy. The synthesis started from pivaldehyde which was converted to the corresponding thioacetal **3.8a** by reaction with propane-1,3-dithiol under solvent-free conditions using $LiBF_4$ as catalyst.[21] Treatment with n-BuLi in THF/abs led to 2-lithio-1,3-dithiane, which was immediately converted to **3.8b** by addition of

acetaldehyde.[22] The α-hydroxyketone **3.8** was obtained after hydrolysis of the thioacetal by treatment with mercury (II) salts in MeOH/H_2O.[22] Finally, 4-*tert*-butyl-5-methyl-1,3-dioxol-2-one **3.9** was obtained by cyclocarbonylation of **3.8** with triphosgene and DMAP as a base.[23]

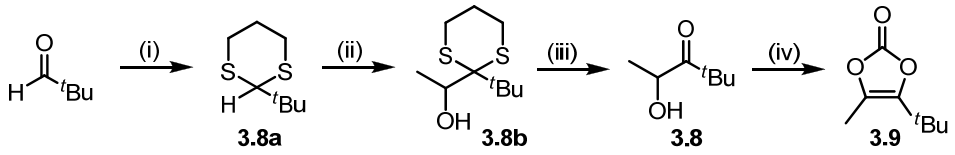

Scheme 3.4. Synthesis of 4-*tert*-butyl-5-methyl-1,3-dioxol-2-one **3.9**. Reagents and conditions: (i) 1,2-propanedithiol (1 eq), $LiBF_4$ (0.1 eq), rt, overnight; (ii) n-BuLi (1.05 eq), THF/abs, -25 °C, 5 h, acetaldehyde (1.5 eq), -78 °C to rt, overnight; (iii) $HgCl_2$ (2.5 eq), HgO (1.5 eq), MeOH/H_2O (9/1 v/v), reflux, 5 h; (iv) DMAP (1.5 eq), triphosgene (0.75 eq), DCM, rt, 2 h, 160 °C, 4 h.

Radical bromination of 4,5-dimethyl-1,3-dioxol-2-one and **3.9** in allylic position using *N*-bromosuccinimide gave the building blocks **3.10** and **3.11,** which were used for the esterification with cilazapril according to Scheme 3.5 to yield the cilazapril prodrugs **3.12** and **3.13**.

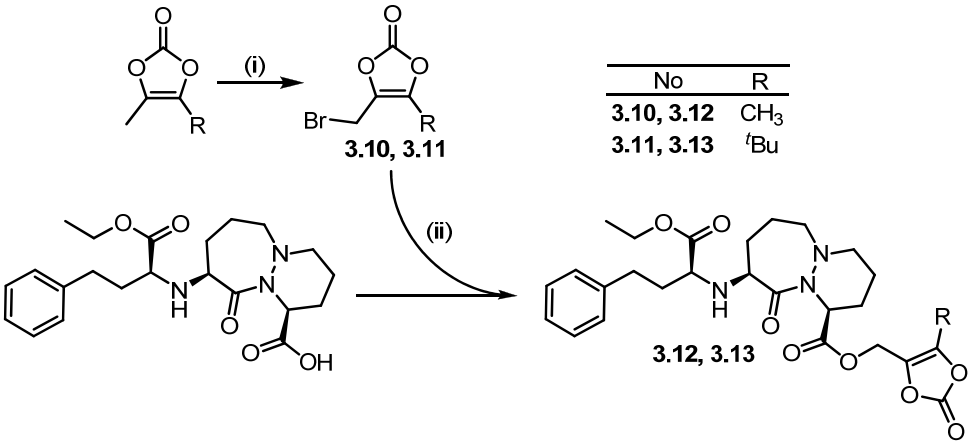

Scheme 3.5. Preparation of building blocks **3.10**, **3.11** and of cilazapril prodrugs **3.12**, **3.13**. Reagents and conditions: (i) NBS (1.1 eq), AIBN (0.05 eq), CCl_4, reflux, 1 h; (ii) **3.10** or **3.11** (1.4 eq), K_2CO_3 (1.5 eq), DMF, 0 °C to rt, overnight.

The morpholinoethyl ester of cilazapril (**3.14**) was prepared by Steglich esterifiaction of cilazapril with 4-(2-hydroxyethyl)morpholine in the presence of DCC as a coupling reagent and DMAP as an acylation catalyst (Scheme 3.6).

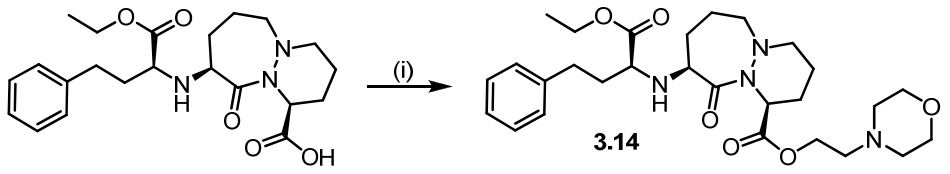

Scheme 3.6. Synthesis of **3.14**. Reagents and conditions: (i) 4-(2-hydroxyethyl)morpholine (1 eq), DCC (1.1 eq), DMAP, DCM/abs, 0 °C – rt overnight.

Scheme 3.7 depicts the synthesis of a basic double ester prodrug of cilazapril (**3.18**). Starting from 1-chloroethyl chloroformate, **3.15** was prepared by a reaction with chlorosulfuric acid and was subsequently used to introduce a 1-chloroethyl-carboxylate moiety by reaction with cilazapril leading to the cilazapril derivate **3.16**.[24] The desired 1-(2-morpholinoacetoxy)ethyl ester **3.18** was finally obtained by a nucleophilic substitution reaction of **3.16** with 2-morpholinoacetic acid **3.17**[25], which was synthesized according to Scheme 3.7 from *tert*-butyl bromoacetate and morpholine followed by acidic cleavage of the *tert*-butyl ester.

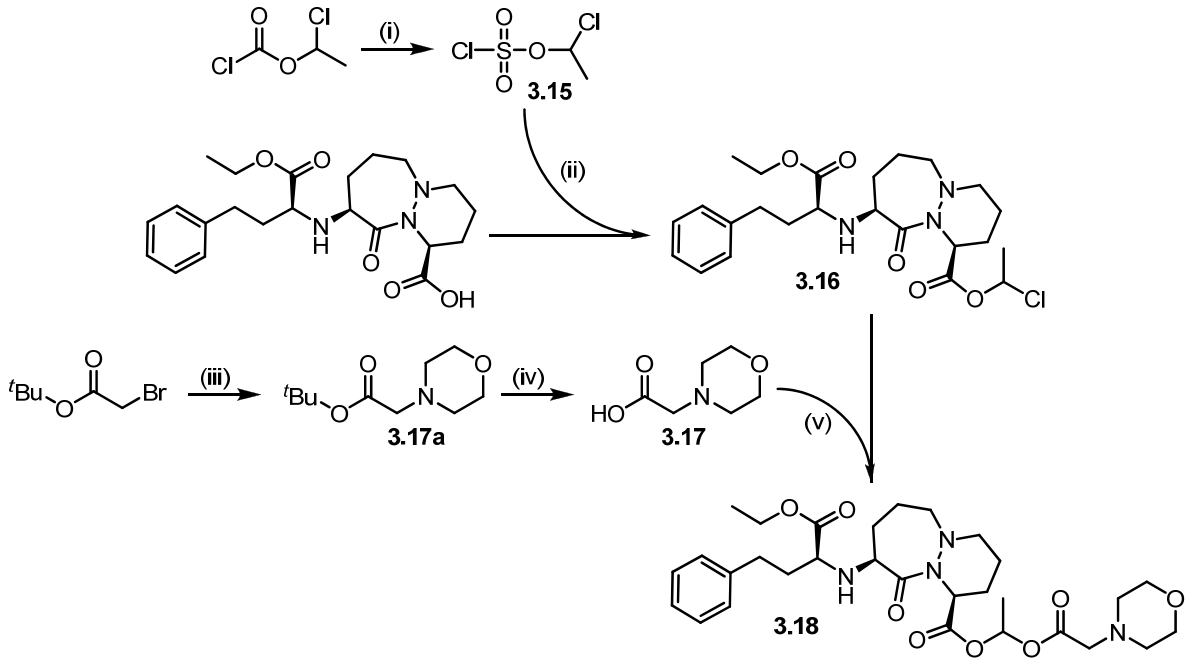

Scheme 3.7. Synthesis of **3.18**. Reagents and conditions: (i) $ClSO_3H$ (1.08 eq), 0 °C, 4 h; (ii) **3.15** (2 eq), $NaHCO_3$ (3.9 eq), $(n\text{-}Bu)_4N(HSO_4)$ (0.1 eq), DCM/H_2O (1/1 v/v), reflux, 4 h, rt overnight; (iii) morpholine (1 eq), NEt_3 (1eq), THF, 0 °C - reflux, 2 h; (iv) TFA (1.6 eq), DCM, 0 °C – rt, overnight; (v) **3.17** (2 eq), $CsCO_3$ (4 eq), DMF, 40 °C, 7 h, rt overnight.

The preparation of *N*-aryl-*N*-alkyloxycarbonylaminomethyl derivatives of cilazapril (**3.25**-**3.27**) is shown in Scheme 3.8. In the first step *N*-arylcarbamic acid alkyl esters (**3.19**-**3.21**) were made by acylation of an aromatic amine with an alkyl chloroformate.[26] Subsequently, **3.19**-**3.21** were chloromethylated with paraformaldehyde and trimethylsilyl chloride yielding the pertinent *N*-aryl-*N*-alkyloxycarbonylaminomethyl chloride building blocks **3.22**-**3.24**.[26-27] Esterification of cilazapril with **3.22**-**3.24** under the afore-mentioned conditions (cf. synthesis of **3.1**-**3.3**) led to the desired derivatives **3.25**-**3.27**.

The synthesis of a simple ethyl ester of cilazapril (**3.28**, Scheme 3.9) was achieved by a common esterification pathway with trimethylsilyl chloride and EtOH/abs serving as both reagent and solvent.

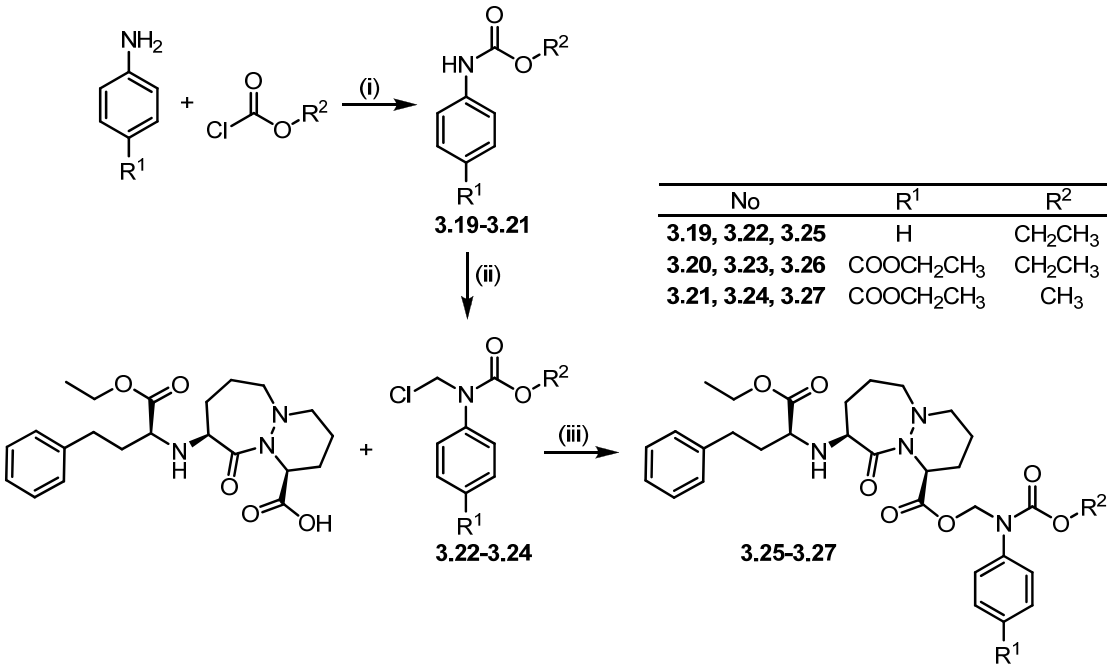

No	R^1	R^2
3.19, 3.22, 3.25	H	CH_2CH_3
3.20, 3.23, 3.26	$COOCH_2CH_3$	CH_2CH_3
3.21, 3.24, 3.27	$COOCH_2CH_3$	CH_3

Scheme 3.8. Preparation of **3.25-3.27**. Reagents and conditions: (i) NH_2PhR^1 (1 eq), $ClCOOR^2$ (1 eq), NEt_3 (1 eq), DCM, 0 °C to rt overnight; (ii) **3.22**: paraformaldehyde (1.7 eq), TMSCl (13 eq), DCM, reflux, 2.5 h; **3.23**, **3.24**: paraformaldehyde (1.1-1.7 eq), TMSCl (5-10 eq), 10 g anhydr. $MgSO_4$, toluol, rt, 2.5 d; (iii) **3.25**-**3.27** (1.5-1.8 eq), K_2CO_3 (1.8 eq), DMF, 0 °C to rt, overnight.

The active principle of cilazapril, cilazaprilat (**3.29**), was prepared to be used as a standard for LC analysis. For this purpose, the ethyl ester moiety in cilazapril was cleaved by treatment with LiOH in methanol (Scheme 3.9).

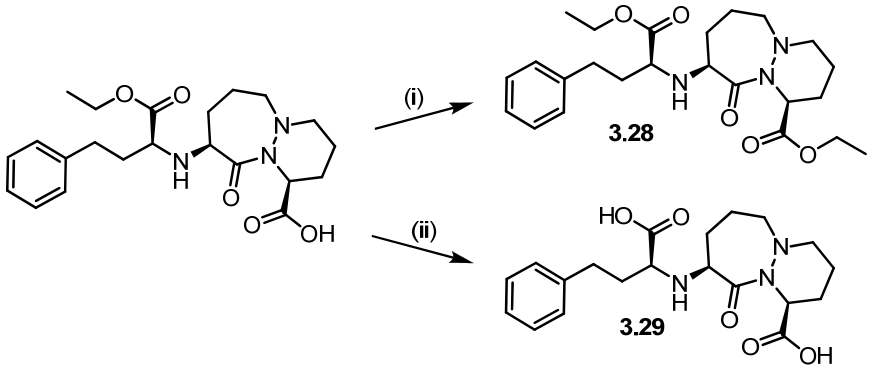

Scheme 3.9. Synthesis of cilazapril derivatives **3.28** and **3.29**. Reagents and conditions: (i) TMSCl (2.2 eq), EtOH/abs, reflux, 4 h; (ii) LiOH (3 eq), MeOH, rt, 6 d.

3.3.2 Candesartan derivatives

The synthesis of the desired candesartan derivatives was achieved by common esterification pathways. In contrast to cilazapril, the introduction of a chiral pro-moiety gives two enantiomers, which cannot be resolved under achiral chromatographic conditions.

Scheme 3.10 summarizes the synthesis of 1-(alkyloxycarbonyloxy)ethyl, 1-(acyloxy)ethyl and (5-alkyl-2-oxo-1,3-dioxol-4-yl)methyl esters of candesartan (**3.31**-**3.34**). In order to avoid side reactions, the acidic tetrazole moiety of candesartan was masked by a reaction with trityl chloride to give the trityl protected intermediate **3.30**. Esterification of **3.30** with the pro-moieties 1-(isopropyloxycarbonyloxy)ethyl chloride, **3.05**, **3.13** and **3.14** under basic conditions in DMF yielded the trityl protected compounds **3.31a**-**3.34a**, which were subsequently deprotected by treatment with aqueous hydrochloric acid in MeOH/THF to yield the candesartan prodrugs **3.31**-**3.34**.

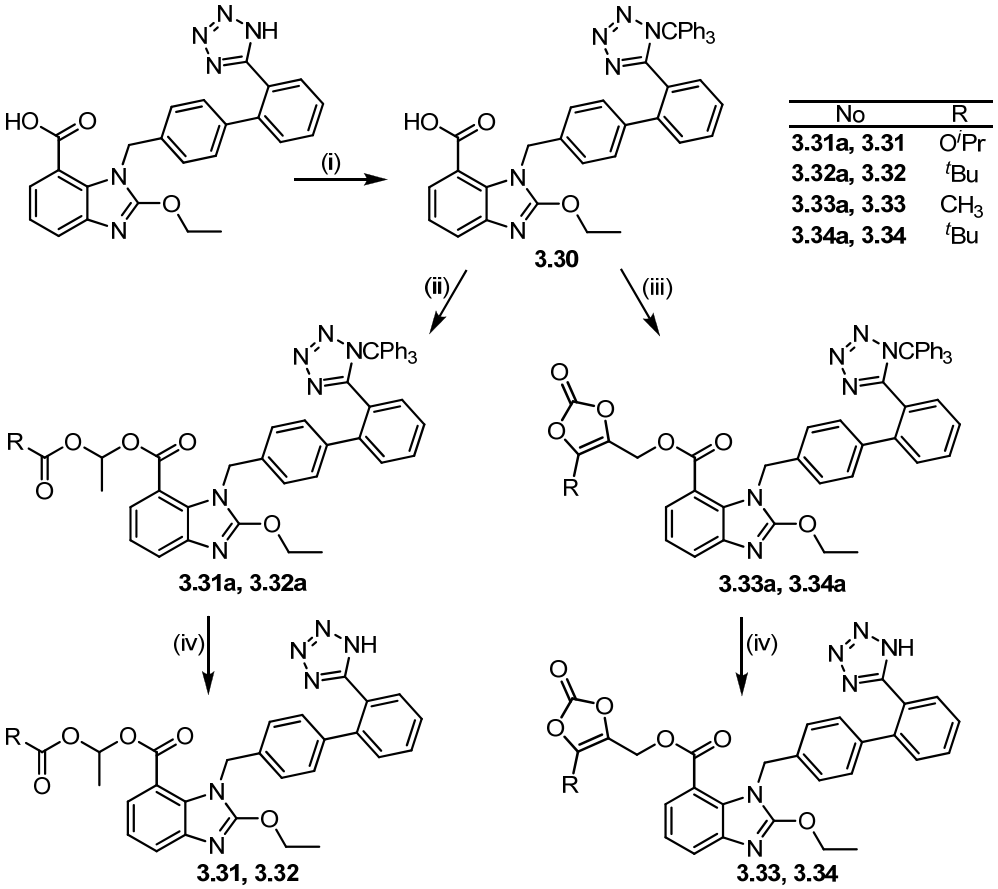

No	R
3.31a, 3.31	O^{i}Pr
3.32a, 3.32	^{t}Bu
3.33a, 3.33	CH_3
3.34a, 3.34	^{t}Bu

Scheme 3.10. Synthesis of candesartan prodrugs **3.31-3.34**. Reagents and conditions: (i) $ClCPh_3$ (1.2 eq), NEt_3 (1.2 eq), DCM, rt, 1 h; (ii) $ClCHCH_3OCOO^{i}Pr$, **3.5** (1.5 eq), K_2CO_3 (1.5 eq), DMF, 0 °C to rt, overnight; (iii) **3.10**, **3.11** (1.5 eq), K_2CO_3 (1.5 eq), DMF, 0 °C to rt, overnight; (iv) aq. HCl, MeOH/THF, rt, 2-5 h.

The synthesis of candesartan morpholinoethyl ester (**3.35**) was performed by a Steglich esterification with DCC and DMAP (Scheme 3.11).

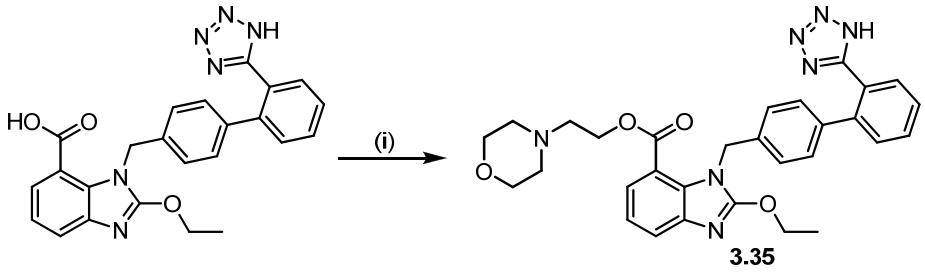

Scheme 3.11. Synthesis of candesartan morpholinoethyl ester **3.35**. Reagents and conditions: (i) 4-(2-hydroxyethyl)morpholine (1 eq), DCC (1.1 eq), DMAP, DMF, 0 °C to rt, overnight.

In the following, various attempts to synthesize basic double esters (1-((alkylamino)oxycarbonyloxy)ethyl and 1-(morpholinylalkyloxycarbonyloxy)ethyl ester) of candesartan are described. Firstly, a 1-chloroethyl 2-morpholinoethyl carbonate (**3.36**) and a 1-chloroethyl 2-(diethylamino)ethyl carbonate (**3.37**) were synthesized according to Scheme 3.12.

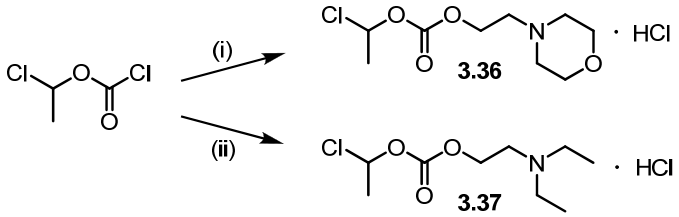

Scheme 3.12. Synthesis of basic double ester building blocks **3.36** and **3.37**. Reagents and conditions: (i) 4-(2-hydroxyethyl)morpholine (1 eq), DCM/abs, 0 °C to rt, 2.5 h; (ii) 2-(diethylamino)ethanol (1 eq), DCM/abs, 0 °C to rt, 2.5 h.

Compounds **3.36** and **3.37** were only stable as hydrochlorides and decomposed when the nitrogen was deprotonated. Therefore, the nucleophilic substitution of **3.36** and **3.37** with tritylated candesartan (**3.31**) under basic conditions was not successful (Scheme 3.13).

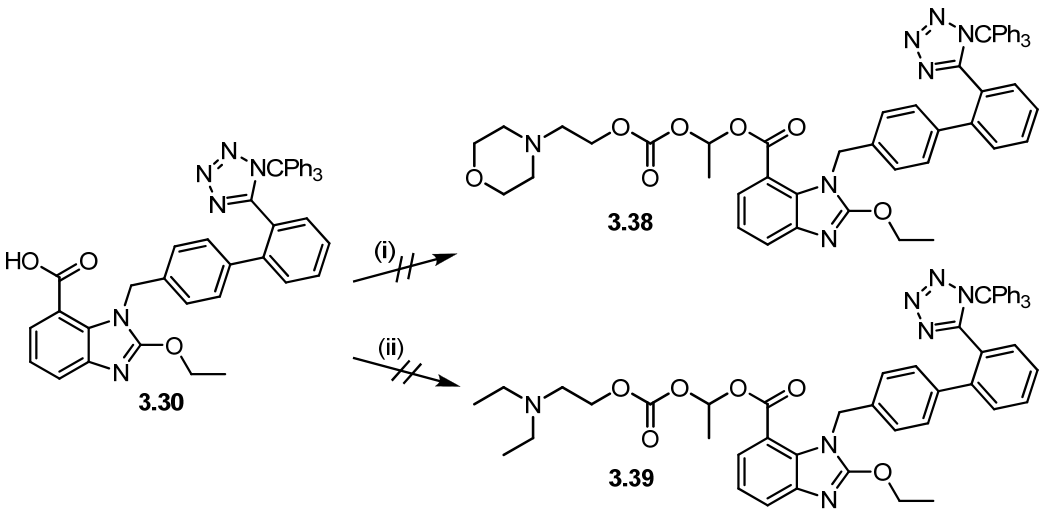

Scheme 3.13. Unsuccessful synthesis of basic double esters of candesartan. Reagents and conditions: (i) **3.36** (1 eq), K_2CO_3 (1.2 eq), DMF, 0 °C to rt, overnight; (ii) **3.37** (1.5 eq), K_2CO_3 (2.5 eq), DMF, 0 - 60 °C, 1.5 h.

Similarly, the reaction with the carboxylate of candesartan, prepared by deprotonation with NaH, and an excess of 1-chloroethyl 2-(diethylamino)ethyl carbonate (**3.37**) according to Scheme 3.14 did not give the desired product **3.39**. However, by ESI-mass spectrometry of the crude product, instead of the basic double ester (**3.39**, *m/z* 869), a pseudomolecular ion [M+H$^+$] at *m/z* 783 was detected. This corresponds to compound **3.40** which might have been formed by a conversion of the starting material involving elimination of CO_2 (Scheme 3.14).

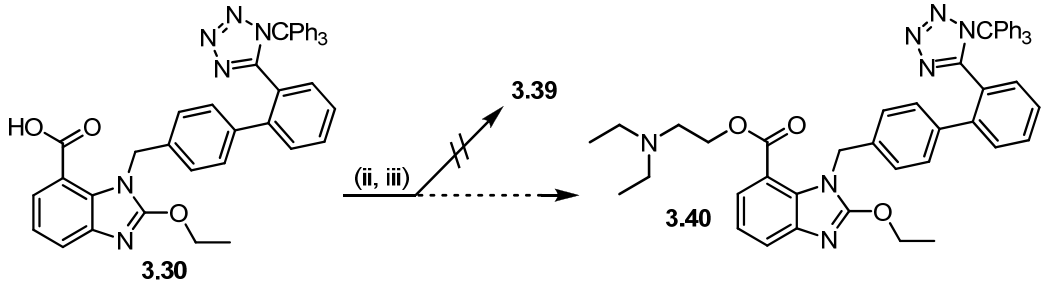

Scheme 3.14. Unsuccessful synthesis of **3.39** and suggested structure (**3.40**) of the product analyzed by mass spectrometry. Reagents and conditions: (i) NaH (1.2 eq), DMF, rt; (iii) **3.37** (1.5 eq), 50 °C, 1 h.

In contrast to synthesis of the 1-(2-morpholinoacetoxy)ethyl ester of cilazapril (**3.18**) basic double esters of candesartan, such as 1-((alkylamino)oxycarbonyloxy)ethyl or 1-(morpholinylalkyloxycarbonyloxy)ethyl esters, were not synthetically accessible in an analogous manner. Due to the above mentioned stability problems this approach was not pursued.

3.4 Physicochemical properties of cilazapril and candesartan prodrugs

To overcome the main barrier of the skin, the stratum corneum, transdermal drugs delivered by passive diffusion must have appropriate physicochemical properties. The stratum corneum can be compared to a “brick and mortar” structure, where the “bricks” are composed of keratin-rich corneocytes, whereas multiple lipid bilayers of ceramides, fatty acids, cholesterol and cholesterol ester comprise the “mortar”. According to this model proposed by Barry[28] the intercellular space is not considered as a simple lipid barrier. The idea is that the “mortar” is rather composed of stacks of intercellular lipid bilayers with an aqueous phase in between (cf. Figure 3.3). Thus, for effective penetration of a compound across the stratum corneum, an optimized balance of lipid and water solubility is a prerequisite.[29] Besides lipophilicity and solubility molecular size, melting point as well as hydrogen bonding are known to affect permeation.[30] Previous studies revealed a characteristic parabolic relationship between skin permeability and lipophilicity of various drugs with maximum permeability at a log *P* of approximately 3-4.[31-32] Recently, Choy and Prausnitz concluded from the investigation of 17 FDA-approved drugs for transdermal delivery that a modified and more stringent version of Lipinski’s Rule of Five (0 ≤ log *P* ≥ 5, molecular weight ≤ 335 Da, no. of H-bond donors ≤ 2, no. of H-bond acceptors ≤ 5) should be applied to transdermal drugs.[33]

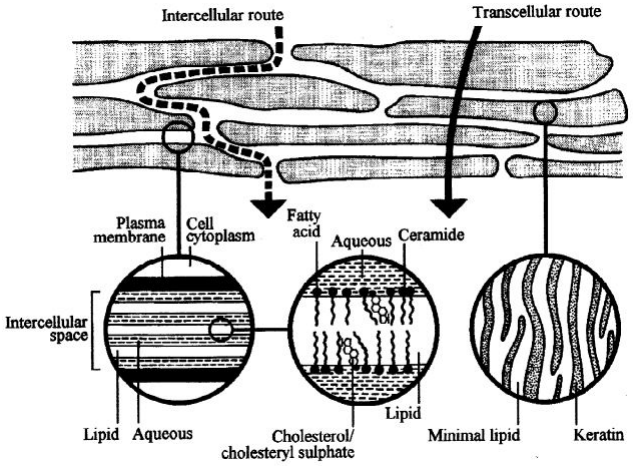

Figure 3.3. Simplified diagram depicting the structure of the stratum corneum and two routes for drug penetration. Reprinted from Barry[28] with permission from Elsevier.

In the following, predicted and experimentally determined physicochemical properties of the synthesized cilazapril and candesartan prodrugs as well as of the active principles cilazaprilat and candesartan will be discussed.

In Table 3.2 physicochemical properties of cilazapril, cilazapril produgs and cilazaprilat are summarized. The molecular weights of all synthesized cilazapril prodrugs lay between approximately 446 and 667 Da. Thus, the modified Rule of Five of Choy and Prausnitz is not fulfilled in terms of molecular weight cut off. However, the molecular weight of the active principle cilazaprilat (~ 389 Da) is considerably lower.

Table 3.2. Physicochemical properties of cilazapril, cilazapril prodrugs and cilazaprilat. The colored pK_a values refer to the correspondingly colored (de-)protonizable moieties of the cilazapril core structure or the pro-moiety.

compound	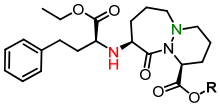 R	molecular weight Da	log *P* calc.[a]	log P_{oct/H_2O} exp.[b]	log $D^{5.5}$ calc.[c]	pK_a calc.[d]	pK_a exp.[e]
cilazapril	H	417.50	2.21 ± 0.56	0.22 ± 0.03	-0.08	5.55 3.88 2.28	6.33 ± 0.01 3.45 ± 0.02
3.1	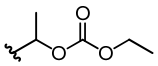	533.61	3.10 ± 0.62	-0.38 ± 0.03	2.94	5.24 2.03	3.28 ± 0.07
3.2	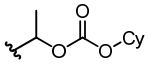	587.70	4.57 ± 0.62	2.70 ± 0.07	4.40	5.24 2.03	4.28 ± 0.06
3.3	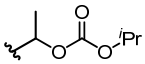	547.64	3.46 ± 0.62	n.d.	3.29	5.24 2.03	n.d.
3.6	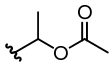	503.59	2.54 ± 0.63	n.d.	2.37	5.24 2.06	n.d.
3.7	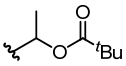	545.67	3.81 ± 0.63	n.d.	3.65	5.24 2.04	n.d.
3.12	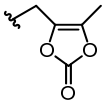	529.58	2.03 ± 0.58	n.d.	1.86	5.26 2.16	n.d.
3.13	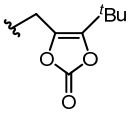	571.66	3.31 ± 0.58	n.d.	3.13	5.26 2.16	n.d.
3.14	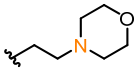	530.66	1.94 ± 0.61	1.07 ± 0.02	1.18	5.94 5.25 2.10	5.49 ± 0.07 4.51 ± 0.05
3.18	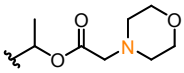	588.69	1.89 ± 0.66	n.d.	1.68	5.24 4.49 2.02	n.d.
3.25	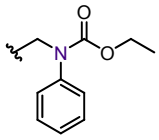	594.70	3.47 ± 0.82	n.d.	3.30	5.25 2.12 -0.37	n.d.
3.26	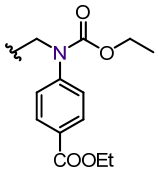	666.76	4.17 ± 0.83	n.d.	4.00	5.25 2.12 -2.92	n.d.
3.27	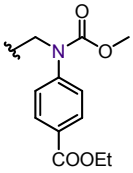	652.73	3.66 ± 0.83	n.d.	3.49	5.25 2.12 -2.94	n.d.
3.28	CH_2CH_3	445.56	2.98 ± 0.56	n.d.	2.81	5.28 2.30	n.d.
cilazaprilat (3.29)	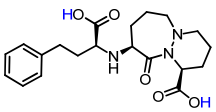	389.45	2.68 ± 0.58	n.d.	-0.72	8.62 3.96 2.52 2.13	n.d.

[a] log *P* values calculated by ACD/PhysChem Suite 12.00 (Advanced Chemistry Development Inc., Toronto, Canada), [b] octanol/water partition coefficient - experimentally determined by potentiometric titration[34], performed by Across Barriers GmbH (Saarbrücken, Germany) and provided by HEXAL AG, [c] calculated log *D* values at pH 5.5 by ACD/PhysChem Suite 12.00, [d] pK_a values calculated with ACD/PhysChem Suite 12.00, [e] pK_a values, experimentally determined by potentiometric titration[35], performed by Across Barriers GmbH and provided by HEXAL AG.

All calculated log *P* values are below 5, namely between 1.89 (**3.18**) and 4.57 (**3.2**), ranking the prodrugs as well as cilazapril and cilazaprilat moderately lipophilic. Given that the log *P* value fails to take into account variations of the lipophilicity with respect to the ionic state of a drug at a given pH, it is more reasonable to use the distribution coefficient log *D*, which refers to a pH-dependent mixture of all charged and uncharged species present at that pH.[36-37] For permeation through the stratum corneum calculation of the log *D* at skin pH (log $D^{5.5}$) is most interesting. At pH 5.5 the mono- and dicarboxylic acids cilazapril and cilazaprilat are fully deprotonated resulting in a difference between calculated log $D^{5.5}$ and log *P* values in the range of two to three log units. Regarding the prodrugs, lowest log $D^{5.5}$ values are calculated for compounds **3.14** and **3.18** due to their ionizable morpholine moiety. In the case of cilazapril, **3.2** and **3.14** the experimentally determined octanol/water partition coefficients and the calculated values are comparable by trend. Regarding the experimentally determined log P_{oct/H_2O} values, cilazapril is found to be the least lipophilic compound followed by **3.14**, whereas **3.2** is the most lipophilic one due to the very unpolar cyclohexyl residue. The log P_{oct/H_2O} of **3.1** appears to be remarkably low. For accurate determination of log P_{oct/H_2O} using the potentiometric method the substance should have high purity, sufficient solubility as well as stability in the titration media (report discussion, Across Barriers GmbH). As the 1-(ethoxycarbonyloxy)ethyl prodrug moiety of **3.1** is known to be prone to hydrolysis in aqueous media, the determined log P_{oct/H_2O} may have been affected by the presence of a defined amount of cilazapril, resulting in a lower log P_{oct/H_2O} value. In summary, the synthesized cilazapril prodrugs seem to be suitable in terms of lipophilicity for adequate transdermal permeation. In particular, prodrugs **3.14** and **3.18** appear to be promising candidates due to their ionizable morpholine moiety providing balanced lipophilicity and water solubility.
Dissociation constants were determined by means of potentiometric titration using methanol as a co-solvent. For cilazapril two pK_a values were obtained referring to the secondary amine and the carboxylic acid (6.33 and 3.45, respectively). For **3.1** and **3.2** the pK_a values of the secondary amine amounted to 3.28 and 4.28, respectively. Prodrug **3.14** showed an additional pK_a referring to the morpholine group (5.49). The experimental data are roughly in agreement with the calculated values.

Table 3.3 summarizes the calculated and experimentally determined physicochemical properties of candesartan and candesartan prodrugs. Comparable to the cilazapril prodrugs the molecular weights of all candesartan prodrugs range from approx. 553 Da to 611 Da. Likewise the active principle candesartan (440.45 Da) does not fulfill the modified Rule of Five molecular weight criterion of Choy and Prausnitz.
The calculated partition coefficients indicate a high lipophilicity of candesartan and all candesartan prodrugs. Due to the ionizable groups (tetrazole, benzimidazole, carboxylic acid, morpholine) the calculated log $D^{5.5}$ values are markedly lower. Candesartan and the morpholinoethyl ester prodrug (**3.35**) show the lowest distribution coefficients with log $D^{5.5}$ values of 1.41 and 2.17, respectively. Strikingly, the experimentally determined

log P_{oct/H_2O} values turned out to be two to four log-units lower than the calculated ones, ranging from approx. 2.4 – 3.6. Compared to log P_{oct/H_2O} exp. values of the cilazapril prodrugs the candesartan prodrugs show a higher lipophilicity, but may be well suited for adequate skin permeation.

Two dissociation constants were obtained by means of potentiometric titration for the candesartan prodrugs **3.31**, **3.32** and **3.33** referring to the benzimidazole and the tetrazole group. An additional pK_a value was determined for **3.35** referring to the morpholine residue. All experimentally determined pK_a values are in good correlation with the calculated ones.

Table 3.3. Physicochemical properties of candesartan and candesartan prodrugs. The colored pK_a values refer to the correspondingly colored (de-)protonizable moieties of the cilazapril core structure or the pro-moiety.

compound	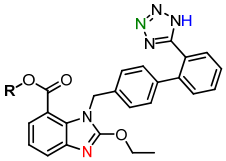 R	molecular weight Da	log *P* calc.[a]	log P_{oct/H_2O} exp.[b]	log $D^{5.5}$ calc.[c]	pK_a calc.[d]	pK_a exp.[e]
candesartan	H	440.45	4.65 ± 0.84	2.80	1.41	5.60 4.15 2.06 0.60	n.d.
3.31	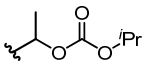	570.60	6.10 ± 0.90	3.34 ± 0.07	4.83	4.16 3.95 0.60	4.65 ± 0.01 4.21 ± 0.06
3.32	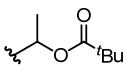	568.62	6.75 ± 0.91	3.56 ± 0.06	5.47	4.16 3.95 0.60	4.60 4.50
3.33	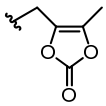	552.54	4.67 ± 0.85	2.41 ± 0.16	3.39	4.16 4.08 0.60	4.49 ± 0.02 3.51 ± 0.06
3.34	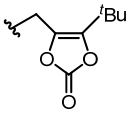	594.62	5.94 ± 0.86	n.d.	4.67	4.16 4.08 0.60	n.d.
3.35	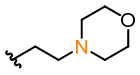	553.61	3.92 ± 0.90	3.45 ± 0.28	2.17	5.89 4.16 4.02 0.60	6.52 6.44 4.86
candesartan cilexetil	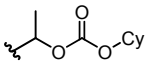	610.66	7.21 ± 0.90	3.10	5.94	4.16 3.94 0.60	n.d.

[a] log *P* values calculated by ACD/PhysChem Suite 12.00 (Advanced Chemistry Development Inc., Toronto, Canada), [b] octanol/water partition coefficient - experimentally determined by potentiometric titration[34], performed by Across Barriers GmbH (Saarbrücken, Germany) and provided by HEXAL AG, [c] calculated log *D* values at pH 5.5 by ACD/PhysChem Suite 12.00, [d] pK_a values calculated with ACD/PhysChem Suite 12.00, [e] pK_a values, experimentally determined by potentiometric titration[35], performed by Across Barriers GmbH and provided by HEXAL AG.

3.5 Bioanalytical studies of candesartan and cilazapril prodrugs

The stability of a drug is a crucial aspect in drug development. It is indispensible to investigate the influence of various storage conditions as well as the stability of the drug in the respective formulation. With respect to prodrugs designed for transdermal application stability as high as possible in the solid state as well as in the TTS-matrix is desired. Furthermore, after release and transdermal absorption the prodrug should be rapidly converted to the active principle. Ester pro-moieties are usually cleaved enzymatically, but spontaneous non-enzymatic ("chemical") hydrolysis should also be taken into consideration. Hence, the stability of the synthesized candesartan and cilazapril prodrug candidates in aqueous buffer solution as well as in the presence of various enzymes was analyzed by means of high performance liquid chromatography (HPLC) in a time-dependent manner. Furthermore, the half-life of hydrolysis ($t_{1/2}$) was determined and products of hydrolysis or degradation were identified by liquid chromatography coupled to tandem mass spectrometry (LC-MS). For the investigation of spontaneous "chemical" hydrolysis sodium phosphate buffer was used; enzymatic hydrolysis was studied by incubation of the compounds with porcine liver esterase, human CPD plasma and porcine skin homogenate, respectively. Moreover, the metabolic stability of the substances in the presence of cultured primary human hepatocytes (PHH) was investigated.

Generally, the half-life ($t_{1/2}$) of enzymatic hydrolysis is determined under substrate saturation conditions, assuming pseudo first-order kinetics. Under these conditions $t_{1/2}$ is independent from the substrate concentration but still influenced by other factors such as the composition of the incubation medium and temperature. For spontaneous hydrolysis in buffer, the assumption of pseudo first-order kinetics is also valid, as the reactant water is present at high excess (approx. 55 M) and its concentration remains almost unchanged. In these simplified cases $t_{1/2}$ can be determined according to Equation 3.1. The slope k can be calculated by linear regression analysis of the half-logarithmic plot of the percental peak area of residual prodrug (determined by HPLC) versus incubation time.

$$t_{1/2} = \frac{\ln(2)}{k}$$

Equation 3.1. Relationship between rate constant k and half-life $t_{1/2}$ of hydrolysis.

In cases where more than one step is involved in the formation of the active principle (AP), $f_{50\%}$ values proved to be more useful and informative than the half-life $t_{1/2}$. The $f_{50\%}$ value represents the time at which 50 % of the drug (AP) have been formed.[38] According to Equation 3.1, $f_{50\%}$ values were determined from the slopes (k) of linear plots of the logarithm of the amount of active principle to be formed (AP_x, calculated according to Equation 3.2) against incubation time.[39]

$$\ln(AP_x) = \ln\,(100 - AP_{t_i})$$

Equation 3.2. Calculation of $\ln(AP_x)$. AP_{t_i} = percentage of active principle after a distinct incubation period.

3.5.1 Solid state stability of candesartan and cilazapril prodrugs

3.5.1.1 Solid state stability of candesartan prodrugs

To investigate the stability of the candesartan prodrugs in solid state, the compounds were stored under defined conditions at different temperature and humidity (rel. h). After a certain period of time the compounds were analyzed by HPLC. The percentage of residual prodrug and degradation products like candesartan or unknown decomposition products were determined from the respective peak areas using the 100 % method.

Table 3.4 summarizes the solid state stability data of candesartan cilexetil, **3.31**, **3.32** and **3.35**. Over a storage period of ten months the double ester prodrugs **3.31** and **3.32** turned out to be sufficiently stable at 5 °C/65 % rel. h. as well as at 25 °C/60 % rel. h. Only small amounts of unidentified degradation products were detected. Under accelerated storage conditions (40 °C/75 % rel. h.) **3.31** remained relatively stable, whereas **3.32** was considerably decomposed, indicated by an increase in decomposition products of unknown structure to 17 %. By contrast, candesartan cilexetil and the morpholinoethyl ester **3.35** showed excellent stability under all storage conditions applied.

Table 3.4. Stability[a] of candesartan prodrugs stored at different temperature and humidity.

No.	t_0	prodrug (%)			candesartan (%)			decomposition products (%)		
	(%)[b]	5 °C/ 65 % rel. h.	25 °C/ 60 % rel. h.	40 °C/ 75 % rel. h.	5 °C/ 65 % rel. h.	25 °C/ 60 % rel. h.	40 °C/ 75 % rel. h.	5 °C/ 65 % rel. h.	25 °C/ 60 % rel. h.	40 °C/ 75 % rel. h.
CAN-CIL[c, d]	100	n.d.	100	100	n.d.	0	0	n.d.	0	0
3.31	100	99	99	98	0	0	0	1	1	2
3.32	100	99	98	83	0	0	0	1	2	17
3.35	100	100	100	100	0	0	0	0	0	0

[a] 6 months stability (**CAN-CIL**), 10 month stability (**3.31**, **3.32**, **3.35**), [b] percentage of compound at the beginning of storage. [c] CAN-CIL = candesartan cilexetil, [D] data provided by HEXAL AG.

In Table 3.5 the results for the analysis of prodrug **3.33** after storage for six and 16 months, respectively, are summarized. The (oxodioxolyl)methyl moiety seems to be highly prone to degradation processes at high temperature or humidity. Storage under accelerated storage conditions resulted in a complete degradation of the compound after 16 months and even at low temperature (5 °C/65 % rel. h.) the compound showed poor stability.

Table 3.5. HPLC analysis of compound **3.33** after storage of 6 and 16 months, respectively at different temperature and humidity.

No.	t_0 (%)[a]	prodrug (%)			candesartan (%)			decomposition products (%)		
		6 months/16 months			6 months/16 months			6 months/16 months		
		5 °C/ 65 % rel. h.	25 °C/ 60 % rel. h.	40 °C/ 75 % rel. h.	5 °C/ 65 % rel. h.	25 °C/ 60 % rel. h.	40 °C/ 75 % rel. h.	5 °C/ 65 % rel. h.	25 °C/ 60 % rel. h.	40 °C/ 75 % rel. h.
3.33	86	77 / 73	63 / 41	39 / 0	0 / 0	1 / 1	10 / 37	23 / 27	36 / 58	51 / 63

[a] percentage of compound existing at the beginning of storage.

3.5.1.2 Solid state stability of cilazapril prodrugs

The solid state stability of a selection of cilazapril prodrugs was determined according to the procedure described in chapter 3.5.1.1. Table 3.6 to Table 3.8 summarize the resulting stability data at 5 °C/65 % rel. h., 25 °C/60 % rel. h. and 40 °C/75 % rel. h., respectively. Beside cilazapril and cilazaprilat a corresponding degradation product of each prodrug was detected resulting from the loss of the ethyl ester of the homophenylalanine substructure, while the introduced pro-moiety remains intact (cf. Scheme 3.15).

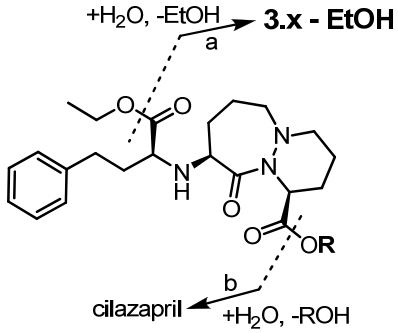

No	R
3.1	$CHCH_3OCOOEt$
3.2	$CHCH_3OCOOCy$
3.3	$CHCH_3OCOO^iPr$
3.6	$CHCH_3OCOCH_3$
3.7	$CHCH_3OCO^tBu$
3.14	CH_2CH_2mo
3.28	CH_2CH_3

Scheme 3.15. Possible pathways for the hydrolysis of cilazapril prodrugs. Pathway a refers to the loss of the ethyl ester of the homophenylalanine substructure resulting in the formation of the corresponding degredation prodrugs "3.x – EtOH". Pathway b describes the loss of the pro-moiety, which leads to the formation of cilazapril. Cilazaprilat results from the cleavage of both ester groups (a + b).

At 5 °C/65 % rel. h. hardly any degradation of all analyzed cilazapril derivatives was observed over a storage period of 16 months. Only the analysis of the double ester prodrugs **3.1** and **3.6** revealed small amounts of cilazapril.

Table 3.6. Solid state stability of a selection of cilazapril prodrugs stored at 5 °C/65 % rel. h. for and 16 months.

No.	t_0 (%)[a]	prodrug (%) 6 months/16 months	cilazapril (%) 6 months/16 months	cilazaprilat (%) 6 months/16 months	"3.x – EtOH" (%)[b] 6 months/16 months
3.1	100	100 / 98	0 / 2	0 / 0	0 / 0
3.2	100	100 / 100	0 / 0	0 / 0	0 / 0
3.3	100	100 / 100	0 / 0	0 / 0	0 / 0
3.6	100	100 / 97	0 / 3	0 / 0	0 / 0
3.7	100	100 / 100	0 / 0	0 / 0	0 / 0
3.14	100	100 / 100	0 / 0	0 / 0	0 / 0
3.28	100	100 / 100	0 / 0	0 / 0	0 / 0

[a] percentage of compound at the beginning of storage. [b] **3.x** refers to the corresponding parent compound. Compounds "**3.x – EtOH**" result from the loss of the ethyl ester of the homophenylalanine substructure. (cf. Scheme 3.15).

At 25 °C/60 % rel. h. a relationship between the structure of the pro-moiety and stability becomes obvious. The stability of the double ester prodrugs **3.1** – **3.3**, **3.6** and **3.7** increased with the steric demand of the alkyl side chain. Thus, **3.2** and **3.7** carrying a cyclohexyl and a *tert*-butyl side chain, respectively, turned out to be most stable, whereas **3.6** with a methyl residue appeared to be most labile. The surprisingly clear difference between the very stable ethyl ester **3.28** and the rather labile morpholinoethyl ester **3.14**

gives rise to the speculation about a catalytic effect of the morpholino group accelerating the degradation.

Under accelerated storage conditions at 40 °C/75 % rel. h. complete degradation of compounds **3.6** and **3.14** occurred within 16 months. Even of the most stable prodrug of this series, compound **3.2**, only 28 % remained unchanged. In general, the stability of all analyzed cilazapril prodrugs, except for **3.28**, under accelerated storage conditions turned out to be insufficient with respect to the development of a TTS. Strikingly, the ethyl ester of the homophenylalanine moiety in **3.28** appeared to be highly stable. However, the combination with a more labile prodrug moiety seems to affect the stability of the homophenylalanine ethyl ester group as well, giving rise to the assumption that as soon as the introduced prodrug ester is cleaved to cilazapril, the ethyl ester also becomes prone to hydrolysis yielding cilazaprilat. It is noteworthy that, regardless of the storage conditions and periods, no diketopiperazine degradation products were detected.

Table 3.7. Six and 16 months solid state stability of a selection of cilazapril prodrugs stored at 25 °C/ 60 % rel. h.

No.	t_0 (%)[a]	prodrug (%) 6 months/16 months	cilazapril (%) 6 months/16 months	cilazaprilat (%) 6 months/16 months	"3.x – EtOH" (%)[b] 6 months/16 months
3.1	100	98 / 89	2 / 7	0 / 0	0 / 4
3.2	100	100 / 98	0 / 2	0 / 0	0 / 0
3.3	100	99 / 96	1 / 4	0 / 0	0 / 0
3.6	100	93 / 34	7 / 41	0 / 18	0 / 7
3.7	100	100 / 97	0 / 3	0 / 0	0 / 0
3.14	100	96 / 70	3 / 25	0 / 3	0 / 2
3.28	100	100 / 100	0 / 0	0 / 0	0 / 0

[a] percentage of compound at the beginning of storage. [b] **3.x** refers to the corresponding parent compound. Compounds "**3.x – EtOH**" result from the loss of the ethyl ester of the homophenylalanine substructure. (cf. Scheme 3.15).

Table 3.8. Six and 16 months solid state stability of a selection of cilazapril prodrugs stored at 40 °C/ 75 % rel. h.

No.	t_0 (%)[a]	prodrug (%) 6 months/16 months	cilazapril (%) 6 months/16 months	cilazaprilat (%) 6 months/16 months	"3.x – EtOH" (%)[b] 6 months/16 months
3.1	100	82 / 6	9 / 9	3 / 68	6 / 17
3.2	100	96 / 28	4 / 15	0 / 38	0 / 19
3.3	100	91 / 14	6 / 12	0 / 52	3 / 22
3.6	100	9 / 0	40 / 0	45 / 92	6 / 8
3.7	100	92 / 10	5 / 10	0 / 59	3 / 21
3.14	100	38 / 0	42 / 0	16 / 100	4 / 0
3.28	100	100 / 91	0 / 9	0 / 0	0 / 0

[a] percentage of compound at the beginning of storage. [b] **3.x** refers to the corresponding parent compound. Compounds "**3.x – EtOH**" result from the loss of the ethyl ester of the homophenylalanine substructure. (cf. Scheme 3.15).

3.5.2 Stability of prodrugs of candesartan and cilazapril in buffer

The rates of "chemical" (non-enzymatic) hydrolysis of prodrugs of candesartan and cilazapril were determined in sodium phosphate buffer (0.1 M, pH 7.4) at 37 °C. At appropriate intervals samples of the prodrug containing incubation mixture were taken and analyzed by HPLC.

3.5.2.1 Spontaneous hydrolysis of candesartan prodrugs

Candesartan cilexetil turned out to be very stable against hydrolysis in buffer. Only about 4 % of the cleavage product candesartan were detected after an incubation period of 72 h (Figure 3.4), corresponding to a half-life $t_{1/2}$ of the prodrug of 57.7 d.

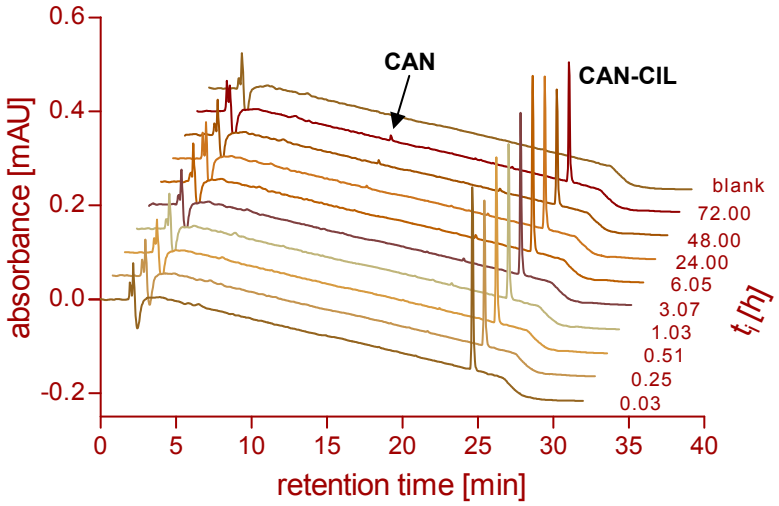

Figure 3.4. Kinetics of hydrolysis of candesartan cilexetil in 0.1 M phosphate buffer, pH 7.4. **CAN-CIL** = candesartan cilexetil, **CAN** = candesartan.

Compared to the cilexetil pro-moiety the less bulky 1-(isopropyloxycarbonyloxy)ethyl residue in **3.31** proved to be less stable; a half life $t_{1/2}$ of 13.8 d was calculated (Figure 3.5).

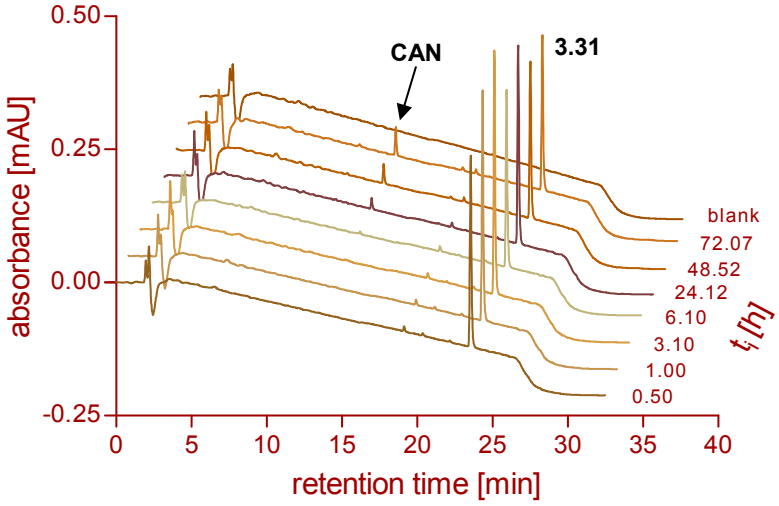

Figure 3.5. Kinetics of hydrolysis of **3.31** in 0.1 M phosphate buffer, pH 7.4, **CAN** = candesartan.

The kinetics of hydrolysis of candesartan 1-(2,2-dimethylpropanoyl)ethyl ester **3.32** is shown in Figure 3.6. The half-life was estimated to be 32.5 d, corresponding to a stability between those of candesartan cilexetil and **3.31**.

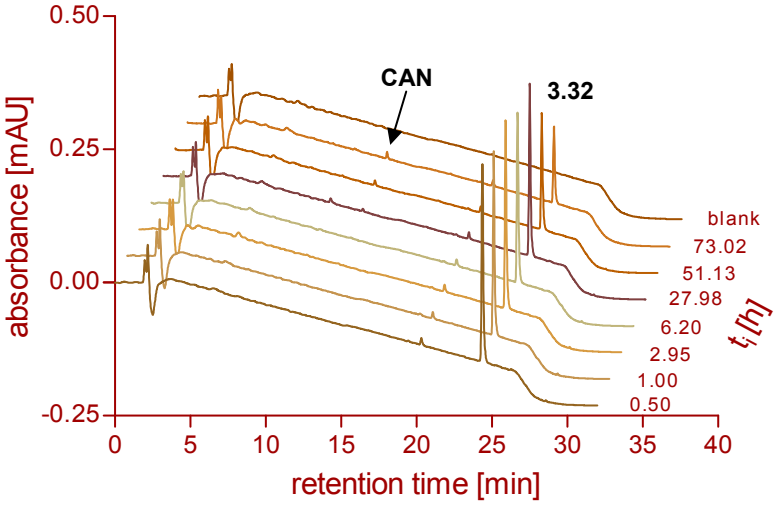

Figure 3.6. Kinetics of hydrolysis of **3.32** in phosphate buffer, **CAN** = candesartan.

Compared to the 1-(alkyloxycarbonyloxy)ethyl and 1-(acyloxy)ethyl prodrugs of candesartan the (5-alkyl-2-oxo-1,3-dioxol-4-yl)methyl esters **3.33** and **3.34** were relatively unstable in buffer ($t_{1/2}$ = 2.3 h and 14.2 h, respectively) (cf. Figure 3.7 and Figure 3.8). In general, the (oxodioxolyl)methyl moiety seems to be very prone to spontaneous hydrolysis. Interestingly, the exchange of the 5-methyl residue against a sterically more demanding *tert*-butyl group leads to a six-fold gain in stability.

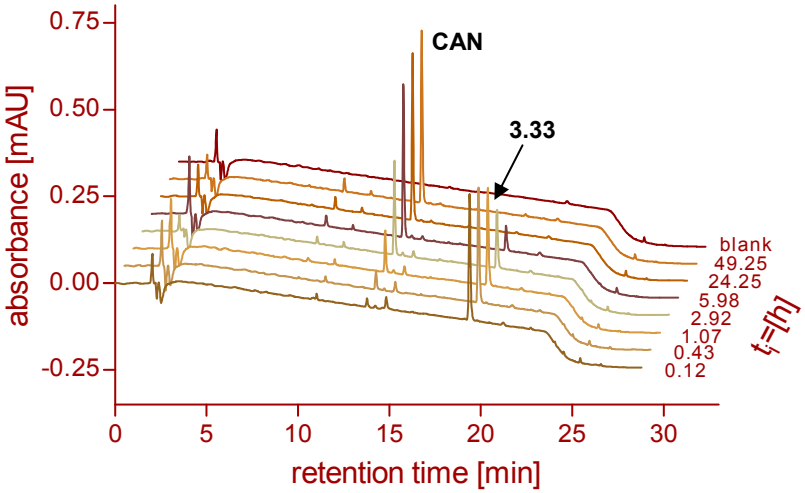

Figure 3.7. Examples of HPLC chromatograms illustrating the kinetics of hydrolysis of **3.33** in phosphate buffer, **CAN** = candesartan.

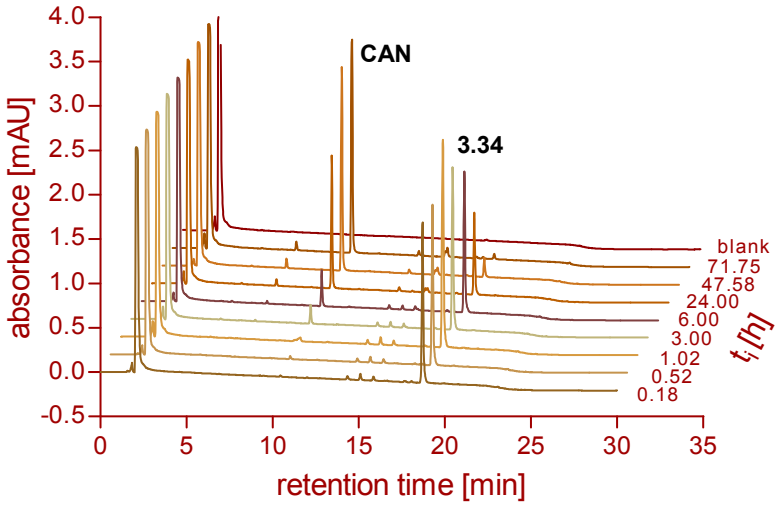

Figure 3.8. Kinetics of hydrolysis of **3.34** in phosphate buffer 0.1 M, pH 7.4, **CAN** = candesartan.

The morpholinoethyl ester **3.35** was reasonably stable in buffer (Figure 3.9). Its half-life of hydrolysis amounted to 6.1 d. In contrast to all other candesartan prodrugs, **3.35** is eluted before candesartan, as the morpholino group is protonated in the presence of the acidic HPLC eluent.

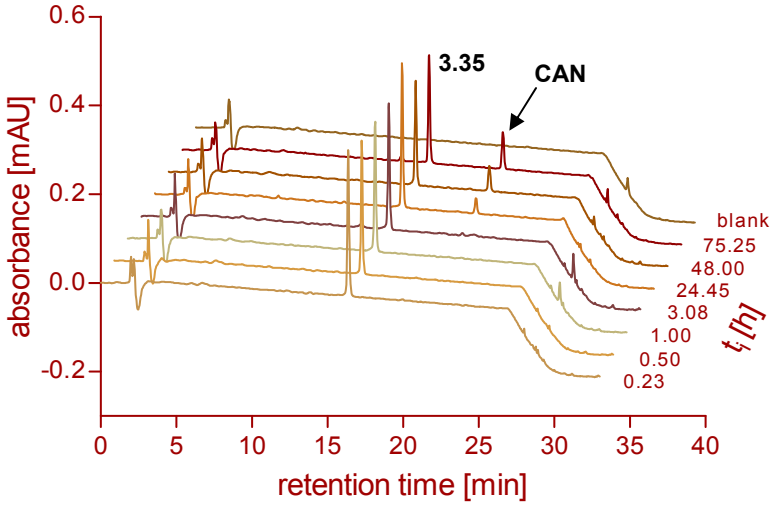

Figure 3.9. Examples of HPLC chromatograms illustrating the kinetics of hydrolysis of **3.35** in phosphate buffer, **CAN** = candesartan.

3.5.2.2 Spontaneous hydrolysis of cilazapril prodrugs

As cilazapril containing a hydrolysable ethyl ester pro-moiety is a prodrug itself, its lifetime in aqueous solution at pH 7.4 is limited. About 16 % of cilazaprilat (**3.29**) were detected after an incubation period of 48.1 h (Figure 3.10). A half-life of 183 h was estimated.

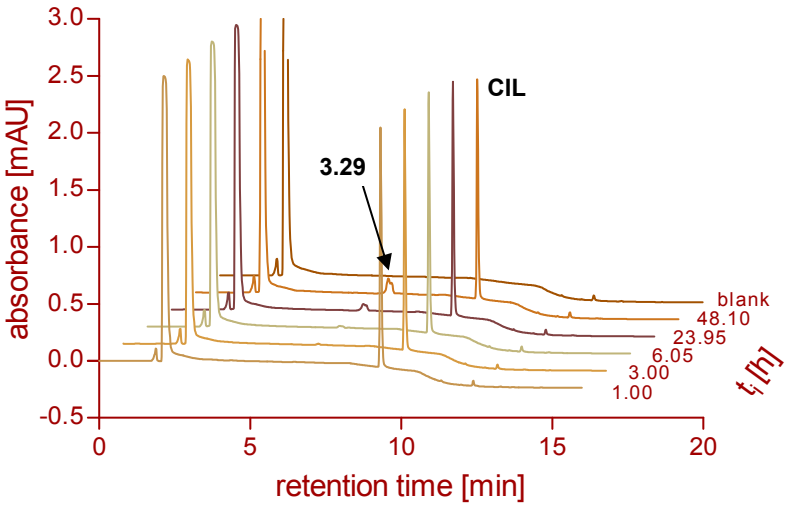

Figure 3.10. Examples of HPLC chromatograms illustrating the kinetics of hydrolysis of cilazapril (**CIL**) in 0.1 M phosphate buffer, pH 7.4.

The $t_{1/2}$ values of the cilazapril 1-(alkyloxycarbonyloxy)ethyl esters **3.1**-**3.3** were found to correlate with the steric demand of the 1-(alkyloxycarbonyloxy)ethyl pro-moiety. Both prodrug esters **3.1** and **3.3** were partially hydrolyzed to cilazapril during an incubation period of about 72 h (cf. appendix, Figure 9.1, Figure 9.2). Whereas $t_{1/2}$ of the 1-(isopropyloxycarbonyloxy)ethyl ester **3.3** only slightly increased ($t_{1/2}$ = 75.7 h) compared to the 1-(ethoxycarbonyloxy)ethyl ester **3.1** ($t_{1/2}$ = 75.0 h), the bulky 1-(cyclohexyloxycarbonyloxy)ethyl ester **3.2** was found to be totally stable over a period of 71.3 h (Figure 3.11).

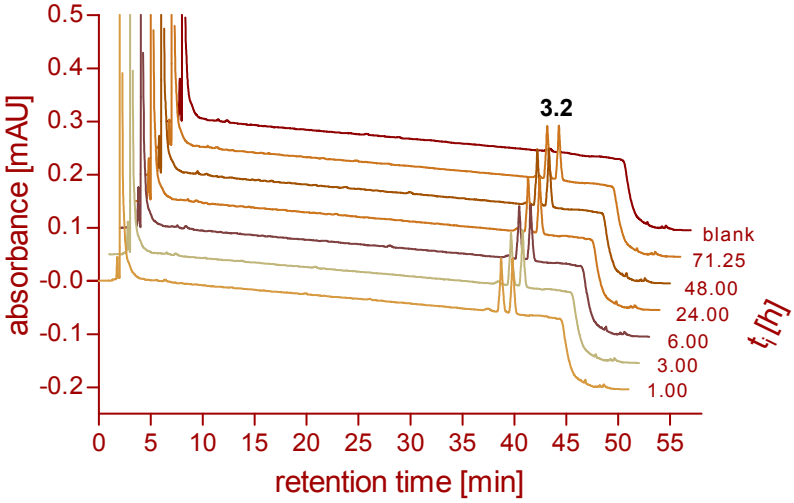

Figure 3.11. Kinetics of hydrolysis of **3.2** (two diastereomers) in phosphate buffer.

An analogous behavior was observed for the cilazapril 1-(acyloxy)ethyl esters **3.6** and **3.7**. Again, the bulkier pro-moiety, the 1-(2,2-dimethylpropanoyl)ethyl residue in **3.7**, conferred higher stability. No degradation of **3.7** was observed within 72 h (cf. appendix, Figure 9.3), whilst **3.6** was found to be considerably less stable ($t_{1/2}$ = 40.3 h). Hence, the degradation products cilazapril as well as cilazaprilat (**3.29**) was detected (Figure 3.12).

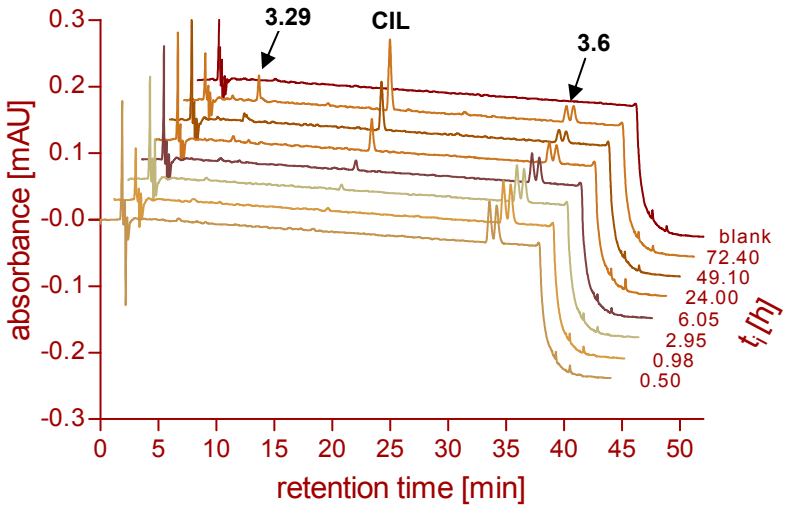

Figure 3.12. Kinetics of hydrolysis of **3.6** (two diastereomers) in phosphate buffer, **CIL** = cilazapril.

The (5-alkyl-2-oxo-1,3-dioxol-4-yl)methyl esters of cilazapril (**3.12** and **3.13**) showed a similar behavior as the analogous derivatives of candesartan (**3.33** and **3.34**). Both prodrugs were rapidly hydrolyzed to give cilazapril and cilazaprilat (**3.29**) (cf. Figure 3.13 and Figure 3.14). The half-life amounted to 3.7 h (**3.12**) and 7.1 h (**3.13**), respectively, indicating that an exchange of the 5-methyl against the 5-*tert*-butyl residue improves stability.

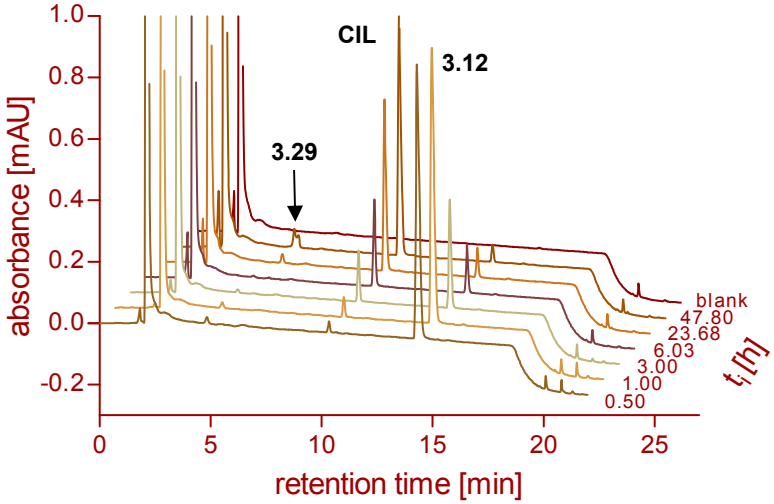

Figure 3.13. Examples of HPLC chromatograms showing the kinetics of hydrolysis of **3.12** in phosphate buffer, **CIL** = cilazapril.

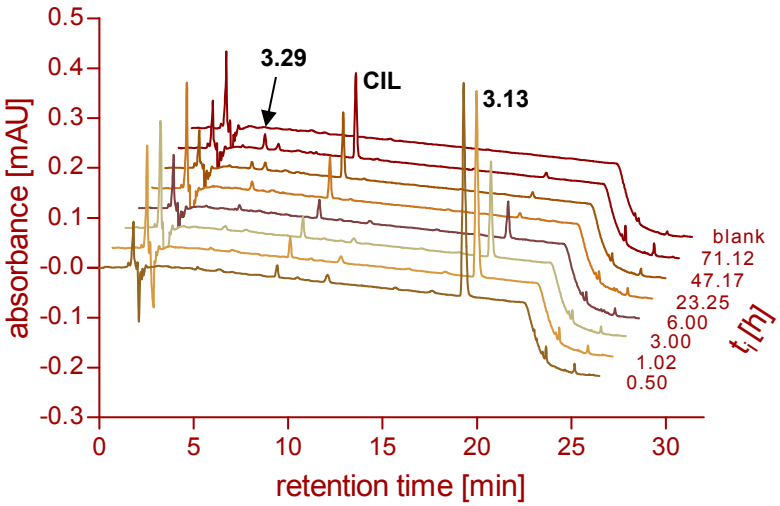

Figure 3.14. Kinetics of hydrolysis of **3.13** in phosphate buffer, **CIL** = cilazapril.

The morpholinoethyl ester **3.14** was found to be only moderately stable in buffer ($t_{1/2}$ = 14.0 h) (cf. Figure 3.15). Cilazapril as well as cilazaprilat (**3.29**) were detected as products of hydrolysis.

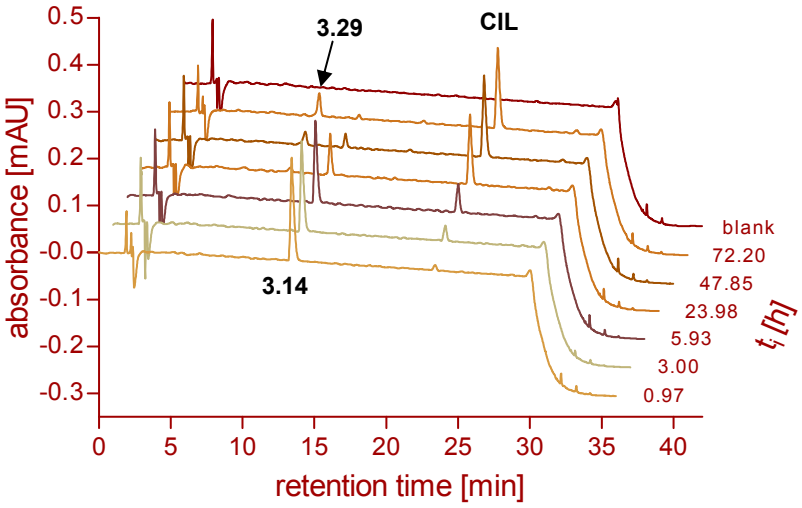

Figure 3.15. Examples of HPLC chromatograms showing the kinetics of hydrolysis of **3.14** in phosphate buffer, **CIL** = cilazapril.

The kinetics of hydrolysis of the cilazapril 1-(2-morpholinoacetoxy)ethyl ester **3.18** (Figure 3.16) was very similar to that of **3.14**, but, with a determined $t_{1/2}$ of 18.6 h, **3.18** was slightly more stable.

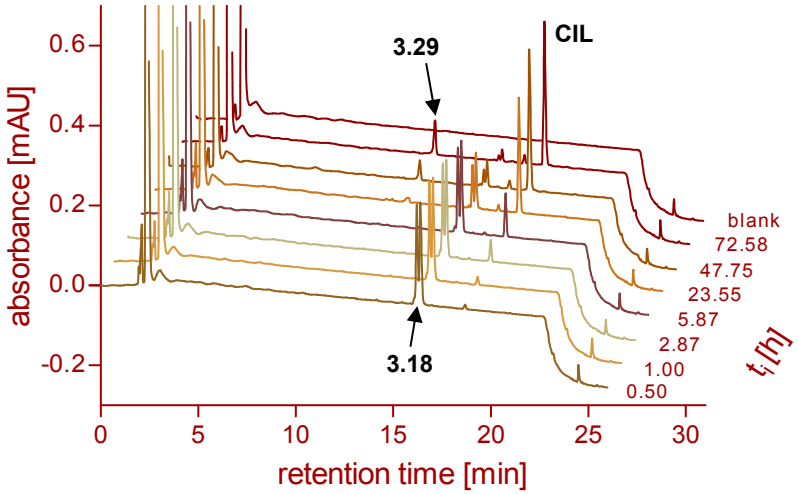

Figure 3.16. Kinetics of hydrolysis of **3.18** (two diastereomers) in phosphate buffer, **CIL** = cilazapril.

From the small set of *N*-aryl-*N*-alkyloxycarbonylaminomethyl prodrugs (**3.25**-**3.27**) only **3.25** was suitable for the determination of half-lives in buffer at pH 7.4, whereas **3.26** and **3.27** turned out to be insufficiently soluble in the incubation buffer. Hence, in case of the latter two compounds, the resulting peak areas in the HPLC chromatograms were too small for reliablequantification. Prodrug **3.25** was degraded to an extent of 97 % in the course of the incubation (cf. Figure 3.17). Its half-life amounted to approximately 12 h. While the peak corresponding to **3.25** decreased with increasing t_i, two peaks were increasing simultaneously. Besides cilazapril at t_R = 9.4 min the peak at t_R = 13.9 min was identified by LC-MS as ethyl phenylcarbamate, a substructure of the degraded promoiety.

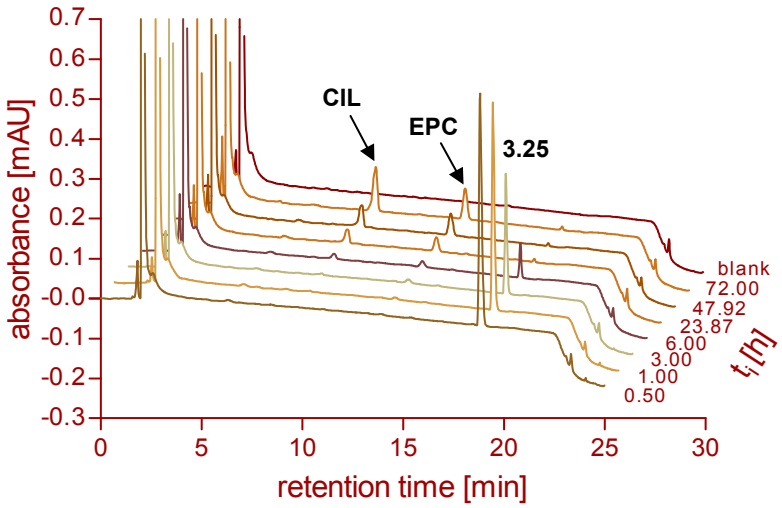

Figure 3.17. Kinetics of hydrolysis of **3.25** in phosphate buffer, **CIL** = cilazapril, **EPC** = ethyl phenylcarbamate.

The simple diethyl ester **3.28** turned out to be the most stable cilazapril prodrug (cf. Figure 3.18). With a half-life of 16.8 d it was even more stable against non-enzymatic hydrolysis than cilazapril itself, supporting the assumption that a free carboxylic acid group at the heterocyclic system renders the homophenylalanine ethyl ester more susceptible to hydrolysis.

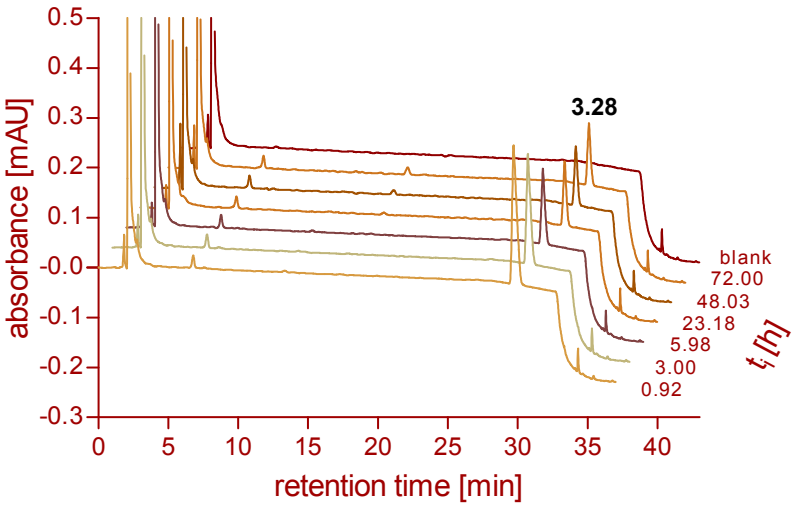

Figure 3.18. Kinetics of hydrolysis of **3.28** in phosphate buffer.

3.5.3 Stability of prodrugs of candesartan and cilazapril against enzymatic hydrolysis

The carrier pro-moiety of all designed cilazapril and candesartan prodrugs is ester-based and can therefore be cleaved by hydrolysis or oxidation, typically by esterases or cytochrome P450 enzymes. In order to investigate the stability of the prodrugs three different enzyme-containing test systems as well as cultured primary human hepatocytes (PHH) were used.

As the synthesized prodrugs should be applicable as transdermal patches, the investigation of their potential hydrolysis in skin is self-evident. It is known that phase I and phase II metabolic reactions can take place in human skin.[40] The metabolizing enzymes, in particular carboxylesterases and cytochrome P450 enzymes[4], are mainly located within the viable epidermis.[40] Since porcine skin is much easier accessible than human skin and shows similarities to the human tissue in terms of distribution and enzyme-activity[41], a homogenate of fresh porcine skin in PBS was prepared and used for metabolic studies.

Another well-established model for studies on enzymatic hydrolysis is human plasma. It contains cholinesterase, acetylcholinesterase and paraoxonase activity.[4] For following studies human CPD plasma was used. As the third enzyme-containing test system a carboxylesterase was considered. Due to its comparably high activity and its low price porcine liver esterase was chosen and used as dilution in phosphate buffer at pH 7.4.

Furthermore, the capability of cultured primary human hepatocytes to metabolize the ester prodrugs should be investigated.

The rates of hydrolysis for each prodrug in the respective enzyme-containing incubation mixture were determined at 37 °C according to the procedure described in section 3.5.2, but, additionally, the samples were deproteinated by addition of ice cold acetonitrile and centrifuged prior to HPLC analysis.

For the investigation of hydrolysis by human liver cells, exemplary substances were incubated at 37 °C with cultured PHH, which were plated on multi-well plates. After an incubation period of one and six hours, respectively, samples were taken, deproteinated, centrifuged and analyzed by HPLC.

3.5.3.1 Enzymatic hydrolysis of candesartan prodrugs

Candesartan cilexetil was selectively hydrolyzed to candesartan on incubation with porcine skin homogenate, human plasma and porcine liver esterase (cf. Figure 3.19-Figure 3.21). The half-lives in porcine skin homogenate and human plasma amounted to 0.27 h and 35.0 h, respectively. Due to the high volume activity of porcine liver esterase used the hydrolysis of candesartan cilexetil was very fast. Thus, $t_{1/2}$ could not be calculated, but was estimated to be < 3 min.

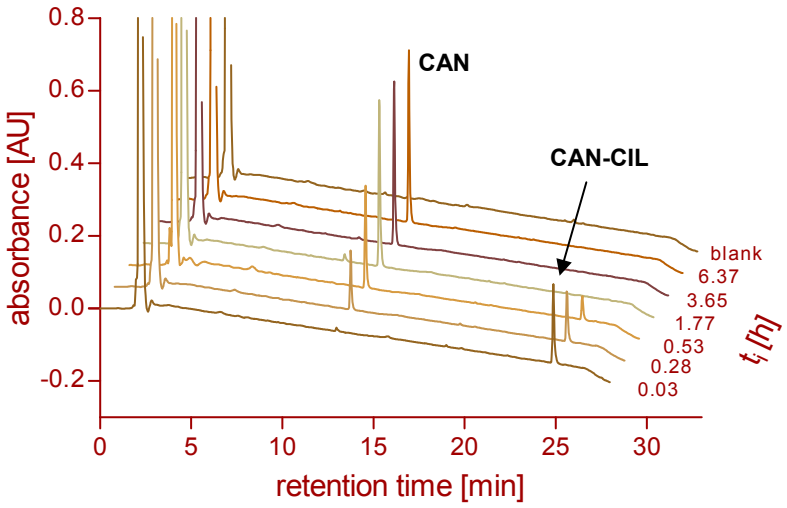

Figure 3.19. Examples of chromatograms showing the kinetics of hydrolysis of candesartan cilexetil (**CAN-CIL**) in the presence of porcine skin homogenate, **CAN** = candesartan.

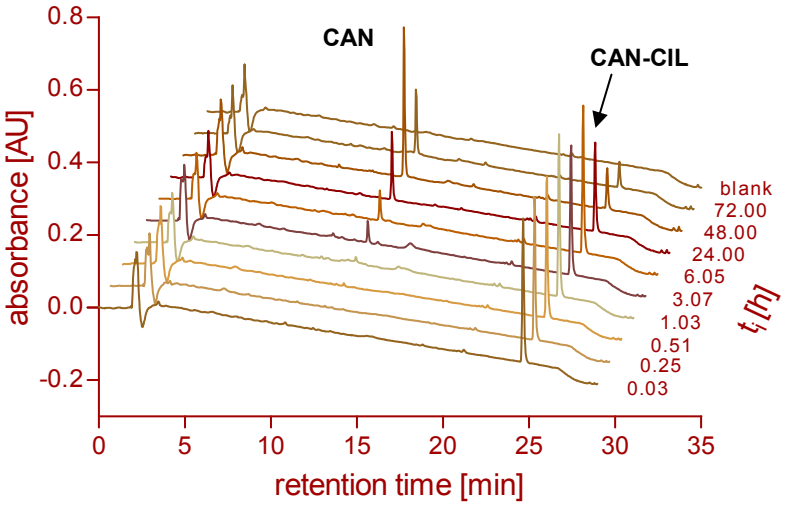

Figure 3.20. Kinetics of hydrolysis of candesartan cilexetil (**CAN-CIL**) in the presence of human plasma, **CAN** = candesartan.

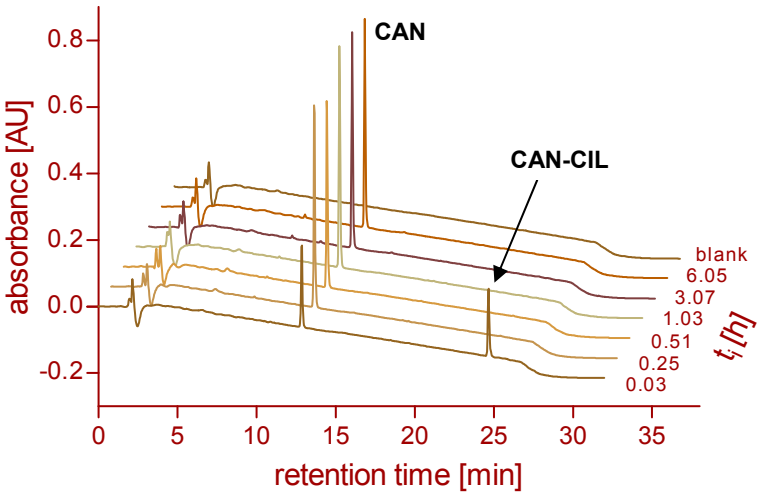

Figure 3.21. Examples of chromatograms showing the kinetics of hydrolysis of candesartan cilexetil (**CAN-CIL**) in the presence of porcine liver esterase, **CAN** = candesartan.

Candesartan 1-(isopropyloxycarbonyloxy)ethyl ester (**3.31**) was also selectively hydrolyzed to candesartan in all three incubation media. In the presence of porcine skin homogenate (Figure 3.22) and porcine liver esterase (Figure 3.23) the hydrolysis proceeded quantitatively with half-life times of 8 min and 6 min, respectively. When incubated with human plasma (Figure 3.24) a $t_{1/2}$ of 47.5 h was calculated.

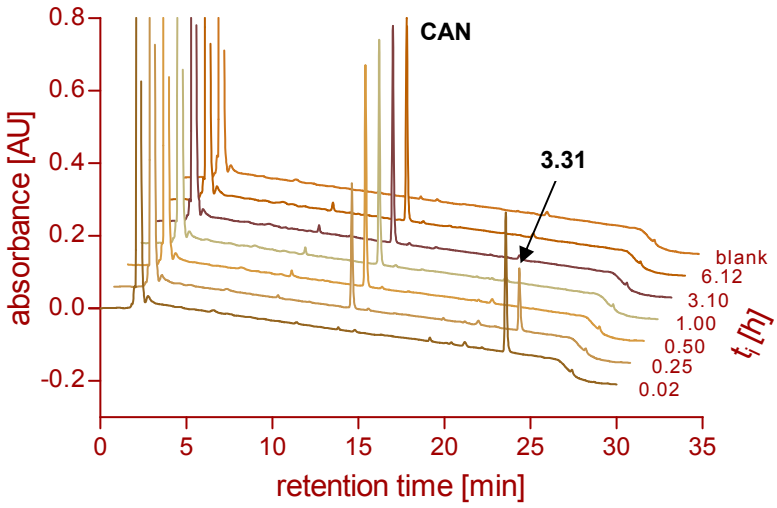

Figure 3.22. Examples of HPLC chromatograms showing the kinetics of hydrolysis of **3.31** in the presence of porcine skin homogenate, **CAN** = candesartan.

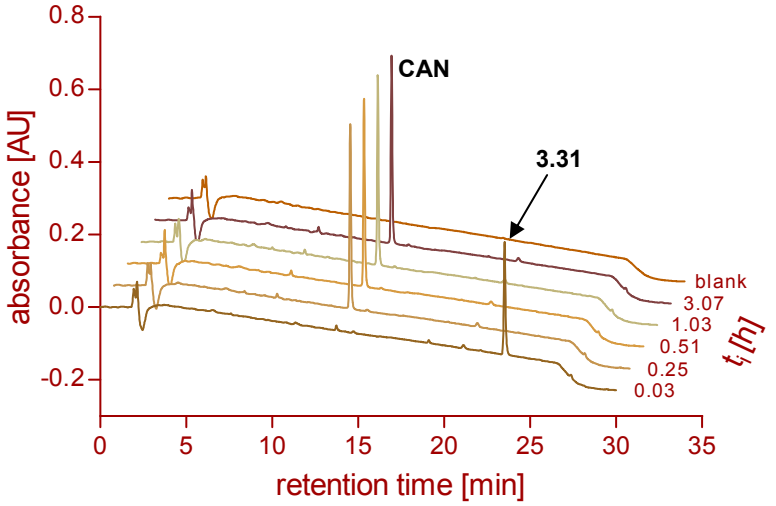

Figure 3.23. Examples of HPLC chromatograms illustrating the kinetics of hydrolysis of **3.31** in the presence of porcine liver esterase, **CAN** = candesartan.

Incubation of **3.31** with primary human hepatocytes revealed that human liver cells are also capable of hydrolyzing the ester pro-moiety. After an incubation period of one hour 47 % of the prodrug was converted to candesartan, whereas after six hours the hydrolysis was quantitative (data not shown).

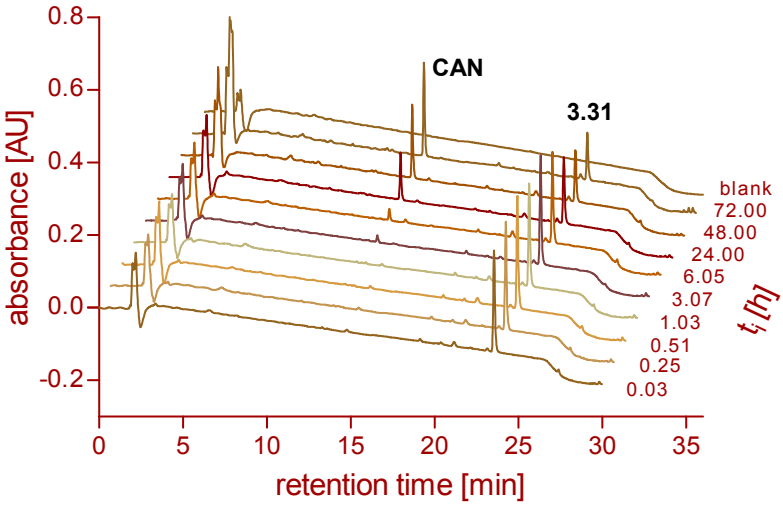

Figure 3.24. Kinetics of hydrolysis of **3.31** in the presence of human plasma, **CAN** = candesartan.

The results of the enzymatic hydrolysis of candesartan 1-(2,2-dimethylpropanoyl)ethyl ester (**3.32**) are similar to those for candesartan cilexetil and **3.31**. **3.32** was also exclusively converted to candesartan in each of the used incubation media resulting in the following half-lives ($t_{1/2}$): 0.45 h (porcine skin homogenate (Figure 3.25)), 32.2 h (human plasma (Figure 3.26)) and 2 min (porcine liver esterase (Figure 3.27)).

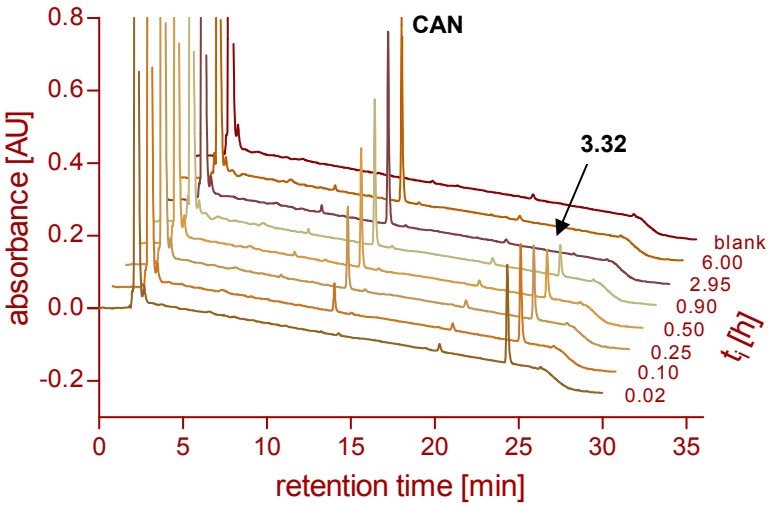

Figure 3.25. Examples of HPLC chromatograms showing the kinetics of hydrolysis of **3.32** in the presence of porcine skin homogenate, **CAN** = candesartan.

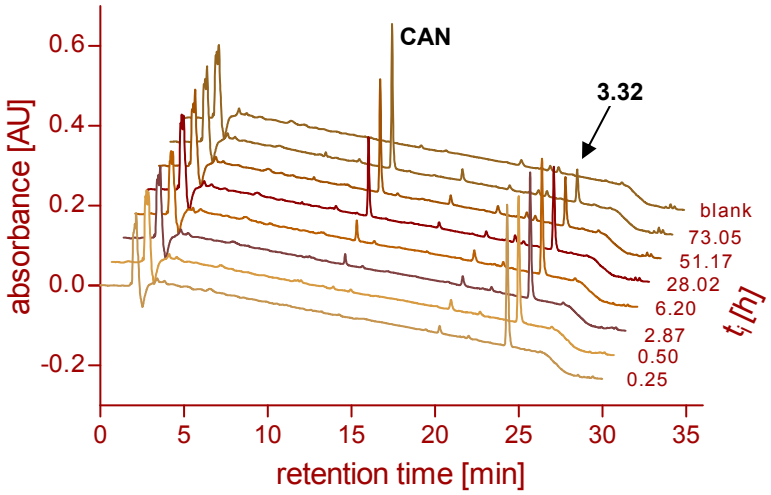

Figure 3.26. Examples of HPLC chromatograms illustrating the kinetics of hydrolysis of **3.32** in the presence of human plasma, **CAN** = candesartan.

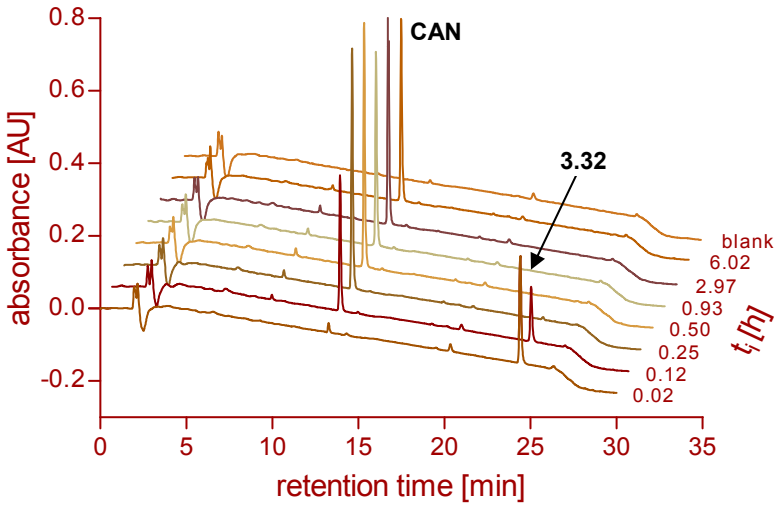

Figure 3.27. Examples of chromatograms showing the kinetics of hydrolysis of **3.32** in the presence of porcine liver esterase, **CAN** = candesartan.

Incubation of **3.32** with primary human hepatocytes for one hour resulted in the formation of 22 % candesartan. After an incubation period of six hours 72 % candesartan were detected (data not shown).

The kinetics of enzymatic hydrolysis of candesartan (5-methyl-2-oxo-1,3-dioxol-4-yl)-methyl ester (**3.33**) by porcine skin homogenate, human plasma and porcine liver esterase are shown in Figure 3.28 to Figure 3.30. In all cases candesartan was detected as the exclusive product of hydrolysis. For the hydrolysis by porcine liver esterase a $t_{1/2}$ of 2.2 h was estimated, which nearly equals the value found for the chemical hydrolysis of **3.33** in buffer (2.3 h). Hence, the parent compound **3.33** seems to be no or only a poor substrate for the carboxylesterase from porcine liver. The generation of candesartan is therefore supposed to take place - at least in part - by spontaneous non-enzymatic hydrolysis.

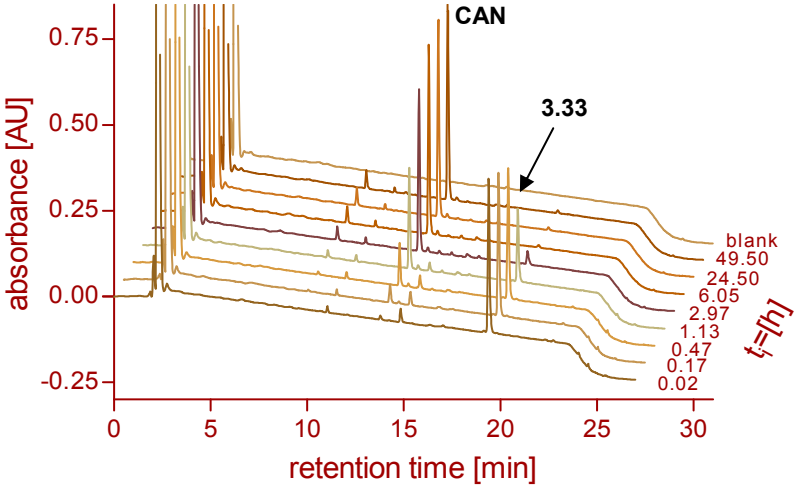

Figure 3.28. Kinetics of hydrolysis of **3.33** in the presence of porcine liver esterase, **CAN** = candesartan.

However, the hydrolysis in porcine skin homogenate was found to be faster ($t_{1/2}$ = 0.95 h) leading to the conclusion that the (5-methyl-2-oxo-1,3-dioxol-4-yl)methyl ester pro-moiety was slightly better accepted as a substrate by esterases present in porcine skin homogenate.

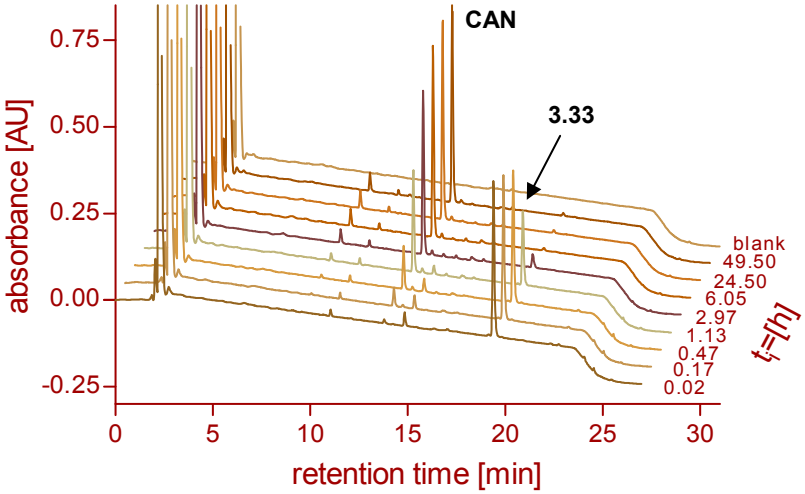

Figure 3.29. Examples of HPLC chromatograms showing the kinetics of hydrolysis of **3.33** in porcine skin homogenate, **CAN** = candesartan.

The degradation of **3.33** in human plasma was strikingly fast. After an incubation period of one minute already 85 % of of the prodrug were converted to candesartan. Thus, $t_{1/2}$ is shorter than one minute. The hydrolysis is supposed to be catalyzed by human serum paraoxonase, which is predominantly found in blood[4] and is known to be capable of hydrolyzing the (5-methyl-2-oxo-1,3-dioxol-4-yl)methyl moiety[42].

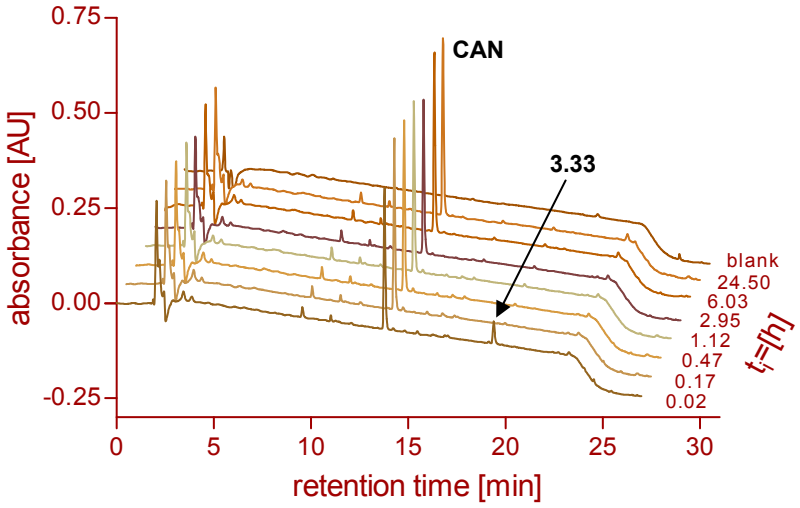

Figure 3.30. Examples of HPLC chromatograms showing the kinetics of hydrolysis of **3.33** in the presence of human plasma, **CAN** = candesartan.

The results of the bioanalytical studies of candesartan (5-*tert*-butyl-2-oxo-1,3-dioxol-4-yl)-methyl ester (**3.34**) are comparable to the results for the analogue **3.33**. The conversion of the prodrug to candesartan was detected on incubation with porcine skin homogenate (Figure 3.31) as well as with porcine liver esterase (Figure 3.32). Since the half-lives (15.9 h and 15.7 h, respectively) were even higher than the value estimated for hydrolysis in buffer (14.2 h), the degradation of the pro-moiety under these conditions can presumably be attributed to non-enzymatic hydrolysis. By contrast, the hydrolysis of **3.34** in the presence of human plasma (Figure 3.33) was fast ($t_{1/2}$ = 0.82 h) suggesting that the (5-*tert*-butyl-2-oxo-1,3-dioxol-4-yl)methyl ester is a substrate of human serum paraoxonase. Compared to **3.33**, the replacement of methyl by *tert*-butyl led to a considerable increase in stability.

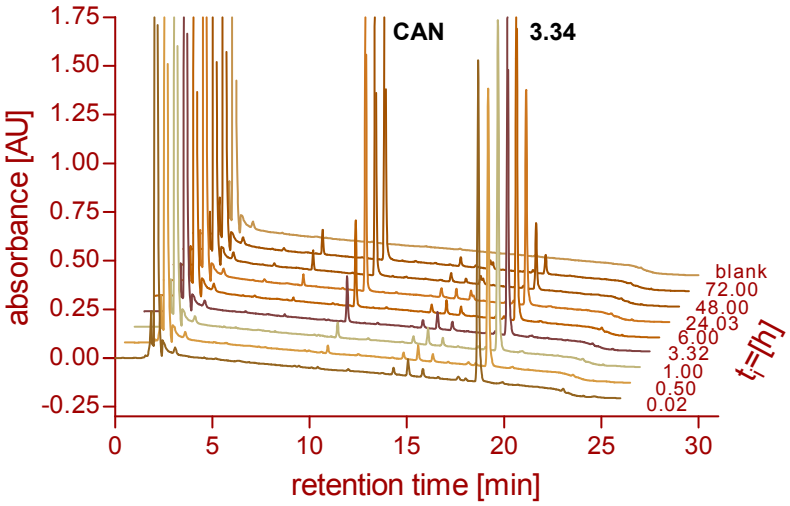

Figure 3.31. Kinetics of hydrolysis of **3.34** in the presence of porcine skin homogenate, **CAN** = candesartan.

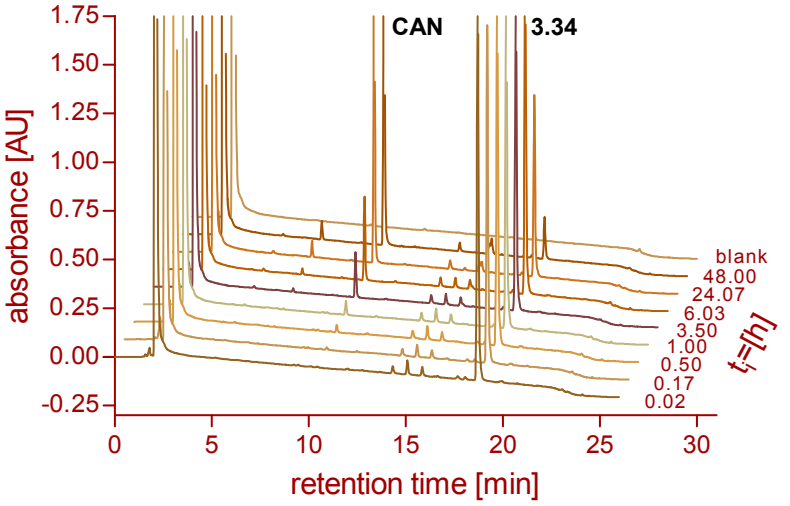

Figure 3.32. Kinetics of hydrolysis of **3.34** in the presence of porcine liver esterase, **CAN** = candesartan.

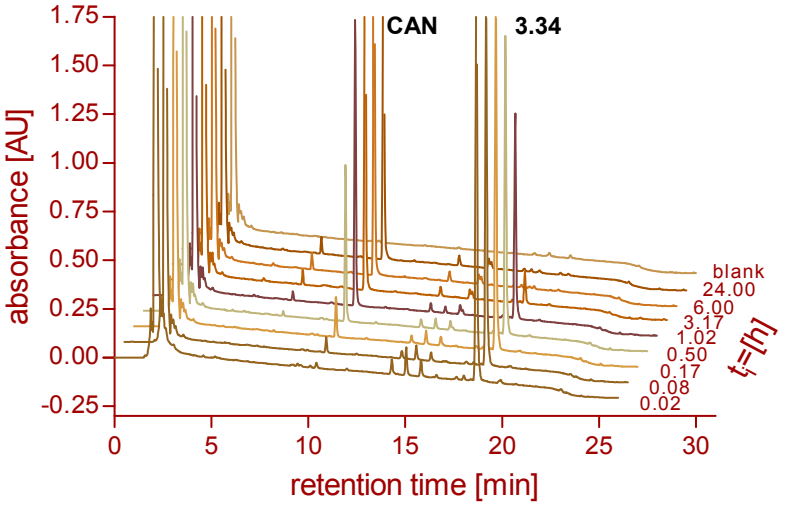

Figure 3.33. Examples of HPLC chromatograms showing the kinetics of hydrolysis of **3.34** in the presence of human plasma, **CAN** = candesartan.

Candesartan morpholinoethyl ester (**3.35**) was hydrolyzed to candesartan in the presence of porcine skin homogenate (Figure 3.34) and by porcine liver esterase (Figure 3.35). The half-life of hydrolysis in porcine skin homogenate was estimated to be 6.1 d, which is comparable to the conversion in buffer. Thus, the cleavage of the morpholinoethyl ester has taken place by non-catalysed hydrolysis rather than enzymatically. In the presence of porcine liver esterase a half-life of 18.0 h was determined.

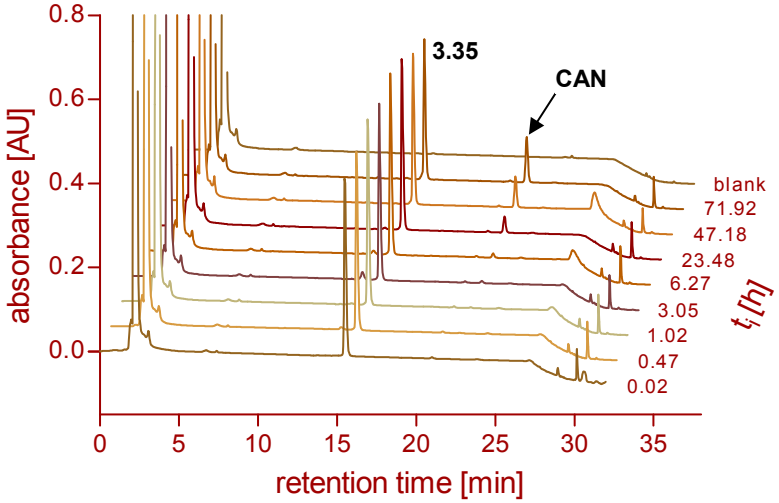

Figure 3.34. Kinetics of hydrolysis of **3.35** in the presence of porcine skin homogenate. **CAN** = candesartan.

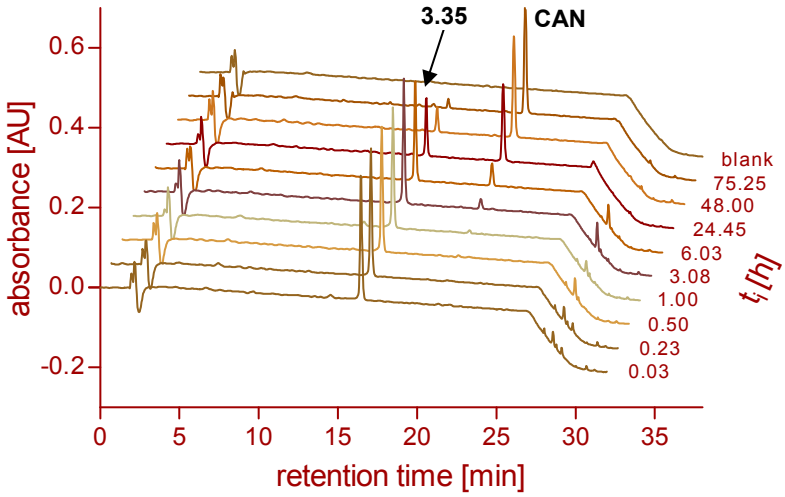

Figure 3.35. Kinetics of hydrolysis of **3.35** in the presence of porcine liver esterase, **CAN** = candesartan.

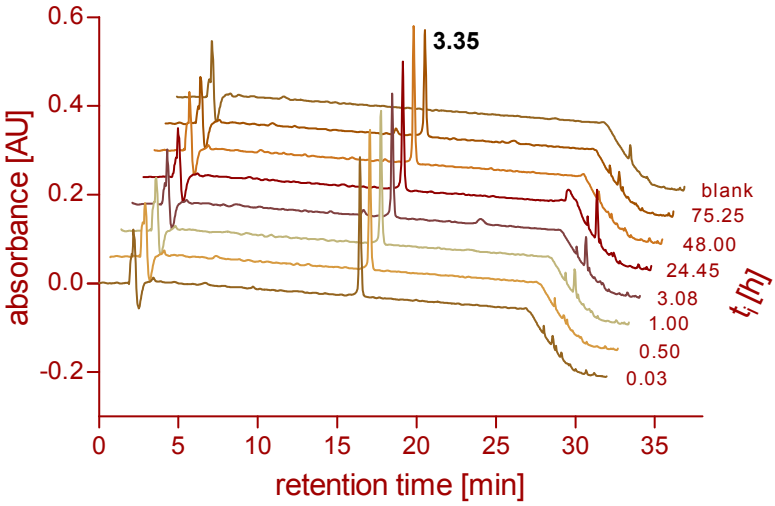

Figure 3.36. Examples of HPLC chromatograms showing the kinetics of hydrolysis of **3.35** in the presence of human plasma.

No conversion of **3.35** was observed in the presence of human plasma within 72 h (Figure 3.36). Surprisingly, even the enzymes present in human hepatocytes were not capable of breaking the ester bond; **3.35** was found to be stable over an incubation period of six hours (cf. Figure 3.37).

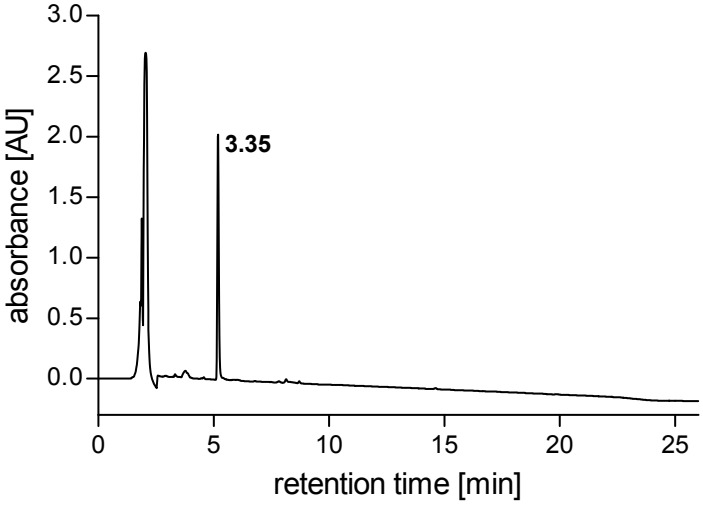

Figure 3.37. HPLC chromatogram of a sample of **3.35** incubated for a period of 6 h with primary human hepatocytes. The peak at t_R ~ 2 min refers to DMSO.

3.5.3.2 Enzymatic hydrolysis of cilazapril prodrugs

Theory:

Considering the results of the stability testing in aqueous solution (chapter 3.5.2.2) it becomes obvious that spontaneous hydrolysis of all cilazapril prodrugs at first occurs at the less stable ester pro-moiety, leading to the formation of cilazapril, and subsequently takes place at the homophenylalanine ethyl ester group to give cilazaprilat. In the case of enzymatic hydrolysis these two reaction steps were found to take place simultaneously according to Scheme 3.16, in which A, B, C and D represent the respective cilazapril prodrug, cilazapril, the respective prodrug ester with cleaved homophenylalanine ethyl ester moiety and cilazaprilat, whilst k_{xy} indicate the respective reaction rate constants.

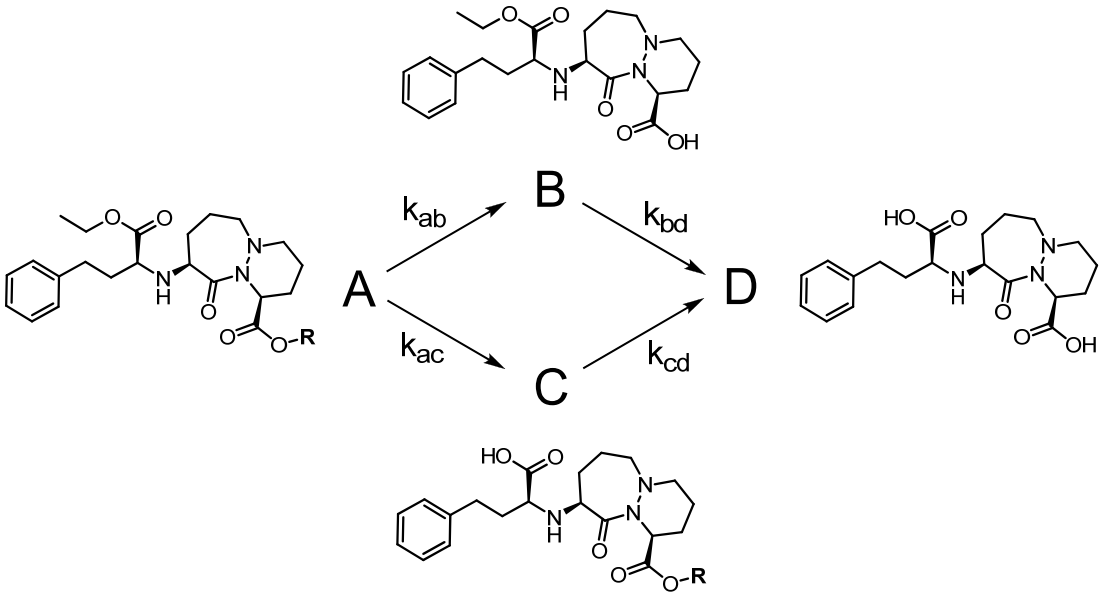

Scheme 3.16. Reaction scheme depicting the enzymatic hydrolysis of cilazapril prodrugs.

Simplifying the simultaneous hydrolysis of A to B and C by presuming pseudo first-order kinetics the half-life $t_{1/2}$ of A can be calculated according to Equation 3.3, in which the factor (k_{ab}+k_{ac}) equals the slopes of linear plots of the logarithm of the percental peak area of residual prodrug against incubation time.

$$t_{1/2} = \frac{\ln(2)}{k_{ab} + k_{ac}}$$

Equation 3.3. Rate of hydrolysis ($t_{1/2}$) according to Scheme 3.16.

According to Equation 3.3, $f_{50\%}$ values for cilazaprilat (D, cf. Scheme 3.16) can be determined from the slopes (k_{bd}+k_{cd}) of linear plots of the logarithm of the amount of cilazaprilat (D_x) to be formed (cf. Equation 3.4) against incubation time.

$$\ln(D_x) = \ln\,(100 - D_{t_i})$$

Equation 3.4. Calculation of ln(D_x). D_{t_i} = percentage of active principle after a distinct incubation period.

A more exact approach to the description of this reaction kinetics is to perform a global fit of the data sets obtained for each partial reaction using following model:

$$\frac{dA(t)}{dt} = -(k_{ab} + k_{ac}) \cdot A(t), \qquad \frac{dB(t)}{dt} = k_{ab} \cdot A(t) - k_{bd} \cdot B(t),$$

$$\frac{dC(t)}{dt} = k_{ac} \cdot A(t) - k_{cd} \cdot C(t), \qquad \frac{dD(t)}{dt} = k_{bd} \cdot B(t) + k_{cd} \cdot C(t)$$

Equation 3.5. Differential rate laws describing the reactions shown in Scheme 3.16.

All four data sets were globally fitted using the least square method by Levenberg-Marquardt[43-44]. From the resulting reaction rate constants the half-life can be calculated according to Equation 3.3.

Results:

As expected, cilazapril was selectively hydrolyzed to cilazaprilat (**3.29**) during incubation with porcine skin homogenate (Figure 3.38), human plasma (Figure 3.39) and porcine liver esterase (Figure 3.40), respectively. In the presence of porcine skin homogenate and porcine liver esterase the hydrolysis was quantitative after incubation periods of approximately 48 h and 24 h, respectively. The half-life amounted to 9.4 h and 3.3 h, respectively. The hydrolysis in human plasma was much slower ($t_{1/2}$ = 88.8 h).

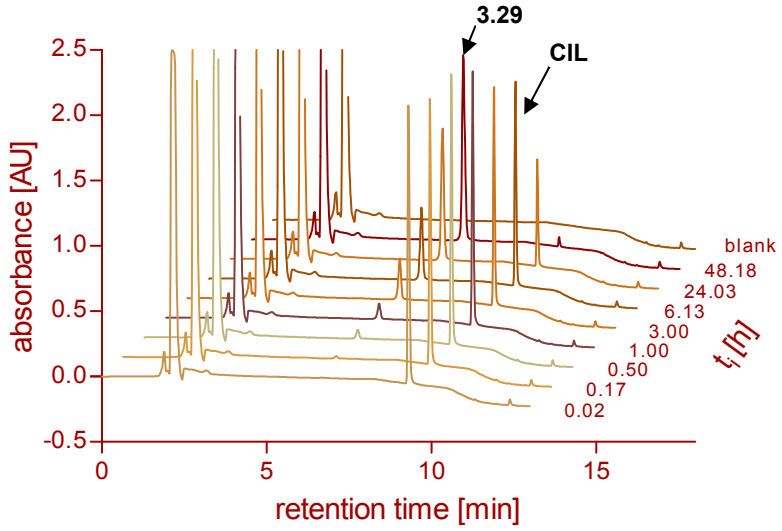

Figure 3.38. Kinetics of hydrolysis of **cilazapril** (**CIL**) in porcine skin homogenate.

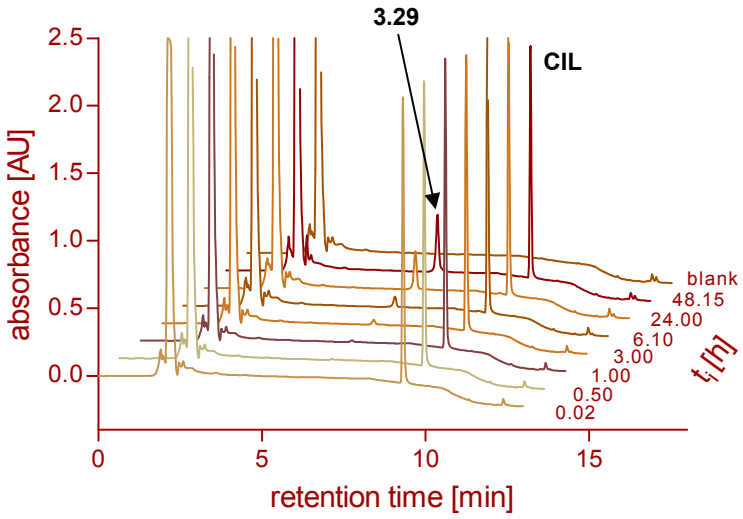

Figure 3.39. Examples of HPLC chromatograms showing the kinetics of hydrolysis of **cilazapril** (**CIL**) in the presence of human plasma.

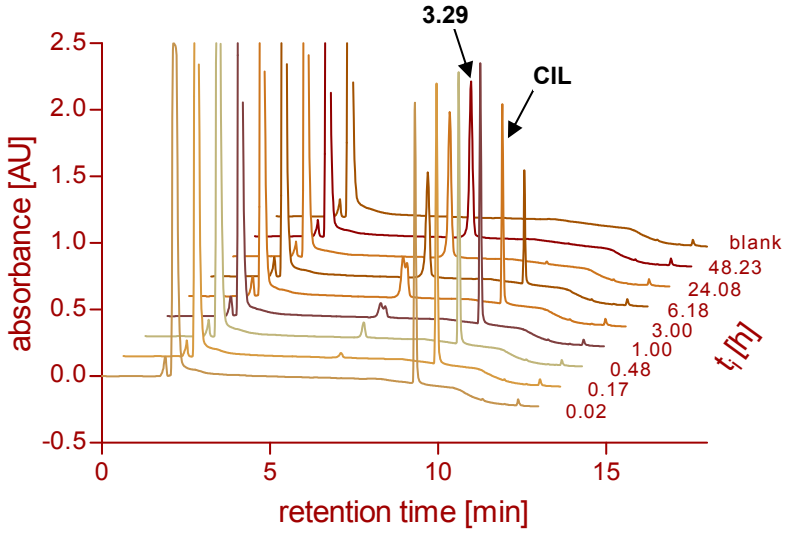

Figure 3.40. Kinetics of hydrolysis of **cilazapril** (**CIL**) in the presence of porcine liver esterase.

Also human hepatocytes were able to metabolize cilazapril to cilazaprilat. 26 % and 89 % of cilazaprilat were formed after incubation periods of 1 h and 6 h, respectively (data not shown).

Cilazapril 1-(ethoxycarbonyloxy)ethyl ester (**3.1**) was completely hydrolyzed to cilazapril (**CIL**) and cilazaprilat (**3.29**) in the presence of porcine skin homogenate, human plasma or porcine liver esterase within an incubation period of 72 h (Figure 3.41 - Figure 3.43).

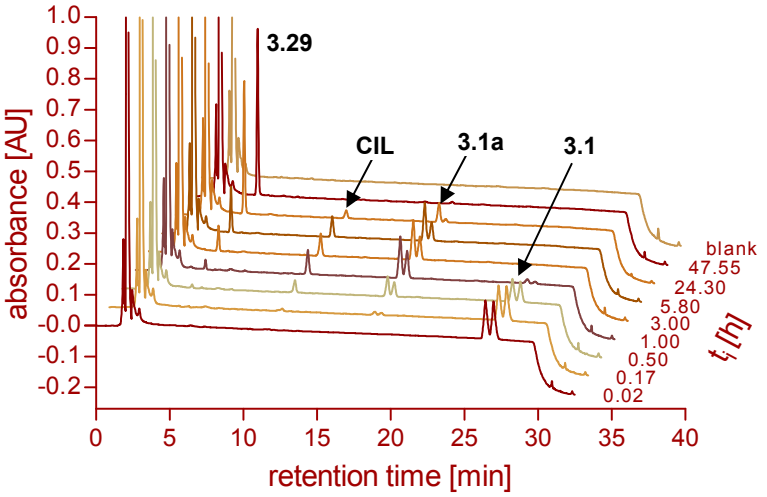

Figure 3.41. Examples of HPLC chromatograms showing the kinetics of hydrolysis of **3.1** in porcine skin homogenate.

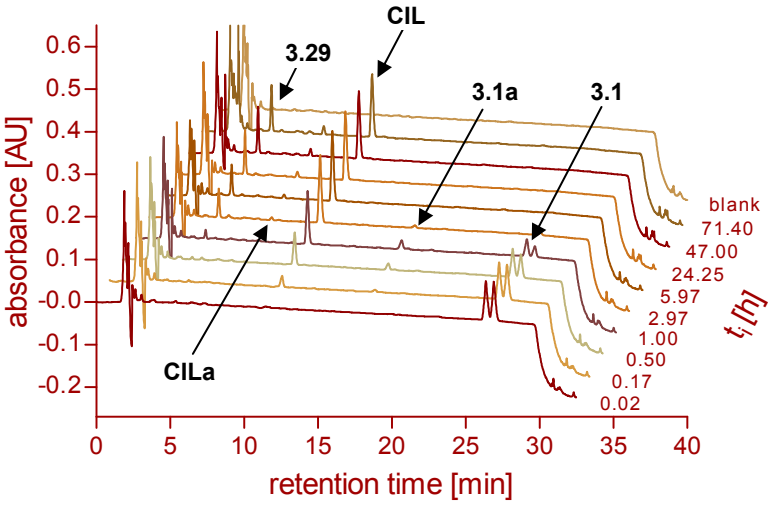

Figure 3.42. Kinetics of hydrolysis of **3.1** in human plasma.

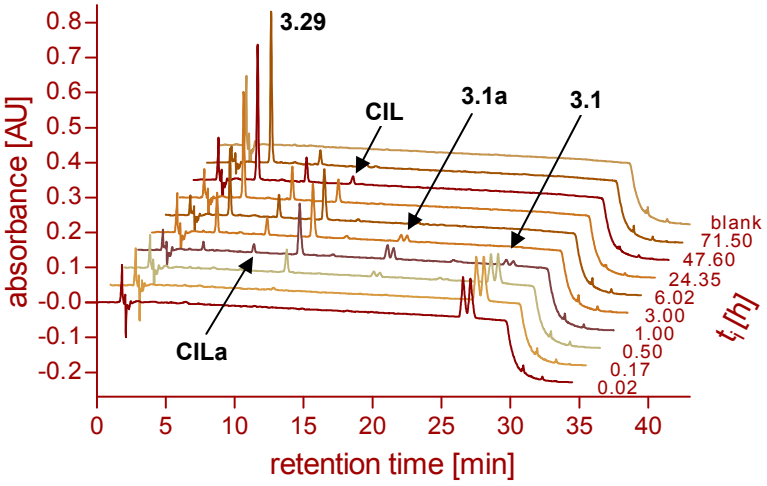

Figure 3.43. Kinetics of hydrolysis of **3.1** in the presence of porcine liver esterase.

Besides cilazapril and cilazaprilat two additional species (cf. Scheme 3.17) were detected by HPLC, which were further characterized by LC-MS (Figure 3.44). Compound **CILa** (t_R ~ 8.6 min, *m/z* 404 (MH^+)) was only detected in the incubation mixtures containing human plasma or porcine liver esterase. The molecular mass of 403 Da corresponds to a methyl ester of cilazapril, which is very likely resulting from transesterification with methanol, which was the solvent of the stock solution of **3.1** used for the aforementioned experiments. By contrast, the stock solution for the incubation with porcine skin homogenate was prepared with DMSO. However, after an initial increase, **CILa** was hydrolyzed to cilazaprilat by porcine liver esterase, whereas in the presence of human plasma the amount of **CILa** increased continuously but very slowly. The two peaks appearing at t_R ~ 19.3 min both possess a pseudomolecular ion (MH^+) at *m/z* 506. Thus, they were identified as two diastereomers of structure **3.1a**, resulting from the hydrolysis of the ethyl ester of compound **3.1**, whereas the 1-(ethoxycarbonyloxy)ethyl ester remained intact. Comparing the results from all three incubation experiments it becomes obvious, that **3.1a** was mainly formed by porcine skin homogenate, whereas in the other incubation mixtures the amounts of **3.1a** were comparably low, suggesting that the esterases present in porcine skin homogenate preferably hydrolyze the ethyl ester, whereas the enzymes in human plasma and the carboxylesterase from porcine liver tend to initially cleave the double ester pro-moiety. Furthermore, the metabolizing enzymes were apparently able to distinguish between the two diastereomers of **3.1** as well as of **3.1a**. This effect was mainly distinctive in the presence of porcine skin homogenate und human plasma.

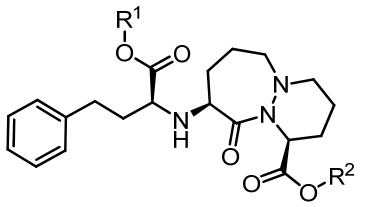

No	R^1	R^2	mass
3.1	CH_2CH_3	$CH(CH_3)OCOOCH_2CH_3$	533.3
3.1a	H	$CH(CH_3)OCOOCH_2CH_3$	505.2
CIL	CH_2CH_3	H	417.2
CILa	CH_3	H	403.2
3.29	H	H	389.2

Scheme 3.17. Structures and exact masses of **3.1** and suggested metabolites detected by LC-MS in different incubation mixtures.

The analysis of the incubation experiment in human plasma revealed a half-life of 0.58 h for **3.1** and a long $f_{50\%}$ time for cilazaprilat (154 h). On incubation with porcine liver esterase $t_{1/2}$ was estimated to be 0.67 h and the $f_{50\%}$ value for cilazaprilat amounted to 23.5 h.

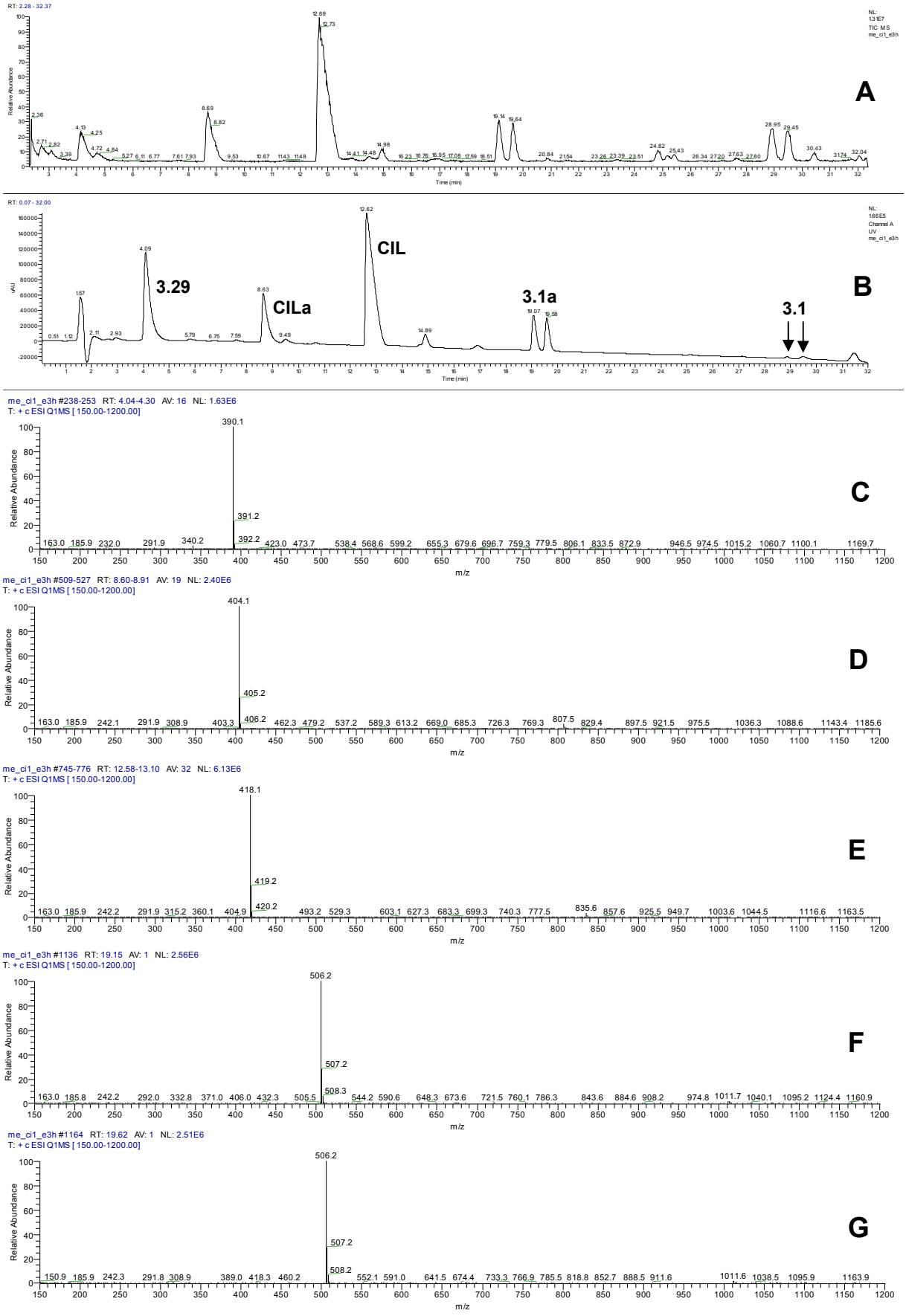

Figure 3.44. LC-MS analysis of a sample of **3.1** incubated for 3 h in the presence of porcine liver esterase. A: TIC, B: UV, C: ESI-MS spectrum of **3.29**, D: ESI-MS spectrum of **CILa**, E: ESI-MS spectrum of **CIL**, F+G: ESI-MS spectra of the two diastereomers of **3.1a**.

The half-life in the presence of porcine skin homogenate was calculated after global fitting of the data using the least square method by Levenberg-Marquardt[43-44], resulting in 0.43 h (Figure 3.45). 50 % of cilazaprilat were formed within 13.0 h.

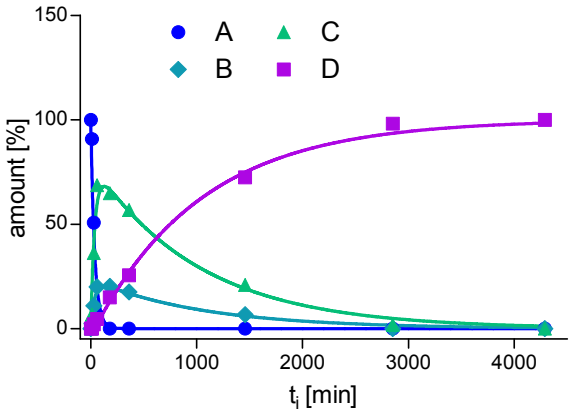

Figure 3.45. Results from a global fit of the data obtained by incubation of **3.1** with porcine skin homogenate. A: **3.1**, B: cilazapril, C: **3.1a**, D: cilazaprilat

Incubating primary human hepatocytes with **3.1** for one hour resulted in the formation of 29 % cilazapril and 36 % cilazaprilat. After an incubation period of six hours 6 % cilazapril and 86 % cilazaprilat were detected (data not shown).

Similar results as for the 1-(ethoxycarbonyloxy)ethyl ester (**3.1**) were found for cilazapril 1-(cyclohexyloxycarbonyloxy)ethyl ester (**3.2**). The hydrolysis by porcine skin homogenate (Figure 3.46) proceeded quantitatively to give cilazaprilat, but **3.2** was found to be more stable than **3.1** corresponding to a calculated half-life of 1.4 h. The $f_{50\%}$ value for cilazaprilat was lower (8.6 h). In contrast to the results for **3.1** only very small amounts of **3.2a** (cf. Scheme 3.18) (cleaved ethyl ester but intact double ester pro-moiety) were detected by HPLC and confirmed by LC-MS (cf. appendix, Figure 9.4).

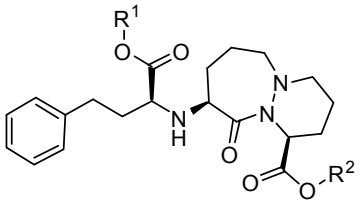

No	R^1	R^2	mass
3.2	CH_2CH_3	$CH(CH_3)OCOOCy$	587.3
3.2a	H	$CH(CH_3)OCOOCy$	559.3
CIL	CH_2CH_3	H	417.2
CILa	CH_3	H	403.2
3.29	H	H	389.2

Scheme 3.18. Structures and exact masses of **3.2** and suggested metabolites detected by LC-MS in different incubation mixtures.

The hydrolysis of **3.2** in human plasma (Figure 3.47) was markedly slower than in case of **3.1** ($t_{1/2}$ = 3.2 h, $f_{50\%\ cilazapril}$ = 4.9 h, $f_{50\%\ cilazaprilat}$ = 228 h). Compound **3.2a** was not detected, but small amounts of the methyl ester **CILa** (formed by transesterification with methanol) were found. Interestingly, comparing the respective chromatograms at t_i ~ 2.8 h (Figure 3.46 and Figure 3.47), it becomes obvious that the hydrolyzing enzymes in porcine skin homogenate prefer one of the diastereomers of **3.2** (cf. peak at longer retention time) as a substrate, whereas in human plasma the second diastereomer (cf. peak at shorter retention time) is preferably hydrolyzed.

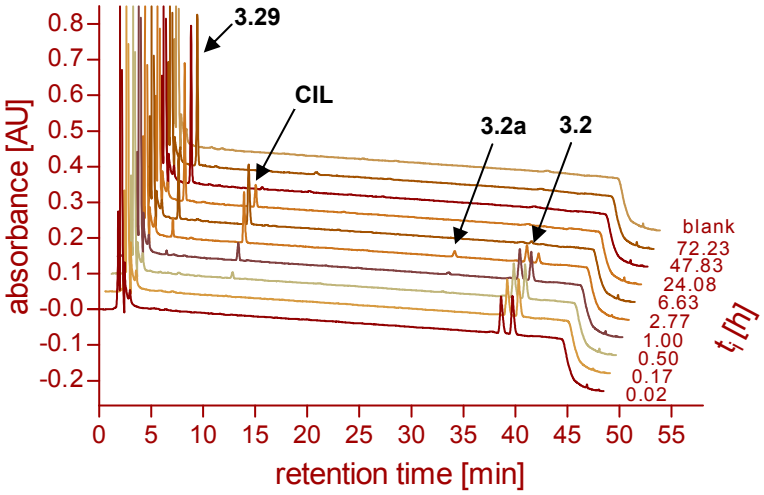

Figure 3.46. Kinetics of hydrolysis of **3.2** in porcine skin homogenate.

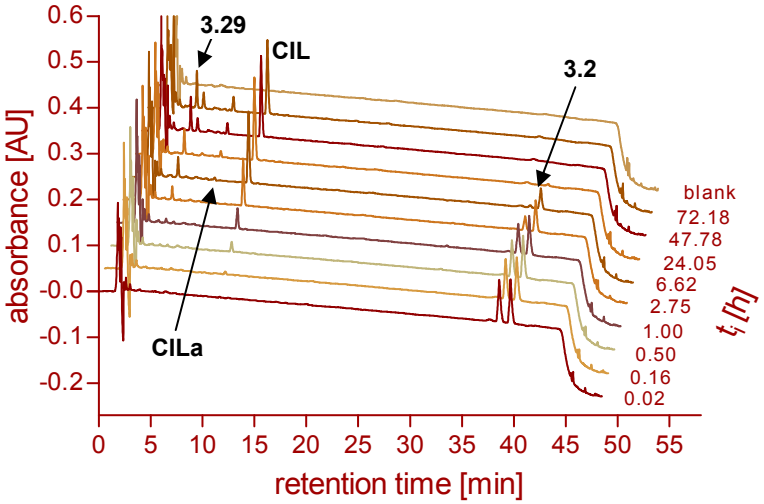

Figure 3.47. Kinetics of hydrolysis of **3.2** in human plasma.

Porcine liver esterase (Figure 3.48) completely hydrolyzed **3.2** to cilazapril and cilazaprilat within approximately 24 h. The half-life was estimated to be 4.2 h and the $f_{50\%\ cilazaprilat}$ amounted to 62.2 h. Again, defined amounts of the methyl ester **CILa** were identified, whereas **3.2a** was not detected.

Primary human hepatocytes hydrolyzed **3.2** at similar rate as **3.1**. After an incubation period of one hour 40 % cilazapril and 42 % cilazaprilat were detected. Incubation for six hours led to the formation of 19 % cilazapril and 81 % cilazaprilat (data not shown).

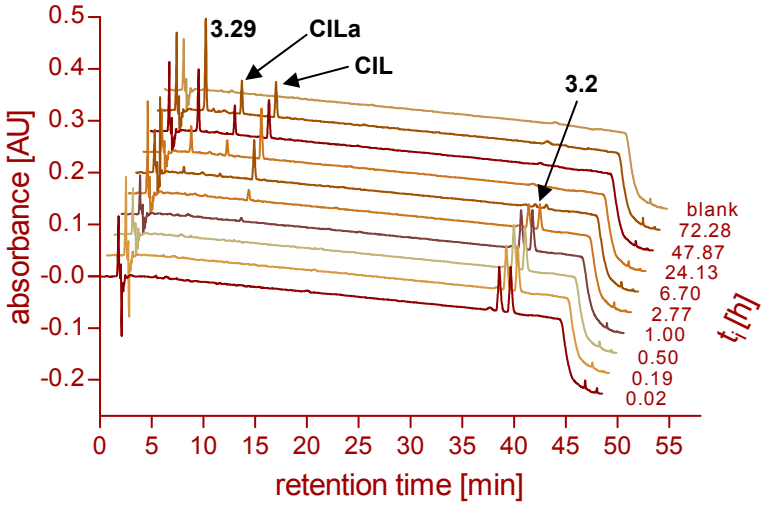

Figure 3.48. Kinetics of hydrolysis of **3.2** in the presence of porcine liver esterase.

In terms of stability against enzymatic hydrolysis cilazapril 1-(isopropyloxycarbonyloxy)ethyl ester (**3.3**) is ranking between the 1-(ethoxycarbonyloxy)ethyl ester (**3.1**) and the 1-(cyclohexyloxycarbonyloxy)ethyl ester (**3.2**). Following half-lives were determined: $t_{1/2}$ = 1.0 h (porcine skin homogenate), $t_{1/2}$ = 1.9 h (human plasma), $t_{1/2}$ = 1.5 h (porcine liver esterase). The hydrolysis of **3.3** by porcine skin homogenate gave cilazaprilat (**3.29**) as final product ($f_{50\%\ cilazaprilat}$ = 11.3 h). Furthermore, the appearance of the intermediate species **3.3a** (two diastereomers, cf. Scheme 3.19) was observed (Figure 3.49).

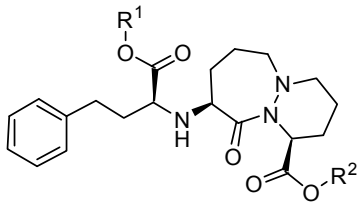

No	R^1	R^2
3.3	CH_2CH_3	$CH(CH_3)OCOO^iPr$
3.3a	H	$CH(CH_3)OCOO^iPr$
CIL	CH_2CH_3	H
CILa	CH_3	H
3.29	H	H

Scheme 3.19. Structures of putative metabolites of **3.3** detected by LC-MS in different incubation mixtures.

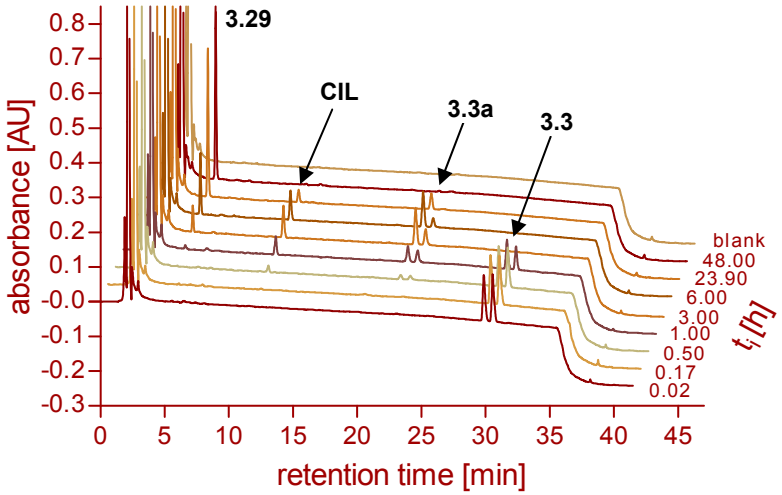

Figure 3.49. Examples of HPLC chromatograms illustrating the kinetics of hydrolysis of **3.3** in porcine skin homogenate.

In human plasma the enzymatic hydrolysis of **3.3** resulted in the formation of cilazapril ($f_{50\%\ cilazapril}$ = 5.4 h) and cilazaprilat ($f_{50\%\ cilazaprilat}$ = 108 h). Moreover, small amounts of the methyl ester **CILa** and the intermediate **3.3a** were detected (Figure 3.50). By analogy with the cleavage of **3.2**, preferred hydrolysis of one or the other diastereomer of **3.3** by human plasma or by porcine skin homogenate is clearly evident from HPLC analysis.
The results from the incubation of **3.3** with porcine liver esterase were very similar to the ones found for **3.1**. The hydrolysis gave cilazaprilat (**3.29**) as major product. The $f_{50\%}$ value for cilazaprilat amounted to 14.2 h. Again, minor amounts of **3.3a** and **CILa** were detected. The discrimination between the two diastereomers of **3.3** is marginal (Figure 3.51).

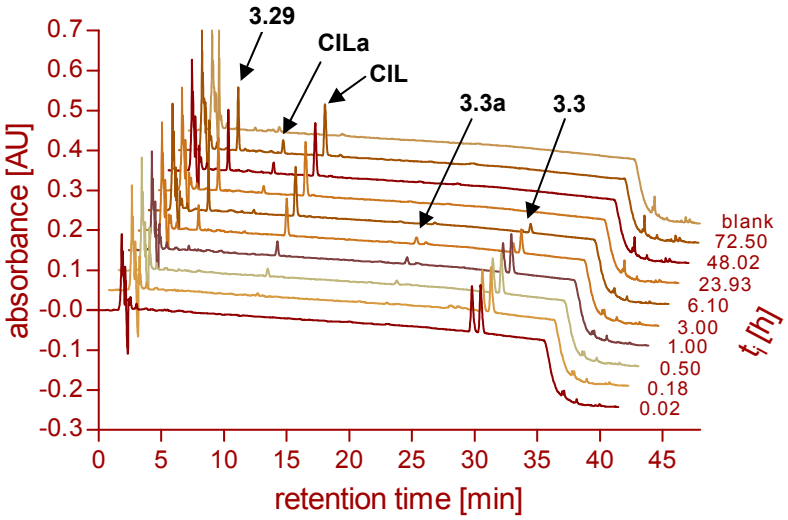

Figure 3.50. Kinetics of hydrolysis of **3.3** in human plasma.

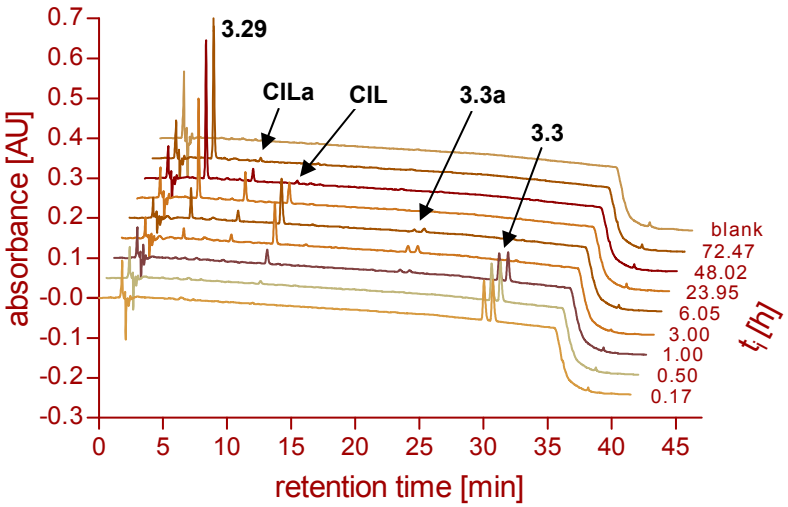

Figure 3.51. Kinetics of hydrolysis of **3.3** in the presence of porcine liver esterase.

Upon incubation with primary human hepatocytes, after an incubation period of six hours nearly the same amounts of cilazapril (6 %) and cilazaprilat (89 %) were found as for **3.1**. After one hour 33 % cilazapril and 28 % cilazaprilat were formed (data not shown).

Cilazapril 1-(acetoxy)ethyl ester (**3.6**) turned out to possess rather short half-lives in all enzyme-containing incubation mixtures. The $t_{1/2}$ values were more or less in the same range as those calculated for **3.1**. In human plasma $t_{1/2}$ of **3.6** amounted to 0.68 h and in the presence of porcine liver esterase $t_{1/2}$ was estimated to be 0.63 h. The half-life in porcine skin homogenate was calculated after global fitting of the data using the least square method by Levenberg-Marquardt[43-44]. In this case two very similar results (0.50 h and 0.53 h) were obtained, although two different starting conditions were used for the fit (Figure 3.52 and Figure 3.53).

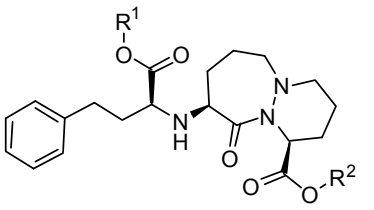

No	R^1	R^2
3.6	CH_2CH_3	$CH(CH_3)OCOCH_3$
3.6a	H	$CH(CH_3)OCOCH_3$
CIL	CH_2CH_3	H
CILa	CH_3	H
3.29	H	H

Scheme 3.20. Structures of **3.6** and putative metabolites of **3.6** detected in different incubation mixtures.

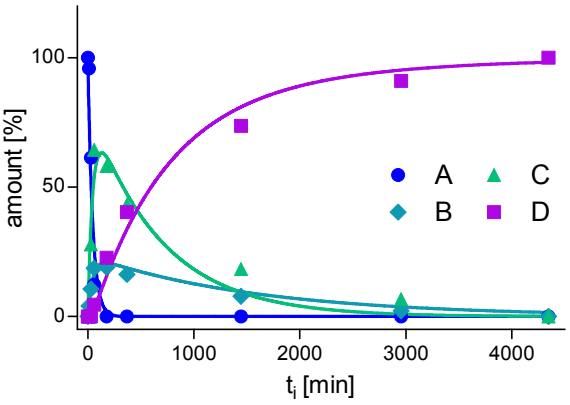

Figure 3.52. Solution 1 of a global fit of the data obtained by incubation of **3.6** with porcine skin homogenate. A: **3.6**, B: cilazapril, C: **3.6a**, D: cilazaprilat.

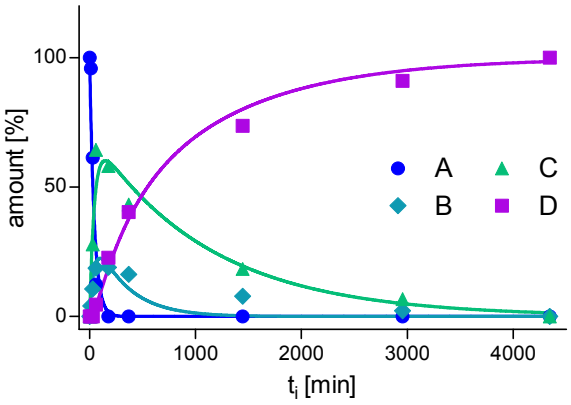

Figure 3.53. Solution 2 of a global fit of the data obtained by incubation of **3.6** with porcine skin homogenate. A: **3.6**, B: cilazapril, C: **3.6a**, D: cilazaprilat.

3.6 was completely hydrolyzed to cilazaprilat (**3.29**) by porcine skin homogenate within 72 h (Figure 3.54). The $f_{50\%}$ of cilazaprilat was estimated to be 14.0 h.

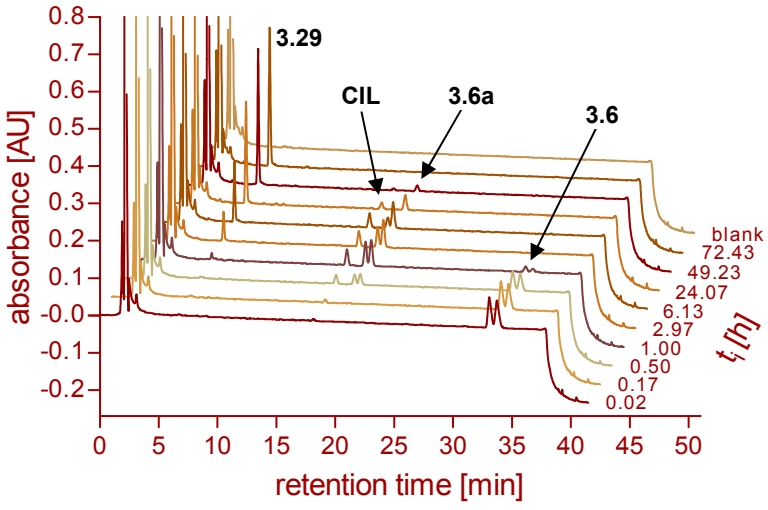

Figure 3.54. Kinetics of hydrolysis of **3.6** in porcine skin homogenate.

In human plasma the formation of 50 % of cilazapril was comparably fast ($f_{50\%\ cilazapril}$ = 2.2 h), whereas the subsequent hydrolysis to cilazaprilat was rather slow ($f_{50\%\ cilazaprilat}$ = 91.2 h) (Figure 3.55). The hydrolysis catalyzed by porcine liver esterase resulted in the formation of 100 % of cilazaprilat within approximately 50 h ($f_{50\%}$ = 9.7 h) (Figure 3.56).

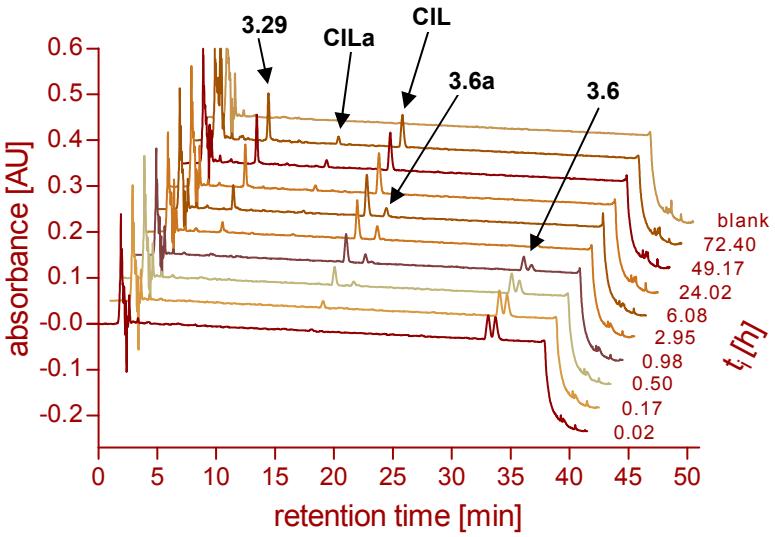

Figure 3.55. Kinetics of hydrolysis of **3.6** in human plasma.

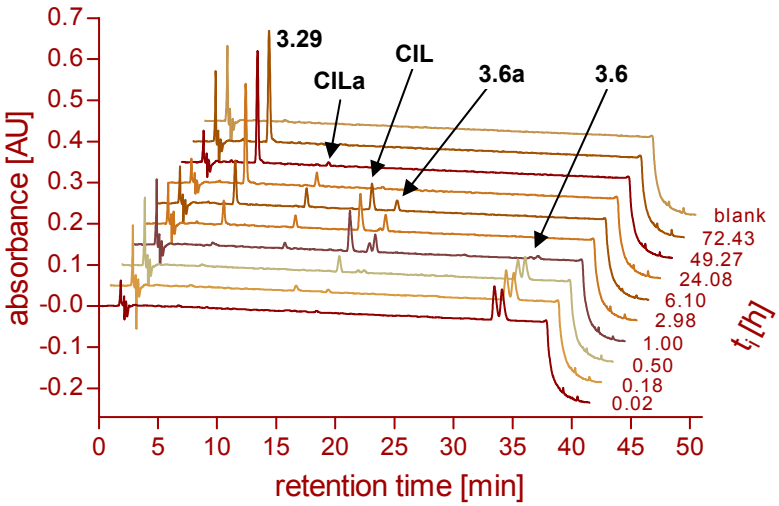

Figure 3.56. Kinetics of hydrolysis of **3.6** in the presence of porcine liver esterase.

As described above for the cilazapril prodrugs **3.1**-**3.3** an intermediate (**3.6a**, two diastereomers, cf. Scheme 3.20) was also detected in all three incubation mixtures, whereas the methyl ester **CILa** only appeared in the samples containing human plasma or porcine liver esterase.

Similar values for the metabolism of **3.6** by primary human hepatocytes were found as for the aforementioned cilazapril prodrugs. After an incubation period of one hour 38 % cilazapril and 24 % cilazaprilat were detected. Incubation for six hours led to the formation of 7 % cilazapril and 82 % cilazaprilat (data not shown).

The exchange of the 1-(acetoxy)ethyl moiety in **3.6** against a 1-(2,2-dimethylpropanoyl)ethyl group led to a considerably increase in stability of compound **3.7** against enzymatic hydrolysis. Following half-life times were calculated: $t_{1/2}$ = 1.0 h in porcine skin homogenate, $t_{1/2}$ = 5.1 h in human plasma and $t_{1/2}$ = 3.8 h in the presence of porcine liver esterase.

Cilazapril 1-(2,2-dimethylpropanoyl)ethyl ester (**3.7**) was quantitatively hydrolyzed to cilazaprilat (**3.29**) in porcine skin homogenate ($f_{50\%\ (cilazaprilat)}$ = 11.5 h). Evidently, either only one diastereomer of the intermediate product **3.7a** was preferably formed or the other one was rapidly further hydrolyzed to cilazaprilat (Figure 3.57).

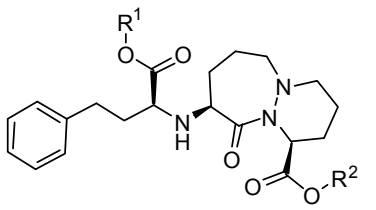

No	R^1	R^2
3.7	CH_2CH_3	$CH(CH_3)OCO^tBu$
3.7a	H	$CH(CH_3)OCO^tBu$
CIL	CH_2CH_3	H
CILa	CH_3	H
3.29	H	H

Scheme 3.21. Structures of **3.7** and putative metabolites of **3.7** detected in different incubation mixtures.

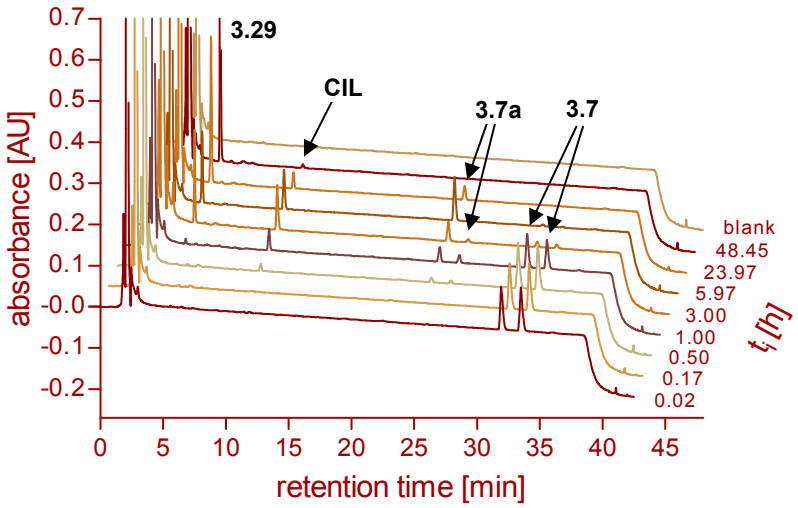

Figure 3.57. Examples of HPLC chromatograms showing the kinetics of hydrolysis of **3.7** in porcine skin homogenate.

The hydrolysis of **3.7** in human plasma resulted in the formation of cilazapril and cilazaprilat. The time required to obtain 50 % of cilazaprilat was estimated to be 33.6 h. Furthermore, small amounts of the methyl ester **CILa** were detected. The discriminative conversion of the two diastereomers of **3.7** and **3.7a**, respectively, was clearly evident from HPLC analysis (Figure 3.58).

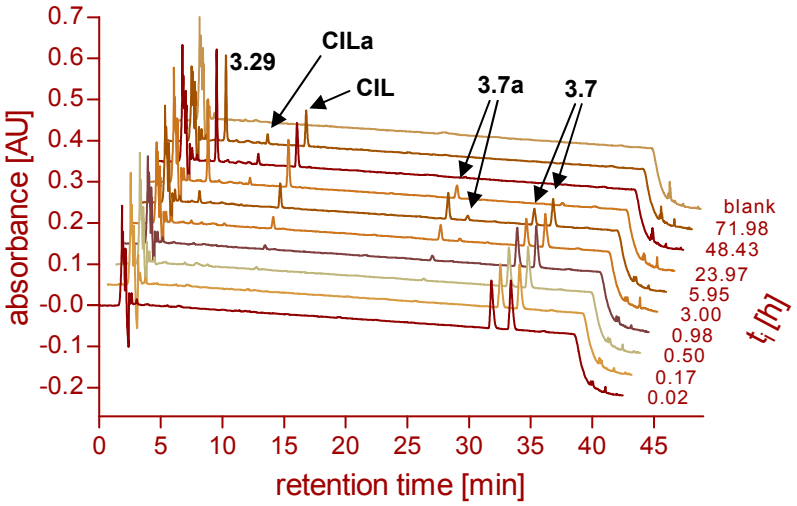

Figure 3.58. Kinetics of hydrolysis of **3.7** in human plasma.

Also porcine liver esterase was capable of hydrolyzing **3.7** to cilazaprilat ($f_{50\%}$ = 16.3 h). In contrast to the results from the incubation with porcine skin homogenate and human plasma hardly any intermediate **3.7a** was detected. However, considerable amounts of the methyl ester **CILa** were identified, which were subsequently hydrolyzed to cilazaprilat (Figure 3.59).

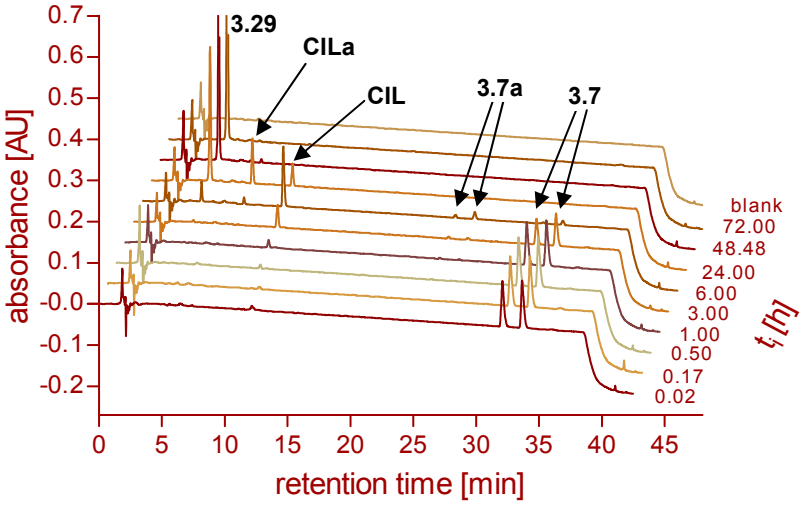

Figure 3.59. Kinetics of hydrolysis of **3.7** in buffered porcine liver esterase.

On incubation with primary human hepatocytes 19 % of cilazapril and 13 % of cilazaprilat were found after one hour. Finally, after an incubation period of six hours the amount of cilazapril decreased to 10 %, whereas the amount of cilazaprilat increased to 72 % (data not shown).

The kinetics of hydrolysis of cilazapril (5-methyl-2-oxo-1,3-dioxol-4-yl)methyl ester (**3.12**) in the presence of porcine skin homogenate, porcine liver esterase and human plasma is shown in Figure 3.60 to Figure 3.62. In all cases cilazapril (**CIL**) and cilazaprilat (**3.29**) were found to be the only products of hydrolysis of **3.12**.

In the incubation mixture containing porcine skin homogenate as well as in the presence of porcine liver esterase the same half-life for **3.12** was determined ($t_{1/2}$ = 1.8 h). As this value is lower than the calculated half-life in buffer (3.7 h) the hydrolysis of the (5-methyl-2-oxo-1,3-dioxol-4-yl)methyl ester pro-moiety must be partly enzymatically catalyzed. Thereby it remains unclear, whether the esterases in porcine skin homogenate and carboxylesterase from porcine liver brake down the pro-moiety at the 5-methyl-2-oxo-1,3-dioxol-4-yl group or directly cleave the ester bond adjacent to the heterocyclic cilazapril core structure. The time, in which 50 % of cilazaprilat were formed, was estimated to be 10.4 h in porcine skin homogenate and 4.3 h in the presence of porcine liver esterase.

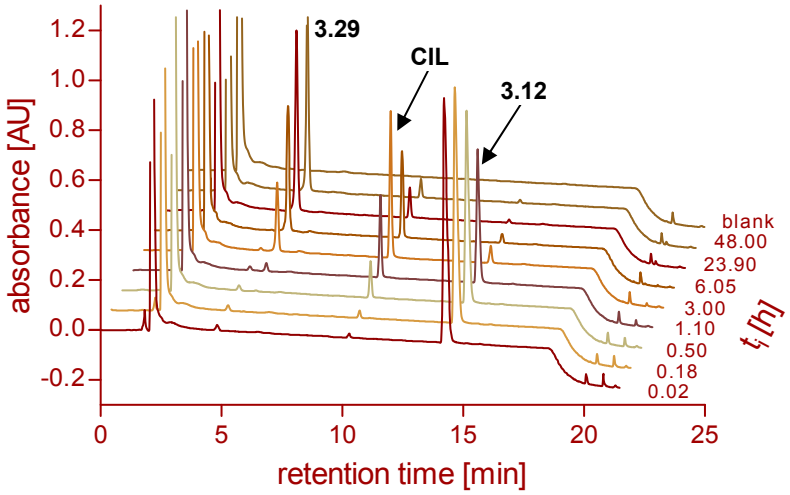

Figure 3.60. Examples of HPLC chromatograms depicting the kinetics of hydrolysis of **3.12** in porcine skin homogenate.

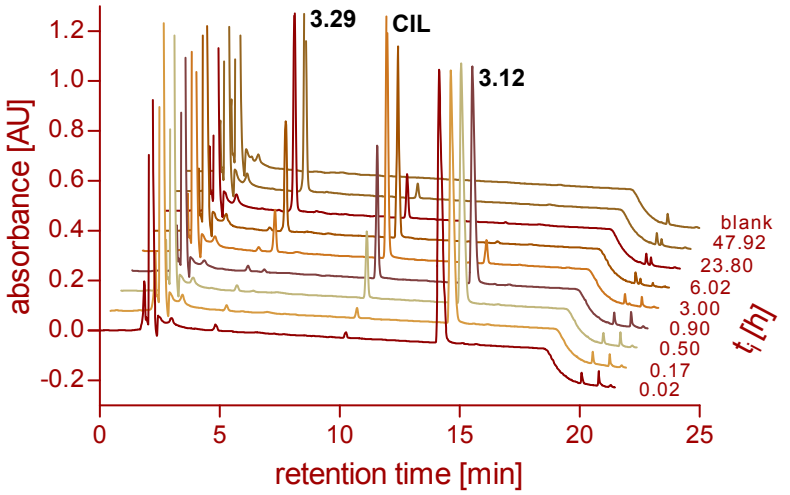

Figure 3.61. Examples of HPLC chromatograms showing the kinetics of hydrolysis of **3.12** in the presence of porcine liver esterase.

According to the results for candesartan (5-methyl-2-oxo-1,3-dioxol-4-yl)methyl ester **3.33** the hydrolysis of **3.12** in human plasma yielding cilazapril was extraordinarily fast ($t_{1/2}$ = 5 min). Presumably, this can be attributed to the high activity of human serum paraoxonase. However, the subsequent conversion to cilazaprilat turned out to be rather slow ($f_{50\%}$ = 250 h).

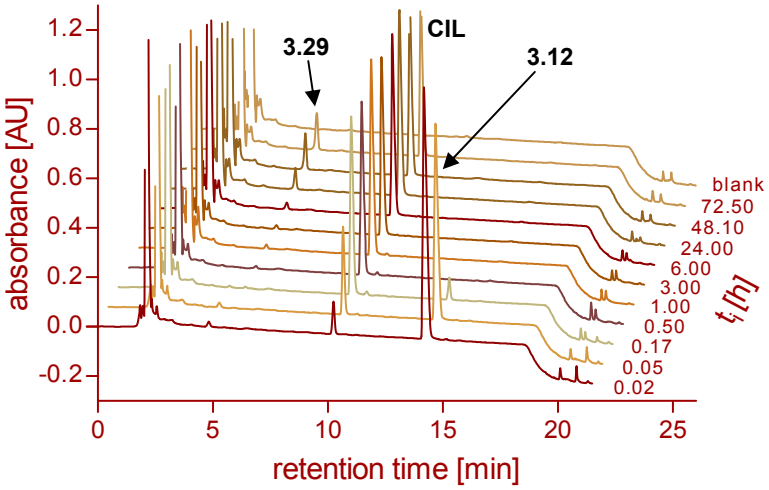

Figure 3.62. Kinetics of hydrolysis of **3.12** in human plasma.

Incubation of **3.12** with primary human hepatocytes resulted in the formation of 66 % cilazapril and 34 % cilazaprilat within one hour. After six hours 15 % cilazapril and 85 % cilazaprilat were detected (data not shown).

Cilazapril (5-*tert*-butyl-2-oxo-1,3-dioxol-4-yl)methyl ester (**3.13**) was completely hydrolyzed to cilazaprilat (**3.29**) by porcine skin homogenate ($t_{1/2}$ = 1.3 h, $f_{50\%\ cilazaprilat}$ = 12.8 h) and porcine liver esterase ($t_{1/2}$ = 4.2 h, $f_{50\%\ cilazaprilat}$ = 5.5 h) within 72 h (cf. Figure 3.63 and Figure 3.64). In contrast to **3.12** cilazapril was not detected as an intermediate product, instead a compound (**3.13a**) resulting from the cleavage of the ethyl ester appeared to be the exclusive intermediate (cf. Scheme 3.22).

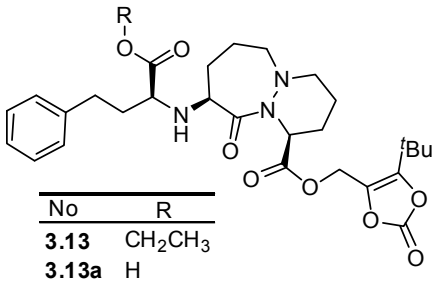

Scheme 3.22. Structure of **3.13** and the putative metabolite **3.13a**.

The exchange of the methyl group against a bulkier *tert*-butyl residue in the (5-alkyl-2-oxo-1,3-dioxol-4-yl)methyl pro-moiety led to a 4-fold increase in stability against enzymatic hydrolysis in human plasma ($t_{1/2}$ = 0.35 h) (Figure 3.65). In contrast to the hydrolysis in porcine skin homogenate and in buffered porcine liver esterase cilazapril (**CIL**) was detected as the main intermediate. The conversion to cilazaprilat was still comparably slow ($f_{50\%}$ = 186 h). Also the enzymes present in primary human hepatocytes were capable of cleaving both ester functions to yield cilazaprilat (data not shown). After an

incubation period of one hour 24 % cilazapril and 42 % cilazaprilat were detected, whereas after six hours the hydrolysis to cilazaprilat was almost complete (cilazapril: 6 %, cilazaprilat: 94 %).

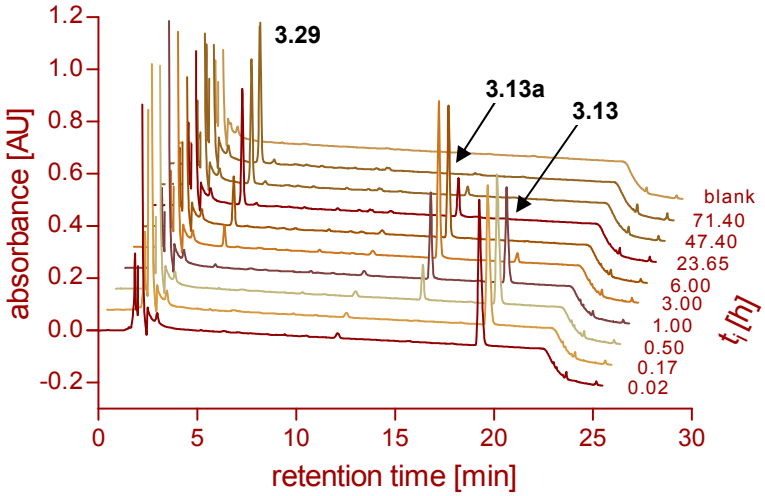

Figure 3.63. Kinetics of hydrolysis of **3.13** in porcine skin homogenate.

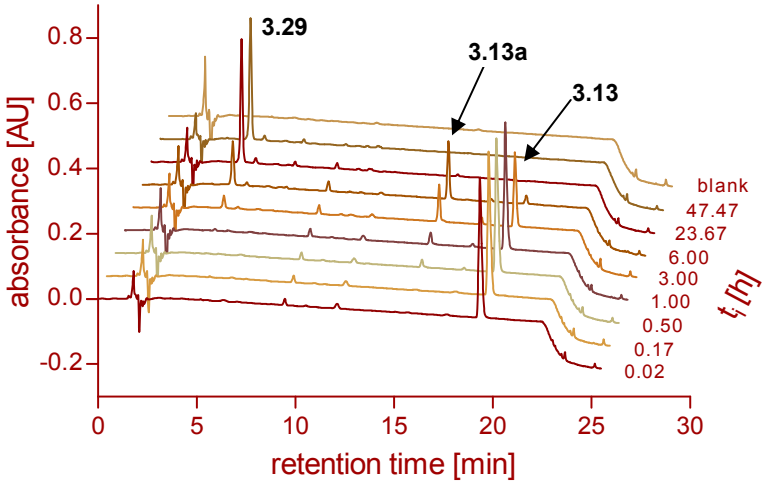

Figure 3.64. Examples of HPLC chromatograms showing the kinetics of hydrolysis of **3.13** in buffered porcine liver esterase.

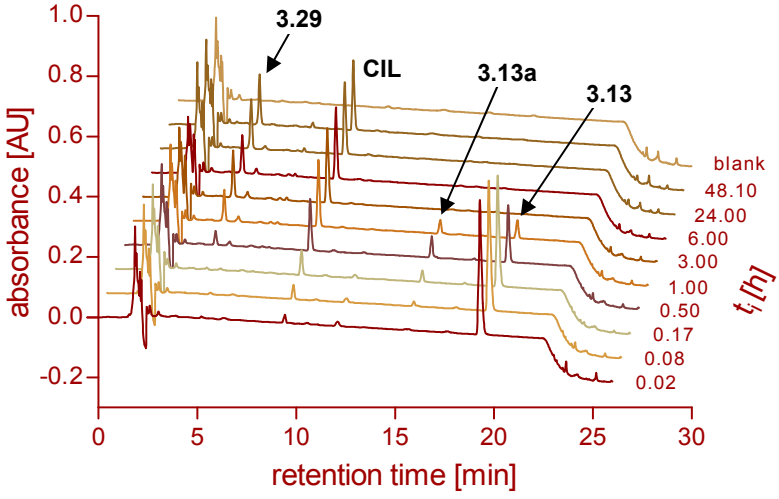

Figure 3.65. Examples of HPLC chromatograms showing the kinetics of hydrolysis of **3.13** in human plasma.

The kinetics of hydrolysis of the *N*-aryl-*N*-alkyloxycarbonylaminomethyl (NArNAOCAM) derivatives of cilazapril (**3.25**-**3.27**) could not be analyzed using the simplified model described at the beginning of this chapter. Determination of the half-life by linearization of the data failed in most of the cases, because the crucial step for the break-down of these pro-moieties is supposed to be based on chemical hydrolysis, whereas, simultaneously, present ethyl ester groups are cleaved enzymatically. Hence, the observed total hydrolysis is composed of the respective fractions of chemical and enzymatic hydrolysis. Moreover, the NArNAOCAM prodrugs turned out to be highly prone to hydrolysis in acidic medium. As the samples taken from the respective incubation mixtures were diluted with mobile phase (MeCN/ 0.05 % TFA) prior to HPLC analysis, it was necessary to perform the chromatographic separation immediately after dilution. Preparation without the addition of 0.05 % TFA resulted in the formation of broad double peaks due to insufficient protonation of the analyte.
In the following, the behavior of the cilazapril NArNAOCAM prodrugs (**3.25**-**3.27**) on incubation with porcine skin homogenate, human plasma and porcine liver esterase is presented. In all three incubation mixtures **3.25**, **3.26** and **3.27** were hydrolyzed to yield cilazapril and cilazaprilat. Special effort was put on the identification of unexpected peaks in the chromatograms be means of LC-MS coupling.

In porcine skin homogenate **3.25** was hydrolyzed to cilazapril (t_R ~ 9.4 min) and cilazaprilat (t_R ~ 4.6 min) (Figure 3.66). A third peak at t_R ~ 13.9 min was afterwards identified as ethyl phenylcarbamate (**EPC**) by LC-MS. The half-life of **3.25** could not be calculated by linear regression, but was estimated to be 28 h. Similar results were obtained for the incubation in the presence of porcine liver esterase ($t_{1/2}$ ~ 4 h, cf. appendix, Figure 9.5).

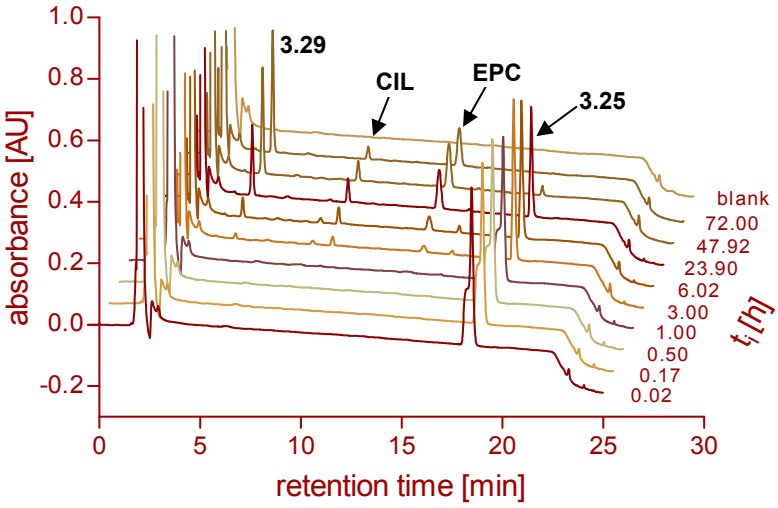

Figure 3.66. Kinetics of hydrolysis of **3.25** in porcine skin homogenate.

Also in human plasma cilazapril and cilazaprilat were observed as products of hydrolysis (Figure 3.67). In this case the data for the kinetics of degradation of **3.25** could be linearized resulting in a calculated $t_{1/2}$ value of 4.1 h.

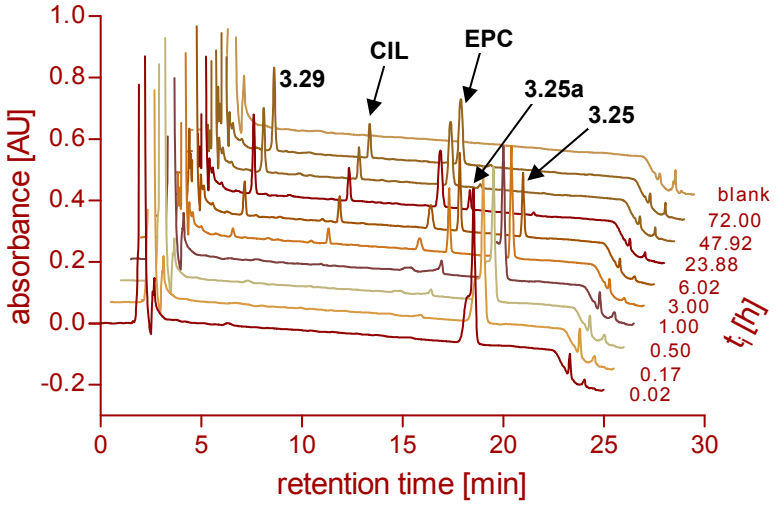

Figure 3.67. Kinetics of hydrolysis of **3.25** in human plasma.

Besides cilazapril and cilazaprilat two additional products were detected and further characterized by LC-MS (data not shown). The peak at t_R ~ 13.9 min corresponded to a pseudomolecular ion (MH^+) at *m/z* 166, presumably referring to ethyl phenylcarbamate (**EPC**), which is a degradation product of the NArNAOCAM pro-moiety. The intermediately formed product **3.25a**, detected at t_R ~ 15.3 min and corresponding to a pseudomolecular ion (MH^+) at *m/z* 567, supposedly resulted from the hydrolysis of the homophenylalanine ethyl ester in **3.25**. Cleavage of the ethyl carbamate would give the same molecular mass, but result in a highly unstable and therefore most probably undetectable carbamic acid.

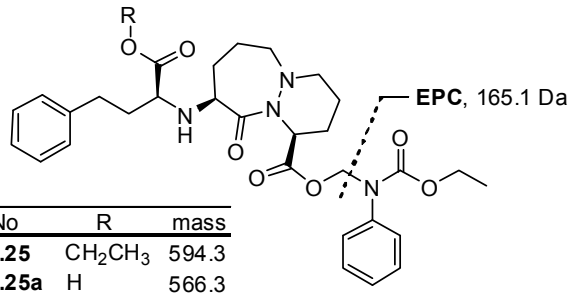

No	R	mass
3.25	CH_2CH_3	594.3
3.25a	H	566.3

Scheme 3.23. Structures and exact masses of **3.25** and potential metabolites of **3.25**.

Incubation of the cilazapril NArNAOCAM prodrug **3.26** with porcine skin homogenate (Figure 3.68) and porcine liver esterase (cf. appendix, Figure 9.6), respectively, gave cilazaprilat (t_R ~ 4.6 min), whereas on incubation with human plasma (Figure 3.69) both cilazaprilat and cilazapril (t_R ~ 9.4 min) could be detected. Furthermore, in all three incubation mixtures a compound was detected at t_R ~ 7.7 min, corresponding to a molecular ion of 453 Da in LC-MS analysis. This compound could only be poorly ionized in the MS resulting in very low signal intensity. Unfortunately, this peak could not be referred to any imaginable degradation product. However, on incubation with human plasma two additional species (t_R ~ 15.2 min and t_R ~ 17.6 min) with the same corresponding pseudomolecular ion (MH^+) at *m/z* 639 were detected. On incubation with porcine skin homogenate and porcine liver esterase, respectively, only one of these molecular species (t_R ~ 17.6 min) was found. Presumably, the formation of these compounds can be explained by enzymatic hydrolysis of the homophenylalanine ethyl ester, resulting in **3.26a**, or the benzoic acid ethyl ester yielding **3.26b**. Furthermore, at t_R ~ 18.9 min small amounts of a compound were detected, which possessed a pseudomolecular ion (MH^+) at *m/z* 238, probably corresponding to ethyl 4-(ethoxycarbonylamino)benzoate (**3.26c**) formed by hydrolysis of the NArNAOCAM pro-moiety (cf. Scheme 3.24).

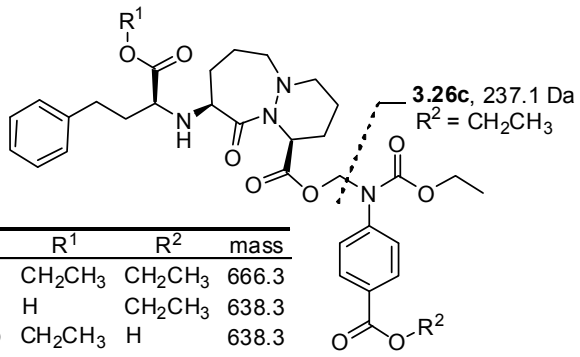

No	R^1	R^2	mass
3.26	CH_2CH_3	CH_2CH_3	666.3
3.26a	H	CH_2CH_3	638.3
3.26b	CH_2CH_3	H	638.3

Scheme 3.24. Structures and exact masses of **3.26** and of potential metabolites of **3.26**.

The half-life of **3.26** in human plasma was calculated to be 5.6 h. In porcine skin homogenate and in the presence of porcine liver esterase the respective $t_{1/2}$ was estimated to be 4 h and 5 h, respectively.

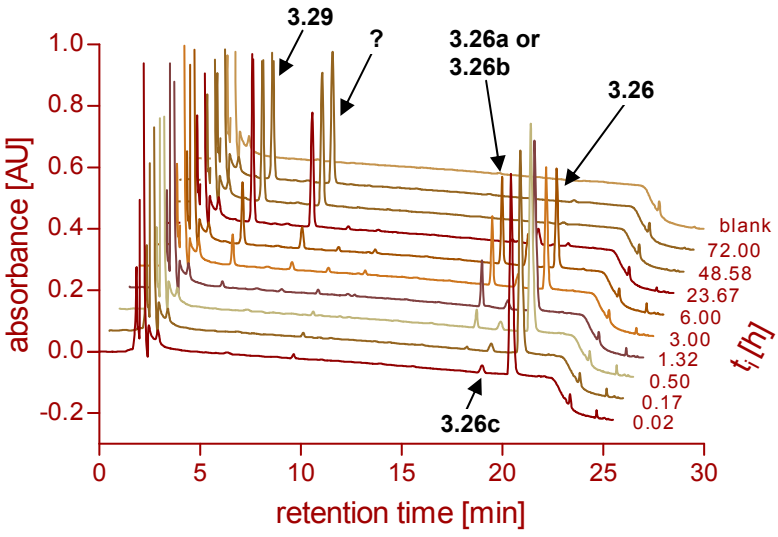

Figure 3.68. Kinetics of hydrolysis of **3.26** in porcine skin homogenate.

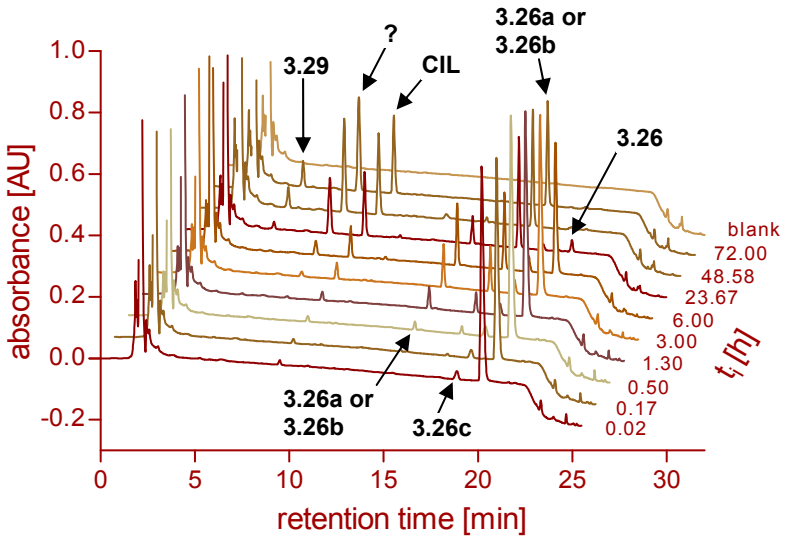

Figure 3.69. Kinetics of hydrolysis of **3.26** in human plasma.

The methyl carbamate analogue **3.27** was found to be hydrolyzed analogously to **3.26** (cf. appendix, Figure 9.7-Figure 9.9). Besides cilazaprilat and cilazapril two compounds having the same molecular mass (625 Da, MH^+) were identified by LC-MS as intermediates resulting from the hydrolysis of the homophenylalanine ethyl ester (**3.27a**) or the benzoic acid ethyl ester (**3.27b**) (cf. Scheme 3.25). Moreover, LC-MS of a sample of **3.27** incubated for 24 h with human plasma revealed small amounts of the degradation product **3.27c** (224 Da, MH^+).

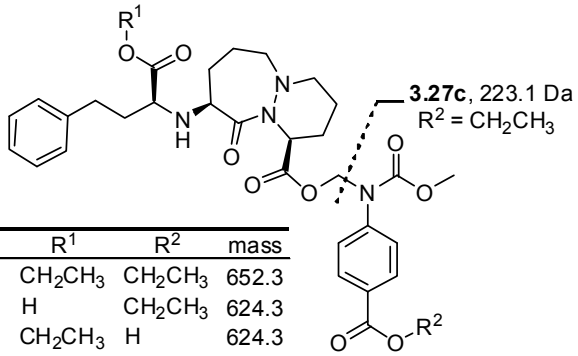

No	R^1	R^2	mass
3.27	CH_2CH_3	CH_2CH_3	652.3
3.27a	H	CH_2CH_3	624.3
3.27b	CH_2CH_3	H	624.3

Scheme 3.25. Structures and exact masses of **3.27** and of potential metabolites of **3.27**.

For the degradation in human plasma the half-life of **3.27**, calculated by linear regression, amounted to 5.2 h. For incubation with porcine skin homogenate and porcine liver esterase the half-life of **3.27** was estimated to be 16 h and 3 h, respectively.

Cilazapril morpholinoethyl ester (**3.14**) was completely hydrolyzed in all three enzyme-containing incubation mixtures (Figure 3.70 to Figure 3.72). However, in contrast to chemical hydrolysis in buffer enzymatic hydrolysis of **3.14** was found to mainly take place at the ethyl ester instead of the morpholinoethyl ester. Hence, during the incubation with porcine skin homogenate cilazapril could not be detected as an intermediate. Only very small amounts of cilazapril (t_R ~ 22.2 min) were detectable in the incubation mixtures containing human plasma and porcine liver esterase, respectively. In all three incubation mixtures compound **3.14a** (t_R ~ 4.7 min) was found as the main intermediate of hydrolysis, which was supposed to derive from **3.14** by cleavage of the ethyl ester. Minor amounts of **3.14b**, supposedly the methyl ester of **3.14**, most likely formed by transesterification of the ethyl ester in **3.14** with methanol, were detected, when methanol-containing stock solutions were used (i.e. human plasma, porcine liver esterase). To further corroborate these assumptions LC-MS studies were performed (cf. appendix, Figure 9.10).

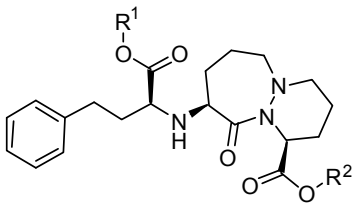

No	R^1	R^2	mass
3.14	CH_2CH_3	CH_2CH_2mo	530.3
3.14a	H	CH_2CH_2mo	502.3
3.14b	CH_3	CH_2CH_2mo	516.3
CIL	CH_2CH_3	H	417.2
3.29	H	H	389.2

Scheme 3.26. Exact masses of **3.14** and of its presumable metabolites observed in different incubation mixtures.

In porcine skin homogenate a fast hydrolysis of **3.14** to **3.14a** was observed ($t_{1/2}$ = 0.50 h) followed by conversion of **3.14a** to cilazaprilat ($f_{50\%}$ = 6.3 h) (Figure 3.70). On incubation with human plasma the half-life of **3.14** was estimated to be 1.3 h. 50 % of cilazaprilat were formed after 10.8 h (Figure 3.71).

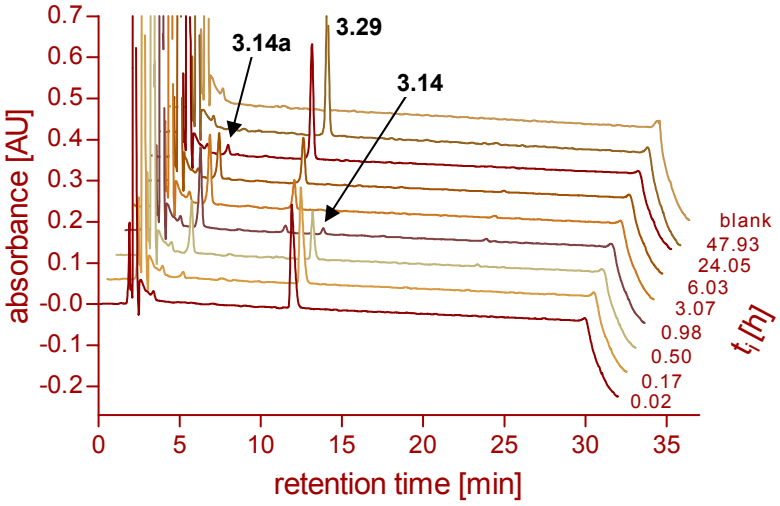

Figure 3.70. Examples of HPLC chromatograms showing the kinetics of hydrolysis of **3.14** in porcine skin homogenate.

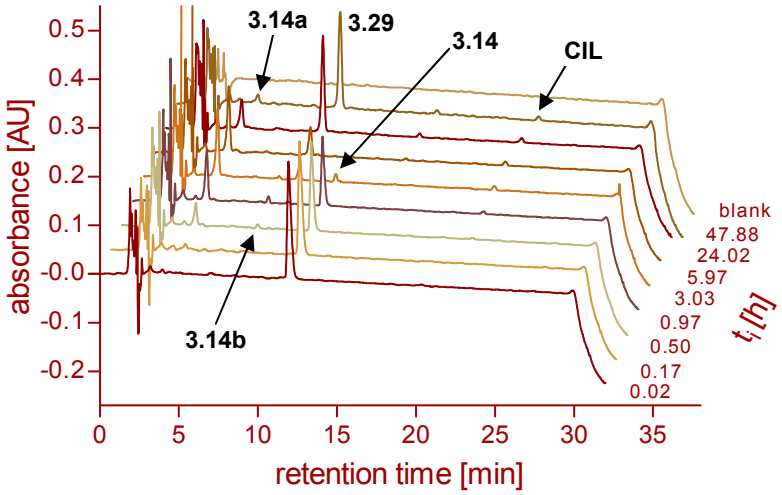

Figure 3.71. Examples of HPLC chromatograms showing the kinetics of hydrolysis of **3.14** in human plasma.

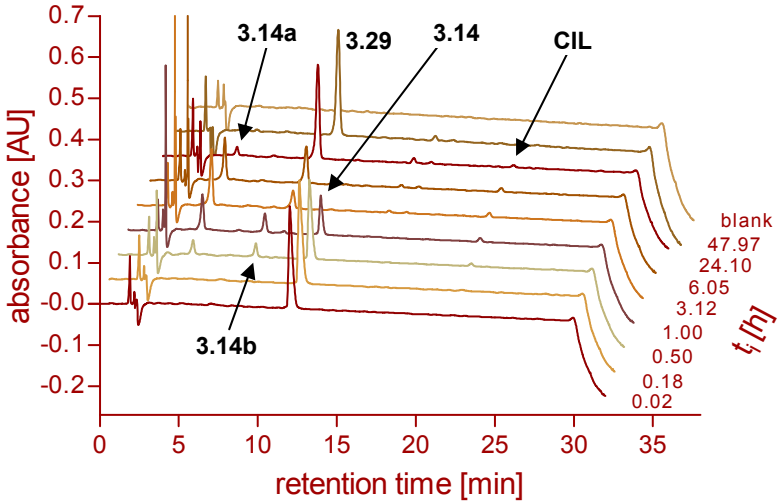

Figure 3.72. Examples of HPLC chromatograms showing the kinetics of hydrolysis of **3.14** in buffered porcine liver esterase.

The half-life of **3.14** in the presence of porcine liver esterase was calculated by global fitting of the data using the least square method by Levenberg-Marquardt[43-44] (Figure 3.73). The $t_{1/2}$ value amounted to 0.95 h. The $f_{50\%}$ value of cilazaprilat was estimated to be 7.5 h.

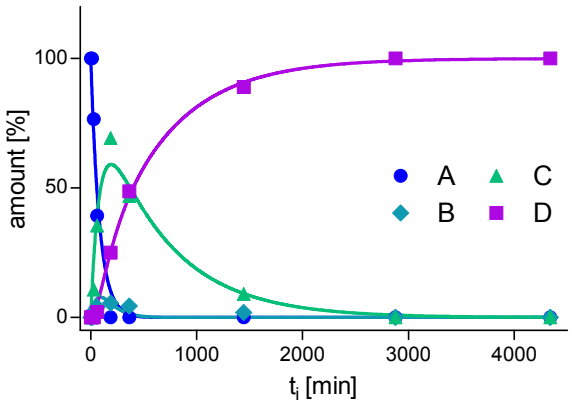

Figure 3.73. Reaction kinetics of **3.14** on incubation with buffered porcine live resterase. Results from global fitting of the data. A: **3.14**, B: cilazapril, C: **3.14a**, D: cilazaprilat.

Also primary human hepatocytes initially cleaved the ethyl ester instead of the morpholinoethyl ester (data not shown). After an incubation period of one hour 6 % of cilazapril and 56 % of **3.14a** were detected. After six hours the amounts of cilazapril and **3.14a** were calculated to 1 % and 54 %, respectively. However, the amount of cilazaprilat increased from 9 % after one hour to 45 % after six hours of incubation.

HPLC-analysis of cilazapril 1-(2-morpholinoacetoxy)ethyl ester (**3.18**) subjected to enzymatic cleavage revealed four different, molecular species (cf. Scheme 3.27). Besides two peaks (t_R ~ 16.1, 16.3 min) referring to the two diastereomers of the prodrug **3.18** and two peaks at t_R ~ 11.7 min and 12.0 min, cilazapril (**CIL**, t_R ~ 18.6 min) as well as cilazaprilat (**3.29**, t_R ~ 13.0 min) were detected. LC-MS analysis (data not shown) of a sample of **3.18** incubated for 30 min with porcine liver esterase revealed a pseudomolecular ion (MH^+) at *m/z* 561 for the compounds detected at t_R ~ 11.7 min and t_R ~ 12.0 min, which were identified as the diastereomeric pair of structure **3.18a** resulting from the hydrolysis of the ethyl ester in **3.18**.

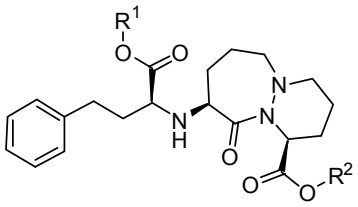

No	R^1	R^2	mass
3.18	CH_2CH_3	$CH(CH_3)OCOCH_2$mo	588.7
3.18a	H	$CH(CH_3)OCOCH_2$mo	560.6
CIL	CH_2CH_3	H	417.2
3.29	H	H	389.2

Scheme 3.27. Exact masses of **3.18** and of its presumable metabolites observed in different incubation mixtures.

In porcine skin homogenate a fast hydrolysis of the ethyl ester in **3.18** resulting in **3.18a** was observed followed by successive conversion to cilazaprilat (Figure 3.74). Cilazapril was only detected as a minor intermediate.

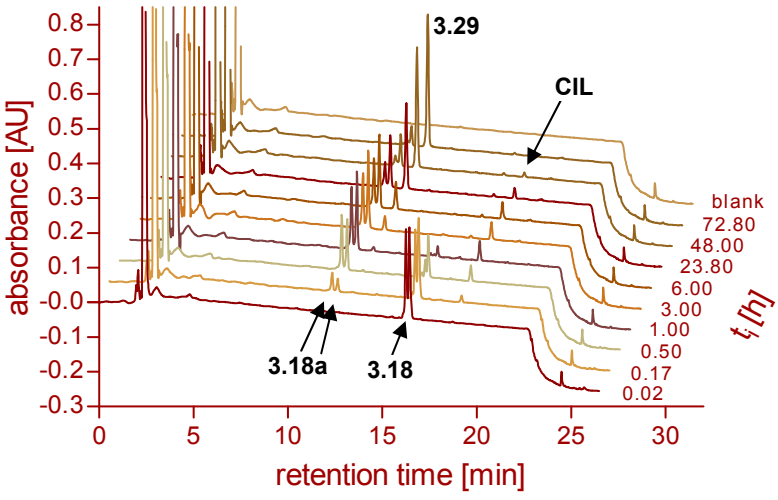

Figure 3.74. Kinetics of hydrolysis of **3.18** in porcine skin homogenate.

After global fitting of the incubation data using the least square method by Levenberg-Marquardt[43-44] (Figure 3.75) the half-life of **3.18** was estimated to be 0.33 h, whereas the $f_{50\%\ cilazaprilat}$ amounted to 24.3 h.

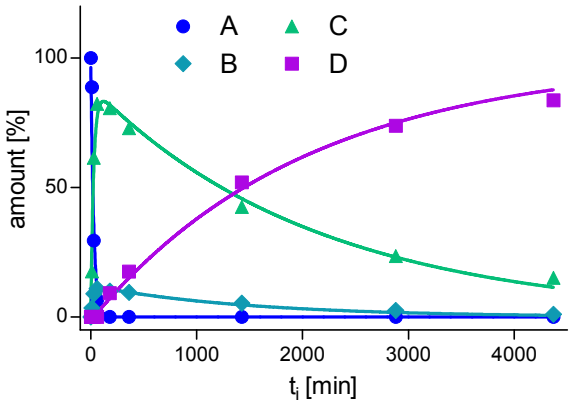

Figure 3.75. Reaction kinetics of **3.18** on incubation with porcine skin homogenate. Results from global fitting of the data. A: **3.18**, B: cilazapril, C: **3.18a**, D: cilazaprilat.

In human plasma the hydrolysis of **3.18** was slower ($t_{1/2}$ = 0.83 h) (Figure 3.76). The diastereomer of **3.18** detected at shorter retention time seemed to be hydrolyzed preferably. In contrast to the incubation with porcine skin homogenate cilazapril was found as the main intermediate, whereas only one diastereomer of **3.18a** was formed in small amounts. The subsequent conversion to cilazaprilat turned out to be very slow ($f_{50\%}$ = 132 h). The half-life of **3.18** in the presence of porcine liver esterase (Figure 3.77) was slightly shorter than in human plasma ($t_{1/2}$ = 0.77 h). 50 % cilazaprilat were formed after 29.3 h. Primary human hepatocytes hydrolyzed **3.18** to cilazapril and cilazaprilat (data not shown). Within one hour 19 % of cilazapril and 38 % of cilazaprilat were formed. After an incubation period of six hours the percentage of cilazapril decreased to 1%, whereas that of cilazaprilat increased to 79 %.

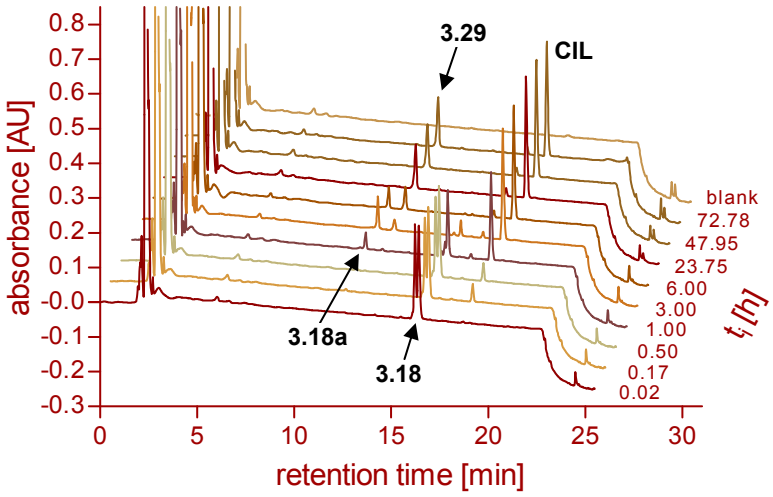

Figure 3.76. Kinetics of hydrolysis of **3.18** in human plasma.

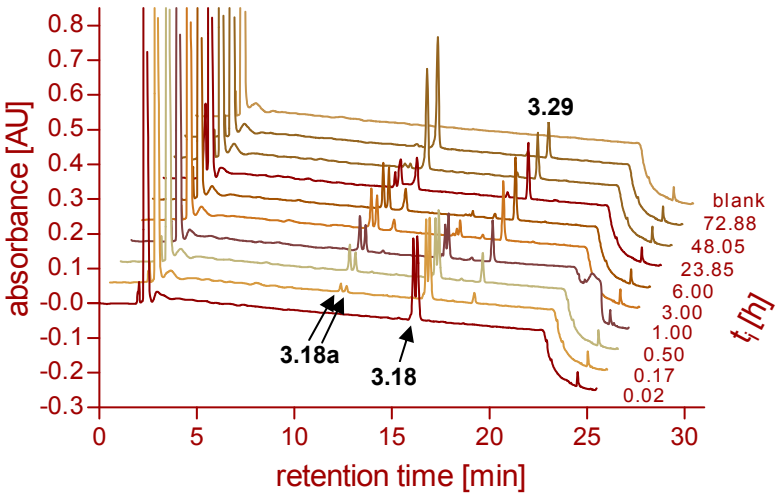

Figure 3.77. Kinetics of hydrolysis of **3.18** in buffered porcine liver esterase.

Cilazapril ethylester (**3.28**) was completely degraded on incubation with porcine skin homogenate, human plasma, porcine liver esterase or primary human hepatocytes resulting exclusively in a compound detected at a retention time of 16.7 min. As confirmed by spiking, this product is not identical with cilazapril, which eluted at $t_R \sim 17.7$ min (Figure 3.78). Hence, the compound presumably corresponds to the monoethyl ester **3.28a** resulting from selective hydrolysis of the homophenylalanine ethyl ester group in **3.28**.

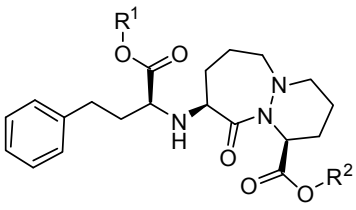

No	R^1	R^2
3.28	CH_2CH_3	CH_2CH_3
3.28a	H	CH_2CH_3
CIL	CH_2CH_3	H
3.29	H	H

Scheme 3.28. Structures of **3.28** and putative metabolites.

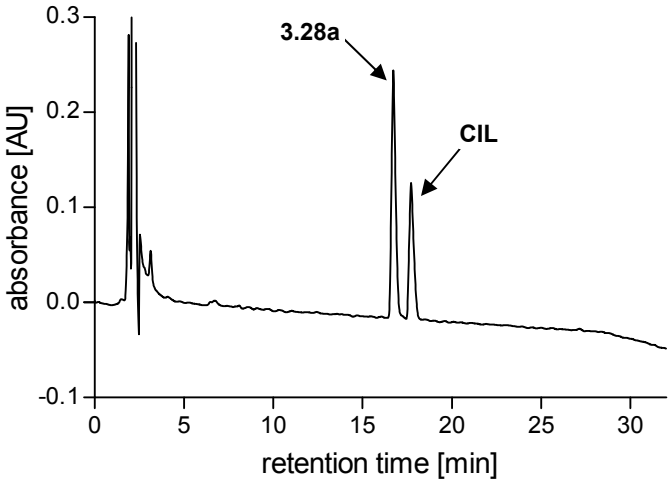

Figure 3.78. HPLC chromatogram of **3.28** incubated for 24 h in porcine skin homogenate spiked with cilazapril (CIL).

In Figure 3.79 the formation of **3.28a** is exemplarily shown in an incubation mixture containing porcine skin homogenate. The incubation of **3.28** in human plasma and in the presence of porcine liver esterase provided similar results (cf. appendix, Figure 9.11,

Figure 9.12). The half-lives of **3.28** in porcine skin homogenate, human plasma and in the presence of porcine liver esterase, respectively, were estimated to be 0.35 h, 11.9 h and 0.69 h. Also primary human hepatocytes were not able to cleave the desired ethyl ester. **3.28a** was found to be the only metabolite amounting to 35 % after an incubation period of one hour and to 99 % after six hours.

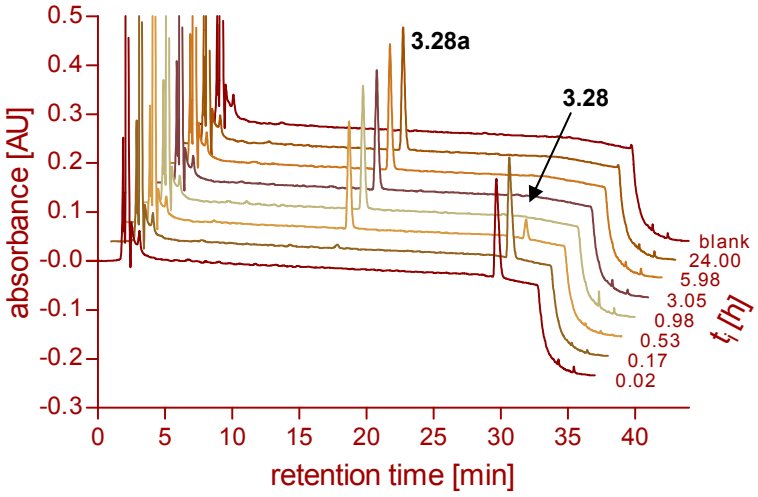

Figure 3.79. Examples of HPLC chromatograms showing the kinetics of hydrolysis of **3.14** in porcine skin homogenate.

3.5.4 Summary: Hydrolytic stability of prodrugs of candesartan and cilazapril

In the following the results of the bioanalytical studies described in chapter 3.5.2 and chapter 3.5.3 are summarized (Table 3.9 to Table 3.12). The half-lives of the respective prodrugs in different incubation media are depicted as well as the observed hydrolysis by primary human hepatocytes.

Table 3.9. Half-lives ($t_{1/2}$) of candesartan prodrugs in porcine skin homogenate, human plasma, buffered porcine liver esterase and phosphate buffer at 37 °C.

prodrug	porcine skin homogenate $t_{1/2}$ (h)	human plasma $t_{1/2}$ (h)	porcine liver esterase $t_{1/2}$ (h)	phosphate buffer (pH 7.4) $t_{1/2}$ (h)
candesartan cilexetil	0.27	35.0	< 0.05	1385
3.31	0.13	47.5	0.10	331
3.32	0.45	32.2	0.03	780
3.33	0.95	< 0.02	2.2	2.3
3.34	15.9	0.82	15.7	14.2
3.35	146	---[a]	18.0	146

[a] No hydrolysis detectable within an incubation period of 72 h.

Table 3.10. Hydrolysis of several candesartan prodrugs by primary human hepatocytes. The percentage of candesartan formed after an incubation period (t_i) of 1 h and 6 h, respectively, is indicated.

prodrug	candesartan (%)	
	t_i = 1 h	t_i = 6 h
3.31	47	100
3.32	22	72
3.35	---[a]	---[a]

[a] No conversion detectable.

Table 3.11. Rate of hydrolysis of cilazapril and cilazapril prodrugs in porcine skin homogenate, human plasma, buffered porcine liver esterase and phosphate buffer at 37 °C.

prodrug	porcine skin homogenate		human plasma		porcine liver esterase		phosphate buffer (pH 7.4)
	$t_{1/2}$ (h)	$f_{50\%}$ (h)[a]	$t_{1/2}$ (h)	$f_{50\%}$ (h)	$t_{1/2}$ (h)	$f_{50\%}$ (h)	$t_{1/2}$ (h)
cilazapril	9.4	9.4	88.8	88.8	3.3	3.3	183
3.1	0.43 [b]	13.0	0.58	154	0.67	23.5	75.0
3.2	1.4	8.6	3.2	228	4.2	62.2	---[c]
3.3	1.0	11.3	1.9	108	1.5	14.2	75.7
3.6	0.50 / 0.52 [b,d]	14.0	0.68	91.2	0.63	9.7	40.3
3.7	1.0	11.5	5.1	33.6	3.8	16.3	---[c]
3.12	1.8	10.4	0.08	250	1.8	4.3	3.7
3.13	1.3	12.8	0.35	186	4.2	5.5	7.1
3.14	0.50	6.3	1.3	10.8	0.95 [c]	7.5	14.0
3.18	0.33 [c]	24.3	0.83	132	0.77	29.3	18.6
3.25	~ 28	---[e]	4.1	---[e]	~ 4	---[e]	~ 12
3.26	~ 4	---[e]	5.6	---[e]	~ 5	---[e]	---[f]
3.27	~ 16	---[e]	5.2	---[e]	~ 3	---[e]	---[f]
3.28	0.35	---[g]	11.9	---[g]	0.69	---[g]	403

[a] $f_{50\%}$ is the time by which 50 % of total cilazaprilat has been formed. [b] $t_{1/2}$ calculated after global fitting of the data using the least square method by Levenberg-Marquardt[43-44]. [c] No hydrolysis detectable within an incubation period of 72 h. [d] Two separate half-lives were obtained due to two different starting conditions of the global fit. [e] Could not be calculated due to unknown reaction kinetics. [f] Not determined because of low solubility in buffer. [g] No conversion to cilazaprilat detectable.

Table 3.12. Hydrolysis of cilazapril and cilazapril prodrugs by primary human hepatocytes. Percentage of cilazapril and cilazaprilat formed after an incubation period (t_i) of 1 h and 6 h, respectively.

prodrug	cilazapril (%)		cilazaprilat (%)	
	t_i = 1 h	t_i = 6 h	t_i = 1 h	t_i = 6 h
cilazapril	74	11	26	89
3.1	29	36	6	86
3.2	40	42	19	81
3.3	33	28	6	89
3.6	38	24	7	82
3.7	19	13	10	72
3.12	66	34	15	85
3.13	24	42	6	94
3.14	6	9	1	45
3.18	19	38	1	79
3.28	---[a]	---[a]	---[a]	---[a]

[a] No conversion to cilazapril or cilazaprilat detectable.

3.6 *Pharmacological investigation of candesartan prodrugs using a spectrofluorimetric Ca^{2+}-assay*

Activation of the angiotensin II AT_1 receptor leads to an increase of the intracellular Ca^{2+} concentration ($[Ca^{2+}]_i$) by a $G\alpha_q$ protein coupled signal transduction pathway. Thus, AT_1 receptor antagonists such as candesartan cause an inhibition of the increase in $[Ca^{2+}]_i$. A subject of previous work was the determination of antagonistic activity at the AT_1 receptor of a small set of candesartan prodrugs in a fura-2 calcium assay with rat glomerular mesangial cells.[45]

In brief, rat mesangial cells were loaded with fura-2 acetoxymethyl ester. After intracellular enzymatic ester cleavage the Ca^{2+}-sensitive dye fura-2 coordinates cytosolic Ca^{2+} ions and $[Ca^{2+}]_i$ can be determined by a ratiometric measurement of the fluorescence according to the Grynkiewicz equation[46] (Equation 3.6).

$$[Ca^{2+}]_i = K_D \cdot \frac{(R - R_{min})}{(R_{max} - R)} \cdot SFB$$

Equation 3.6. The Grynkiewicz equation for calculation of the intracellular Ca^{2+} concentration. K_D: dissociation constant of the fura-2-Ca^{2+} complex; R: ratio of fluorescence intensity at 510 nm after excitation at 340 and 380 nm; R_{min}: fluorescence ratio in absence of free Ca^{2+}; R_{max}: fluorescence ratio in presence of a saturating Ca^{2+} concentration; SFB: correction factor.

Treatment of the rat cells with angiotensin II causes an increase in $[Ca^{2+}]_i$. This signal can be inhibited by angiotensin II AT_1 receptor antagonists such as candesartan (Figure 3.80). After preincubation with variable concentrations of antagonist the $[Ca^{2+}]_i$ signal was induced by addition of 100 nM angiotensin II (approximate agonist concentration inducing about 80 % of the maximal response). Using antagonist concentrations reducing the angiotensin II-induced fluorescence signal to 20 % - 80 % the percental inhibition (P) relative to control (no antagonist) was determined by Equation 3.7.

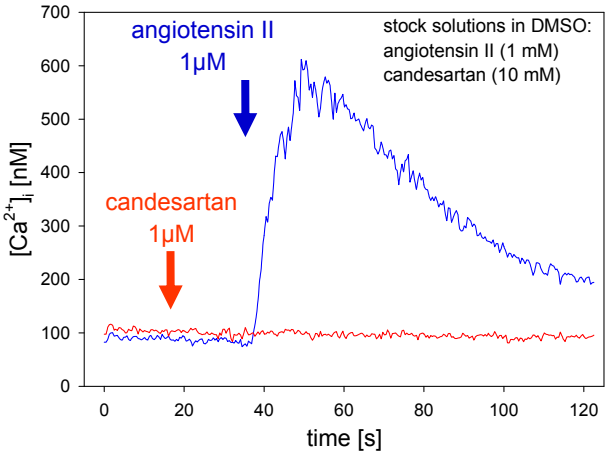

Figure 3.80. AT_1 receptor mediated mobilization of intracellular Ca^{2+} in rat glomerular mesangial cells induced by stimulation with 1 µM angiotensin II (blue curve); inhibition of mobilization of intracellular Ca^{2+} by 1 µM candesartan (red curve).

$$\text{Percentage inhibition [\%]} = P = \left(100 - \frac{[Ca^{2+}]_i - \text{slope (compound + 100 nM angiotensin II)[µM]}}{[Ca^{2+}]_i - \text{slope (control)[µM]}}\right)$$

Equation 3.7. Calculation of the percental inhibition P.

After logit-transformation following Equation 3.8 and plotting of the resulting logit (P) values versus the logarithm of the corresponding compound concentration the log (IC_{50}) value was obtained as intersection point of the regression line with the x-axis.

$$\mathrm{logit(P)} = \log\left(\frac{\mathrm{P}}{100 - \mathrm{P}}\right)$$

Equation 3.8. Logit-log Transformation

A logit-log-plot is shown in Figure 3.81 for candesartan as an example.

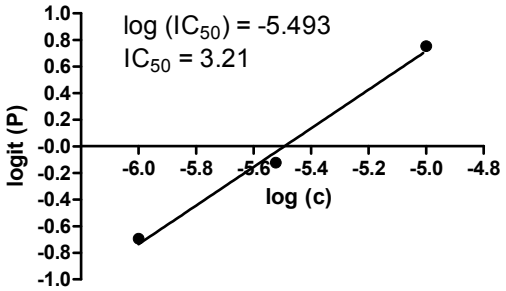

Figure 3.81. Logit-log-plot of candesartan.

The calculated IC_{50} values were converted to dissociation constants (K_b) according to the Cheng-Prusoff equation[47] (Equation 3.9) using an EC_{50} value of 19.7 nM for angiotensin II (mean value from 2 independently determined concentration-effect curves on rat glomerular mesangial cells).

$$\mathrm{K_b} = \mathrm{IC_{50}} \cdot \frac{\mathrm{EC_{50}}}{\mathrm{EC_{50}} + [\mathrm{L}]}$$

Equation 3.9. Cheng-Prusoff equation for functional assays. K_b: dissociation constant; EC_{50}: angiotensin II concentration which induces 50 % of the maximal effect (determined to 19.7 nM); [L]: angiotensin II concentration (100 nM).

The results from the fura-2 calcium assay for candesartan and the candesartan prodrugs are summarized in Table 3.13.

All investigated candesartan derivatives were able to antagonize the effect of the agonist angiotensin II on rat glomerular mesangial cells with IC_{50} values in the one- to two-digit nanomolar range (4.8 nM – 47.2 nM) and corresponding K_b values ranging from 0.8 nM to 7.8 nM. The parent compound candesartan showed an IC_{50} of 3.2 nM and a corresponding K_b of 0.5 nM, which is in good correlation with results reported in literature (K_i = 0.64 nM)[48]. Surprisingly, besides candesartan the synthesized prodrugs, in particular the 1-(2,2-dimethylpropanoyl)ethyl ester **3.32** (IC_{50} = 4.8 nM, K_b = 0.8 nM) as well as the morpholinoethyl ester **3.35** (IC_{50} = 6.0 nM, K_b = 1.0 nM), turned out to be potent antagonists. Whereas **3.32** and **3.35** were about as potent as candesartan, the antagonistic activities of the (oxodioxolyl)methyl ester prodrugs **3.33** and **3.34** were approximately four to five times lower, and the 1-(alkyloxycarbonyloxy)ethyl esters **3.31**

and candesartan cilexetil were about 12 to 15 times less potent. From these data a clear structure-activity-relationship is not evident. However, a sterically more demanding ester moiety such as the cilexetil group seems to decrease the antagonistic activity more strongly than smaller ester moieties. Comparing the compounds with similar type of ester side chains (**3.31** and candesartan cilexetil as well as **3.33** and **3.34**) the bulkier substituent leads to a weaker antagonistic activity. Since there is only a slight difference between the IC_{50} values of candesartan and the prodrug esters **3.32** or **3.35** it is likely, that the affinity for the AT_1 receptor is mainly caused by the tetrazolylbiphenylmethyl partial structure and the benzimidazole ring. The introduction of certain ester pro-moieties seems to have a rather insignificant impact on the antagonistic activity.

Table 3.13. Antagonistic activity at the AT_1 receptor of candesartan and candesartan prodrugs in a spectrofluorimetric Ca^{2+}-assay (fura-2 assay) on rat glomerular mesangial cells given as mean values ± SEM from 3-5 independent experiments.

	No.	R	IC_{50} [nM]	K_b [nM]
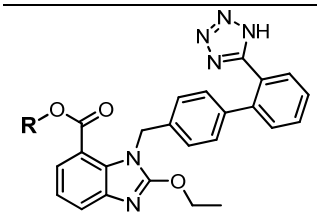	**Candesartan**	H	3.2 ± 0.5	0.5 ± 0.1
	3.31	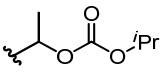	38.6 ± 17.0	6.4 ± 2.8
	3.32	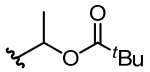	4.8 ± 0.4	0.8 ± 0.1
	3.33	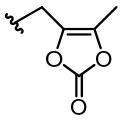	11.7 ± 4.2	1.9 ± 0.7
	3.34	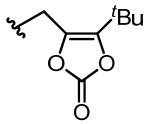	15.4 ± 2.1	2.5 ± 0.3
	3.35	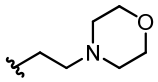	6.0 ± 0.6	1.0 ± 0.1
	Candesartan cilexetil	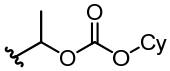	47.2 ± 21.8	7.8 ± 3.6

However, the most important conclusion from the pharmacological studies is that the investigated candesartan derivatives due to their partly high potency at the AT_1 receptor must not be considered as inactive prodrugs. In fact, they represent new chemical entities.

3.7 Summary and conclusion

Inspired by structures of therapeutically well-established or promising experimental carrier-prodrugs, a set of potential candesartan and cilazapril prodrugs, which should fulfill the requirements for application *via* a transdermal therapeutic system (TTS), was synthesized. Starting from candesartan and cilazapril, respectively, the desired compounds were accessible by esterification. In terms of physicochemical properties, in particular with respect to lipophilicity (log *P*, log *D*), the synthesized candesartan and cilazapril prodrugs are considered suitable for skin permeation. Especially, compounds containing an ionizable morpholine moiety (**3.14**, **3.18**, **3.35**) are interesting candidates due to balanced lipophilicity and water solubility.

Candesartan prodrugs: The candesartan double ester prodrugs (candesartan cilexetil, **3.31** and **3.32**) as well as the candesartan morpholinoethyl ester (**3.35**) exhibited excellent solid state stabilities at long-term storage conditions. The candesartan double ester prodrugs were also sufficiently stable against spontaneous, non-enzymatic hydrolysis in buffer pH 7.4. On the contrary, the prodrugs were enzymatically converted to candesartan in the presence of porcine skin homogenate, human plasma, porcine liver esterase and upon incubation with primary human hepatocytes. In contrast, enzymatic hydrolysis of **3.33** and **3.34** to candesartan was only observed in the presence of human plasma. Moreover, the (oxodioxolyl)methyl moiety appeared to be highly prone to non-enzymatic hydrolysis. Surprisingly, the morpholinoethyl ester of candesartan (**3.35**) was only hydrolyzed in the presence of porcine skin homogenate and porcine liver esterase, whereas high stability was observed in human plasma and upon incubation with primary human hepatocytes. Thus, it can be assumed that hydrolysis is impaired due to the short distance between the core structure and the cleavage site. Surprisingly, in a spectrofluorimetric Ca^{2+}-assay (fura-2 assay) on rat glomerular mesangial cells both, the 1-(2,2-dimethylpropanoyl)ethyl ester **3.32** (K_b = 0.8 nM) and the morpholinoethyl ester **3.35** (K_b = 1.0 nM) turned out to be potent angiotensin II AT_1 receptor antagonists. Therefore, these candesartan derivatives must not be considered as inactive prodrugs, but as new pharmacologically active chemical entities.

Cilazapril prodrugs: The investigation of the solid state stability of a selection of cilazapril prodrugs (**3.1**-**3.3**, **3.6**, **3.7**, **3.14**, **3.28**) revealed high stabilities of all compounds at 5 °C/65 % rel. h. Except for the simple ethyl ester (**3.28**), which was found to be remarkably stable at all storage conditions, the stabilities of **3.1**-**3.14** were considerably decreasing at long-term as well as at accelerated storage conditions. In contrast to prodrugs of the ACE inhibitor trandolapril (previous in-house investigations), the chemical stability of cilazapril prodrugs is increased, as the intramolecular formation of diketopiperazine is precluded due to the more rigid structure of cilazapril. Moreover, there was no intermolecular formation of diketopiperazine. The cilazapril double ester prodrugs **3.1**-**3.3**, **3.6** and **3.7** showed high to moderate stabilities towards non-enzymatic hydrolysis in buffer. Enzyme-containing incubation mixtures as well as primary human

hepatocytes led to a fast degradation of the prodrugs and to the formation of cilazaprilat as the final metabolite. Interestingly, double ester prodrugs, containing a stereogenic center in the pro-moiety, were stereoselectively cleaved in most cases, when used as a mixture of two diastereomers. In accordance to the candesartan prodrugs **3.33** and **3.34**, the (oxodioxolyl)methyl prodrugs of cilazapril (**3.12**, **3.13**) showed strikingly fast hydrolysis in human plasma, but insufficient stability in buffer pH 7.4. Furthermore, fast reaction kinetics concerning enzymatic hydrolysis and moderate stability towards non-enzymatic hydrolysis were observed for compounds **3.14** and **3.18**, which contain an ionizable morpholinoethyl and 1-(2-morpholinoacetoxy)ethyl moiety, respectively. In view of their application *via* a TTS, *N*-aryl-*N*-alkyloxycarbonylaminomethyl (NArNAOCAM) esters of cilazapril are considered rather unsuitable, since they are prone to hydrolysis at low pH values and kinetics of hydrolysis is complex. The ethyl ester of cilazapril (**3.28**) turned out to be completely stable against enzymatic cleavage of the additional ethyl carboxylate group, whereas hydrolysis occurred exclusively at the homophenylalanine ethyl ester moiety. This result corroborates previous findings from our laboratory on the cleavage of trandolapril ethyl ester.

In conclusion, several promising prodrugs of candesartan and cilazapril were synthesized. Their physicochemical properties are presumably adequate for transdermal application, as they are enzymatically hydrolyzed, yielding the active principles candesartan and cilazaprilat.

3.8 Experimental section

3.8.1 General experimental conditions

Commercially available chemicals and reagents were purchased from Acros Organics (Geel, Belgium), Alfa Aesar GmbH & Co. KG (Karlsruhe, Germany), Merck KGaA (Darmstadt, Germany), Sigma-Aldrich Chemie GmbH (München, Germany) or Wako Pure Chemical Industries (Osaka, Japan). Cilazapril and candesartan were kindly provided by Hexal AG (Holzkirchen, Germany). All solvents used were of analytical grade or distilled before use. Reactions were usually monitored by thin layer chromatography (TLC) on Merck silica gel F_{254} aluminium sheets and spots were visualized with UV light at 254 nm or ammonium molybdate/cerium (IV) sulfate solution. For flash column chromatography Merck silica gel 60 (0.040-0.063 mm) was used. Purification by preparative HPLC was performed on a RP-column (Nucleodur 100-5 C18 ec, 250 x 21 mm, 5 µm; Machery-Nagel, Düren, Germany) with a system consisting of two K-1800 pumps (Knauer, Berlin, Germany) and a UV-VIS detector model K-2000 (Knauer). UV-detection was done at 220 nm, the temperature was 30 °C and the flow rate 22 ml/min. Melting points (mp) were determined with a Büchi 510 melting point apparatus and are uncorrected. Nuclear Magnetic Resonance (^{1}H-NMR and ^{13}C-NMR) spectra were recorded on an Avance 300 (^{1}H: 300 MHz), an Avance 600 (^{1}H: 600 MHz) or an Avance III

600 spectrometer (^{1}H: 600 MHz) (Bruker BioSpin GmbH, Rheinstetten, Germany) with per-deuterated solvents (Deutero GmbH, Kastellaun, Germany). The chemical shift δ is given in parts per million (ppm) with reference to the chemical shift of the residual protic solvent compared to tetramethylsilane (δ = 0). Multiplicities are specified with the following abbreviations: s (singlet), d (doublet), t (triplet), q (quartet), sept (septet), m (multiplet) and bs (broad singlet). The multiplicity of carbon atoms was determined by DEPT 135 (distortionless enhancement by polarization transfer) and is indicated as follows: "+" for primary and tertiary carbon atoms (positive DEPT 135 signal), "-" for secondary carbon atoms (negative DEPT 135 signal), "quat" for quaternary carbon atoms. 2D-NMR techniques (COSY, TOCSY, HSQC, HMBC) were partially performed to support interpretation of 1D spectra. Mass spectrometry analysis (MS) was performed on a Finnigan MAT 95 (EI-MS 70eV, HR-MS), a Finnigan SSQ 710A (EI-MS 70 eV, CI-MS (NH_3)) and on a Finnigan ThermoQuest TSQ 7000 (ES-MS) spectrometer. The peak-intensity in % relative to the strongest signal is given in parenthesis. Elemental analysis was carried out in the Department of Microanalysis, University of Regensburg. Analytical HPLC analysis was performed on a system from Thermo Separation Products (Thermo Scientific) consisting of a SN400 controller, a P4000 pump, an AS3000 autosampler, a Spectra Focus UV-VIS detector and a RP-column (Luna C18-2, 150 x 4.6 mm, 3 µm; Phenomenex, Aschaffenburg, Germany) at a flow rate of 0.75 mL/min and a column temperature varying between 25 to 60 °C. Absorbance was detected at 210 nm. The mobile phase consisted of MeCN and 0.05 % trifluoroacetic acid (TFA) in Millipore water. All samples were filtered prior to injection using 0.2 µm Phenex-NY Syringe Filters (0.2 µm pore size, 4 mm diameter) (Phenomenex, Aschaffenburg, Germany). For the determination of compound purity following gradients were used: Gradient a: 0 min: MeCN/0.05% TFA/aq 10/90, 25 min: 90/10, 26-31 min: 95/5; Gradient b: 0 min: MeCN/0.05% TFA/aq 10/90, 20 min: 90/10, 21-29 min: 95/5. The retention (capacity) factor k was calculated from the retention time t_R and the hold-up time t_0 according to $k = (t_R - t_0)/t_0$ with t_0 = 2.88 min for Luna C18-2, 150 x 4.6 mm, 3 µm. Millipore water was used throughout for the preparation of buffers and HPLC eluents. The loading buffer for the fura-2 assay on rat mesangial cells consisted of 7.013 g/l NaCl, 0.373 g/l KCl, 0.407 g/l $MgCl_2 \cdot 6\ H_2O$, 0.221 g/l $CaCl_2 \cdot 2\ H_2O$, 5.958 g/l HEPES, 1.802 g/l glucose. The pH was adjusted to 7.4 with NaOH followed by sterile filtration.

3.8.2 Chemistry: Experimental protocols and analytical data

In the following the correlation of ^{1}H and ^{13}C nuclear magnetic resonance signals of the (1*S*,9*S*)-10-oxooctahydro-1H-pyridazino-[1,2-a][1,2]diazepine-1-carboxylic acid core structure will be reported according to the atom numbering depicted on the right side. That means that the signal C-x refers to carbon atom no. x and the signal x-H refers to the hydrogen atom/atoms connected to the carbon atom no. x.

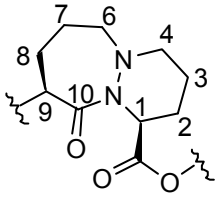

3.8.2.1 General procedure for the synthesis of 1-(alkyloxycarbonyloxy)ethyl esters (3.1-3.3) and 1-(acyloxy)ethyl esters (3.6-3.7)

K_2CO_3 (1.2 eq) was added to a solution of cilazapril (1eq) in DMF (H_2O < 0.01 %) and the solution was stirred for 10 min. The corresponding 1-(alkyloxycarbonyloxy)ethyl chloride or 1-chloroethyl alkanoate (cf. 3.8.2.2) (1.3 eq) was added dropwise at 0 °C. After stirring at room temperature overnight the reaction mixture was poured into water and extracted three times with ethyl acetate. The combined organic layers were washed with water, dried over anhydrous $MgSO_4$, filtered and evaporated under reduced pressure. The crude product was purified by flash chromatography.

(1*S*,9*S*)-1-(Ethoxycarbonyloxy)ethyl 9-((*S*)-1-ethoxy-1-oxo-4-phenylbutan-2-ylamino)-10-oxooctahydro-1*H*-pyridazino[1,2-a][1,2]diazepine-1-carboxylate (3.1): The title compound was prepared from cilazapril (2.4 mmol, 1.00 g), K_2CO_3 (2.9 mmol, 0.40 g) and 1-chloroethyl(ethyl)carbonate (3.1 mmol, 0.48 g) in DMF (H_2O < 0.01 %) (5 ml) following the general procedure 3.8.2.1. The desired product was obtained after flash chromatography (PE/EtOAc 3/2 v/v) as a yellowish oil (0.80 g, 62 %). ^{1}H-NMR ($CDCl_3$) δ ppm: 1.27 (m, 3H, C***H*₃**CH_2OCOO), 1.30 (m, 3H, C***H*₃**CH_2OCOCH), 1.37 and 1.72 (m, 2H, 3-H_2), 1.48 and 2.03 (m, 2H, 8-H_2), 1.53 (m, 3H, OCHC***H*₃**O), 1.72 and 1.85 (m, 2H, 7-H_2), 1.82 and 2.23 and 2.35 (m, 2H, 2-H_2), 2.03 (m, 2H, $PhCH_2C$***H*₂**), 2.50 (bs, 1H, NH), 2.50 and 3.27 and 3.44 (m, 2H, 6-H_2), 2.73 (m, 2H, PhC***H*₂**), 2.94 and 3.07 (m, 2H, 4-H_2), 3.37 (m, 1H, $PhCH_2CH_2C$***H***), 4.17 (m, 1H, 9-H), 4.18 (m, 2H, CH_3C***H*₂**OCOCH), 4.20 (m, 2H, CH_3C***H*₂**OCOO), 5.01 and 5.08 (m, 1H, 1-H), 6.73 and 6.80 (m, 1H, OC***H***CH_3O), 7.17 (m, 3H, Ph***H***), 7.25 (m, 2H, Ph***H***). ^{13}C-NMR ($CDCl_3$) δ ppm: 14.08 (+, ***C***H_3CH_2OCOO), 14.29 (+, ***C***H_3CH_2OCOCH), 15.81 and 16.21 (-, C-3), 19.41 and 19.47 (+, OCH***C***H_3O), 24.82 and 24.89 (-, C-2), 24.99 and 25.26 (-, C-7), 29.83 and 29.98 (-, C-8), 32.17 (-, Ph***C***H_2), 34.99 and 35.05 (-, $PhCH_2$***C***H_2), 49.30 and 49.94 (+, C-1), 51.08 (-, C-6), 51.62 and 51.81 (-, C-4), 57.17 and 57.30 (+, C-9), 60.49 and 60.55 (+, $PhCH_2CH_2$***C***H), 60.62 (-, CH_3***C***H_2OCOCH), 64.48 and 64.52 (-, CH_3***C***H_2OCOO), 91.96 and 92.04 (+, O***C***HCH_3O), 125.84 (+, Ph***C***), 128.25 and 128.30 (2C, +, Ph***C***), 128.37 (2C, +, Ph***C***), 141.48 (quat, Ph***C***), 152.91 and 152.09 (quat, CH_3CH_2O***C***OO), 169.46 and 169.50 (quat, C-1-***C***OO), 174.37 (quat, CH_3CH_2O***C***OCH), 174.88 and 174.96 (quat, C-10). HRMS: EI-MS: *m/z* for ($C_{27}H_{39}N_3O_8$) calcd. 533.2737, found: 533.27304. Analytical HPLC: purity 100 %, t_R = 15.61 min (gradient a), k = 4.42. $C_{27}H_{39}N_3O_8$ (547.61).

(1*S*,9*S*)-1-(Cyclohexyloxycarbonyloxy)ethyl 9-((*S*)-1-ethoxy-1-oxo-4-phenylbutan-2-ylamino)-10-oxooctahydro-1*H*-pyridazino[1,2-a][1,2]diazepine-1-carboxylate (3.2): The title compound was prepared according to the general procedure 3.8.2.1 using cilazapril (0.6 mmol, 0.25 g), K_2CO_3 (0.7 mmol, 0.10 g) and 1-chloroethyl(cyclohexyl)carbonate (0.8 mmol, 0.16 g) in DMF (H_2O < 0.01 %) (3 ml) and was obtained after flash chromatography (PE/EtOAc 3/2 v/v) as a yellowish oil (0.26 g, 74 %). ^{1}H-NMR ($CDCl_3$) δ ppm: 1.27 (m, 3H, C***H*₃**CH_2), 1.27 and 1.52 (m, 2H, cy-4-H_2), 1.35 and 1.73 (m, 4H, cy-3-

H_2, cy-5-H_2), 1.35 and 1.73 (m, 2H, 3-H_2), 1.47 and 1.90 (m, 4H, cy-2-H_2, cy-6-H_2), 1.47 and 2.03 (m, 2H, 8-H_2), 1.52 (m, 3H, OCHC***H*****$_3$**O), 1.73 and 1.90 (m, 2H, 7-H_2), 1.90 and 2.26 and 2.35 (m, 2H, 2-H_2), 2.02 (m, 2H, PhCH_2C***H*****$_2$**), 2.35 (bs, 1H, NH), 2.50 and 3.27 and 3.44 (m, 2H, 6-H_2), 2.73 (m, 2H, PhC***H*****$_2$**), 2.94 and 3.06 (m, 2H, 4-H_2), 3.37 (m, 1H, PhCH_2CH_2C***H***), 4.16 (m, 1H, 9-H), 4.18 (m, 2H, CH_3C***H*****$_2$**), 5.01 and 5.08 (m, 1H, 1-H), 6.73 and 6.80 (m, 1H, OC***H***CH_3O), 7.17 (m, 3H, Ph***H***), 7.25 (m, 2H, Ph***H***). ^{13}C-NMR ($CDCl_3$) δ ppm: 14.35 (+, ***C***H_3CH_2), 15.84 and 16.21 (-, C-3), 19.42 and 19.49 (+, OCH***C***H_3O), 23.51 (2C, -, cy-C-4), 24.81 and 24.89 (-, C-2), 25.04 and 25.27 (-, C-7), 25.09 (4C, -, cy-C-3, cy-C-5), 29.88 and 30.06 (-, C-8), 31.32 (4C, -, cy-C-2, cy-C-6), 32.18 (-, Ph***C***H_2), 35.04 and 35.09 (-, PhCH_2***C***H_2), 49.30 and 49.95 (+, C-1), 51.08 (-, C-6), 51.63 and 51.81 (-, C-4), 57.16 and 57.28 (+, C-9), 60.51 (+, PhCH_2CH_2***C***H), 60.59 (-, CH_3***C***H_2), 77.47 and 77.50 (+, cy-C-1), 91.85 and 91.97 (+, O***C***HCH_3O), 125.84 (+, Ph***C***), 128.30 (2C, +, Ph***C***), 128.37 (2C, +, Ph***C***), 141.50 (quat, Ph***C***), 152.43 and 152.60 (quat, cy-O***C***OO), 169.46 and 169.52 (quat, C-1-***C***OO), 174.43 (quat, CH_3CH_2O***C***O), 175.00 (quat, C-10). HRMS: EI-MS: *m/z* for ($C_{31}H_{45}N_3O_8$) calcd. 587.3207, found: 587.32002. Analytical HPLC: purity 100 %, two diastereomeres, t_R = 18.41, 18.65 min (gradient a), k = 5.39, 5.48. $C_{31}H_{45}N_3O_8$ (587.70).

(1*S*,9*S*)-1-(Isopropyloxycarbonyloxy)ethyl 9-((*S*)-1-ethoxy-1-oxo-4-phenylbutan-2-ylamino)-10-oxooctahydro-1*H*-pyridazino[1,2-a][1,2]diazepine-1-carboxylate (3.3): The title compound was prepared from cilazapril (0.6 mmol, 0.25 g), K_2CO_3 (0.7 mmol, 0.10 g) and 1-chloroethyl(isopropyl)carbonate (0.8 mmol, 0.13 g) in DMF (H_2O < 0.01 %) (3 ml) according to the general procedure 3.8.2.1 and was obtained after flash chromatography (PE/EtOAc 1/1 v/v) as a yellowish oil (0.28 g, 84 %). ^{1}H-NMR ($CDCl_3$) δ ppm: 1.27 (m, 3H, C***H*****$_3$**CH_2), 1.29 (m, 6H, CH(C***H*****$_3$)$_2$), 1.36 and 1.72 (m, 2H, 3-H_2), 1.48 and 2.03 (m, 2H, 8-H_2), 1.52 (m, 3H, OCHC***H*****$_3$**O), 1.72 and 1.85 (m, 2H, 7-H_2), 1.82 and 2.26 and 2.35 (m, 2H, 2-H_2), 2.03 (m, 2H, PhCH_2C***H*****$_2$**), 2.43 (bs, 1H, NH), 2.50 and 3.27 and 3.44 (m, 2H, 6-H_2), 2.73 (m, 2H, PhC***H*****$_2$**), 2.94 and 3.07 (m, 2H, 4-H_2), 3.37 (m, 1H, PhCH_2CH_2C***H***), 4.17 (m, 1H, 9-H), 4.19 (m, 2H, CH_3C***H*****$_2$**), 4.87 (m, 1H, C***H***$(CH_3)_2$), 5.01 and 5.08 (m, 1H, 1-H), 6.73 and 6.80 (m, 1H, OC***H***CH_3O), 7.17 (m, 3H, Ph***H***), 7.25 (m, 2H, Ph***H***). ^{13}C-NMR ($CDCl_3$) δ ppm: 14.32 (+, ***C***H_3CH_2), 15.82 and 16.21 (-, C-3), 19.42 and 19.49 (+, OCH***C***H_3O), 21.58 and 21.62 (2C, +, CH(***C***$H_3)_2$), 24.82 and 24.89 (-, C-2), 25.03 and 25.25 (-, C-7), 29.86 and 30.03 (-, C-8), 32.18 (-, Ph***C***H_2), 35.02 and 35.08 (-, PhCH_2***C***H_2), 49.33 and 49.95 (+, C-1), 51.10 (-, C-6), 51.64 and 51.80 (-, C-4), 57.17 and 57.29 (+, C-9), 60.51 and 60.56 (+, PhCH_2CH_2***C***H), 60.61 (-, CH_3***C***H_2), 72.73 and 72.78 (+, ***C***H$(CH_3)_2$), 91.83 and 91.94 (+, O***C***HCH_3O), 125.84 (+, Ph***C***), 128.31 (2C, +, Ph***C***), 128.38 (2C, +, Ph***C***), 141.49 (quat, Ph***C***), 152.42 and 152.61 (quat, $(CH_3)_2$CHO***C***OO), 169.46 and 169.52 (quat, C-1-***C***OO), 174.41 (quat, CH_3CH_2O***C***O), 174.99 (quat, C-10). HRMS: EI-MS: *m/z* for ($C_{28}H_{41}N_3O_8$) calcd. 547.2894, found: 547.28848. Analytical HPLC: purity 100 %, two diastereomeres, t_R = 16.56, 16.72 min (gradient a), k = 4.75, 4.81. $C_{28}H_{41}N_3O_8$ (547.64).

3.8.2.2 General procedure for the synthesis of 1-chloroethyl alkanoates 3.4, 3.5[20]

A catalytic amount of $ZnCl_2$ was added to the corresponding acid chloride (1 eq). Under stirring acetaldehyde (1.04 eq) was added dropwise at -20 °C. The reaction mixture was stirred below 0 °C for 1 h and then at room temperature for 1-3 h. The resulting reaction mixture was poured into cold water and extracted three times with diethylether. The pooled organic layers were washed with saturated sodium hydrogen carbonate solution and twice with brine, dried over anhydrous $MgSO_4$, filtered and evaporated under reduced pressure. The resulting brown liquid was purified by distillation under reduced pressure (57 mm Hg).

1-Chloroethyl acetate (3.4): The title compound was prepared according to general procedure 3.8.2.2 using acetyl chloride (171 mmol, 12.17 ml) and acetaldehyde (177 mmol, 10 ml). Distillation under reduced pressure yielded the desired product as a colorless liquid (12.57 g, 60 %). Bp: 32-34 °C/ 57 mmHg. ^{1}H-NMR ($CDCl_3$) δ ppm: 1.79 (d, 3H, ^3J = 5.8 Hz, ClCHC***H*****$_3$**), 2.12 (s, 3H, OCOC***H*****$_3$**), 6.53 (q, 1H, ^3J = 5.8 Hz, ClC***H***CH_3). ^{13}C-NMR ($CDCl_3$) δ ppm: 20.92 (OCO***C***H_3), 25.19 (Cl***C***HCH_3), 80.67 (Cl***C***HCH_3), 168.63 (***C***=O). CI-MS (NH_3) *m/z* (%): 140 (100) $[M+NH_4]^+$. $C_4H_7ClO_2$ (122.55).

1-Chloroethyl-2,2-dimethyl propanoate (3.5): The title compound was prepared from pivaloyl chloride (171 mmol, 20.98 ml) and acetaldehyde (177 mmol, 10 ml) according to the general procedure 3.8.2.2. Distillation under reduced pressure yielded the desired product as a colorless liquid (14.92 g, 53 %). Bp: 50-53 °C/ 57 mmHg. ^{1}H-NMR ($CDCl_3$) δ ppm: 1.22 (s, 9H, C(C***H*****$_3$**$)_3$), 1.79 (d, 3H, ^3J = 5.8 Hz, ClCHC***H*****$_3$**), 6.54 (q, 1H, ^3J = 5.8 Hz, ClC***H***CH_3). ^{13}C-NMR ($CDCl_3$) δ ppm: 25.07 (+, ClCH***C***H_3), 26.73 (3C, +, C(***C***$H_3)_3$), 38.66 (quat, ***C***$(CH_3)_3$), 80.87 (+, Cl***C***HCH_3), 176.06 (quat, ***C***=O). CI-MS (NH_3) *m/z* (%): 182 (100) $[M+NH_4]^+$. $C_7H_{13}ClO_2$ (164.63).

(1*S*,9*S*)-1-Acetoxyethyl 9-((*S*)-1-ethoxy-1-oxo-4-phenylbutan-2-ylamino)-10-oxo-octahydro-1*H*-pyridazino[1,2-a][1,2]diazepine-1-carboxylate (3.6): The title compound was prepared according to the general procedure 3.8.2.1 using cilazapril (0.6 mmol, 0.25 g), K_2CO_3 (0.7 mmol, 0.10 g) and **3.4** (0.8 mmol, 0.11 g) in DMF (H_2O < 0.01 %) (3 ml) and was obtained after flash chromatography (PE/EtOAc 5/4 to 1/2 v/v) as a pale yellow oil (0.18 g, 70 %). ^{1}H-NMR ($CDCl_3$) δ ppm: 1.27 (m, 3H, C***H*****$_3$**CH_2), 1.37 and 1.72 (m, 2H, 3-H_2), 1.48 (d, 3H, ^3J = 5.5 Hz, OCHC***H*****$_3$**O), 1.48 and 2.02 (m, 2H, 8-H_2), 1.72 and 1.89 (m, 2H, 7-H_2), 1.83 and 2.23 and 2.34 (m, 2H, 2-H_2), 2.02 (m, 2H, $PhCH_2C$***H*****$_2$**), 2.03 and 2.07 (2 s, 3H, C***H*****$_3$**COO), 2.50 and 3.26 and 3.43 (m, 2H, 6-H_2), 2.73 (m, 2H, PhC***H*****$_2$**), 2.93 and 3.06 (m, 2H, 4-H_2), 3.37 (m, 1H, $PhCH_2CH_2C$***H***), 4.15 (m, 1H, 9-H), 4.18 (m, 2H, CH_3C***H*****$_2$**), 5.00 and 5.06 (m, 1H, 1-H), 6.81 and 6.89 (m, 1H, OC***H***CH_3O), 7.17 (m, 3H, Ph***H***), 7.25 (m, 2H, Ph***H***). ^{13}C-NMR ($CDCl_3$) δ ppm: 14.30 (+, ***C***H_3CH_2), 15.79 and 16.15 (-, C-3), 19.35 and 19.41 (+, OCH***C***H_3O), 20.70 and 20.75 (+, ***C***H_3COO), 24.76 and 24.91 (-, C-2), 25.00 and 25.28 (-, C-7), 29.91 and 30.06 (-, C-8),

32.17 (-, Ph***C***H_2), 35.04 and 35.10 (-, $PhCH_2$***C***H_2), 49.24 and 49.86 (+, C-1), 51.02 and 51.55 (-, C-6), 51.62 and 51.80 (-, C-4), 57.15 and 57.26 (+, C-9), 60.52 (+, $PhCH_2CH_2$***C***H), 60.59 (-, CH_3***C***H_2), 89.21 and 89.27 (+, O***C***HCH_3O), 125.83 and 125.84 (+, Ph***C***), 128.30 (2C, +, Ph***C***), 128.36 (2C, +, Ph***C***), 141.48 and 141.51 (quat, Ph***C***), 168.70 and 169.02 (quat, CH_3***C***OO), 169.46 and 169.52 (quat, C-1-***C***OO), 174.46 (quat, CH_3CH_2O***C***O), 174.94 and 175.02 (quat, C-10). HRMS: EI-MS: *m/z* for ($C_{26}H_{37}N_3O_7$) calcd. 503.2632, found: 503.26416. Analytical HPLC: purity 99 %, t_R = 14.65 min (gradient a), k = 4.09. $C_{26}H_{37}N_3O_7$ (503.59).

(1*S*,9*S*)-1-(2,2-Dimethylpropanoyl)ethyl 9-((*S*)-1-ethoxy-1-oxo-4-phenylbutan-2-yl-amino)-10-oxooctahydro-1*H*-pyridazino[1,2-a][1,2]diazepine-1-carboxylate (3.7): The title compound was prepared from cilazapril (0.6 mmol, 0.25 g), K_2CO_3 (0.7 mmol, 0.10 g) and **3.5** (0.8 mmol, 0.14 g) in DMF (H_2O < 0.01 %) (3 ml) according to the general procedure 3.8.2.1 and was obtained after flash chromatography (PE/EtOAc 1/1 v/v) as a pale yellow oil (0.29 g, 87 %). ^{1}H-NMR ($CDCl_3$) δ ppm: 1.16 and 1.19 (2s, 9H, $C(CH_3)_3$), 1.27 (m, 3H, C***H₃***CH_2), 1.36 and 1.71 (m, 2H, 3-H_2), 1.45 and 2.02 (m, 2H, 8-H_2), 1.48 (d, 3H, ^3J = 5.5 Hz, OCHC***H₃***O), 1.71 and 1.82 (m, 2H, 7-H_2), 1.83 and 2.21 and 2.33 (m, 2H, 2-H_2), 2.01 (m, 2H, $PhCH_2$C***H₂***), 2.44 (bs, 1H, NH), 2.50 and 3.31 and 3.44 (m, 2H, 6-H_2), 2.72 (m, 2H, PhC***H₂***), 2.93 and 3.06 (m, 2H, 4-H_2), 3.36 (m, 1H, $PhCH_2CH_2$C***H***), 4.15 (m, 1H, 9-H), 4.19 (m, 2H, CH_3C***H₂***), 5.00 and 5.06 (m, 1H, 1-H), 6.81 and 6.85 (m, 1H, OC***H***CH_3O), 7.17 (m, 3H, Ph***H***), 7.25 (m, 2H, Ph***H***). ^{13}C-NMR ($CDCl_3$) δ ppm: 14.30 (+, ***C***H_3CH_2), 15.78 and 16.19 (-, C-3), 19.21 and 19.38 (+, OCH***C***H_3O), 24.79 and 24.92 (-, C-2), 25.11 and 25.38 (-, C-7), 26.79 and 26.82 (3C, +, C(***C***$H_3)_3$), 29.99 and 30.26 (-, C-8), 32.17 and 32.20 (-, Ph***C***H_2), 35.10 and 35.17 (-, $PhCH_2$***C***H_2), 38.59 and 38.64 (quat, ***C***$(CH_3)_3$), 49.24 and 49.84 (+, C-1), 51.08 and 51.57 (-, C-6), 51.64 and 51.82 (-, C-4), 57.11 and 57.22 (+, C-9), 60.52 (-, CH_3***C***H_2), 60.64 (+, $PhCH_2CH_2$***C***H), 89.19 and 89.63 (+, O***C***HCH_3O), 125.81 and 125.82 (+, Ph***C***), 128.28 (2C, +, Ph***C***), 128.36 (2C, +, Ph***C***), 141.53 and 141.56 (quat, Ph***C***), 169.44 and 169.65 (quat, C-1-***C***OO), 174.58 (quat, CH_3CH_2O***C***O), 175.02 and 175.14 (quat, C-10), 176.20 and 176.46 (quat, $C(CH_3)_3$***C***OO). HRMS: EI-MS: *m/z* for ($C_{29}H_{43}N_3O_7$) calcd. 545.3101, found: 545.30947. Analytical HPLC: purity 99 %, two diastereomers, t_R = 17.26, 17.64 min (gradient a), k = 4.99, 5.13. $C_{29}H_{43}N_3O_7$ (545.67).

2-*tert*-Butyl-1,3-dithiane (3.8a)[21]: Propane-1,3-dithiol (1 eq, 0.18 mol, 19.4 g) was added dropwise to a mixture of pivaldehyde (1.3 eq, 0.24 mol, 20.3 g) and lithium tetrafluoroborate (0.1 eq, 0.018 mol, 1.0 g). The reaction mixture was allowed to stir overnight. Excess pivaldehyde was removed by distillation at atmospheric pressure. The desired product was obtained by distillation under reduced pressure as a light yellowish liquid (25.92 g, 82%). Bp.: 58-60 °C/ 0.2 mbar (ref.[49]: 108-110 °C/ 12 torr). ^{1}H-NMR ($CDCl_3$) δ ppm: 1.11 (s, 9H, $(CH_3)_3$), 1.80 and 2.07 (m, 2H, 1,3-dithiane-5-H_2), 2.89 (m,

4H, 1,3-dithiane-4-H_2 and 1,3-dithiane-6-H_2), 3.99 (s, 1H, 1,3-dithiane-2-H). CI-MS (NH_3) *m/z* (%): 177 (100) $[M+H]^+$. $C_8H_{16}S_2$ (176.34).

1-(2-*tert*-Butyl-1,3-dithian-2-yl)ethanol (3.8b)[22]: 3.8a (1 eq, 108 mmol, 19.11 g) was dissolved in 217 ml THF/abs to give a 0.5 mol/l solution. A 1.6 mol/l solution of butyllithium in hexane (1.05 eq, 114 mmol, 71.1 ml) was added dropwise to the stirred reaction mixture under nitrogen at -25 °C. The reaction mixture was kept stirring for 5 h at -25 °C, cooled down to -78 °C and acetaldehyde (1.5 eq, 163 mmol, 9.2 ml) was added dropwise. The mixture was stirred overnight and allowed to warm to room temperature, poured into 600 ml H_2O and extracted three times with $CHCl_3$. The pooled organic layers were washed twice with 10 % potassium hydroxide solution and once with H_2O, dried over anhydrous $MgSO_4$ and filtered. The volatiles were rotary evaporated. The resulting material was fractionally distilled under reduced pressure to yield a light yellowish liquid (14.59 g, 61 %). Bp.: 92-95 °C/ 0.2 mbar. ^{1}H-NMR ($CDCl_3$) δ ppm: 1.23 (s, 9H, $(CH_3)_3$), 1.57 (d, 3H, ^3J = 6.5 Hz, CHC***H₃***), 1.82 and 2.02 (m, 2H, 1,3-dithiane-5-H_2), 2.65 and 2.95 (m, 4H, 1,3-dithiane-4-H_2, 1,3-dithiane-6-H_2), 3.12 (d, 1H, ^3J = 2.0 Hz, OH), 4.36 (dq, 1H, ^3J = 2.7 Hz, ^3J = 6.6 Hz, CH). ^{13}C-NMR ($CDCl_3$) δ ppm: 19.69 (+, CH***C***H_3), 23.80 (-, 1,3-dithiane-C-5), 25.88 and 26.78 (-, 2C, 1,3-dithiane-C-4 and 1,3-dithiane-C-6), 28.26 (+, C(***C***$H_3)_3$), 41.31 (quat, ***C***$(CH_3)_3$), 67.49 (+, CH), 70.76 (quat, 1,3-dithiane-C-2). CI-MS (NH_3) *m/z* (%): 238 (100) $[M+NH_4]^+$. $C_{10}H_{20}OS_2$ (220.40).

4-Hydroxy-2,2-dimethylpentan-3-one (3.8)[22]: $HgCl_2$ (2.5 eq, 166 mmol, 44.93 g) and HgO (1.5 eq, 99 mmol, 21.51 g) were added to a solution of **3.8b** (1 eq, 66 mmol, 14.59 g) in MeOH/H_2O (9/1 v/v). The reaction mixture was heated to reflux for 5 h. Solids were removed by filtration and washed with little amounts of diethylether. The filtrate was diluted with ca. 700 ml H_2O and extracted with diethylether three times. The pooled organic layers were successively washed with H_2O, saturated ammonium chloride solution and H_2O, dried over anhydrous $MgSO_4$ and concentrated under reduced pressure. The resulting material was objected to fractional distillation to yield the desired product as a colorless liquid (3.83 g, 44.4 %). Bp.: 35-38 °C/ 0.2 mbar. ^{1}H-NMR ($CDCl_3$) δ ppm: 1.21 (s, 9H, $C(CH_3)_3$), 1.35 (d, 3H, ^3J = 6.8 Hz, CH_3), 2.83 (bs, 1H, OH), 4.60 (q, 1H, ^3J = 6.8 Hz, CH). ^{13}C-NMR ($CDCl_3$) δ ppm: 21.68 (+, CH_3), 26.74 (+, C(***C***$H_3)_3$), 42.63 (quat, ***C***$(CH_3)_3$), 68.57 (+, CH), 218.43 (quat, C=O). CI-MS (NH_3) *m/z* (%): 148 (100) $[M+NH_4]^+$. $C_7H_{14}O_2$ (130.18).

4-*tert*-Butyl-5-methyl-1,3-dioxol-2-one (3.9)[23]: A solution of triphosgene (0.75 eq, 22.1 mmol, 6.55 g) in 15 ml of DCM to a mixture of **3.8** (1 eq, 29.4 mmol, 3.83 g) and dimethylaniline (1.5 eq, 44.1 mmol, 5.57 ml) in 60 ml of DCM was added over a period of 30 min. The reaction mixture was stirred at room temperature for 2 h. The solvent was rotary evaporated, and the residue was heated to reflux at 160 °C for 4 h. The crude product was purified by fractional distillation under reduced pressure. The product containing fractions were pooled, dissolved in diethylether and washed with 1 mol/l HCl

solution. The organic phase was dried over anhydrous $MgSO_4$, filtered and evaporated under reduced pressure to yield the title compound as a colorless liquid (1.84 g, 40 %). Bp.: 39-43 °C/ 0.2 mbar (ref.[23]: 108-112 °C/ 1 torr). ^{1}H-NMR ($CDCl_3$) δ ppm: 1.24 (s, 9H, $C(CH_3)_3$), 2.13 (s, 3H, CH_3). ^{13}C-NMR ($CDCl_3$) δ ppm: 10.52 (+, CH_3), 28.22 (+, $C(\boldsymbol{C}H_3)_3$), 31.54 (quat, $\boldsymbol{C}(CH_3)_3$), 132.85 (quat, $CH_3\boldsymbol{C}$=C^{t}Bu), 145.03 (quat, CH_3C=$\boldsymbol{C}^t$Bu), 152.96 (quat, C=O). EI-MS (70 eV) m/z (%): 192 (8) [$M^{+\cdot}$]. EI-MS (70 eV) *m/z* (%): 156 (21) [$M^{+\cdot}$]. $C_8H_{12}O_3$ (156.18).

4-(Bromomethyl)-5-methyl-1,3-dioxol-2-one (3.10): *N*-bromosuccinimide (1.1 eq, 9.7 mmol, 1.72 g) and azobisisobutyronitrile (0.02 eq, 0.1 mmol, 22 mg) were added to a solution of 4,5-dimethyl-1,3-dioxol-2-one (1 eq, 8.8 mmol, 1.00 g) in ca. 40 ml CCl_4. The reaction mixture was carefully heated to reflux. After the reaction started with vigorous boiling the reaction mixture was heated to reflux for 1 h. Solids were removed by filtration and the filtrate was concentrated under reduced pressure. The resulting material was subjected to distillation under reduced pressure to yield the title compound as a yellow liquid (1.12 g, 66 %). Bp: 90 °C/ 1 mbar (ref.[50]:115-120 °C/ 5 torr). ^{1}H-NMR ($CDCl_3$) δ ppm: 2.13 (s, 3H, CH_3), 4.18 (s, 2H, CH_2). ^{13}C-NMR ($CDCl_3$) δ ppm: 9.49 (+, CH_3), 17.78 (-, CH_2), 134.46 (quat, CH_3C=$\boldsymbol{C}CH_2$), 136.57 (quat, $CH_3\boldsymbol{C}$=CCH_2), 137.89 (quat, C=O). EI-MS (70 eV) *m/z* (%): 192 (8) [$M^{+\cdot}$]. $C_5H_5BrO_3$ (193.00).

4-(Bromomethyl)-5-*tert*-butyl-1,3-dioxol-2-one (3.11): The title compound was prepared following the procedure described for the synthesis of **3.10**, using **3.9** (1 eq, 6.4 mmol, 1.0 g), *N*-bromosuccinimide (1.1 eq, 7.0 mmol, 1.25 g) and azobisisobutyronitrile (0.05 eq, 0.5 mmol, 87 mg) in ca. 50 ml CCl_4, and was obtained after distillation under reduced pressure as a pale yellow liquid (1.29 g, 86%). Bp.: 60-64 °C/ 0.2 mbar (ref.[51]: 112-115 °C/ 4 torr). ^{1}H-NMR ($CDCl_3$) δ ppm: 1.31 (s, 9H, $C(CH_3)_3$), 4.29 (s, 2H, CH_2). ^{13}C-NMR ($CDCl_3$) δ ppm: 19.54 (-, CH_2), 27.76 (+, $C(\boldsymbol{C}H_3)_3$), 32.30 (quat, $\boldsymbol{C}(CH_3)_3$), 133.01 (quat, $CH_2\boldsymbol{C}$=C^{t}Bu), 148.09 (quat, CH_2C=$\boldsymbol{C}^t$Bu), 151.42 (quat, C=O). EI-MS (70 eV) *m/z* (%): 234 (10) [$M^{+\cdot}$]. $C_8H_{11}BrO_3$ (235.08).

3.8.2.3 General procedure for the synthesis of (5-alkyl-2-oxo-1,3-dioxol-4-yl)methyl esters (3.12, 3.13)

K_2CO_3 (1.5 eq) was added to a solution of cilazapril (1 eq) in DMF (H_2O < 0.01 %). A solution of the appropriate 4-(bromomethyl)-5-alkyl-1,3-dioxol-2-one (1.4 eq) in DMF (H_2O < 0.01 %) was added dropwise at 0 °C. The reaction mixture was warmed to room temperature and stirred overnight. The solvent was evaporated under reduced pressure and the residue was taken up in EtOAc/H_2O 1/1 v/v. The layers were separated and the aqueous phase was extracted twice with EtOAc. The combined organic phases were washed with brine, dried over anhydrous $MgSO_4$, filtered and evaporated to dryness. Flash chromatography of the crude material yielded the title cilazapril derivatives.

(1*S*,9*S*)-(5-Methyl-2-oxo-1,3-dioxol-4-yl)methyl 9-((*S*)-1-ethoxy-1-oxo-4-phenylbutan-2-ylamino)-10-oxooctahydro-1*H*-pyridazino[1,2-a][1,2]diazepine-1-carboxylate (3.12): The title compound was prepared according to the general procedure 3.8.2.3, using cilazapril (1.2 mmol, 0.50 g), K_2CO_3 (1.8 mmol, 0.25 g) and **3.10** (1.48 eq, 1.8 mmol, 0.34 g) in DMF (H_2O < 0.01 %) (5 ml), and was obtained after flash chromatography (PE/EtOAC 2/1 to 1/1 v/v) as a yellow oil (0.36 g, 61 %). ^{1}H-NMR ($CDCl_3$) δ ppm: 1.27 (t, 3H, ^3J = 7.2 Hz, C***H*₃**CH_2), 1.39 and 1.68 (m, 2H, 3-H_2), 1.44 and 2.02 (m, 2H, 8-H_2), 1.72 and 1.84 (m, 2H, 7-H_2), 1.85 and 2.29 (m, 2H, 2-H_2), 2.01 (m, 2H, $PhCH_2C$***H*₂**), 2.16 (s, 3H, CH_3C=C), 2.51 and 3.24 (m, 2H, 6-H_2), 2.72 (m, 2H, Ph***C*H₂**), 2.94 and 3.08 (m, 2H, 4-H_2), 3.34 (m, 1H, $PhCH_2CH_2C$***H***), 4.13 (m, 1H, 9-H), 4.17 (m, 2H, CH_3C***H*₂**), 4.88 (s, 2H, OCH_2C=C), 5.06 (m, 1H, 1-H), 7.17 (m, 3H, Ph***H***), 7.25 (m, 2H, Ph***H***). ^{13}C-NMR ($CDCl_3$) δ ppm: 9.38 (+, ***C***H_3C=C), 14.28 (+, ***C***H_3CH_2), 15.93 (-, C-3), 24.87 (-, C-2), 24.95 (-, C-7), 29.98 (-, C-8), 32.16 (-, Ph***C***H_2), 35.13 (-, $PhCH_2$***C***H_2), 49.53 (+, C-1), 51.28 (-, C-6), 51.58 (-, C-4), 54.37 (-, O***C***H_2C=C), 57.09 (+, C-9), 60.43 (+, $PhCH_2CH_2$***C***H), 60.58 (-, CH_3***C***H_2), 125.83 (+, Ph***C***), 128.29 (2C, +, Ph***C***), 128.35 (2C, +, Ph***C***), 133.00 (quat, CH_3***C***=C), 140.35 (quat, CH_3C=***C***), 141.49 (quat, Ph***C***), 151.86 (quat, OC(O)O), 171.44 (quat, C-1-**C**OO), 174.61 (quat, CH_3CH_2O***C***O), 175.11 (quat, C-10). HRMS: EI-MS: *m/z* for ($C_{27}H_{35}N_3O_8$) calcd. 529.2424, found: 529.24212. Analytical HPLC: purity 98 %, t_R = 12.41 min (gradient b), k = 3.31. $C_{27}H_{35}N_3O_8$ (529.58).

(1*S*,9*S*)-(5-*tert*-Butyl-2-oxo-1,3-dioxol-4-yl)methyl 9-((*S*)-1-ethoxy-1-oxo-4-phenylbutan-2-ylamino)-10-oxooctahydro-1*H*-pyridazino[1,2-a][1,2]diazepine-1-carboxylate (3.13): The title compound was prepared from cilazapril (1.2 mmol, 0.50 g), K_2CO_3 (1.7 mmol, 0.23 g) and **3.11** (1.7 mmol, 0.40 g) in DMF (H_2O < 0.01 %) (5 ml) according to the general procedure 3.8.2.3 and was obtained after flash chromatography (PE/EtOAC 3/1 v/v) as a yellow oil (0.42 g, 66 %). ^{1}H-NMR ($CDCl_3$) δ ppm: 1.28 (m, 3H, C***H*₃**CH_2), 1.29 (s, 9H, $(CH_3)_3$), 1.48 and 1.70 (m, 2H, 3-H_2), 1.48 and 2.05 (m, 2H, 8-H_2), 1.72 and 1.85 (m, 2H, 7-H_2), 1.85 and 2.30 (m, 2H, 2-H_2), 2.05 (m, 2H, $PhCH_2C$***H*₂**), 2.53 and 3.29 (m, 2H, 6-H_2), 2.73 (m, 2H, Ph***C*H₂**), 2.94 and 3.08 (m, 2H, 4-H_2), 3.39 (m, 1H, $PhCH_2CH_2C$***H***), 4.16 (m, 1H, 9-H), 4.20 (m, 2H, CH_3C***H*₂**), 5.00 (m, 2H, O***C*H₂**C=C), 5.05 (m, 1H, 1-H), 7.17 (m, 3H, Ph***H***), 7.25 (m, 2H, Ph***H***). ^{13}C-NMR ($CDCl_3$) δ ppm: 14.33 (+, ***C***H_3CH_2), 16.01 (-, C-3), 25.03 (2C, -, C-2 and C-7), 27.92 (3C, +, C(***C***$H_3)_3$), 29.58 (-, C-8), 32.17 (-, Ph***C***H_2), 34.86 (-, $PhCH_2$***C***H_2), 40.87 (quat, ***C***$(CH_3)_3$), 49.82 (+, C-1), 51.42 (-, C-6), 51.70 (-, C-4), 55.89 (-, O***C***H_2C=C), 57.31 (+, C-9), 60.40 (+, $PhCH_2CH_2$***C***H), 60.87 (-, CH_3***C***H_2), 125.96 (+, Ph***C***), 128.38 (2C, +, Ph***C***), 128.44 (2C, +, Ph***C***), 131.13 (quat, $(CH_3)_3CC$=***C***), 141.35 (quat, Ph***C***), 150.17 (quat, $(CH_3)_3C$***C***=C), 151.72 (quat, OC(O)O), 170.80 (quat, C-1-**C**OO), 174.02 (quat, CH_3CH_2O***C***O), 174.72 (quat, C-10). HRMS: EI-MS: *m/z* for ($C_{30}H_{41}N_3O_8$) calcd. 571.2894, found: 571.2890. Analytical HPLC: purity 97 %, t_R = 14.11 min (gradient b), k = 3.90. $C_{30}H_{41}N_3O_8$ (571.66).

(1*S*,9*S*)-2-Morpholinoethyl 9-((*S*)-1-ethoxy-1-oxo-4-phenylbutan-2-ylamino)-10-oxo-octahydro-1*H*-pyridazino[1,2-a][1,2]diazepine-1-carboxylate (3.14): A catalytic amount of 4-(dimethylamino)pyridine and 4-(2-hydroxyethyl)morpholine (1 eq, 2.4 mmol, 0.29 ml) were added to a solution of cilazapril (1 eq, 2.4 mmol, 1.00 g) in DCM/abs (5 ml). A solution of *N,N'*-dicyclohexylcarbodiimide (1.1 eq, 2.6 mmol, 0.55 g) in DCM/abs (2 ml) was added dropwise at 0 °C under an atmosphere of argon. The reaction mixture was stirred at 0 °C for 1 h and at room temperature overnight. Solids were removed by filtration. Rotary evaporation of the filtrate gave the crude product, which was subjected to flash chromatography (PE/EtOAc 1/3 + 0.5 % NEt_3 v/v) to yield the desired product as a yellow oil (0.91 g, 72 %). ^{1}H-NMR ($CDCl_3$) δ ppm: 1.27 (t, 3H, ^3J = 7.1 Hz, C***H*****$_3$**CH_2), 1.37 and 1.72 (m, 2H, 3-H_2), 1.46 and 2.01 (m, 2H, 8-H_2), 1.72 and 1.85 (m, 2H, 7-H_2), 1.85 and 2.31 (m, 2H, 2-H_2), 2.01 (m, 2H, $PhCH_2C$***H*****$_2$**), 2.22 (bs, 1H, NH), 2.47 (m, 4H, mo-3-H_2, mo-5-H_2), 2.50 and 3.40 (m, 2H, 6-H_2), 2.60 (m, 2H, $OCOCH_2C$***H*****$_2$**N), 2.73 (m, 2H, PhC***H*****$_2$**), 2.94 and 3.08 (m, 2H, 4-H_2), 3.52 (t, 1H, ^{3}J = 6.6 Hz, $PhCH_2CH_2C$***H***), 3.67 (m, 4H, mo-2-H_2, mo-6-H_2), 4.14 (m, 1H, 9-H), 4.18 (m, 2H, CH_3C***H*****$_2$**), 4.21 and 4.29 (m, 2H, OCOC***H*****$_2$**CH_2N), 5.03 (m, 1H, 1-H), 7.17 (m, 3H, Ph***H***), 7.25 (m, 2H, Ph***H***). ^{13}C-NMR ($CDCl_3$) δ ppm: 14.29 (+, ***C***H_3CH_2), 16.06 (-, C-3), 25.13 (2C, -, C-2 and C-7), 30.15 (-, C-8), 32.19 (-, Ph***C***H_2), 35.16 (-, $PhCH_2$***C***H_2), 49.78 (+, C-1), 51.38 (-, C-6), 51.74 (-, C-4), 53.67 (2C, -, mo-C-3, mo-C-5), 56.96 (-, $OCOCH_2$***C***H_2N), 57.13 (+, C-9), 60.50 (-, CH_3***C***H_2), 60.56 (+, $PhCH_2CH_2$***C***H), 61.81 (-, OCO***C***H_2CH_2N), 66.87 (2C, -, mo-C-2, mo-C-6), 125.80 (+, Ph***C***), 128.28 (2C, +, Ph***C***), 128.35 (2C, +, Ph***C***), 141.55 (quat, Ph***C***), 171.34 (quat, C-1-***C***OO), 174.61 (quat, CH_3CH_2O***C***O), 175.14 (quat, C-10). HRMS: EI-MS: *m/z* for ($C_{28}H_{42}N_4O_6$) calcd. 530.3104, found: 530.31032. Analytical HPLC: purity 100 %, t_R = 8.49 min (gradient b), k = 1.95. $C_{28}H_{42}N_4O_6$ (530.66).

Chlorosulfuric acid 1-chloroethyl ester (3.15)[24]: Chlorosulfuric acid (1.08 eq, 45 mmol, 3.00 ml) was added dropwise to 1-chloroethyl chloroformate (1 eq, 42 mmol, 4.57 ml) at 0 °C. The reaction mixture was stirred for 4 h until gas evolution ceased and was then poured into a mixture of ice water and DCM (1/1 v/v). The phases were separated and the aqueous layer was extracted with DCM twice. The pooled organic layers were washed twice with saturated $NaHCO_3$ solution and once with brine, dried over anhydrous $MgSO_4$ and filtered. The volatiles were rotary evaporated and the residue was purified by distillation under reduced pressure to yield the title compound as a colorless liquid (4.15 g, 55 %). Bp.: 63-65 °C/ 57 mmHg (ref.[24]: 49-50 °C/ 10 torr). ^{1}H-NMR ($CDCl_3$) δ ppm: 1.99 (d, 1H, ^3J = 5.8 Hz, CH), 6.48 (q, 3H, ^3J = 5.8 Hz, CH_3). ^{13}C-NMR ($CDCl_3$) δ ppm: 26.31 (+, CH_3), 90.98 (+, CH). $C_2H_4Cl_2O_3S$ (179.02).

(1*S*,9*S*)-1-Chloroethyl 9-((*S*)-1-ethoxy-1-oxo-4-phenylbutan-2-ylamino)-10-oxooctahydro-1*H*-pyridazino[1,2-a][1,2]diazepine-1-carboxylate (3.16)[24]: Compound **3.15** (2 eq, 2.9 mmol, 0.52 g) was added dropwise to a mixture of cilazapril (1 eq, 1.4 mmol,

0.60 g), $NaHCO_3$ (3.9 eq, 5.6 mmol, 0.47 g) and tetrabutylammonium hydrogensulfate (0.1 eq, 0.14 mmol, 49 mg) in DCM/H_2O (1/1 v/v). The reaction mixture was vigorously stirred under reflux for 4 h and at room temperature overnight. The phases were separated and the aqueous layer was extracted with DCM twice. The combined organic layers were washed twice with saturated $NaHCO_3$ solution and once with brine, dried over anhydrous $MgSO_4$, filtered and evaporated to dryness. The title compound was obtained after flash chromatography (PE/EtOAC 2/1 v/v) as a yellow oil (0.44 g, 63 %). ^{1}H-NMR ($CDCl_3$) δ ppm: 6.52 (m, 1H, CHCl). ^{13}C-NMR ($CDCl_3$) δ ppm: 25.03 and 25.25 (+, C***H*****$_3$**CHCl), 81.47 and 81.37 (+, CH_3C***H***Cl). ES-MS (DCM/MEOH + 10 mM NH_4OAc) *m/z* (%): 480 (100) $[M+H]^+$. $C_{24}H_{34}ClN_3O_5$ (480.00).

***tert*-Butyl 2-morpholinoacetate (3.17a)[25]:** To a solution of *tert*-butyl bromoacetate (1 eq, 28.5 mmol, 5.56 g) in THF a mixture of morpholine (1 eq, 28.5 mmol, 2.50 g) and triethylamine (1 eq, 28.5 mmol, 4 ml) was added dropwise at 0 °C. The reaction mixture was heated to reflux for 2 h and then cooled down to 0 °C again. The resulting suspension was filtered and the filtrate was evaporated to dryness. The oily residue was dissolved in ethyl acetate and washed with H_2O. After the organic phase was dried over anhydrous $MgSO_4$ and filtered the solvent was removed under reduced pressure to yield the desired product as a yellow oil (5.17 g, 90 %). ^{1}H-NMR ($CDCl_3$) δ ppm: 1.39 (s, 9H, $C(CH_3)_3$), 2.50 (m, 4H, mo-3-H_2, mo-5-H_2), 3.03 (s, 2H, CH_2), 3.68 (m, 4H, mo-2-H_2, mo-6-H_2). $C_{10}H_{19}NO_3$ (201.26).

2-Morpholinoacetic acid (3.17)[25]: TFA (1.6 eq, 42 mmol, 32 ml) was added dropwise to a solution of **3.17a** (1 eq, 26 mmol, 5.17 g) in DCM at 0 °C. The reaction mixture was stirred at room temperature overnight and was afterwards evaporated to dryness. Treatment of the residue with diisopropylether resulted in crystallization of the product, which was filtered off and dried under reduced pressure. The off-white crystalline product was obtained as a non-stoichiometric salt with TFA (6.16 g). ^{1}H-NMR (DMSO-d_6) δ ppm: 3.26 (m, 4H, mo-3-H_2, mo-5-H_2), 3.83 (m, 4H, mo-2-H_2, mo-6-H_2), 4.08 (s, 2H, CH_2), 10.68-14.10 (bs, 2H, OH). ES-MS (DCM/MEOH + 10 mM NH_4OAc) *m/z* (%): 146 (100) $[M+H]^+$. $C_6H_{11}NO_3$ (145.16).

(1*S*,9*S*)-1-(2-Morpholinoacetoxy)ethyl 9-((*S*)-1-ethoxy-1-oxo-4-phenylbutan-2-ylamino)-10-oxooctahydro-1*H*-pyridazino[1,2-a][1,2]diazepine-1-carboxylate (3.18): Cs_2CO_3 (4 eq, 3.76 mmol, 1.23 g) was added to a solution of the **3.17** (2 eq, 1.88 mmol, 0.49 g) in DMF (H_2O < 0.01 %) (6 ml). A solution of **3.16** (1 eq, 0.94 mmol, 0.45 g) in DMF (H_2O < 0.01 %) (1 ml) was added dropwise. The mixture was stirred for 7 h at 40 °C and overnight at room temperature. The solvent was evaporated under reduced pressure and the residue was taken up in EtOAc/H_2O 1/1 v/v. The layers were separated and the aqueous phase was extracted with EtOAc twice. The pooled organic phases were washed with brine, dried over anhydrous $MgSO_4$, filtered and evaporated to dryness. Flash chromatography (PE/EtOAc 1/1 + NH_3 to 1/2 + NH_3 v/v) of the crude material

yielded the target compound as a yellow oil (0.17 g, 31 %). ^{1}H-NMR ($CDCl_3$) δ ppm: 1.27 (t, 3H, ^{3}J = 7.1 Hz, C***H₃***CH_2), 1.36 and 1.71 (m, 2H, 3-H_2), 1.44 and 2.00 (m, 2H, 8-H_2), 1.50 (d, 3H, ^{3}J = 5.5 Hz, OCHC***H₃***O), 1.70 and 1.85 (m, 2H, 7-H_2), 1.85 and 2.22 and 2.30 (m, 2H, 2-H_2), 2.01 (m, 2H, $PhCH_2C$***H₂***), 2.49 and 3.28 and 3.39 (m, 2H, 6-H_2), 2.56 (m, 4H, mo-3-H_2, mo-5-H_2), 2.71 (m, 2H, PhC***H₂***), 2.93 and 3.06 (m, 2H, 4-H_2), 3.18 and 3.22 (2 s, 2H, mo-***CH₂***CO), 3.34 (m, 1H, $PhCH_2CH_2C$***H***), 3.71 (m, 4H, mo-2-H_2, mo-6-H_2), 4.14 (m, 1H, 9-H), 4.17 (m, 2H, CH_3C***H₂***), 5.00 and 5.05 (m, 1H, 1-H), 6.85 and 6.91 (2 q, 1H, ^{3}J = 5.4 Hz, OC***H***CH_3O), 7.17 (m, 3H, Ph***H***), 7.25 (m, 2H, Ph***H***). ^{13}C-NMR ($CDCl_3$) δ ppm: 14.28 (+, ***C***H_3CH_2), 15.77 and 16.04 (-, C-3), 19.37 and 19.47 (+, OCH***C***H_3O), 24.79 and 24.94 (-, C-2), 24.85 and 25.13 (-, C-7), 29.88 and 30.04 (-, C-8), 32.15 (-, Ph***C***H_2), 35.08 and 35.12 (-, $PhCH_2$***C***H_2), 49.29 and 49.74 (+, C-1), 51.10 and 51.50 (-, C-6), 51.54 and 51.66 (-, C-4), 52.94 and 53.00 (2C, -, mo-C-3, mo-C-5), 57.06 and 57.12 (+, C-9), 58.98 and 59.12 (-, mo-***CH₂***CO), 60.48 and 60.52 (+, $PhCH_2CH_2$***C***H), 60.54 (-, CH_3***C***H_2), 66.65 and 66.66 (2C, -, mo-C-2, mo-C-6), 89.28 and 89.38 (+, O***C***HCH_3O), 125.81 and 125.82 (+, Ph***C***), 128.28 (2C, +, Ph***C***), 128.33 (2C, +, Ph***C***), 141.46 and 141.48 (quat, Ph***C***), 167.92 and 168.17 (mo-CH_2***C***O), 169.42 and 169.55 (quat, C-1-***C***OO), 174.52 (quat, CH_3CH_2O***C***O), 174.97 and 175.07 (quat, C-10). HRMS: EI-MS: *m/z* for ($C_{30}H_{44}N_4O_8$) calcd. 588.3159, found: 588.31599. Analytical HPLC: purity 98 %, t_R = 10.49 min (gradient a), k = 2.64. $C_{30}H_{44}N_4O_8$ (588.69).

Ethyl phenylcarbamate (3.19)[26]: Triethylamine (1 eq, 20 mmol, 1.44 g) and aniline (1 eq, 20 mmol, 1.86 g) were added dropwise to a solution of ethyl chloroformate (1 eq, 20 mmol, 2.17 g) in DCM at 0 °C. The reaction mixture was allowed to warm to room temperature and was stirred overnight. The solution was washed with brine three times. The organic layer was dried over $MgSO_4$, filtered and concentrated under reduced pressure to yield the title compound as a yellow solid (2.79 g, 84 %). ^{1}H-NMR ($CDCl_3$) δ ppm: 1.30 (t, 3H, ^{3}J = 7.1 Hz, CH_3), 4.23 (q, 2H, ^{3}J = 7.1 Hz, CH_2), 6.87 (bs, 1H, NH), 7.05 (m, 1H, Ph***H***), 7.29 (m, 2H, Ph***H***), 7.40 (m, 2H, Ph***H***). $C_9H_{11}NO_2$ (165.19).

Ethyl 4-(ethoxycarbonylamino)benzoate (3.20)[26]: The title compound was prepared following the procedure described for the synthesis of **3.19** using ethyl 4-aminobenzoate (1 eq, 20 mmol, 3.30 g), triethylamine (1 eq, 20 mmol, 2.77 ml) and ethyl chloroformate (1 eq, 20 mmol, 2.17 g) and was obtained as a yellow solid (2.45 g, 52 %). EI-MS (70 eV) *m/z* (%): 237 (73) [$M^{+\cdot}$]. $C_{12}H_{15}NO_4$ (237.25).

Ethyl 4-(methoxycarbonylamino)benzoate (3.21)[26]: The title compound was prepared following the procedure described for the synthesis of **3.19** using ethyl 4-aminobenzoate (1 eq, 20 mmol, 3.30 g), triethylamine (1 eq, 20 mmol, 2.77 ml) and methyl chloroformate (1 eq, 20 mmol, 1.55 ml) and was obtained as a yellow solid (2.35 g, 53 %). EI-MS (70 eV) *m/z* (%): 223 (56) [$M^{+\cdot}$]. $C_{11}H_{13}NO_4$ (223.23).

Ethyl chloromethyl(phenyl)carbamate (3.22)[26]: A mixture of **3.19** (1 eq, 17 mmol, 2.79 g), paraformaldeyde (1.7 eq, 29 mmol, 0.86 g) and trimethylsilyl chloride (13 eq, 219 mmol, 28 ml) was heated to reflux for 2.5 h. The reaction mixture was diluted with DCM and the solids were filtered off. The filtrate was concentrated under reduced pressure and the resulting oily residue was triturated with hexane overnight. The suspension was filtered and evaporated to dryness to give the desired product as a yellow oil (3.03 g, 84 %). ^{1}H-NMR ($CDCl_3$) δ ppm: 1.25 (t, 3H, ^3J = 7.1 Hz, CH_3), 4.25 (q, 2H, ^3J = 7.1 Hz, $CH_3C\boldsymbol{H_2}$), 5.57 (s, 2H, $ClCH_2$), 7.28-7.45 (m, 5H, Ph***H***). CI-MS (NH_3) *m/z* (%): 231 (71) $[M+NH_4]^+$. $C_{10}H_{12}ClNO_2$ (213.66).

4-[(Chloromethyl)(ethoxycarbonyl)amino]benzoate (3.23)[27]: A suspension of **3.20** (1 eq, 10 mmol, 2.38 g), paraformaldehyde (1.1 eq, 11 mmol, 0.36 g), trimethylsilyl chloride (5 eq, 50 mmol, 6.3 ml) and 10 g of anhydrous $MgSO_4$ in toluol was stirred at room temperature for 2.5 d. After the solids were removed by filtration the filtrate was concentrated under reduced pressure to yield the title compound as yellow oil (1.41 g, 49 %). ^{1}H-NMR ($CDCl_3$) δ ppm: 1.26 (t, 3H, ^3J = 7.1 Hz, $C\boldsymbol{H_3}CH_2OCON$), 1.39 (t, 3H, ^3J = 7.1 Hz, $C\boldsymbol{H_3}CH_2OCOPh$), 4.26 (q, 2H, ^3J = 7.1 Hz, $CH_3C\boldsymbol{H_2}OCON$), 4.38 (q, 2H, ^3J = 7.1 Hz, $CH_3C\boldsymbol{H_2}OCOPh$), 5.57 (s, 2H, $ClCH_2$), 7.43 (m, 2H, aminobenzoate-3-H, aminobenzoate-5-H), 8.07 (m, 2H, aminobenzoate-2-H, aminobenzoate-6-H). ^{13}C-NMR ($CDCl_3$) δ ppm: 14.33 (2C, +, ***C***H_3CH_2OCON, ***C***H_3CH_2OCOPh), 61.19, 61.46 (-, $ClCH_2$, CH_3***C***H_2OCOPh), 63.21 (-, CH_3***C***H_2OCON), 126.19 (+, 2C, aminobenzoate-C-2, aminobenzoate-C-6), 129.45 (quat, aminobenzoate-C-4), 130.53 (+, 2C, aminobenzoate-C-3, aminobenzoate-C-5), 144.28 (quat, aminobenzoate-C-1), 154.05 (quat, OCON), 165.81 (quat, O***C***OPh). CI-MS (NH_3) *m/z* (%): 303 (100) $[M+NH_4]^+$. $C_{13}H_{16}ClNO_4$ (285.72).

4-[(Chloromethyl)(methoxycarbonyl)amino]benzoate (3.24)[27]: The title compound was prepared following the procedure for the synthesis of **3.23** using **3.21** (1 eq, 8.2 mmol, 1.82 g), paraformaldehyde (1.7 eq, 14 mmol, 0.46 g), trimethylsilyl chloride (10 eq, 82 mmol, 10.4 ml) and 10 g of anhydrous $MgSO_4$ and was obtained as yellow oil (0.95 g, 43 %). ^{1}H-NMR ($CDCl_3$) δ ppm: 1.39 (t, 3H, ^3J = 7.1 Hz, $C\boldsymbol{H_3}CH_2$), 3.79 (s, 3H, CH_3OCO), 4.38 (q, 2H, ^3J = 7.1 Hz, $CH_3C\boldsymbol{H_2}$), 5.56 (s, 2H, $ClCH_2$), 7.43 (m, 2H, aminobenzoate-3-H, aminobenzoate-5-H), 8.08 (m, 2H, aminobenzoate-2-H, aminobenzoate-6-H). ^{13}C-NMR ($CDCl_3$) δ ppm: 14.33 (+, ***C***H_3CH_2), 53.96 (+, CH_3O), 61.21, 61.44 (-, $ClCH_2$, CH_3***C***H_2), 126.34 (+, 2C, aminobenzoate-C-2, aminobenzoate-C-6), 129.67 (quat, aminobenzoate-C-4), 130.60 (+, 2C, aminobenzoate-C-3, aminobenzoate-C-5), 144.10 (quat, aminobenzoate-C-1), 154.57 (quat, OCON), 165.74 (quat, O***C***OPh). CI-MS (NH_3) *m/z* (%): 303 (100) $[M+NH_4]^+$. $C_{12}H_{14}ClNO_4$ (271.70).

3.8.2.4 General procedure for the synthesis of cilazapril derivatives 3.25-3.27

K_2CO_3 (1.8 eq) was added to a solution of cilazapril (1 eq) in DMF (H_2O < 0.01 %). A solution of ethyl chloromethyl(phenyl)carbamate (1.5 eq) or the appropriate ethyl 4-((chloromethyl)(alkyloxycarbonyl)amino)benzoate (1.8 eq) in DMF (H_2O < 0.01 %) was added dropwise at 0 °C. The reaction mixture was warmed to room temperature and stirred overnight. The solvent was evaporated under reduced pressure and the residue was taken up in EtOAc/H_2O 1/1 v/v. The layers were separated and the aqueous phase was extracted twice with EtOAc. The combined organic phases were washed with brine, dried over anhydrous $MgSO_4$, filtered and evaporated to dryness. Flash chromatography of the crude material yielded the title cilazapril derivatives.

(1*S*,9*S*)-[Ethoxycarbonyl(phenyl)amino]methyl 9-((*S*)-1-ethoxy-1-oxo-4-phenylbutan-2-ylamino)-10-oxooctahydro-1*H*-pyridazino[1,2-a][1,2]diazepine-1-carboxylate (3.25): The title compound was prepared according to the general procedure 3.8.2.4 from cilazapril (0.36 mmol, 0.15 g), K_2CO_3 (1.5 eq, 0.54 mmol, 75 mg) and **3.22** (0.54 mmol, 115 mg) in DMF (H_2O < 0.01 %) (3 ml) and was obtained after flash chromatography (PE/EtOAc 2/1 v/v) as a pale yellow oil (60 mg, 28 %). ^{1}H-NMR ($CDCl_3$) δ ppm: 1.22 (t, 3H, ^3J = 6.9 Hz, C***H*₃**CH_2OCON), 1.27 (t, 3H, ^3J = 7.1 Hz, C***H*₃**CH_2OCOCH), 1.37 and 1.67 (m, 2H, 3-H_2), 1.37 and 1.98 (m, 2H, 8-H_2), 1.67 and 1.81 (m, 2H, 7-H_2), 1.81 and 2.30 (m, 2H, 2-H_2), 2.02 (m, 2H, $PhCH_2C$***H*₂**), 2.48 and 3.31 (m, 2H, 6-H_2), 2.74 (m, 2H, Ph***H*₂**), 2.93 and 3.07 (m, 2H, 4-H_2), 3.36 (t, 1H, ^3J = 6.6 Hz, $PhCH_2CH_2C$***H***), 4.14 (m, 1H, 9-H), 4.18 (m, 4H, CH_3C***H*₂**$OCON$ and CH_3C***H*₂**$OCOCH$), 5.07 (m, 1H, 1-H), 5.63 and 5.74 (m, 2H, OCH_2N), 7.18 (m, 3H, Ph***H***), 7.26 (m, 5H, aniline-***H***, Ph***H***), 7.36 (m, 2H, aniline-***H***). ^{13}C-NMR ($CDCl_3$) δ ppm: 14.28 (+, ***C***H_3CH_2OCOCH), 14.33 (+, ***C***H_3CH_2OCON), 16.02 (-, C-3), 24.96 (-, C-2), 25.11 (-, C-7), 30.06 (-, C-8), 32.20 (-, Ph***C***H_2), 35.17 (-, $PhCH_2$***C***H_2), 49.64 (+, C-1), 51.25 (-, C-6), 51.79 (-, C-4), 57.11 (+, C-9), 60.60 (+, $PhCH_2CH_2$***C***H), 60.63 (-, CH_3***C***H_2OCOCH), 62.52 (-, CH_3***C***H_2OCON), 75.33 (-, OCH_2N), 125.82 (+, Ph***C***), 126.80 (+, aniline-***C***), 127.32 (2C, +, aniline-***C***), 128.29 (2C, +, Ph***C***), 128.36 (2C, +, Ph***C***), 129.05 (2C, +, aniline-***C***), 140.63 (quat, aniline-***C***), 141.55 (quat, Ph***C***), 155.02 (quat, CH_3CH_2O***C***ON), 170.78 (quat, C-1-***C***OO), 174.59 (quat, CH_3CH_2O***C***OCH), 175.19 (quat, C-10). HRMS: LSI-MS: *m/z* for ($C_{32}H_{42}N_4O_7$ + H^+) calcd. 595.3126, found: 595.31148. Analytical HPLC: purity 96 %, t_R = 13.63 min (gradient b), k = 3.73. $C_{32}H_{42}N_4O_7$ (594.70).

(1*S*,9*S*)-{Ethoxycarbonyl[4-(ethoxycarbonyl)phenyl]amino}methyl 9-((*S*)-1-ethoxy-1-oxo-4-phenylbutan-2-ylamino)-10-oxooctahydro-1*H*-pyridazino[1,2-a][1,2]diazepine-1-carboxylate (3.26): The title compound was prepared from cilazapril (0.48 mmol, 0.20 g), K_2CO_3 (0.86 mmol, 0.12 g) and **3.23** (0.86 mmol, 0.25 g) in DMF (H_2O < 0.01 %) (5 ml) according to the general procedure 3.8.2.4 and was obtained after flash chromatography (PE/EtOAc 5/2 to 2/1 v/v) as a pale yellow oil (0.19 g, 59 %). ^{1}H-NMR ($CDCl_3$) δ ppm: 1.26 (m, 6H, C***H*₃**CH_2OCON and C***H*₃**CH_2OCOPh), 1.37 (m, 3H,

C***H₃***CH_2OCOCH), 1.37 and 1.67 (m, 2H, 3-H_2), 1.37 and 2.02 (m, 2H, 8-H_2), 1.67 and 1.81 (m, 2H, 7-H_2), 1.81 and 2.30 (m, 2H, 2-H_2), 2.02 (m, 2H, $PhCH_2C$***H₂***), 2.02 (m, 1H, NH), 2.49 and 3.31 (m, 2H, 6-H_2), 2.74 (m, 2H, PhC***H₂***), 2.93 and 3.07 (m, 2H, 4-H_2), 3.36 (t, 1H, ^3J = 6.6 Hz, $PhCH_2CH_2C$***H***), 4.14 (m, 1H, 9-H), 4.18 (m, 2H, CH_3C***H₂***OCOCH), 4.21 (m, 2H, CH_3C***H₂***OCON), 4.36 (m, 2H, CH_3C***H₂***$OCOC_6H_5$) 5.07 (m, 1H, 1-H), 5.71 (m, 2H, OCH_2N), 7.18 (m, 3H, Ph***H***), 7.26 (m, 2H, Ph***H***), 7.35 (m, 2H, EtOOCPh***H***), 8.05 (m, 2H, EtCOOPh***H***). ^{13}C-NMR ($CDCl_3$) δ ppm: 14.07 (+, ***C***H_3CH_2OCON), 14.26 (+, ***C***H_3CH_2OCOPh), 14.29 (+, ***C***H_3CH_2OCOCH), 16.00 (-, C-3), 24.96 (-, C-2), 25.14 (-, C-7), 30.08 (-, C-8), 32.21 (-, Ph***C***H_2), 35.19 (-, $PhCH_2$***C***H_2), 49.68 (+, C-1), 51.33 (-, C-6), 51.78 (-, C-4), 57.09 (+, C-9), 60.52 (+, $PhCH_2CH_2$***C***H), 60.55 (-, CH_3***C***H_2OCOCH), 61.07 (-, CH_3***C***H_2OCOPh), 62.86 (-, CH_3***C***H_2OCON), 74.81 (-, OCH_2N), 125.83 (+, Ph***C***), 126.08 (2C, +, EtCOOPh***C***), 128.30 (2C, +, Ph***C***), 128.37 (2C, +, Ph***C***), 129.05 (quat, EtCOOPh***C***), 130.44 (2C, +, EtCOOPh***C***), 141.54 (quat, Ph***C***), 144.64 (quat, EtCOOPh***C***), 154.46 (quat, CH_3CH_2O***C***ON), 165.79 (quat, CH_3CH_2O***C***OPh), 170.75 (quat, C-1-**C**OO), 174.61 (quat, CH_3CH_2O***C***OCH), 175.24 (quat, C-10). HRMS: LSI-MS: *m/z* for ($C_{35}H_{46}N_4O_9$ + H^+) calcd. 667.3338, found: 676.33251. Analytical HPLC: purity 95 %, t_R = 14.33 min (gradient b), k = 3.98. $C_{35}H_{46}N_4O_9$ (666.76).

(1*S*,9*S*)-{[4-(Ethoxycarbonyl)phenyl](methoxycarbonyl)amino}methyl 9-((*S*)-1-ethoxy-1-oxo-4-phenylbutan-2-ylamino)-10-oxooctahydro-1*H*-pyridazino[1,2-a][1,2]diazepine-1-carboxylate (3.27): The title compound was prepared from cilazapril (0.48 mmol, 0.20 g), K_2CO_3 (0.86 mmol, 0.12 g) and **3.24** (0.86 mmol, 0.23 g) in DMF (H_2O < 0.01 %) (5 ml) according to the general procedure 3.8.2.4 and was obtained after flash chromatography (PE/EtOAc 5/2 to 1/1 v/v) as a pale yellow oil (0.25 g, 80 %). ^{1}H-NMR ($CDCl_3$) δ ppm: 1.27 (t, 3H, ^3J = 7.1 Hz, C***H₃***CH_2OCOCH), 1.37 (m, 3H, C***H₃***CH_2OCOPh), 1.37 and 1.67 (m, 2H, 3-H_2), 1.37 and 2.02 (m, 2H, 8-H_2), 1.67 and 1.80 (m, 2H, 7-H_2), 1.80 and 2.30 (m, 2H, 2-H_2), 2.02 (m, 2H, $PhCH_2C$***H₂***), 2.49 and 3.30 (m, 2H, 6-H_2), 2.74 (m, 2H, PhC***H₂***), 2.93 and 3.07 (m, 2H, 4-H_2), 3.36 (t, 1H, ^3J = 6.6 Hz, $PhCH_2CH_2C$***H***), 3.75 (s, 3H, CH_3OCO), 4.14 (m, 1H, 9-H), 4.18 (m, 2H, CH_3C***H₂***OCOCH), 4.36 (m, 2H, CH_3C***H₂***$OCOC_6H_5$) 5.07 (m, 1H, 1-H), 5.70 (m, 2H, OCH_2N), 7.18 (m, 3H, Ph***H***), 7.26 (m, 2H, Ph***H***), 7.35 (m, 2H, EtOOCPh***H***), 8.05 (m, 2H, EtCOOPh***H***). ^{13}C-NMR ($CDCl_3$) δ ppm: 14.26 (+, ***C***H_3CH_2OCOPh), 14.29 (+, ***C***H_3CH_2OCOCH), 16.00 (-, C-3), 24.94 (-, C-2), 25.16 (-, C-7), 30.09 (-, C-8), 32.21 (-, Ph***C***H_2), 35.19 (-, $PhCH_2$***C***H_2), 49.67 (+, C-1), 51.34 (-, C-6), 51.79 (-, C-4), 53.65 (+, ***C***H_3OCO), 57.10 (+, C-9), 60.52 (+, $PhCH_2CH_2$***C***H), 60.54 (-, CH_3***C***H_2OCOCH), 61.09 (-, CH_3***C***H_2OCOPh), 74.83 (-, OCH_2N), 125.83 (+, Ph***C***), 126.25 (2C, +, EtCOOPh***C***), 128.30 (2C, +, Ph***C***), 128.38 (2C, +, Ph***C***), 129.29 (quat, EtCOOPh***C***), 130.52 (2C, +, EtCOOPh***C***), 141.56 (quat, Ph***C***), 144.49 (quat, EtCOOPh***C***), 155.00 (quat, CH_3O***C***O), 165.74 (quat, CH_3CH_2O***C***OPh), 170.77 (quat, C-1-**C**OO), 174.62 (quat, CH_3CH_2O***C***OCH), 175.27 (quat, C-10). HRMS: LSI-MS: *m/z* for ($C_{34}H_{44}N_4O_9$+ H^+) calcd.

653.3181, found: 653.31693. Analytical HPLC: purity 97 %, t_R = 13.72 min (gradient b), k = 3.76. $C_{34}H_{44}N_4O_9$ (652.73).

(1*S*,9*S*)-Ethyl 9-((*S*)-1-ethoxy-1-oxo-4-phenylbutan-2-ylamino)-10-oxooctahydro-1*H*-pyridazino[1,2-a][1,2]diazepine-1-carboxylate (3.28): Trimethylsilyl chloride (2.2 eq, 0.79 mmol, 0.1 ml) was added to a solution of cilazapril (1 eq, 0.36 mmol, 0.15 g) in EtOH/abs (5 ml). The reaction mixture was heated at reflux for 4 h. The solution was evaporated to dryness. The resulting residue was taken up in EtOAc and the organic layer was washed with saturated $NaHCO_3$ solution twice. The organic layer was dried over anhydrous $MgSO_4$, filtered and rotary evaporated. The crude product was submitted to flash chromatography (PE/EtOAc 1/1 v/v) to obtain the title compound as a pale yellow oil (0.12 g, 73 %). ^{1}H-NMR ($CDCl_3$) δ ppm: 1.27 (m, 6H, C***H*****$_3$**CH_2OCOCHNH, C***H*****$_3$**CH_2OCOCHN<), 1.36 and 1.72 (m, 2H, 3-H_2), 1.46 and 2.02 (m, 2H, 8-H_2), 1.72 and 1.85 (m, 2H, 7-H_2), 1.85 and 2.31 (m, 2H, 2-H_2), 2.01 (m, 2H, PhCH_2C***H*****$_2$**), 2.21 (bs, 1H, NH), 2.50 and 3.35 (m, 2H, 6-***H*****$_2$**), 2.73 (m, 2H, PhC***H*****$_2$**), 2.94 and 3.08 (m, 2H, 4-H_2), 3.36 (m, 1H, PhCH_2CH_2C***H***), 4.14 (m, 1H, 9-H), 4.17 (m, 4H, CH_3C***H*****$_2$**OCOCHNH, CH_3C***H*****$_2$**OCOCHN<), 5.02 (m, 1H, 1-H), 7.17 (m, 3H, Ph***H***), 7.25 (m, 2H, Ph***H***). ^{13}C-NMR ($CDCl_3$) δ ppm: 14.08 (+, ***C***H_3CH_2OCOCHN<), 14.29 (+, ***C***H_3CH_2OCOCHNH), 16.05 (-, C-3), 25.05 (2C, -, C-2 and C-7), 30.11 (-, C-8), 32.21 (-, Ph***C***H_2), 35.16 (-, PhCH_2***C***H_2), 49.78 (+, C-1), 51.30 (-, C-6), 51.74 (-, C-4), 57.17 (+, C-9), 60.53 (-, CH_3***C***H_2OCOCHNH), 60.60 (+, PhCH_2CH_2***C***H), 61.30 (-, CH_3***C***H_2OCOCHN<), 125.81 (+, Ph***C***), 128.29 (2C, +, Ph***C***), 128.36 (2C, +, Ph***C***), 141.57 (quat, Ph***C***), 171.44 (quat, C-1-COO), 174.61 (quat, CH_3CH_2O***C***OCHNH), 175.11 (quat, C-10). HRMS: EI-MS: *m/z* for ($C_{24}H_{35}N_3O_5$) calcd. 445.2577, found: 445.25801. Analytical HPLC: purity 97 %, t_R = 12.08 min (gradient b), k = 3.19. $C_{24}H_{35}N_3O_5$ (445.56).

(1*S*,9*S*)-9-((*S*)-1-carboxy-3-phenylpropylamino)-10-oxooctahydro-1*H*-pyridazino-[1,2-a][1,2]diazepine-1-carboxylic acid (3.29): A mixture of cilazapril (1 eq, 0.31 mmol, 0.13 g) and LiOH (3 eq, 0.93 mmol, 22 mg) in methanol was stirred for 6 d at room temperature. The reaction mixture was acidified by addition of TFA (10%). Subsequently, the volatiles were removed *in vacuo* and the residue was purified by preparative HPLC yielding the title compound as a white solid (0.11 g, 67 %). Mp.: 144-146 °C. ^{1}H-NMR (CD_3OD) δ ppm: 1.42 and 1.74 (m, 2H, 3-H_2), 1.79 and 2.18 (m, 2H, 8-H_2), 1.86 and 2.13 (m, 2H, 7-H_2), 2.13 and 2.38 (m, 2H, 2-H_2), 2.25 (m, 2H, PhCH_2C***H*****$_2$**), 2.59 and 3.48 (m, 2H, 6-H_2), 2.83 (m, 2H, PhC***H*****$_2$**), 3.03 and 3.15 (m, 2H, 4-H_2), 3.96 (t, 1H, ^3J = 5.9 Hz, PhCH_2CH_2C***H***), 4.84 (t, 1H, ^3J = 7.8 Hz, 9-H), 4.92 (m, 1H, 1-H), 7.20 (m, 1H, Ph***H***), 7.25 (m, 2H, Ph***H***), 7.28 (m, 2H, Ph***H***). ^{13}C-NMR (CD_3OD) δ ppm: 16.99 (-, C-3), 25.79 (-, C-2), 25.82 (-, C-7), 26.64 (-, C-8), 32.21 (-, Ph***C***H_2), 33.43 (-, PhCH_2***C***H_2), 51.57 (+, C-1), 51.81 (-, C-6), 52.64 (-, C-4), 60.20 (+, C-9), 60.73 (+, PhCH_2CH_2***C***H), 127.51 (+, Ph***C***), 129.44 (2C, +, Ph***C***), 129.67 (2C, +, Ph***C***), 141.44 (quat, Ph***C***), 169.71 (quat, C-10), 171.47 (quat, NHCH***C***OOH), 173.69 (quat, C-1-***C***OO). HRMS: EI-MS: *m/z* for

($C_{20}H_{27}N_3O_5$) calcd. 389.1951, found: 389.19426. Prep. HPLC: MeCN/0.05% TFA/aq 25/75, 10 min: 45/55, 10.1-20 min: 95/5. Analytical HPLC: purity 100 %, t_R = 8.49 min (gradient b), k = 1.95. Anal. ($C_{20}H_{27}N_3O_5 \cdot C_2HF_3O_2 \cdot 0.75H_2O$) C, H, N. $C_{20}H_{27}N_3O_5$ · 1 TFA (503.47).

2-Ethoxy-1-{[2'-(1-triphenylmethyl-1*H*-tetrazole-5-yl)biphenyl-4-yl]methyl}benzimidazole-7-carboxylic acid (3.30)[52]: 2-Ethoxy-1-[[2'-(1*H*-tetrazole-5-yl)biphenyl-4-yl]methyl]benzimidazole-7-carboxylic acid (1 eq, 11.4 mmol, 5.00 g) was suspended in 22 ml of DCM. After addition of triethylamine (1.2 eq, 13.7 mmol, 1.92 ml) a solution of trityl chloride (1.2 eq, 13.7 mmol, 3.81 g) in 10 ml of DCM was added dropwise. The reaction mixture was stirred at room temperature for one hour and washed with water. The organic layer was dried over anhydrous $MgSO_4$, filtered and concentrated under reduced pressure. The crude product was purified by flash chromatography (PE/EtOAC 2/1 to 2/3 + 0.1 % acetic acid v/v) to give colorless crystals (4.43 g, 57 %). Mp: 166-169 °C (ref.[52]: 168-170 °C). ^{1}H NMR (DMSO-d_6) δ ppm: 1.28 (t, 3H, ^3J = 7.0 Hz, $OCH_2C\boldsymbol{H_3}$), 4.50 (q, 2H, ^3J = 7.0 Hz, $OC\boldsymbol{H_2}CH_3$), 5.64 (s, 2H, $NC\boldsymbol{H_2}$-p-phenylene), 6.86 (m, 8H, CPh_3, p-phenylene-2-H, p-phenylene-6-H), 6.96 (d, 2H, ^3J = 8.2 Hz, p-phenylene-3-H, p-phenylene-5-H), 7.13 (t, 1H, ^3J = 7.8 Hz, Ar***H***), 7.34 (m, 10H, CPh_3, Ar***H***), 7.54 (m, 4H, CPh_3, Ar***H***), 7.76 (m, 1H, Ar***H***), 13.12 (br s, COOH). ES-MS (DCM/MEOH + 10 mM NH_4OAc) *m/z* (%): 683 (100) [$M+H^+$]. $C_{43}H_{34}N_6O_3$ (682.77).

3.8.2.5 General procedure for the esterification of 3.30

The corresponding alkyloxycarbonyloxyethylchloride, acyloxyethylchloride or 4-(bromomethyl)-5-alkyl-1,3-dioxol-2-one (1.5 eq) was added dropwise to a mixture of **3.30** (1 eq) and K_2CO_3 (1.5 eq) in DMF (H_2O < 0.01 %) at 0 °C. The reaction mixture was stirred overnight at room temperature and concentrated *in vacuo*. The residue was distributed between water and ethyl acetate. The organic layer was separated and the aqueous layer was extracted two times with ethyl acetate. The combined organic phases were washed with water, dried over anhydrous $MgSO_4$, filtered and evaporated to dryness. The crude product was subjected to flash chromatography.

1-(Isopropyloxycarbonyloxy)ethyl 2-ethoxy-1-{[2'-(1-triphenylmethyl-1*H*-tetrazole-5-yl)biphenyl-4-yl]methyl}benzimidazole-7-carboxylate (3.31a): The title compound was prepared according to the general procedure 3.8.2.5, using **3.30** (1 eq, 3.2 mmol, 2.18 g), K_2CO_3 (1.5 eq, 4.8 mmol, 0.66 g) and 1-chloroethyl(isopropyl)carbonate (1.5 eq, 4.8 mmol, 0.80 g), and was obtained after flash chromatography (PE/EtOAc 2/1 v/v) as colorless crystals (2.16 g, 83 %). ES-MS (DCM/MEOH + 10 mM NH_4OAc) *m/z* (%): 813 (100) [$M+H^+$]. $C_{49}H_{44}N_6O_6$ (812.91).

1-(2,2-Dimethylpropanoyloxy)ethyl 2-ethoxy-1-[[2'-(1-triphenylmethyl-1*H*-tetrazole-5-yl)biphenyl-4-yl]methyl]benzimidazole-7-carboxylate (3.32a): The title compound was prepared according to the general procedure 3.8.2.5, using **3.30** (1 eq, 5.3 mmol, 3.62 g), K_2CO_3 (1.5 eq, 8.0 mmol, 1.11 g) and **3.5** (1.5 eq, 8.0 mmol, 1.32 g), and was obtained after flash chromatography (PE/EtOAc 2/1 v/v) as colorless crystals (4.30 g, 80 %). ES-MS (DCM/MEOH + 10 mM NH_4OAc) *m/z* (%): 811 (100) [$M+H^+$]. $C_{50}H_{46}N_6O_5$ (810.94).

(5-Methyl-2-oxo-1,3-dioxol-4-yl)methyl 2-ethoxy-1-{[2'-(1-triphenylmethyl-1*H*-tetrazole-5-yl)biphenyl-4-yl]methyl}benzimidazole-7-carboxylate (3.33a): The title compound was prepared according to the general procedure 3.8.2.5, using **3.30** (1 eq, 0.3 mmol, 0.20 g), K_2CO_3 (1.5 eq, 0.4 mmol, 60 mg) and **3.10** (1.5 eq, 0.4 mmol, 77 mg), and was obtained after flash chromatography (PE/EtOAc 2/1 v/v) as colorless crystals (0.20 g, 87 %). ^{1}H NMR ($CDCl_3$) δ ppm: 1.42 (t, 3H, ^3J = 7.1 Hz, $OCH_2C\boldsymbol{H_3}$), 4.62 (q, 2H, ^3J = 7.1 Hz, $OC\boldsymbol{H_2}CH_3$), 4.73 (s, 2H, OCH_2C=C), 5.58 (s, 2H, $NC\boldsymbol{H_2}$-p-phenylene), 6.73 (m, 2H, Ar***H***), 6.93-7.03 (m, 8H, Ar***H***), 7.20-7.28 (m, 6H, Ar***H***), 7.15-7.25 (m, 6H, Ar***H***), 7.29-7.37 (m, 4H, Ar***H***), 7.39-7.56 (m, 3H, Ar***H***), 7.79 (m, 2H, Ar***H***). ES-MS (DCM/MEOH + 10 mM NH_4OAc) *m/z* (%): 795 (100) [$M+H^+$]. $C_{48}H_{38}N_6O_6$ (794.85).

(5-*tert*-Butyl-2-oxo-1,3-dioxol-4-yl)methyl 2-ethoxy-1-{[2'-(1-triphenylmethyl-1*H*-tetrazole-5-yl)biphenyl-4-yl]methyl}benzimidazole-7-carboxylate (3.34a): The title compound was prepared from **3.30** (1 eq, 0.7 mmol, 0.50 g), K_2CO_3 (1.5 eq, 1.1 mmol, 0.15 g) and **3.11** (1.5 eq, 1.1 mmol, 0.26 g) according to the general procedure 3.8.2.5 and was obtained after flash chromatography (PE/EtOAc 2/1 v/v) as colorless crystals (0.54 g, 88 %). ^{1}H NMR ($CDCl_3$) δ ppm: 1.23 (s, 9H, $C(CH_3)_3$), 1.43 (t, 3H, ^3J = 7.1 Hz, $OCH_2C\boldsymbol{H_3}$), 4.66 (q, 2H, ^3J = 7.0 Hz, $OC\boldsymbol{H_2}CH_3$), 4.90 (s, 2H, OCH_2C=C), 5.58 (s, 2H, $NC\boldsymbol{H_2}$-p-phenylene), 6.72 (m, 2H, Ar***H***), 6.94 (m, 6H, Ar***H***), 6.99 (m, 2H, Ar***H***), 7.20-7.28 (m, 6H, Ar***H***), 7.32 (m, 5H, Ar***H***), 7.45 (m, 2H, Ar***H***), 7.57 (m, 1H, Ar***H***), 7.83 (m, 2H, Ar***H***). ES-MS (DCM/MEOH + 10 mM NH_4OAc) *m/z* (%): 837 (100) [$M+H^+$]. $C_{51}H_{44}N_6O_6$ (836.93).

3.8.2.6 General procedure for the deprotection of the trityl-protected compounds 3.31a-3.34a to generate the compounds 3.31-3.34

The corresponding compound **3.31a**-**3.34a** was dissolved in a mixture of methanol and tetrahydrofurane. After addition of 1M hydrochloric acid the reaction mixture was stirred at room temperature for 2 to 5 h (DC control). The solution was neutralized with 1 M NaOH and evaporated to dryness. The residue was taken up in ethyl acetate and H_2O. The phases were separated and the aqueous layer was extracted two times with ethyl acetate. The combined organic phases were dried over anhydrous $MgSO_4$, and the solvent was evaporated. The crude product was purified by flash chromatography. The product containing fractions were neutralized by washing with saturated $NaHCO_3$

solution and dried over $MgSO_4$. After filtration and removal of the solvents under reduced pressure the resulting solid was recrystallized.

1-(Isopropoxycarbonyloxy)ethyl 2-ethoxy-1-[[2'-(1*H*-tetrazole-5-yl)biphenyl-4-yl]methyl]benzimidazole-7-carboxylate (3.31): The title compound was prepared according to the general procedure 3.8.2.6 by stirring of **3.31a** (5 mmol, 4.06 g) in 70 ml MeOH/THF 1/1 v/v under addition of 15 ml of 1M HCl for 5 h. After workup, flash chromatography (PE/EtOAc 3/2 + 0.1% acetic acid v/v) and recrystallization from ethanol the desired product was obtained as a white solid (1.80 g, 63 %). Mp: 92-94 °C. ^{1}H NMR ($CDCl_3$) δ ppm: 1.19 (t, 6H, ^3J = 6.0 Hz, (C***H*****$_3$**)$_2$CH), 1.33 (d, 3H, ^3J = 5.4 Hz, OCHC***H*****$_3$**O), 1.43 (t, 3H, ^3J = 7.1 Hz, OCH_2C***H*****$_3$**), 4.16-4.52 (m, 2H, OC***H*****$_2$**CH_3), 4.77 (sept, 1H, ^3J = 6.3 Hz, $(CH_3)_2$C***H***), 5.62 (s, 2H, NC***H*****$_2$**-p-phenylene), 6.67 (q, 1H, ^3J = 5.4 Hz, OC***H***CH_3O), 6.75 (d, 2H, ^3J = 8.0 Hz, p-phenylene-2-H, p-phenylene-6-H), 6.87 (d, 2H, ^3J = 8.2 Hz, p-phenylene-3-H, p-phenylene-5-H), 6.99 (m, 2H, Ar***H***), 7.31 (m, 1H, Ar***H***), 7.50 (m, 1H, Ar***H***), 7.58 (m, 2H, Ar***H***), 8.01 (m, 1H, Ar***H***), 15.08 (bs, tetrazole-***H***). ^{13}C-NMR ($CDCl_3$) δ ppm: 14.56 (+, OCH_2***C***H_3), 19.25 (+, OCH***C***H_3O), 21.53, 21.57 (+, (***C***$H_3)_2$CH), 46.93 (-, N***C***H_2-p-phenylene), 67.73 (-, CH_3***C***H_2OCO), 72.99 (+, $(CH_3)_2$***C***H), 91.86 (+, O***C***HCH_3O), 115.28 (quat, benzim-C-7), 121.19, 121.29 (+, Ar***C***), 123.30 (quat, Ar***C***), 124.27 (+, Ar***C***), 125.30 (+, 2C, p-phenylene-C-2, p-phenylene-C-6), 128.34 (+, Ar***C***), 129.48 (+, 2C, p-phenylene-C-3, p-phenylene-C-5), 130.58 (+, Ar***C***), 130.72 (quat, Ar***C***), 131.20, 131.30 (+, Ar***C***),136.62, 138.16, 140.04, 140.90 (quat, Ar***C***), 152.41 (quat, $(CH_3)_2$CHO***C***O), 154.66 (quat, benzim-***C-2***), 158.01 (quat, tetrazole), 163.35 (quat, O***C***O-benzim). ES-MS (DCM/MEOH + 10 mM NH_4OAc) *m/z* (%): 571 (100) [M+H$^+$]. Anal. ($C_{30}H_{30}N_6O_6 \cdot H_2O$) C, H, N. $C_{30}H_{30}N_6O_6$ (570.60).

1-(2,2-Dimethylpropanoyloxy)ethyl 2-ethoxy-1-{[2'-(1*H*-tetrazole-5-yl)biphenyl-4-yl]-methyl}benzimidazole-7-carboxylate (3.32): The title compound was prepared according to the general procedure 3.8.2.6 by stirring of **3.32a** (10.4 mmol, 8.43 g) in 150 ml MeOH/THF 1/1 v/v under addition of 35 ml of 1M HCl for 3.5 h. Workup, followed by flash chromatography (PE/EtOAc 2/1 + 0.1% acetic acid v/v) and recrystallization from ethanol gave the desired product as a white solid (3.96 g, 67 %). Mp: 100-102 °C. ^{1}H NMR ($CDCl_3$) δ ppm: 1.11 (s, 9H, (C***H*****$_3$**)$_3$C), 1.23 (d, 3H, ^3J = 5.4 Hz, OCHC***H*****$_3$**O), 1.41 (t, 3H, ^3J = 7.1 Hz, OCH_2C***H*****$_3$**), 4.28 (m, 2H, OC***H*****$_2$**CH_3), 5.61 (s, 2H, NC***H*****$_2$**-p-phenylene), 6.71 (m, 3H, OC***H***CH_3O, Ar***H***), 6.82 (m, 2H, Ar***H***), 6.90 (t, 1H, ^3J = 7.8 Hz, Ar***H***), 7.28 (m, 1H, Ar***H***), 7.42 (d, 1H, ^3J = 7.7 Hz, Ar***H***), 7.59 (m, 2H, Ar***H***), 7.99 (m, 1H, Ar***H***), 15.98 (bs, tetrazole-***H***). ^{13}C-NMR ($CDCl_3$) δ ppm: 14.55 (+, OCH_2***C***H_3), 19.11 (+, OCH***C***H_3O), 26.78 (3C, +, (***C***$H_3)_3$C), 38.65 (quat, $(CH_3)_3$***C***), 46.97 (-, N***C***H_2-p-phenylene), 67.73 (-, O***C***H_2CH_3), 89.28 (+, O***C***HCH_3O), 115.46 (quat, benzim-C-7), 121.10, 121.28 (+, Ar***C***), 123.35 (quat, Ar***C***), 124.14 (+, Ar***C***), 125.32 (+, 2C, p-phenylene-C-2, p-phenylene-C-6), 128.31 (+, Ar***C***), 129.44 (+, 2C, p-phenylene-C-3, p-phenylene-C-5), 130.08 (quat, Ar***C***), 130.54, 131.20, 131.27 (+, Ar***C***), 136.77, 138.17, 140.05, 140.90 (quat, Ar***C***), 154.82

(quat, benzim-C-2), 158.01 (quat, tetrazole-***H***), 163.42 (quat, O***C***O-benzim), 176.81 (quat, $(CH_3)_3$***C***OO). ES-MS (DCM/MEOH + 10 mM NH_4OAc) *m/z* (%): 569 (100) $[M+H^+]$. Anal. ($C_{31}H_{32}N_6O_5 \cdot H_2O$) C, H, N. $C_{31}H_{32}N_6O_5$ (568.62).

(5-Methyl-2-oxo-1,3-dioxol-4-yl)methyl 2-ethoxy-1-{[2'-(1*H*-tetrazole-5-yl)biphenyl-4-yl]methyl}benzimidazole-7-carboxylate (3.33): Following the general procedure 3.8.2.6 **3.33a** (0.25 mmol, 0.20 g) was stirred in 7 ml MeOH/THF 5/2 v/v under addition of 1 ml of 1M HCl for 2.25 h the title compound was obtained after workup, followed by flash chromatography (PE/EtOAc 1/1 to 1/2 + 0.1% acetic acid v/v) and recrystallization from cyclohexane/ *tert*-butyl methylether/ hexane as a white solid (53 mg, 38 %). Mp: 98-100 °C. ^{1}H NMR (CD_3OD) δ ppm: 1.45 (t, 3H, ^3J = 7.1 Hz, $OCH_2C\boldsymbol{H_3}$), 2.16 (s, 3H, $C\boldsymbol{H_3}C$=C), 4.60 (q, 2H, ^3J = 7.1 Hz, $OC\boldsymbol{H_2}CH_3$), 5.03 (s, 2H, $OC\boldsymbol{H_2}$C=C), 5.61 (s, 2H, $NC\boldsymbol{H_2}$-p-phenylene), 6.87 (m, 2H, Ar***H***), 6.99 (m, 2H, Ar***H***), 7.21 (t, 1H, ^3J = 7.9 Hz, Ar***H***), 7.52 (m, 2H, Ar***H***), 7.61 (m, 3H, Ar***H***), 7.68 (m, 1H, Ar***H***). ^{13}C-NMR (CD_3OD) δ ppm: 9.38 (+, ***C***H_3C=C), 14.93 (+, $OCH_2\boldsymbol{C}H_3$), 48.05 (-, N***C***H_2-p-phenylene), 55.85 (-, O***C***H_2C=C), 68.50 (-, O***C***H_2CH_3), 116.47 (quat, benzim-C-7), 122.44, 123.10 (+, Ar***C***), 124.51 (quat, $CH_3C\boldsymbol{C}$=C), 125.51 (+, Ar***C***), 127.65 (+, 2C, p-phenylene-C-2, p-phenylene-C-6), 129.02 (+, Ar***C***), 130.43 (+, 2C, p-phenylene-C-3, p-phenylene-C-5), 131.59, 131.97, 132.50 (+, Ar***C***), 132.67 (quat, Ar***C***), 135.05 (quat, CH_3CC=***C***), 138.19, 140.00, 142.08, 142.74, 143.04 (quat, Ar***C***), 153.84 (quat, O***C***OO), 156.90 (quat, benzim-C-2), 160.20 (quat, tetrazole), 166.83 (quat, O***C***O-benzim). ES-MS (DCM/MeOH + 10 mM NH_4OAc) *m/z* (%): 553 (100) $[M+H^+]$. Anal. ($C_{29}H_{24}N_6O_6 \cdot 0.5\ C_5H_{12}O \cdot 0.5\ H_2O$) C, H, N. $C_{29}H_{24}N_6O_6$ (552.54).

(5-*tert*-Butyl-2-oxo-1,3-dioxol-4-yl)methyl 2-ethoxy-1-{[2'-(1*H*-tetrazole-5-yl)biphenyl-4-yl]methyl}benzimidazole-7-carboxylate (3.34): The title compound was prepared according to the general procedure 3.8.2.6 by stirring of **3.34a** (0.65 mmol, 0.54 g) in 30 ml MeOH/THF 2/1 v/v under addition of 7.5 ml of 1M HCl for 3 h and was obtained after workup and flash chromatography (PE/EtOAc 1/2 + 0.5% acetic acid v/v) as a white solid (0.63 g, 16 %). Mp: 103-105 °C. ^{1}H NMR ($CDCl_3$) δ ppm: 1.20 (s, 9H, $(C\boldsymbol{H_3})_3$C), 1.41 (t, 3H, ^3J = 7.1 Hz, $OCH_2C\boldsymbol{H_3}$), 4.28 (q, 2H, ^3J = 6.9 Hz, $OC\boldsymbol{H_2}CH_3$), 4.80 (s, 2H, $OC\boldsymbol{H_2}$C=C), 5.58 (s, 2H, $NC\boldsymbol{H_2}$-p-phenylene), 6.70 (m, 2H, Ar***H***), 6.85 (m, 3H, Ar***H***), 6.93 (t, 1H, ^3J = 7.8 Hz, Ar***H***), 7.34 (m, 1H, Ar***H***), 7.45 (m, 1H, Ar***H***), 7.60 (m, 2H, Ar***H***), 7.97 (m, 1H, Ar***H***), 15.64 (bs, tetrazole-***H***). ^{13}C-NMR ($CDCl_3$) δ ppm: 14.55 (+, $OCH_2\boldsymbol{C}H_3$), 27.89 (3C, +, $(\boldsymbol{C}H_3)_3$C), 32.12 (quat, $(CH_3)_3\boldsymbol{C}$), 46.98 (-, N***C***H_2-p-phenylene), 56.09 (-, O***C***H_2C=C), 67.88 (-, O***C***H_2CH_3), 115.09 (quat, benzim-C-7), 121.32, 121.55 (+, Ar***C***), 123.11 (quat, Ar***C***), 124.24 (+, Ar***C***), 125.52 (+, 2C, p-phenylene-C-2, p-phenylene-C-6), 128.45 (+, Ar***C***), 129.50 (+, 2C, p-phenylene-C-3, p-phenylene-C-5), 130.39 (quat, Ar***C***), 130.89 (+, Ar***C***), 131.06 (quat, $(CH_3)_3CC$=***C***), 131.17, 131.49 (+, Ar***C***), 136.35, 138.49, 139.99, 140.69 (quat, Ar***C***), 150.08 (quat, $(CH_3)_3C\boldsymbol{C}$=C), 151.88 (quat, O***C***OO), 154.80 (quat, benzim-C-2), 158.00 (quat, tetrazole), 165.11 (quat, O***C***O-benzim). ES-MS

(DCM/MeOH + 10 mM NH_4OAc) *m/z* (%): 595 (100) [$M+H^+$]. Anal. ($C_{32}H_{30}N_6O_6 \cdot 1.1\ C_2H_4O_2$) C, H, N. $C_{32}H_{30}N_6O_6$ (594.62).

2-Morpholinoethyl 1-{[2'-(1*H*-tetrazole-5-yl)biphenyl-4-yl]methyl}-2-ethoxy-benzimidazole-7-carboxylate (3.35): 3.30 (1 eq, 3.4 mmol, 1.50 g) was dissolved in DMF (H_2O < 0.01 %) (8 ml). A catalytic amount of 4-(dimethylamino)pyridine and 4-(2-hydroxyethyl)-morpholine (1 eq, 3.4 mmol, 0.41 ml) were added. A solution of *N,N'*-dicyclohexylcarbodiimide (1.1 eq, 3.8 mmol, 0.78 g) in DMF (H_2O < 0.01 %) (15 ml) was added dropwise at 0 °C. The reaction mixture was stirred for 1 h at 0 °C and overnight at room temperature. The solids were removed by filtration and the solvent was rotary evaporated. The resulting crude solid was purified by recrystallization from ethyl acetate/hexane to yield the title compound as pale beige crystals (0.96 g, 51 %). Mp: 181-183 °C. ^{1}H NMR ($CDCl_3$) δ ppm: 1.47 (t, 3H, ^3J = 7.1 Hz, $OCH_2C\boldsymbol{H_3}$), 2.61 (m, 4H, mo-3-H, mo-5-H), 2.97 (m, 2H, $NC\boldsymbol{H_2}CH_2O$), 3.39 (m, 4H, mo-2-H, mo-6-H), 4.10 (m, 2H, $NCH_2C\boldsymbol{H_2}O$), 4.64 (q, 2H, ^3J = 7.1 Hz, $OC\boldsymbol{H_2}CH_3$), 5.55 (s, 2H, $NC\boldsymbol{H_2}$-p-phenylene), 6.74 (d, 2H, ^3J = 8.3 Hz, p-phenylene-2-H, p-phenylene-6-H), 6.97 (d, 2H, ^3J = 8.3 Hz, p-phenylene-3-H, p-phenylene-5-H), 7.19 (t, 1H, ^3J = 7.9 Hz, Ar***H***), 7.49 (m, 2H, Ar***H***), 7.73 (m, 4H, Ar***H***), 9.22 (bs, tetrazole-***H***). ^{13}C-NMR ($CDCl_3$) δ ppm: 14.62 (+, $OCH_2\boldsymbol{C}H_3$), 46.69 (-, $N\boldsymbol{C}H_2$-p-phenylene), 53.07 (-, 2C, mo-C-2, mo-C-6), 56.34 (-, $N\boldsymbol{C}H_2CH_2O$), 62.31 (-, $N\boldsymbol{C}H_2CH_2O$), 65.31 (-, 2C, mo-C-3, mo-C-5), 67.01 (-, $O\boldsymbol{C}H_2CH_3$), 116.01 (quat, benzim-C-7), 121.08, 121.78, 122.49 (+, Ar***C***), 124.89 (quat, Ar***C***), 125.60 (+, 2C, p-phenylene-C-2, p-phenylene-C-6), 128.11 (+, Ar***C***), 129.09 (+, 2C, p-phenylene-C-3, p-phenylene-C-5), 130.25 (+, Ar***C***), 130.69 (quat, Ar***C***), 130.98, 131.35 (+, Ar***C***), 136.55, 138.25, 140.31, 141.60 (quat, Ar***C***), 156.87 (quat, benzim-C-2), 158.51 (quat, tetrazole), 165.65 (quat, O***C***O-benzim). ES-MS (DCM/MeOH + 10 mM NH_4OAc) *m/z* (%): 554 (100) [$M+H^+$]. Anal. ($C_{30}H_{31}N_7O_4 \cdot 0.5\ H_2O$) C, H, N. $C_{30}H_{31}N_7O_4$ (553.61).

3.8.3 Bioanalytical investigations

Solid state stability of cilazapril and candesartan prodrugs (3.1-3.3, **3.6**, **3.7**, **3.14**, **3.28, 3.31-3.35).** A few milligrams of each substance were stored at 5 °C/ 65 % rel. h., 25 °C/ 60 % rel. h. and 40 °C/ 75 % rel. h., respectively. After respective storage periods of 6, 10 or 16 months the compounds were dissolved in methanol to yield 10 mM stock solutions, diluted to 100 µM with mobile phase and subsequently analyzed by analytical HPLC using following gradients. **3.1**: 0 min: MeCN/0.05% TFA/aq 25/75, 23 min: 39/61, 27 min: 43/57, 28-34 min: 95/5, 35-43 min: 25/75. **3.2**: 0 min: MeCN/0.05% TFA/aq 25/75, 36 min: 47/53, 42 min: 53/47, 43-49 min: 95/5, 50-58 min: 25/75. **3.3**: 0 min: MeCN/0.05% TFA/aq 25/75, 23 min: 39/61, 33 min: 49/51, 34-40 min: 95/5, 41-49 min: 25/75. **3.6**: 0 min: MeCN/0.05% TFA/aq 22/78, 35 min: 36/64, 36-42 min: 95/5, 43-51 min: 22/78. **3.7**: 0 min: MeCN/0.05% TFA/aq 25/75, 36 min: 49/51, 37-43 min: 95/5, 44-52 min: 25/75. **3.14**: 0 min: MeCN/0.05% TFA/aq 18/82, 27 min: 33/67, 29-35 min: 95/5,

36-44 min: 18/82. **3.28**: 0 min: MeCN/0.05% TFA/aq 22/78, 25 min: 32/68, 30 min: 40/60, 31-37 min: 95/5, 38-46 min: 22/78. **3.31**-**3.35**: 0 min: MeCN/0.05% TFA/aq 30/70, 20 min: 85/15, 21-36 min: 95/5, 27-35 min: 30/70.

Preparation of porcine skin homogenate. From fresh full-thickness porcine skin the subcutaneous fatty tissue was removed and the skin was cut in thin slices. 50 g (25 % w/w) of porcine skin were added to 150 ml of PBS and homogenized with an ultra-turrax under cooling.[53] The resulting homogenate was centrifuged at 35000 g for 20 min at 5 °C. After removal of the upper fatty layer the homogenate was aliquoted and stored at -78 °C.

Determination of esterase activity in porcine skin homogenate, human CPD plasma and of porcine liver esterase.[54] Esterase activity was determined by a continuous spectrophotometric rate measurement using 2-nitrophenyl butyrate as a substrate. In acryl cuvettes suitable volumina of potassium phosphate buffer (0.1 M, pH 7.4, 1.42-1.48 ml) and of a 100 mM stock solution of 2-nitrophenyl butyrate in DMSO (15-30 µl) were mixed and equilibrated to 25 °C in a Cary 100 UV/VIS spectrophotometer (Varian Inc., Palo Alto, USA). After addition of a suitable volume of enzyme solution (5-50 µl) and mixing by inversion the increase in the absorption of 2-nitrophenol at 414 nm was recorded for approximately 5 min. A sample containing the same volume of phosphate buffer instead of enzyme solution was measured simultaneously as a reference. The maximum linear rate of ΔA_{414nm} vs. time was used to determine the volume activity V_A according to Equation 3.10.

$$V_A = \frac{\frac{\Delta A_{414nm}}{t} \cdot V}{\varepsilon \cdot d \cdot v}$$

Equation 3.10. Volume activity V_A. V = total volume (ml), ε = molar extinction coefficient of 2-nitrophenol = 3190 $l \cdot mol^{-1} \cdot cm^{-1}$ [55], d = path length (cm), v = volume of enzyme solution (ml).

The results from the determination of esterase activity in porcine skin homogenate and different batches of human CPD plasma and of porcine liver esterase are listed below.

	V_A (U/ml)
porcine skin homogenate	0.65
human CPD plasma (charge a (07/1999))	2.17
human CPD plasma (charge b (01/2004))	3.82
porcine liver esterase [a]	2369

[a] (EC 3.1.1.1.), suspension in 3.2 M $(NH_4)_2SO_4$ solution, pH 8, Lot 67H7175 (Sigma-Aldrich Chemie GmbH (München, Germany)).

Determination of the stability of cilazapril and candesartan prodrugs in different incubation media. A defined volume of the respective prodrug stock solution or the same volume of solvent was added to potassium phosphate buffer (0.1 M, pH 7.4), porcine skin homogenate (PSH), human plasma and buffered porcine liver esterase (PLE), respectively. All samples were incubated in a water bath at 37 °C. Over a period of up to 72 h samples of the prodrug containing incubation mixtures (200 µl) were collected. To all samples 400 µl of ice-cold acetonitrile were added. After vortex mixing the samples were allowed to stand in a refrigerator for approx. 30 min. The samples were then centrifuged at 13000 g for 5 min. The supernatants were collected and stored at -78 °C until HPLC analysis. To 200 µl of each supernatant 400 µl of aqueous 0.05 % TFA were added prior to injection. Samples containing **3.25**, **3.26** or **3.27** were partially diluted 1:1:1 with MeCN and 0.05 % TFA.

In Table 3.14 the compositions of the respective incubation mixtures for all studied cilazapril and candesartan prodrugs are summarized.

Table 3.14. Incubation mixtures used for bioanalytical studies of cilazapril and candesartan prodrugs.

No.	incubation mixture	volume (µl)							
		phosphate buffer	porcine skin homogenate	human plasma[a]	porcine liver esterase dilution[b]	stock solution in MeOH		stock solution in DMSO	
						conc. (mM)	µl	conc. (mM)	µl
Cila-za-pril	buffer	1960	-	-	-	-	-	100	40
	PSH	-	1960	-	-	-	-	100	40
	human plasma	-	-	1960	-	-	-	100	40
	buffered PLE	1920	-	-	40	-	-	100	40
3.1	buffer	1960	-	-	-	50	40	-	-
	PSH	-	1960	-	-	-	-	50	40
	human plasma	-	-	1960	-	50	40	-	-
	buffered PLE	1920	-	-	40	50	40	-	-
3.2	buffer	1960	-	-	-	-	-	50	40
	PSH	-	1960	-	-	-	-	50	40
	human plasma	-	-	1960	-	50	40	-	-
	buffered PLE	1920	-	-	40	50	40	-	-
3.3	buffer	1960	-	-	-	50	40	-	-
	PSH	-	1960	-	-	-	-	50	40
	human plasma	-	-	1960	-	50	40	-	-
	buffered PLE	1920	-	-	40	50	40	-	-
3.6	buffer	1960	-	-	-	50	40	-	-
	PSH	-	1960	-	-	-	-	50	40
	human plasma	-	-	1960	-	50	40	-	-
	buffered PLE	1920	-	-	40	50	40	-	-
3.7	buffer	1960	-	-	-	50	40	-	-
	PSH	-	1960	-	-	-	-	50	40
	human plasma	-	-	1960	-	50	40	-	-
	buffered PLE	1920	-	-	40	50	40	-	-
3.12	buffer	1960	-	-	-	-	-	100	40
	PSH	-	1960	-	-	-	-	100	40
	human plasma	-	-	1960	-	-	-	100	40
	buffered PLE	1920	-	-	40	-	-	100	40

Table 3.14 continued

3.13	buffer	1960	-	-	-	50	40	-	-
	PSH	-	1960	-	-	-	-	50	40
	human plasma	-	-	1960	-	50	40	-	-
	buffered PLE	1920	-	-	40	50	40	-	-
3.14	buffer	1960	-	-	-	50	40	-	-
	PSH	-	1960	-	-	-	-	50	40
	human plasma	-	-	1960	-	50	40	-	-
	buffered PLE	1920	-	-	40	50	40	-	-
3.18	buffer	1960	-	-	-	-	-	50	40
	PSH	-	1960	-	-	-	-	50	40
	human plasma	-	-	1960	-	-	-	50	40
	buffered PLE	1920	-	-	40	-	-	50	40
3.25	buffer	1960	-	-	-	-	-	50	40
	PSH	-	1960	-	-	-	-	50	40
	human plasma	-	-	1960	-	-	-	50	40
	buffered PLE	1920	-	-	40	-	-	50	40
3.26	buffer	1960	-	-	-	-	-	50	40
	PSH	-	1960	-	-	-	-	50	40
	human plasma	-	-	1960	-	-	-	50	40
	buffered PLE	1920	-	-	40	-	-	50	40
3.27	buffer	1960	-	-	-	-	-	50	40
	PSH	-	1960	-	-	-	-	50	40
	human plasma	-	-	1960	-	-	-	50	40
	buffered PLE	1920	-	-	40	-	-	50	40
3.28	buffer	1960	-	-	-	50	40	-	-
	PSH	-	1960	-	-	-	-	50	40
	human plasma	-	-	1960	-	50	40	-	-
	buffered PLE	1920	-	-	40	50	40	-	-
CAN-CIL[c]	buffer	1960	-	-	-	10	40	-	-
	PSH	-	1960	-	-	-	-	10	40
	human plasma	-	-	1960 [d]	-	10	40	-	-
	buffered PLE	1955	-	-	5 [e]	10	40	-	-
3.31	buffer	1960	-	-	-	10	40	-	-
	PSH	-	1960	-	-	-	-	10	40
	human plasma	-	-	1960 [d]	-	10	40	-	-
	buffered PLE	1953	-	-	7	10	40	-	-
3.32	buffer	1960	-	-	-	10	40	-	-
	PSH	-	1960	-	-	-	-	10	40
	human plasma	-	-	1960	-	10	40	-	-
	buffered PLE	1959	-	-	0.75 [e]	10	40	-	-
3.33	buffer	1960	-	-	-	10	40	-	-
	PSH	-	1960	-	-	-	-	10	40
	human plasma	-	-	1960	-	10	40	-	-
	buffered PLE	1950	-	-	10	10	40	-	-
3.34	buffer	1960	-	-	-	-	-	50	40
	PSH	-	1960	-	-	-	-	50	40
	human plasma	-	-	1960	-	-	-	50	40
	buffered PLE	1920	-	-	40	-	-	50	40
3.35	buffer	1960	-	-	-	10	40	-	-
	PSH	-	1960	-	-	-	-	10	40
	human plasma	-	-	1960 [d]	-	10	40	-	-
	buffered PLE	1955	-	-	5 [e]	10	40	-	-

[a] Human CPD plasma batch b (01/2004) unless otherwise indicated. [b] Porcine liver esterase was diluted with phosphate buffer 1:100 (v:v) prior to incubation unless otherwise indicated. [c] Candesartan cilexetil. [d] Human CPD plasma batch b (07/1999) [e] Porcine liver esterase was used undiluted.

The following analytical HPLC gradients were applied:
Cilazapril: 0 min: MeCN/0.05% TFA/aq 20/80, 5 min: 30/70, 8 min: 55/45, 9-15 min: 95/5, 16-24 min: 20/80. **3.1**: 0 min: MeCN/0.05% TFA/aq 25/75, 23 min: 39/61, 27 min: 43/57, 28-34 min: 95/5, 35-43 min: 25/75. **3.2**: 0 min: MeCN/0.05% TFA/aq 25/75, 36 min: 47/53, 42 min: 53/47, 43-49 min: 95/5, 50-58 min: 25/75. **3.3**: 0 min: MeCN/0.05% TFA/aq 25/75, 23 min: 39/61, 33 min: 49/51, 34-40 min: 95/5, 41-49 min: 25/75. **3.6**: 0 min: MeCN/0.05% TFA/aq 22/78, 35 min: 36/64, 36-42 min: 95/5, 43-51 min: 22/78. **3.7**: 0 min: MeCN/0.05% TFA/aq 25/75, 36 min: 49/51, 37-43 min: 95/5, 44-52 min: 25/75. **3.12**: 0 min: MeCN/0.05% TFA/aq 25/75, 18 min: 51/49, 19-25 min: 95/5, 26-34 min: 25/75. **3.13**: 0 min: MeCN/0.05% TFA/aq 25/75, 20 min: 50/50, 21-27 min: 95/5, 28-36 min: 25/75. **3.14**: 0 min: MeCN/0.05% TFA/aq 18/82, 27 min: 33/67, 29-35 min: 95/5, 36-44 min: 18/82. **3.18**: 0 min: MeCN/0.05% TFA/aq 10/90, 20 min: 40/60, 21-28 min: 95/5, 29-37 min: 10/90. **3.25**-**3.27**: 0 min: MeCN/0.05% TFA/aq 25/75, 10 min: 38/62, 20 min: 55/45, 21-27 min: 95/5, 28-36 min: 25/75. **3.28**: 0 min: MeCN/0.05% TFA/aq 22/78, 25 min: 32/68, 30 min: 40/60, 31-37 min: 95/5, 38-46 min: 22/78. **Candesartan cilexetil**: 0 min: MeCN/0.05% TFA/aq 20/80, 24 min: 80/20, 25-29 min: 95/5, 31-39 min: 20/80. **3.31**: 0 min: MeCN/0.05% TFA/aq 20/80, 24 min: 73/27, 25-30 min: 95/5, 32-42 min: 20/80. **3.32**: 0 min: MeCN/0.05% TFA/aq 20/80, 24 min: 77/23, 25-29 min: 95/5, 31-39 min: 20/80. **3.33**: 0 min: MeCN/0.05% TFA/aq 20/80, 21 min: 66/34, 22-26 min: 95/5, 27-35 min: 20/80. **3.34**: 0 min: MeCN/0.05% TFA/aq 25/75, 20 min: 80/20, 21-27 min: 95/5, 28-36 min: 25/75. **3.35**: 0 min: MeCN/0.05% TFA/aq 20/80, 24 min: 43/57, 27-31 min: 95/5, 32-40 min: 20/80.

Preparation of primary human liver cell culture. Tissue samples were obtained and experimental procedures were performed according to the guidelines of the charitable state controlled foundation HTCR, with the informed patient's consent.[56-57] Briefly, primary human liver cells (hepatocytes) were seeded in a 96-well plate coated with rat tail collagen type I (Biocoat Cell Environments Collagen I Cellware 96-well plate, Becton Dickinson Labware, Bedford, USA) at a density of $0.15 \cdot 10^6$ cells/cm^2 ($0.48 \cdot 10^5$ cells/well). The medium consisted of DMEM with 5 % fetal calf serum (FCS) and the following supplements: 125 mU/ml insulin, 60 ng/ml hydrocortisone, 10 ng/ml glucagon, 100 mg/ml streptomycin, 100 mU/ml penicillin. After 24 h the culture medium was replaced by fresh medium.

Protocol for determination of the stability of cilazapril and candesartan prodrugs in different incubation media. The test compounds were dissolved in DMSO (stock solution, 50 mM) and prior to use diluted with hepatocyte culture medium yielding a final concentration of 150 µM. 48 h after seeding, four wells each were treated with 200 µl of fresh culture medium containing the respective test compound or DMSO as a control. After incubation periods (37 °C) of one and six hours, respectively, 150 µl were collected in duplicate and immediately stored at -78 °C. Prior to analysis to each sample (150 µl)

300 µl of MeCN were added. Prior to HPLC analysis, the samples were thawed and 300 µl of MeCN were added to each sample. After vortex mixing the samples were stored in a refrigerator for approx. 30 min, then vortexed again and centrifuged at 13000 g for 5 min. The supernatants were evaporated to dryness using a speed vac. The resulting residues were dissolved in 450 µl of mobile phase, shortly sonicated and analyzed by HPLC applying the following gradient: 0 min: MeCN/0.05% TFA/aq 10/90, 15 min: 30/70, 30 min: 75/25, 31-36 min: 95/5, 37-45 min: 10/90. For the HPLC analysis of samples containing candesartan prodrugs the following gradient was used: 0 min: MeCN/0.05% TFA/aq 30/70, 20 min: 85/15, 21-26 min: 95/5, 27-35 min: 30/70.

3.8.4 Investigation for AT_1 receptor antagonism on rat mesangial cells

Fura-2 assay on rat mesangial cells. Glomerular rat mesangial cells (kindly provided by the work group of Prof. Dr. A Kurtz, Institute of Physiology, University of Regensburg) were passaged 4-5 days prior to the experiment, and the content of a confluent 25 cm^2 culture flask was divided to four 175 cm^2 culture flasks. The cells were cultured in RPMI1640 medium supplemented with 10 % FCS and 0.24 mg/l insulin at 37 °C and 5 % CO_2 in a saturated humidity atmosphere. On the day of the experiment the cells were trypsinized, suspended in medium and centrifuged (7 min, 200 g). The cells were re-suspended in 40 ml of loading buffer and 30 µl of fura-2/AM (1 mM in DMSO), 37.5 µl Pluronic F-127 (20 % in DMSO) and 200 mg of BSA were added. After an incubation period of 30 min at ambient temperature under exclusion of light the cells were centrifuged, transferred to fresh loading buffer und incubated for additional 60 min. The cells were washed with loading buffer, suspended in 25 ml of loading buffer and were allowed to stand for at least 15 min under light protection. 200-fold concentrated solutions of the test compounds were prepared by dilution of the respective stock solutions (10 mM in DMSO) with DMSO/H_2O (1:1 v:v). One ml of cell suspension and 10 µl of the appropriate substance concentration were added to 1 ml of loading buffer in an acryl cuvette equipped with a small stirring bar. After incubation for 1 min at 25 °C, the Ca^{2+}-signal was stimulated by addition of angiotensin II (100 nM in DMSO). The fluorescence intensity was recorded using a Perkin-Elmer LS50 B spectrofluorometer (Perkin Elmer, Überlingen, Germany) with following settings: λ_{ex} = 340 and 380 nm (alternating), slit = 10 nm; λ_{em} =510 nm, slit = 10 nm. For each concentration a sample containing 10 µl of loading buffer instead of test substance was measured simultaneously and gave the uninhibited control value. The maximal fluorescence signal was detected by adding 10 µl of digitonin solution (2 % in H_2O) instead of 10 µl of test substance and the minimal fluorescence signal resulted from the subsequent addition of 50 µl of EGTA solution (600 mM in 1 M tris buffer, pH 8.7).

3.9 References

1. Albert, A. Chemical aspects of selective toxicity. *Nature* **1958**, 182, 421-422.
2. Bundesverband der Pharmazeutischen Industrie. *Rote Liste 2002 : Arzneimittelverzeichnis für Deutschland (einschl. EU-Zulassungen und bestimmter Medizinprodukte)*. Editio Cantor Verl.: Aulendorf/Württ., 2002; p Getr. Pag +.
3. Ettmayer, P.; Amidon, G. L.; Clement, B.; Testa, B. Lessons learned from marketed and investigational prodrugs. *J. Med. Chem.* **2004**, 47, 2393-2404.
4. Liederer, B. M.; Borchardt, R. T. Enzymes involved in the bioconversion of ester-based prodrugs. *J. Pharm. Sci.* **2006**, 95, 1177-1195.
5. Testa, B.; Mayer, J. M. *Hydrolysis in drug and prodrug metabolism : chemistry, biochemistry, and enzymology*. Verl. Helvetica Chimica Acta [u.a.]: Zürich, 2003; p XX, 780 S.
6. Crauste-Manciet, S.; Decroix, M.; Farinotti, R.; Chaumeil, J. Cefpodoxime-proxetil hydrolysis and food effects in the intestinal lumen before absorption: in vitro comparison of rabbit and human material. *Int. J. Pharm.* **1997**, 157, 153-161.
7. Jarvinen, T.; Poikolainen, M.; Suhonen, P.; Vepsalainen, J.; Alaranta, S.; Urtti, A. Comparison of enzymatic hydrolysis of pilocarpine prodrugs in human plasma, rabbit cornea, and butyrylcholinesterase solutions. *J. Pharm. Sci.* **1995**, 84, 656-660.
8. Potter, P. M.; Wadkins, R. M. Carboxylesterases--detoxifying enzymes and targets for drug therapy. *Curr. Med. Chem.* **2006**, 13, 1045-1054.
9. Thompson, R. H.; Whittaker, V. P. The esterases of skin. *Biochem. J.* **1944**, 38, 295-299.
10. Billecke, S.; Draganov, D.; Counsell, R.; Stetson, P.; Watson, C.; Hsu, C.; La Du, B. N. Human serum paraoxonase (PON1) isozymes Q and R hydrolyze lactones and cyclic carbonate esters. *Drug Metab. Disposition* **2000**, 28, 1335-1342.
11. Parkinson, A.; Ogilvie, B. W. Biotransformation of Xenobiotics. In *Casarett and Doull's toxicology : the basic science of poisons*, 7. ed.; Casarett, L. J.; Doull, J.; Klaassen, C. D., Eds., McGraw-Hill: New York, NY [u.a.], 2008; pp XV, 1310 S.
12. Attwood, M. R.; Francis, R. J.; Hassall, C. H.; Krohn, A.; Lawton, G.; Natoff, I. L.; Nixon, J. S.; Redshaw, S.; Thomas, W. A. New potent inhibitors of angiotensin converting enzyme. *FEBS Lett.* **1984**, 165, 201-206.
13. Gu, L.; Strickley, R. G. Diketopiperazine formation, hydrolysis, and epimerization of the new dipeptide angiotensin-converting enzyme inhibitor RS-10085. *Pharm. Res.* **1987**, 4, 392-397.
14. Deget, F.; Brogden, R. N. Cilazapril: A Review of its Pharmacodynamic and Pharmacokinetic Properties, and Therapeutic Potential in Cardiovascular Disease. *Drugs* **1991**, 41, 799-820.
15. Morsing, P.; Adler, G.; Brandt-Eliasson, U.; Karp, L.; Ohlson, K.; Renberg, L.; Sjoquist, P. O.; Abrahamsson, T. Mechanistic differences of various AT1-receptor blockers in isolated vessels of different origin. *Hypertension* **1999**, 33, 1406-1413.
16. Easthope, S. E.; Jarvis, B. Candesartan cilexetil: an update of its use in essential hypertension. *Drugs* **2002**, 62, 1253-1287.
17. Beaumont, K.; Webster, R.; Gardner, I.; Dack, K. Design of ester prodrugs to enhance oral absorption of poorly permeable compounds: challenges to the discovery scientist. *Curr. Drug Metab.* **2003**, 4, 461-485.
18. Brass, E. P. Pivalate-generating prodrugs and carnitine homeostasis in man. *Pharmacol. Rev.* **2002**, 54, 589-598.
19. Majumdar, S.; Sloan, K. B. N-Alkyl-N-alkyloxycarbonylaminomethyl (NANAOCAM) prodrugs of carboxylic acid containing drugs. *Bioorg. Med. Chem. Lett.* **2007**, 17, 1447-1450.
20. Uchida, K.; Masumoto, S.; Tohno, M.; Mimura, M.; Okumura, M.; Ichikawa, K.; Matsumura, M. Biphenylylpropionic acid derivative, with antiinflammatory, analgesic and antipyretic activities. EP 103265, 1984.
21. Kazahaya, K.; Tsuji, S.; Sato, T. Entirely solvent-free procedure for the synthesis of distillable 1,3-dithianes using lithium tetrafluoroborate as a reusable catalyst. *Synlett* **2004**, 1640-1642.
22. Seebach, D. Nucleophile Acylierung mit 2-Lithium-1,3-dithianen bzw. -1,3,5-trithianen. *Synthesis* **1969**, 1969, 17,36.
23. Sahu, D. P. A convenient and safe synthesis of 4,5-disubstituted-2-oxo-1,3-dioxolenes. *Indian J. Chem., Sect. B Org. Chem. Incl. Med. Chem.* **2002**, 41B, 1722-1723.
24. Adam, F.; Blumbach, J.; Duerckheimer, W.; Fischer, G.; Mencke, B.; Isert, D.; Seibert, G. Preparation of (alkanoyloxy)alkyl cephemcarboxylates as antibiotics. DE3901405, 1989.

25. Fedi, V.; Altamura, M.; Balacco, G.; Canfarini, F.; Criscuoli, M.; Giannotti, D.; Giolitti, A.; Giuliani, S.; Guidi, A.; Harmat, N. J.; Nannicini, R.; Pasqui, F.; Patacchini, R.; Perrotta, E.; Tramontana, M.; Triolo, A.; Maggi, C. A. Insertion of an aspartic acid moiety into cyclic pseudopeptides: synthesis and biological characterization of potent antagonists for the human Tachykinin NK-2 receptor. *J. Med. Chem.* **2004**, 47, 6935-6947.
26. Majumdar, S.; Sloan, K. B. Practical synthesis of N-alkyl-N-alkyloxycarbonylaminomethyl prodrug derivatives of acetaminophen, theophylline, and 6-mercaptopurine. *Synth. Commun.* **2006**, 36, 3537-3548.
27. Ortiz, J.; Guijarro, A.; Yus, M. alpha-aminated methyllithium by DTBB-catalysed lithiation of a N-(chloromethyl)carbamate. *Tetrahedron* **1999**, 55, 4831-4842.
28. Barry, B. W. Novel mechanisms and devices to enable successful transdermal drug delivery. *Eur. J. Pharm. Sci.* **2001**, 14, 101-114.
29. Sloan, K. B.; Wasdo, S. C.; Rautio, J. Design for optimized topical delivery: Prodrugs and a paradigm change. *Pharm. Res.* **2006**, 23, 2729-2747.
30. Zhang, Q.; Grice, J. E.; Li, P.; Jepps, O. G.; Wang, G. J.; Roberts, M. S. Skin solubility determines maximum transepidermal flux for similar size molecules. *Pharm. Res.* **2009**, 26, 1974-1985.
31. Diez, I.; Colom, H.; Moreno, J.; Obach, R.; Peraire, C.; Domenech, J. A comparative in vitro study of transdermal absorption of a series of calcium channel antagonists. *J. Pharm. Sci.* **1991**, 80, 931-934.
32. Kim, M. K.; Lee, C. H.; Kim, D. D. Skin permeation of testosterone and its ester derivatives in rats. *J. Pharm. Pharmacol.* **2000**, 52, 369-375.
33. Choy, Y. B.; Prausnitz, M. R. The Rule of Five for Non-Oral Routes of Drug Delivery: Ophthalmic, Inhalation and Transdermal. *Pharm. Res.* **2010**.
34. Avdeef, A. pH-metric log P. II: Refinement of partition coefficients and ionization constants of multiprotic substances. *J. Pharm. Sci.* **1993**, 82, 183-190.
35. Avdeef, A.; Box, K. J.; Comer, J. E.; Gilges, M.; Hadley, M.; Hibbert, C.; Patterson, W.; Tam, K. Y. PH-metric log P 11. pKa determination of water-insoluble drugs in organic solvent-water mixtures. *J. Pharm. Biomed. Anal.* **1999**, 20, 631-641.
36. Bhal, S. K.; Kassam, K.; Peirson, I. G.; Pearl, G. M. The Rule of Five revisited: applying log D in place of log P in drug-likeness filters. *Mol. Pharmacol.* **2007**, 4, 556-560.
37. Liu, X.; Testa, B.; Fahr, A. Lipophilicity and Its Relationship with Passive Drug Permeation. *Pharm. Res.* **2010**.
38. Jarvinen, T.; Suhonen, P.; Urtti, A.; Peura, P. O,O'-(1,4-Xylylene) Bispilocarpic Acid-Esters as New Potential Double Prodrugs of Pilocarpine for Improved Ocular Delivery .2. Physicochemical Properties, Stability, Solubility and Enzymatic-Hydrolysis. *Int. J. Pharm.* **1991**, 75, 259-269.
39. Rautio, J.; Taipale, H.; Gynther, J.; Vepsalainen, J.; Nevalainen, T.; Jarvinen, T. In vitro evaluation of acyloxyalkyl esters as dermal prodrugs of ketoprofen and naproxen. *J. Pharm. Sci.* **1998**, 87, 1622-1628.
40. Täuber, U. Metabolism of drugs on and in the skin. In *Dermal and transdermal absorption*, Brandau, R.; Lippold, B. H.; Hook, M., Eds., Wiss. Verl.-Ges.: Stuttgart, 1982; pp 133-151.
41. Meyer, W.; Neurand, K. The distribution of enzymes in the skin of the domestic pig. *Lab. Anim.* **1976**, 10, 237-247.
42. Tougou, K.; Nakamura, A.; Watanabe, S.; Okuyama, Y.; Morino, A. Paraoxonase has a major role in the hydrolysis of prulifloxacin (NM441), a prodrug of a new antibacterial agent. *Drug Metab. Disposition* **1998**, 26, 355-359.
43. Levenberg, K. A Method for the Solution of Certain Problems in Least Squares. *Quart. Appl. Math.* **1944**, 2, 164-168.
44. Marquardt, D. An Algorithm for Least Squares Estimation on Nonlinear Parameters. *SIAM J. Appl. Math.* **1963**, 11, 431–441.
45. Ertel, M. Potentielle Prodrugs von ACE-Hemmern und Angiotensin II AT_1-Rezeptorantagonisten: Synthese und analytische Untersuchungen. Diploma, Regensburg, Regensburg, 2006.
46. Grynkiewicz, G.; Poenie, M.; Tsien, R. Y. A new generation of Ca2+ indicators with greatly improved fluorescence properties. *J. Biol. Chem.* **1985**, 260, 3440-3450.
47. Cheng, Y.; Prusoff, W. H. Relationship between the inhibition constant (K1) and the concentration of inhibitor which causes 50 per cent inhibition (I50) of an enzymatic reaction. *Biochem. Pharmacol.* **1973**, 22, 3099-3108.

48. Noda, M.; Shibouta, Y.; Inada, Y.; Ojima, M.; Wada, T.; Sanada, T.; Kubo, K.; Kohara, Y.; Naka, T.; Nishikawa, K. Inhibition of rabbit aortic angiotensin II (AII) receptor by CV-11974, a new nonpeptide AII antagonist. *Biochem. Pharmacol.* **1993**, 46, 311-318.
49. Stahl, I. 1,3-Dithienium- und 1,3-Dithioleniumsalze, IV. 1,3-Dithian-2-ylium-tetrafluoroborate – neue Agenzien zur Synthese von 1-Deuterioaldehyden. *Chem. Ber.* **1985**, 118, 3166-3171.
50. Shiyouji, I. S., F.; Tsukamoto, G. 7-Aminocephalosporanic acid esters. JP 58013591, 1983.
51. Ikeda, S.; Sakamoto, F.; Kondo, H.; Moriyama, M.; Tsukamoto, G. Studies on prodrugs. III. A convenient and practical preparation of ampicillin prodrugs. *Chem. Pharm. Bull.* **1984**, 32, 4316-4322.
52. Naka, T.; Nishikawa, K.; Kato, T. Preparation of benzimidazole derivatives as angiotensin II antagonists. EP 459136, 1991.
53. Ngawhirunpat, T.; Opanasopit, P.; Prakongpan, S. Comparison of skin transport and metabolism of ethyl nicotinate in various species. *Eur. J. Pharm. Biopharm.* **2004**, 58, 645-651.
54. Stoops, J. K.; Horgan, D. J.; Runnegar, M. T.; De Jersey, J.; Webb, E. C.; Zerner, B. Carboxylesterases (EC 3.1.1). Kinetic studies on carboxylesterases. *Biochemistry (Mosc).* **1969**, 8, 2026-2033.
55. Lockridge, O.; La Du, B. N. Comparison of atypical and usual human serum cholinesterase. Purification, number of active sites, substrate affinity, and turnover number. *J. Biol. Chem.* **1978**, 253, 361-366.
56. Thasler, W. E.; Weiss, T. S.; Schillhorn, K.; Stoll, P. T.; Irrgang, B.; Jauch, K. W. Charitable State-Controlled Foundation Human Tissue and Cell Research: Ethic and Legal Aspects in the Supply of Surgically Removed Human Tissue For Research in the Academic and Commercial Sector in Germany. *Cell. Tissue. Bank.* **2003**, 4, 49-56.
57. Weiss, T. S.; Jahn, B.; Cetto, M.; Jauch, K. W.; Thasler, W. E. Collagen sandwich culture affects intracellular polyamine levels of human hepatocytes. *Cell Prolif.* **2002**, 35, 257-267.

Chapter 4
Novel Transdermal Therapeutic Systems Containing Prodrugs of Candesartan or Cilazapril: Making and Characterization

4.1 Introduction

Transdermal therapeutic systems (TTS), also known as transdermal drug delivery systems (TDDS), are drug-loaded adhesive patches, designed to deliver a therapeutically effective amount of drug across a patient's skin.[1-2] Common transdermal drug delivery typically involves passive diffusion of a drug through the skin, whereas novel strategies intend to improve transdermal delivery by using e.g. chemical enhancers, electrically-assisted approaches (iontophoresis, electroporation), ultrasound (sonophoresis), heat or strategies for increasing permeability of the skin (microneedles, microdermabrasion).[3]

Typical designs of passive transdermal therapeutic systems are shown in Figure 4.1. In the simplest form, the adhesive matrix or drug-in-adhesive design (Figure 4.1 a), the drug is dissolved, dispersed or suspended in a pressure-sensitive adhesive (PSA) polymer matrix, which provides skin adhesion, storage of the drug, and control over the drug delivery rate.[2] The adhesive matrix is supported on the topside by an impermeable backing film, and on the side that faces the skin, it is laminated with a removable release liner. The liquid reservoir design (Figure 4.1 c) consists of a liquid reservoir compartment containing the drug and a permeation enhancer either in solution or dispersed. It is positioned between a backing film and a rate-controlling membrane adjacent to a skin-contacting PSA layer and a release liner. For both designs the release liner usually consists of a layer of release coating (e.g. fluoro-polymer, silicone) applied to a carrier substrate (e.g. polyester).[4] Also copolymers such as

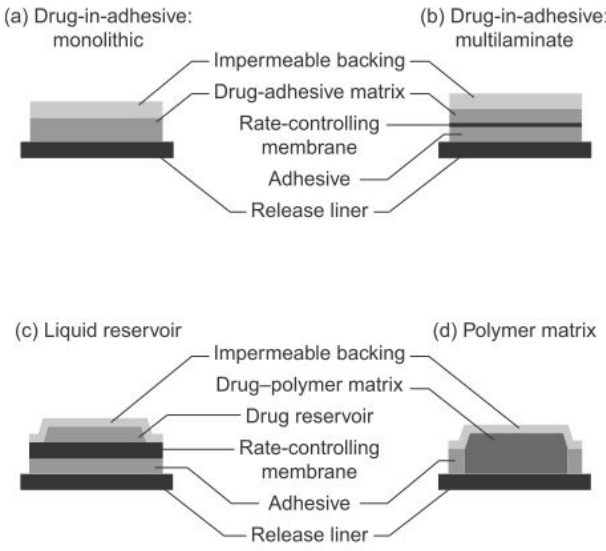

Figure 4.1. Typical designs of passive transdermal therapeutic systems. Reprinted from Tan and Pfister[2] with permission from Elsevier.

ethylene vinyl acetate, coated papers or aluminium foil are used.[5] The backing layer is often prepared from polyethylene, polypropylene, polyester, polyurethane or less occlusive polyvinylchloride.[5]

Three classes of PSA polymers are widely used in TTS development: polyisobutylene (PIB)-based adhesives, acrylics and silicone-based PSAs. Ideally, the PSA should provide solubility and long-term stability of the drug and potential excipients.

Furthermore, it should be biologically inert, non-irritating and non-sensitizing to the skin, exhibit strong adhesion for the prescribed application period, easily removable without any residues on the skin and comfortable to wear.[1-2]

Silicone PSAs (Scheme 4.1) are well established adhesives for application in TTS devices. They have a highly flexible and extremely open macromolecular architecture with a high void volume resulting in a high permeability to vapor, gases and a variety of therapeutic molecules.[2] To avoid condensation reactions of reactive silanol end groups with basic drugs, the residual SiOH groups are end-capped to yield an amine-compatible silicone PSA.[6]

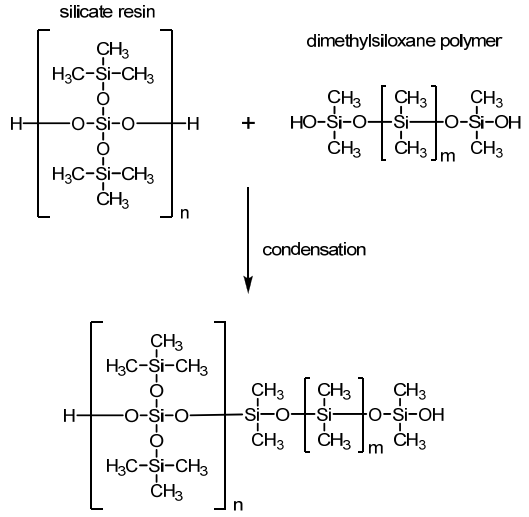

Scheme 4.1. Processing of silicone pressure sensitive adhesive. Adapted from Tan and Pfister.[2]

4.2 Selection of most promising prodrug candidates for TTS development

In the previous chapter synthesis and physicochemical properties of potential prodrugs of candesartan and cilazapril are presented. Furthermore, the compounds were characterized in terms of solid state stability, enzymatic and non-enzymatic (spontaneous) cleavage as well as pharmacological activity in case of the candesartan prodrugs. According to these criteria a set of the three most promising candidates each had to be selected for upscaling of the synthesis to manufacture TTS. Adequate lipophilicity and preferably fast enzymatic hydrolysis to the active metabolite are classified as crucial criteria. Since prodrug activation ideally takes place in the viable epidermis, and because porcine skin shows similarities to the integument of humans in terms of enzyme activity and distribution[7], hydrolysis in porcine skin homogenate was considered the most predictive criterion.

Among the candesartan prodrugs the cascade esters **3.31** and **3.32** as well as the morpholinoethyl ester **3.35** (Table 4.1) were chosen for development of TTS. **3.31** and **3.32** showed high stability against non-enzymatic hydrolysis, short half-lives in porcine skin homogenate and similar experimentally determined octanol/water partition

coefficients as the reference candesartan cilexetil. The hydrolysis of **3.35** in porcine skin homogenate was found to be rather slow, but the possibility of salt formation and the fact that the putative prodrugs **3.35** and **3.32** are potent AT_1 receptor antagonists led to the decision to short-list **3.35** as a third potential development candidate.
Similar considerations led to the selection of the cilazapril cascade prodrugs **3.1**, **3.2** and the morpholinoethyl ester **3.14** as TTS development candidates (cf. Table 4.1). These compounds are characterized by ease of synthesis, adequate lipophilicity, high to moderate stability against non-enzymatic hydrolysis and fast cleavage in porcine skin homogenate. (5-alkyl-2-oxo-1,3-dioxol-4-yl)methyl esters (**3.12**, **3.13**) and *N*-aryl-*N*-alkyl-oxycarbonylaminomethyl esters (**3.25**-**3.27**) of cilazapril do not fulfill the criteria, because they are prone to spontaneous hydrolysis. By contrast, the simple ethyl ester **3.28** was disregarded due to very high resistance against enzymatic hydrolysis.

Subsequently, approximately 5 g of each selected prodrug (Table 4.1) were synthesized for further TTS development.

Table 4.1. Prodrugs of candesartan and cilazapril chosen for TTS development.

candesartan prodrugs		cilazapril prodrugs	
compound	structure	compound	structure
3.31	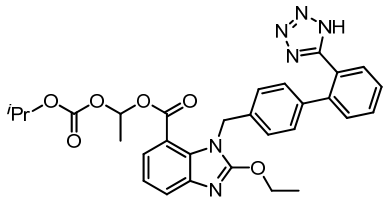	**3.1**	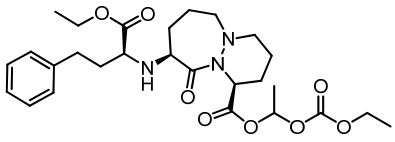
3.32	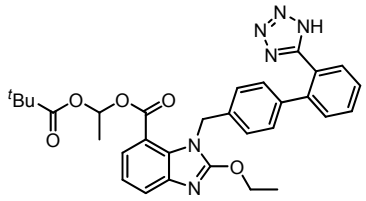	**3.2**	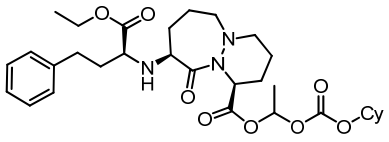
3.35	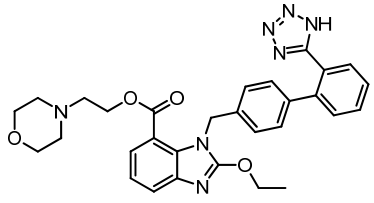	**3.14**	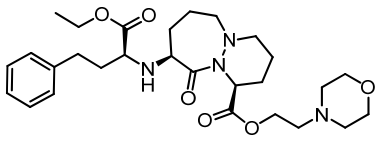
reference standard		reference standard	
candesartan cilexetil	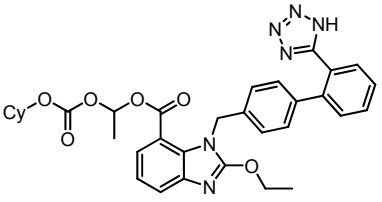	**cilazapril**	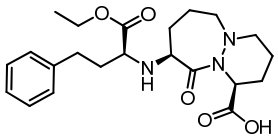

4.3 Manufacturing of transdermal therapeutic systems

For the preparation of monolithic drug-in-adhesive type transdermal patches used for analytical studies and permeation experiments the respective prodrug was dissolved in an appropriate amount of organic solvent (ethyl acetate), and the required amount of a silicone pressure-sensitive adhesive (PSA) in organic solvent (ethyl acetate) was added. After homogenizing, the resulting mixture was coated on a fluorosiliconized polyester-based film laminate serving as the release liner by means of a motorized film applicator. The solvent was removed in a drying cabinet. Subsequently, the adhesive coating was covered with a thin PET backing foil and round patches with an area of 10 cm^2 or 2.5 cm^2 were punched out using appropriate cutting tools. The TTS were then separately packed in sachets and vacuum sealed.

TTS batches with different intended drug dosages were prepared, aiming at masses per unit area in the range between 60 to 80 g/m^2. The resulting drug dose per TTS is assumed to provide adequate permeability to reach therapeutic levels. Table 4.2 summarizes the produced TTS batches for analytical studies and permeation experiments containing either a candesartan prodrug (**3.31**, **3.32**, **3.35**) or a cilazapril prodrug (**3.1**, **3.2**, **3.14**). Additionally, batches of TTS containing candesartan cilexetil and cilazapril, respectively, were produced for the purpose of comparative studies.

Table 4.2. Manufactured TTS batches containing candesartan prodrugs, cilazapril prodrugs or cilazapril.

TTS batch	compound	intended conc. [%]	calculated drug conc.[a] [%]	intended mass per unit area [g/m^2]	actual matrix mass per unit area[b] [g/m^2]	drug dose per 10 cm^2 TTS [mg/TTS]
PCAN0001TTS	**3.31**	5	4.68	80	131.93	6.18
PCAN0002TTS	**3.32**	5	4.79	80	141.13	6.76
PCAN0003TTS	**3.35**	5	4.90	80	171.93	8.42
PCAN0004TTS	**3.31**	10	9.82	80	70.01	6.87
PCAN0005TTS	**3.32**	10	9.94	80	71.14	7.07
PCAN0006TTS	**3.35**	10	9.42	80	49.74	4.68
PCAN0009TTS	**3.31**	10	10.09	60	66.82	6.74
PCAN0010TTS	**3.32**	10	9.76	60	63.62	6.21
PCAN0011TTS	**3.35**	10	10.08	60	65.90	6.64
CAN0043TTS	**CAN-CIL**	10	9.52	80	72.25	6.88
CAN0044TTS	**CAN-CIL**	10	9.94	60	60.00	5.96
PCIL0002TTS	**3.1**	10	10.12	80	74.07	7.49
PCIL0003TTS	**3.2**	10	10.70	80	74.76	8.00
PCIL0004TTS	**3.14**	10	9.79	80	75.18	7.36
PCIL0011TTS	**3.1**	10	9.71	70	62.92	6.11
PCIL0012TTS	**3.2**	10	10.39	70	63.98	6.65
PCIL0013TTS	**3.14**	10	10.28	70	63.88	6.57
CIL0025TTS	**cilazapril**	10	9.76	75	96.57	9.42
CIL0027TTS	**cilazapril**	10	10.17	70	65.18	6.63

[a] Calculated from the weight of added compound and PSA. [b] Theoretical mass per unit area of the TTS matrix calculated from the weight of TTS samples by subtraction of the weights of release liner and backing foil.

As the initial formulations of candesartan prodrug TTS batches with intended drug concentrations of 5 % (PCAN0001TTS – PCAN0003TTS) were successful, loading was increased to 10 %. Thereby, the apparent difference between intended and actual drug concentration can be attributed to the fact that, with respect to the small batch size, the exact manual addition of a small amount of semi-solid PSA was challenging. The calculated drug concentration represents only a theoretical value. Because of inequalities of the coating mixture, variations of the true drug concentration of each TTS cannot be excluded. High discrepancies between the intended and the actual TTS matrix mass were mainly caused by an unsuitable gap width of the film applicator during coating, which led to thicker and heavier patches, when the gap width was adjusted too broad. The TTS matrix mass at the edges of the laminate is generally smaller due to a reduced thickness of the coating mass. Regarding the solubility of the respective prodrugs in ethyl acetate and in the resulting coating mixture, it became apparent that the 1-(2,2-dimethylpropanoyloxy)ethyl ester **3.32** was most soluble in ethyl acetate and showed only slight turbidity after addition of the PSA. The solubility of the 1-(isopropyloxy-carbonyloxy)ethyl ester **3.31** and candesartan cilexetil in ethyl acetate turned out to be dependent on the amount of solvent added. The prodrugs became insoluble, when slightly decreased amounts of ethyl acetate were used. The resulting suspension was then mixed with PSA and intensively stirred to obtain a homogeneous coating mixture. The candesartan morpholinoethyl ester **3.35** turned out to be the least soluble prodrug. In the case of PCAN0003TTS a clear prodrug stock solution in ethyl acetate was obtained after addition of a larger solvent volume and heating, but the addition of PSA led to precipitation of the prodrug. Since a high solvent content can affect the properties of the resulting laminate, **3.35** was only suspended in ethyl acetate and homogeneously distributed in the coating mixture for following TTS batches.

The manufacturing of cilazapril prodrug-containing TTS batches was very promising. The intended drug concentrations of 10 % were successfully achieved, as all prodrugs were highly soluble in ethyl acetate resulting in clear prodrug stock solutions. Addition of silicone PSA did not compromise the properties of the coating mixtures, which stayed clear and homogeneous. Furthermore, the semi-solid nature of the prodrugs was considered rather beneficial than disadvantageous for the formulation. However, the preparation of TTS batches with a drug concentration of 12.5 % failed, due to inhomogeneity of the matrix after coating and drying (data not shown). Cilazapril is poorly soluble in ethyl acetate. Therefore, it was suspended and mixed after addition of PSA until a homogeneous coating mixture was obtained.

4.4 Characterization of transdermal therapeutic systems

In the following, examples of TTS batches containing candesartan prodrugs, cilazapril prodrugs and cilazapril, respectively are characterized in terms of quality including evaluation of the visual and microscopic appearance and relevant properties like ease of release (removal from the release liner), adhesive strength and cold flow. Furthermore, the stabilities of the individual TTS batches were studied visually as well as by means of HPLC for determination of drug content.

4.4.1 TTS quality

The relevant quality features of the respective candesartan and cilazapril prodrug-containing TTS batches, determined immediately after manufacturing, are summarized in Table 4.3 and Table 4.4. The release was determined by the ease of removal of the release liner. The adhesive strength was assayed by categorizing the power needed to remove the TTS from a plane surface. For the characterization of the cold flow, the tendency of the TTS to form matrix strings during cutting and to stick to the sachet was evaluated.

Table 4.3. Properties of candesartan prodrug TTS batches.

TTS batch	visual appearance	release	adhesive strength	cold flow
PCAN0001TTS	turbid, homogenous	good	good	not present
PCAN0002TTS	turbid, homogenous	good	good	not present
PCAN0003TTS	turbid, inhomogeneous, particles/ crystals visible	good	good	not present
PCAN0004TTS	turbid, homogenous	easy and complete	very good	not present
PCAN0005TTS	turbid, homogenous	easy and complete	moderate	not present
PCAN0006TTS	clear, homogeneous, particles/ crystals visible	easy and complete	good	not present
PCAN0009TTS	turbid, homogenous	good	moderate	hardly present
PCAN0010TTS	turbid, homogenous	good	moderate	hardly present
PCAN0011TTS	turbid, particles/ crystals visible	good	moderate	hardly present
CAN0043TTS	turbid, homogenous	easy and complete	moderate	not present
CAN0044TTS	turbid, homogenous	easy and complete	moderate	hardly present

Almost all TTS batches had a turbid and milky, but still homogeneous appearance after removal of the solvents (Table 4.3). Regarding batches containing the prodrug **3.35**, unsolved prodrug particles or crystals were visible, caused by the use of **3.35** as suspension in the coating mixture. The release of all batches was convincing, as the release liner could be removed easily and without any residual matrix. The adhesive strength was adequate, too. Furthermore, no or hardly any cold flow was identified.

Table 4.4. Properties of cilazapril and cilazapril prodrug TTS batches.

TTS batch	visual appearance	release	adhesive strength	cold flow
PCIL0002TTS	turbid, homogenous	easy and complete	good	hardly present
PCIL0003TTS	turbid, homogenous	easy and complete	good	hardly present
PCIL0004TTS	turbid, homogenous	easy and complete	good	hardly present
PCIL0011TTS	turbid, homogenous	bad, matrix sticks on the RL, BF was removed instead	moderate	hardly present
PCIL0012TTS	turbid, homogenous	easy and complete	moderate	hardly present
PCIL0013TTS	turbid, homogenous	bad at the edges	moderate	hardly present
CIL0025TTS	turbid, homogenous	easy and complete	good	hardly present
CIL0027TTS	turbid, homogenous	good	moderate	hardly present

All batches of cilazapril prodrugs depicted in Table 4.4 were characterized showing turbid and homogenous visual appearance, moderate to good adhesive strength and hardly any cold flow. In most of the cases the release liner could be removed easily and completely without any residual matrix. Only in case of batch PCIL0011TTS, removal of the release liner from the matrix was impossible, but the backing foil was removed quite easily instead. A rather difficult release at the edges of each TTS was observed for PCIL0013TTS.

For further characterization of the TTS matrix-structures microscopic images of exemplary TTS batches were taken directly after manufacturing (cf. Figure 4.2 A-H). Regarding the batches PCAN0004TTS, PCAN0005TTS and PCAN0010TTS homogeneous matrices with dispersed emulsion droplets were visible. For CAN0043TTS single crystals distributed in a homogeneous matrix were found, whereas the matrices of PCAN0009TTS and CAN0044TTS appeared to be more crystalline, containing scattered drug agglomerates. The images of PCAN0006TTS and PCAN0011TTS revealed crystals and small particles, which were either embedded in clear (PCAN0006TTS) or turbid (PCAN0011TTS) matrices. In summary, homogeneous matrices containing emulsion droplets were only found, when the drug was dissolved in the coating mixture. However, when the drug was processed as a suspension, particles and crystals of the drug were clearly visible in the TTS matrix.
Images taken from examples of cilazapril prodrug TTS batches (Figure 4.3 A-H) showed very homogeneous, finely structured matrices with scattered emulsion droplets. The matrices of cilazapril containing TTS batches appeared to be slightly more inhomogeneous due to comparatively more voluminous (CIL0027TTS) or rather amorphous (CIL0025TTS) emulsion droplets. Although cilazapril was used as a suspension in the coating mixture, particles or crystals of the drug were not detected in the TTS, indicating that the suspension was resolved after coating on the release liner.

A: PCAN0004TTS, objective: 10 x

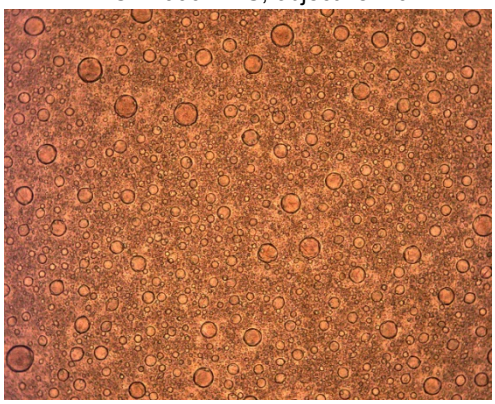

B: PCAN0005TTS, objective: 10 x

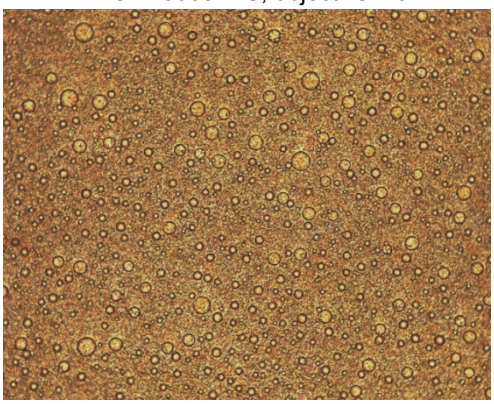

C: PCAN0006TTS, objective: 10 x

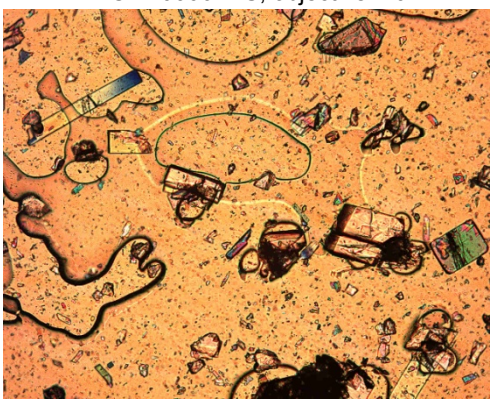

D: CAN0043TTS, objective: 10 x

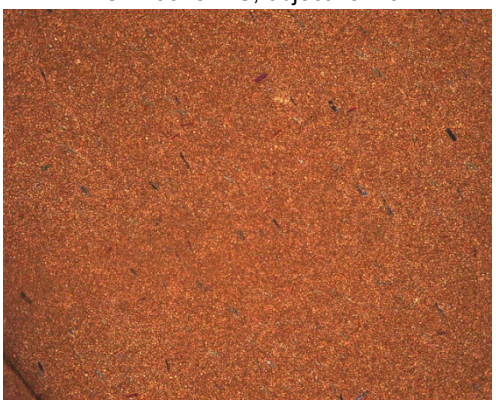

E: PCAN0009TTS, objective: 25 x

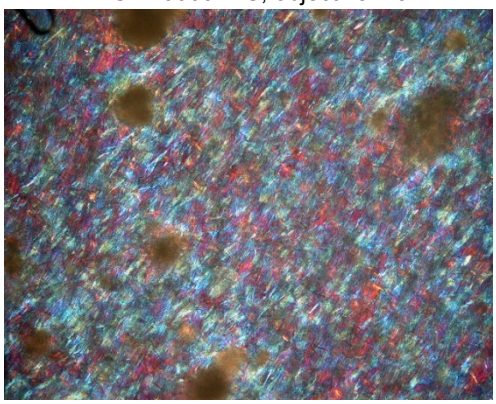

F: PCAN0010TTS, objective: 25 x

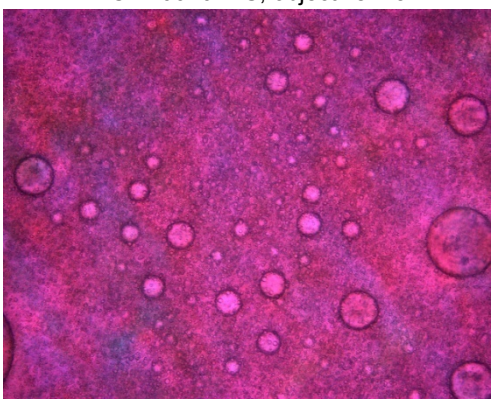

G: PCAN0011TTS, objective: 25 x

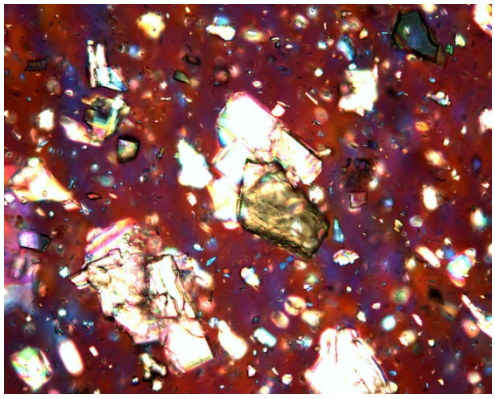

H: CAN0044TTS, objective: 25 x

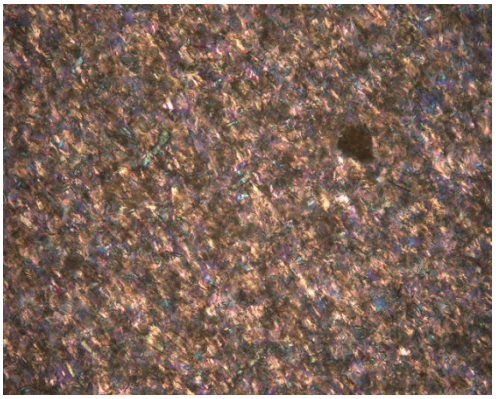

Figure 4.2 A-H. Microscopic images of candesartan prodrug TTS batches, provided by Hexal AG.

A: PCIL0002TTS, objective: 40 x

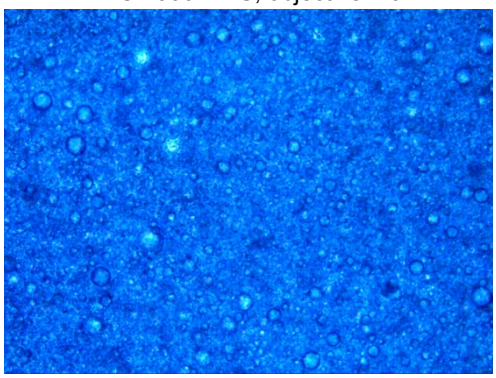

B: PCIL0003TTS, objective: 40 x

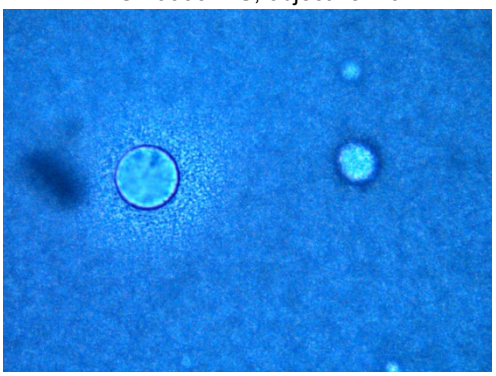

C: PCIL0004TTS, objective: 40 x

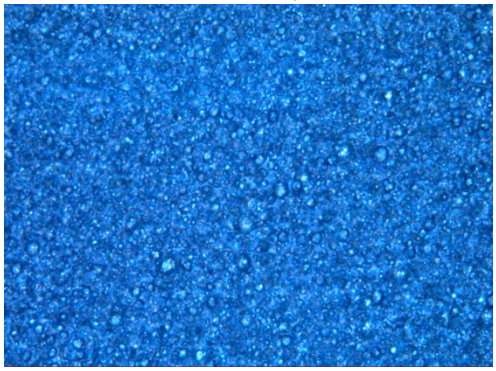

D: CIL0025TTS, objective: 40 x

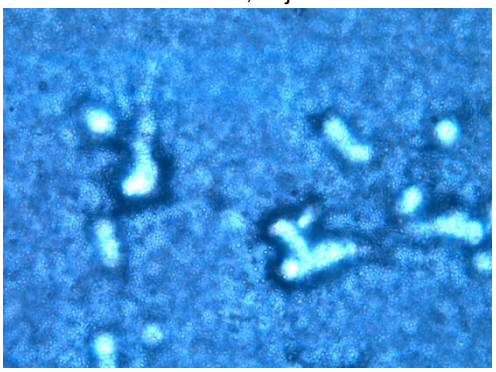

E: PCIL0011TTS, objective: 25 x

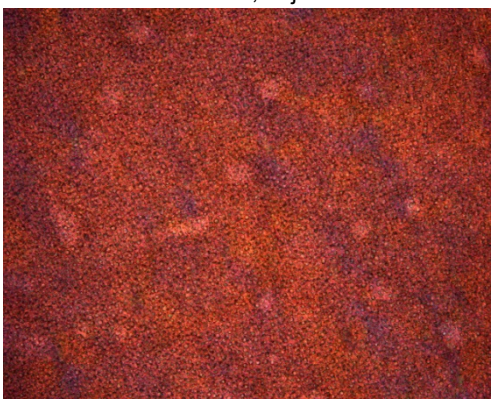

F: PCIL0012TTS, objective: 25 x

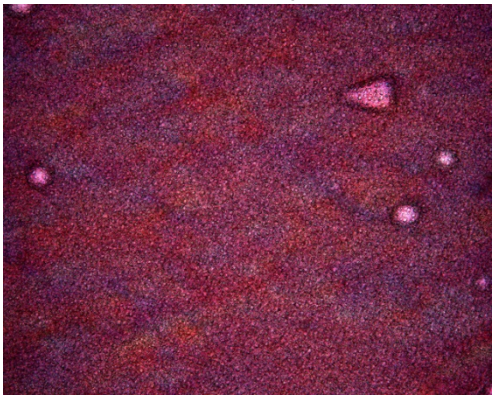

G: PCIL0013TTS, objective: 25 x

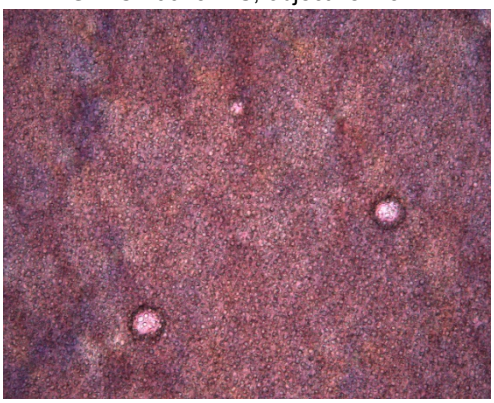

H: CIL0027TTS, objective: 25 x

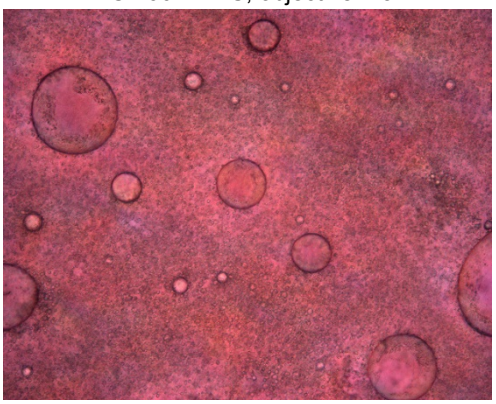

Figure 4.3 A-H. Microscopic images of cilazapril and cilazapril prodrug TTS batches, provided by Hexal AG.

4.4.2 TTS stability

The stability of the different TTS formulations was determined after storage for different periods of time at various temperatures and humidities (rel. h.) by extraction of examples of the respective TTS batches with an organic solvent and subsequent analysis by HPLC using the 100 % method. Furthermore, visible changes of the TTS quality were controlled by light microscopy.

The stability of TTS batches containing candesartan prodrugs in a silicone PSA matrix at different conditions is summarized in Table 4.5 and illustrated in Figure 4.4. It became obvious that all candesartan prodrugs remained stable during storage at 5 °C/65 % rel. h. for eight months. Storage at 25 °C/60 % rel. h. over a period of eight months led to a slight decrease in drug content of the batches PCAN0004TTS, PCAN0005TTS and CAN0043TTS. Furthermore, storage over a period of two months under accelerated storage conditions (40 °C/75 % rel. h.) resulted in a significant decrease in the content of the double ester prodrugs **3.31**, **3.32** and candesartan cilexetil. With respect to the initial value (0 months, promptly determined after TTS preparation), degradation of **3.32** and candesartan cilexetil was comparable. By contrast, **3.31** revealed the lowest stability in the accelerated stability test. Regarding the morpholinoethyl ester **3.35**, excellent stability was observed, irrespective of the storage conditions. However, **3.35** was not dissolved in the TTS matrix. In contrast to PCAN0004TTS, PCAN0005TTS and CAN0043TTS, PCAN0006TTS contained the prodrug in a crystalline form.
Surprisingly, in all TTS batches candesartan was either not detectable or present only in negligible amounts as impurity. For **3.31**, **3.32** and candesartan cilexetil two major impurities each were detected (highlighted in *italics* in Table 4.5 and indicated by black arrows in Figure 4.4), one with shorter, one with longer retention time compared to the respective prodrug. Since each pair of impurities showed a Δt_R ~ 8 min the corresponding decomposition reaction might have occurred at the same positions in the respective prodrugs but not at the pro-moiety.

Table 4.5. Stability of candesartan prodrugs in a silicone PSA matrix after different storage periods at different temperatures and humidities.[a]

batch/ **prodrug**	**prodrug** or impurity (I)[c, d]	content [%]	content (Δ)[b] [%]		content (Δ)[b] [%]	
		0 months	2 months 25 °C/ 60 % rel. h.	2 months 40 °C/ 75 % rel. h.	8 months 5 °C/ 65 % rel. h.	8 months 25 °C/ 60 % rel. h.
PCAN0004TTS/	**3.31**	**92.8**	**93.3 (-0.5)**	**53.3 (39.5)**	**95.3 (-2.5)**	**90.7 (2.1)**
3.31	*I_133*	*3.4*	*3.7*	*18.8*	*2.8*	*5.0*
	I_156	0.1	0.1	2.3	0.0	0.2
	I_178	0.1	0.1	8.9	0.0	0.3
	I_198	0.9	0.9	3.9	0.7	1.1
	I_221	*2.0*	*1.8*	*12.8*	*1.2*	*2.6*
	I_rest [e]	0.7	0.1	0.0	0.0	0.1
PCAN0005TTS/	**3.32**	**93.2**	**93.2 (0)**	**79.4 (13.8)**	**95.6 (-2.4)**	**91.0 (2.2)**
3.32	*I_152*	*3.1*	*3.5*	*9.9*	*2.6*	*4.7*
	I_198	0.2	0.2	1.9	0.0	0.3
	I_217	0.6	0.6	1.9	0.6	0.9
	I_238	*1.3*	*1.7*	*5.7*	*1.1*	*2.3*
	I_rest [e]	1.6	0.8	1.2	0.1	0.8
PCAN0006TTS/	**3.35**	**99.0**	**99.5 (-0.5)**	**99.4 (-0.4)**	**100.0 (-1.0)**	**100.0 (-1.0)**
3.35	I_rest [e]	1.0	0.5	0.6	0.0	0.0
CAN0043TTS/	**CAN-CIL**	**94.9**	**94.4 (0.5)**	**82.3 (12.6)**	**97.3 (-2.4)**	**92.8 (2.1)**
candesartan	*I_165*	*2.5*	*3.0*	*8.9*	*1.8*	*3.9*
cilexetil	I_209	0.0	0.1	1.3	0.0	0.3
(**CAN-CIL**)	I_228	0.3	0.5	1.5	0.0	0.6
	I_245	*1.0*	*1.6*	*5.4*	*0.8*	*2.3*
	I_rest [e]	1.3	0.4	0.6	0.1	0.1

[a] Mean values of two independently analyzed TTS samples. [b] decrease of prodrug content with respect to the 0 months value [c] Not further characterized impurities (I) with > 1 % abundance are listed separately and are highlighted in *italics*. [d] I_xxx stands for impurity eluting at t_R ~ xx.x min. [d] I_rest: sum of all impurities not separately listed.

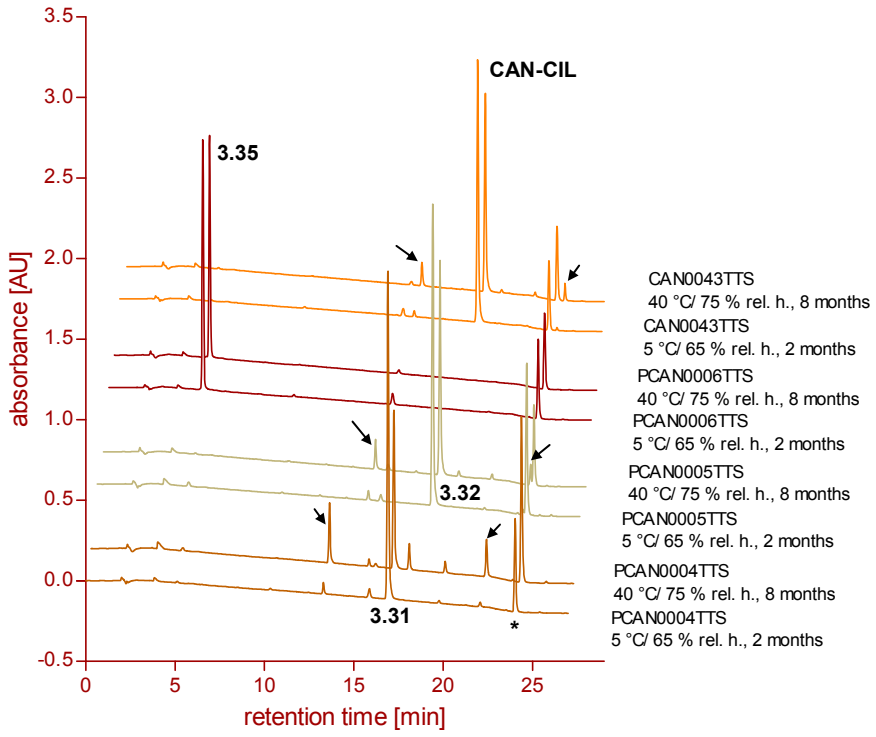

Figure 4.4. Examples of HPLC chromatograms illustrating the analysis of candesartan prodrug containing TTS batches after two different storage periods (1 and 8 months) and at different conditions. Black arrows indicate major impurities. Asterisk refers to an impurity from the used organic solvent.

In Table 4.6 the stabilities of cilazapril and cilazapril prodrugs in silicone PSA matrices are summarized and illustrated in Figure 4.4. Surprisingly, masking of the free carboxylic acid group in cilazapril with a promoiety seemed to be beneficial in terms of drug stability in a silicone PSA matrix, since the prodrugs **3.1** and **3.2** showed a slightly better stability at long-term stability conditions (25 °C, 60 % rel. h.) and were clearly superior to cilazapril under accelerated conditions (40 °C, 75 % rel. h.) over nine months. By contrast, the presence of a basic group in the pro-moiety as in **3.14** led to accelerated degradation compared to cilazapril, although the stability at 25 °C/60 % rel. h. over nine months was still satisfactory and comparable to cilazapril. It becomes obvious from Table 4.6 and Figure 4.4 that (apart from small amounts of cilazaprilat and not further characterized impurities) cilazapril was the major degradation product of **3.1**, **3.2** and **3.14**, whereas the major degradation product of cilazapril was cilazaprilat.

Table 4.6. Stability of cilazapril and cilazapril prodrugs in a silicone PSA matrix after different storage periods at different temperatures and humidities.[a, b]

			content (Δ)[c] [%]	
batch/ **prodrug**	molecular species	0 months	9 months 25 °C/60 % rel. h.	9 months 40 °C/75 % rel. h.
PCIL0002TTS/	**3.1**	**99.7**	**98.0 (1.7)**	**94.1 (5.6)**
3.1	cilazapril	0.3	0.4	3.5
	cilazaprilat	0.0	0.0	0.2
	I_rest[d]	0.0	1.6	2.2
PCIL0003TTS/	**3.2**	**100.0**	**98.3 (1.7)**	**95.9 (4.1)**
3.2	cilazapril	0.0	0.2	1.9
	cilazaprilat	0.0	0.0	0.1
	I_rest[d]	0.0	1.5	2.1
PCIL0004TTS/	**3.14**	**98.0**	**94.7 (3.3)**	**69.1 (28.9)**
3.14	cilazapril	0.6	0.6	21.5
	cilazaprilat	0.0	0.0	1.7
	I_rest[d]	1.4	4.7	7.7
CIL0025TTS/	**cilazapril**	**100.0**	**97.0 (3.0)**	**76.8 (23.2)**
cilazapril	cilazaprilat	0.0	2.1	21.2
	I_rest[d]	0.0	0.9	2.0

[a] Data represent values from the respective “worst case chromatograms” of two analyzed TTS. [b] Data provided from Hexal AG. [c] decrease of prodrug content with respect to the 0 months value. [d] I_rest: sum of all not further characterized impurities or degradation products not separately listed.

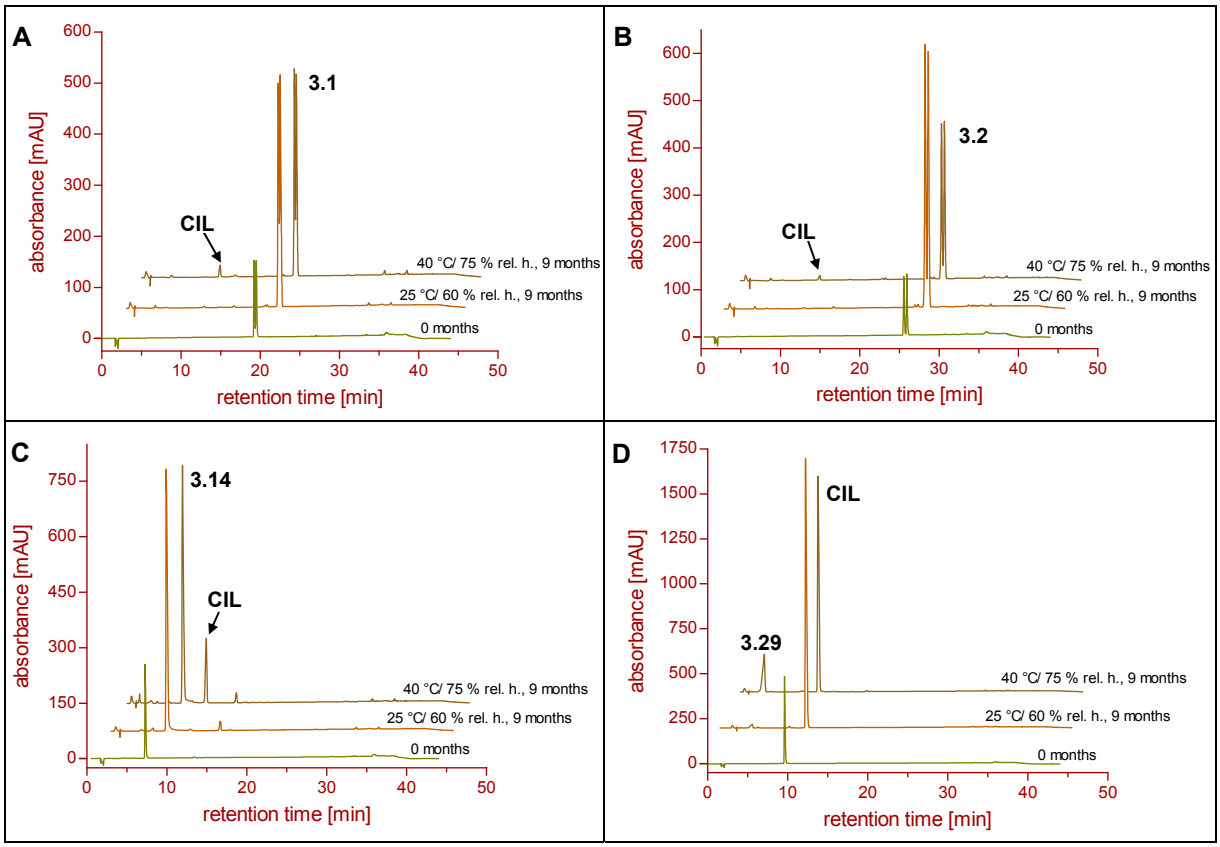

Figure 4.5. HPLC chromatograms of PCIL0002TTS (**A**), PCIL0003TTS (**B**), PCIL0004TTS (**C**) and CIL0025TTS (**D**) stored at given conditions and periods of time. Raw data was provided from Hexal AG and processed by M. Ertel.

After a storage period of five months at 25 °C/60 % rel. h. and 40 °C/75 % rel. h., respectively, the TTS batches PCAN0004TTS, PCAN0005TTS, PCAN0006TTS and CAN0043TTS were inspected and documented by microscopic images in order to detect potential alterations in the TTS matrix structures. From Figure 4.6 it becomes obvious, that compared to long-term stability conditions storage under accelerated conditions led to considerable changes in the appearance of the TTS batches PCAN0004TTS, PCAN0005TTS and CAN0043TTS, which were characterized by a grainier matrix and an increase in the size of present emulsion droplets. This became particularly obvious for PCAN0005TTS by determination of the diameter of randomly chosen spherical emulsion droplets by means of an image processing software (ImageJ 1.43u). Comparing two samples stored at 25 °C/60 % rel. h. and 40 °C/75 % rel. h., respectively, the average diameter increased from ~18 µm to ~71 µm under accelerated storage conditions.

The TTS batch PCAN0006TTS seemed not to be affected during storage in the accelerated stability test, showing single drug crystals or agglomerates and some bubbles. However, the patches revealed a strong tendency to cake, resulting in a considerably more difficult release of the release liner.

A: PCAN0004TTS, 25 °C, 60 % rel. h., objective: 10 x

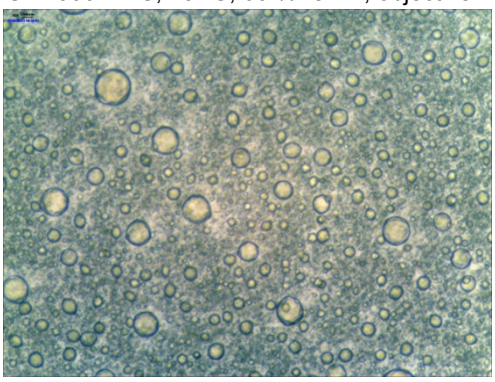

B: PCAN0004TTS, 40 °C, 75 % rel. h., objective: 10 x

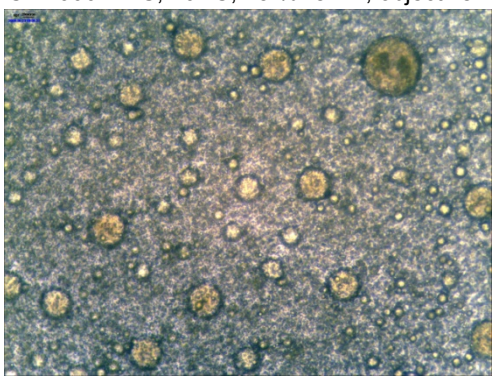

C: PCAN0005TTS, 25 °C, 60 % rel. h., objective: 10 x

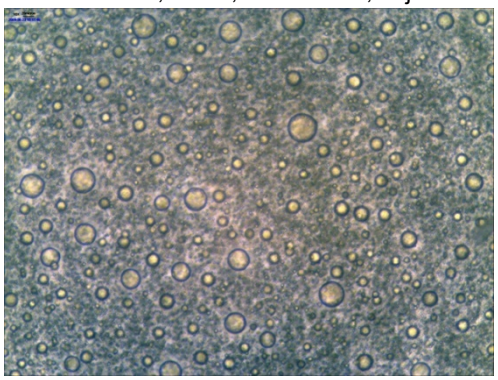

D: PCAN0005TTS, 40 °C, 75 % rel. h., objective: 10 x

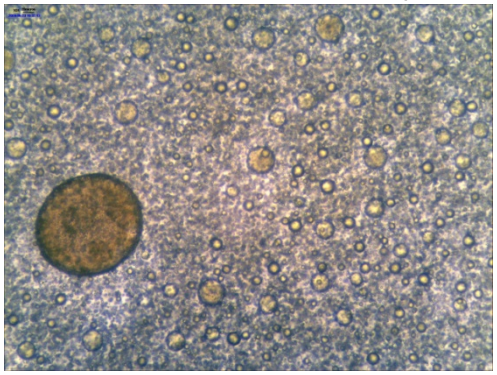

E: PCAN0006TTS, 25 °C, 60 % rel. h., objective: 4 x, polarized light

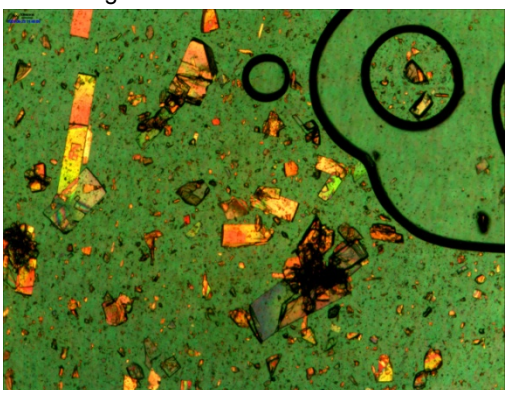

F: PCAN0006TTS, 40 °C, 75 % rel. h., objective: 4 x, polarized light

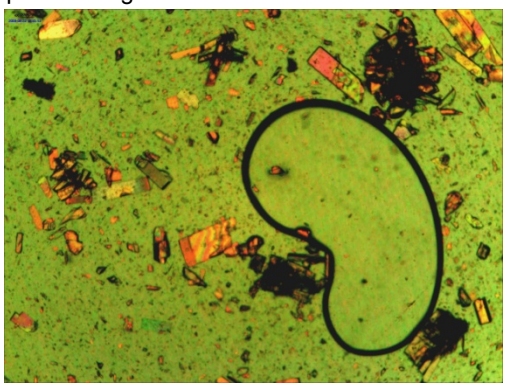

G: CAN0043TTS, 25 °C, 60 % rel. h., objective: 10 x

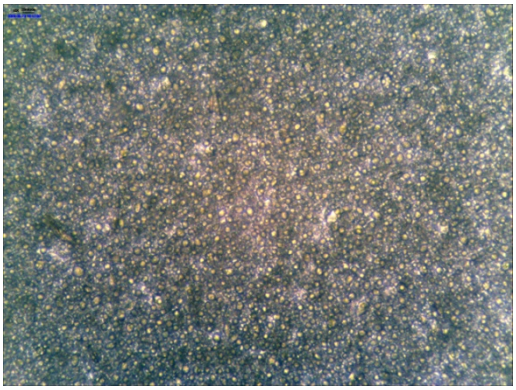

H: CAN0043TTS, 40 °C, 75 % rel. h., objective: 10 x

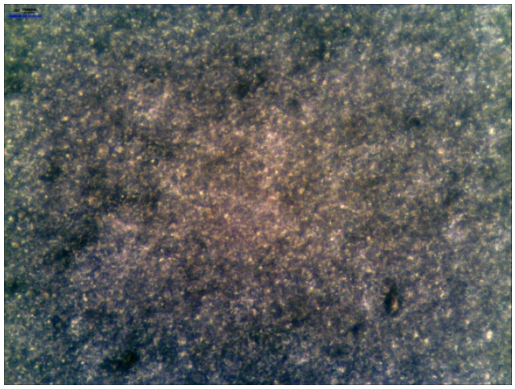

Figure 4.6 A-H. Microscopic images of candesartan prodrug TTS batches stored for five months at given temperature and humidity conditions.

Microscopic studies of examples of the cilazapril and cilazapril prodrug containing TTS batches PCIL0002TTS, PCIL0003TTS, PCIL0004TTS and CIL0025TTS after a storage period of 26 months at 25 °C/60 % rel. h. and 40 °C/75 % rel. h., respectively, revealed promising results for the prodrug containing systems (Figure 4.7). Even over a relatively long storage period at 25 °C/60 % rel. h. no crystallization was observed for PCIL0002TTS, PCIL0003TTS and PCIL0004TTS, and the appearance of the respective matrices was quite satisfactory. As also noticed for candesartan prodrug TTS batches, storage under accelerated storage conditions led to a decrease in homogeneity resulting in a grainier matrix. In PCIL0004TTS yellowish emulsion drops were detected. However, it should be kept in mind that, irrespective of the storage conditions, degradation of all prodrugs took place to a certain degree; this might contribute to the changes in the appearance of the TTS. Investigation of the cilazapril containing TTS CIL0025TTS showed a generally more homogeneous matrix with numerous randomly shaped emulsion structures, which tended to agglomerate under accelerated conditions.

A: PCIL0002TTS, 25 °C, 60 % rel. h., objective: 10 x

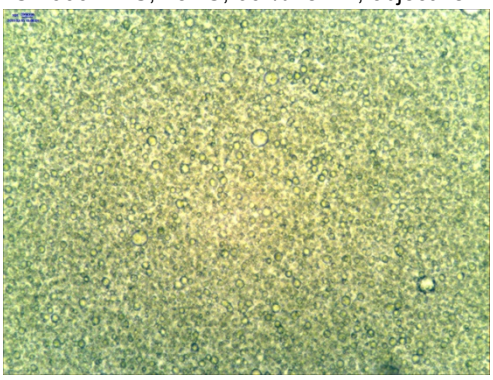

B: PCIL0002TTS, 40 °C, 75 % rel. h., objective: 10 x

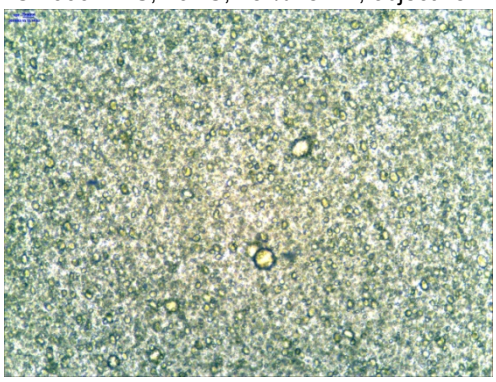

C: PCIL0003TTS, 25 °C, 60 % rel. h., objective: 10 x

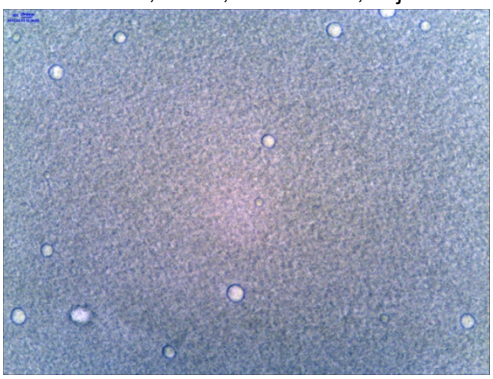

D: PCIL0003TTS, 40 °C, 75 % rel. h., objective: 10 x

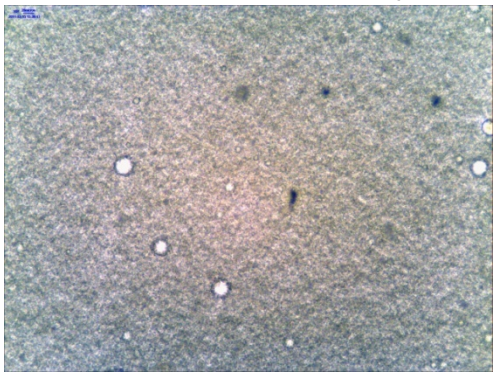

E: PCIL0004TTS, 25 °C, 60 % rel. h., objective: 10 x

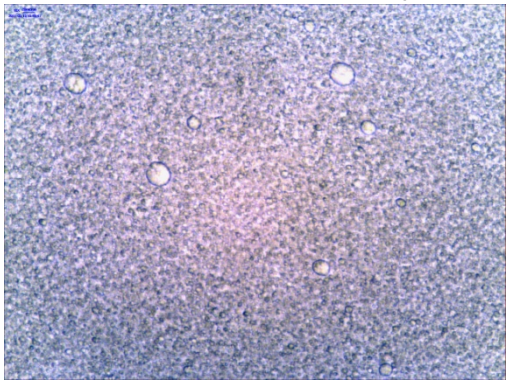

F: PCIL0004TTS, 40 °C, 75 % rel. h., objective: 10 x

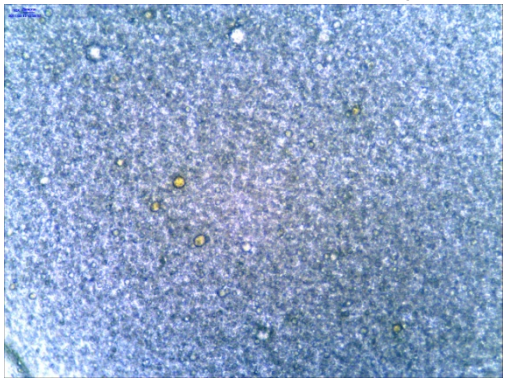

G: CIL0025TTS, 25 °C, 60 % rel. h., objective: 20 x

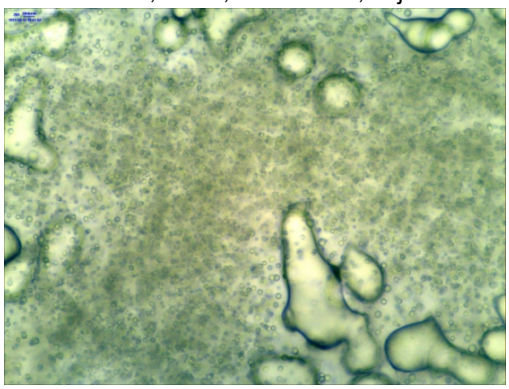

H: CIL0025TTS, 40 °C, 75 % rel. h., objective: 20 x

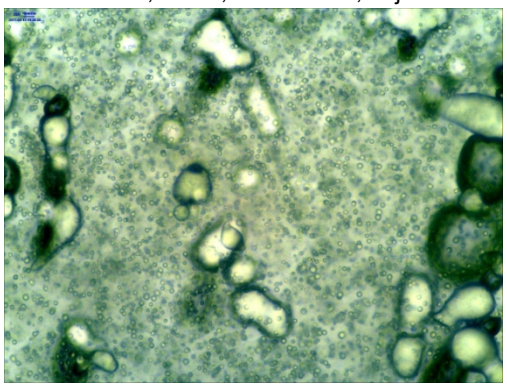

Figure 4.7 A-H. Microscopic images of cilazapril and cilazapril prodrug TTS batches stored for 26 months at given temperature and humidity conditions.

4.5 Summary

In consideration of synthesis, physicochemical properties as well as bioanalytical and pharmacological studies of a set of candesartan and cilazapril prodrugs, respectively, i.e. the three most promising candidates of each group, was selected for TTS development.
Regarding the candesartan prodrugs candesartan 1-(isopropyloxycarbonyloxy)ethyl ester (**3.31**), candesartan 1-(2,2-dimethylpropanoyloxy)ethyl ester (**3.32**) and candesartan morpholinoethyl ester (**3.35**), TTS batches based on silicone PSA with drug concentrations of 10 % were successfully manufactured. The formulate-ability of **3.31** and **3.32** was comparable or even superior to that of candesartan cilexetil. By contrast, the use of **3.35** resulted in inhomogeneous TTS matrices with scattered drug crystals, made visible by microscopy. The manufactured TTS exhibited comparable properties as the candesartan cilexetil containing TTS in terms of release (removal of the release liner), adhesive strength and cold flow. HPLC analysis of examples of TTS batches revealed promising stabilities of all prodrugs at low temperatures and under long-term stability conditions. Moreover, alterations of the matrix structure during storage were controlled by microscopic studies.
Among the selected cilazapril prodrugs, cilazapril 1-(ethoxycarbonyloxy)ethyl ester (**3.1**), cilazapril 1-(cyclohexyloxycarbonyloxy)ethyl ester (**3.2**) and cilazapril morpholinoethyl ester (**3.14**) turned out to be very promising in terms of formulate-ability. The semi-solid prodrugs proved to have favorable properties to successfully manufacture TTS based on silicone PSA with drug concentrations of 10 %, showing homogeneous matrices with finely dispersed emulsion droplets. At low temperature the stability of **3.1**, **3.2** and **3.14** in these TTS was very good, and, surprisingly, under accelerated storage conditions the double esters **3.1** and **3.2** were significantly more stable than cilazapril. Furthermore, microscopic studies of such TTS showed no tendency for crystallization over 26 months.

In summary, the prodrugs **3.31**, **3.32**, **3.35** and **3.1**, **3.2**, **3.14** were found to be comparable or even superior to the reference compounds candesartan cilexetil and cilazapril with respect to formulate-ability, TTS quality and stability in a silicone PSA matrix. Thus, the selected prodrugs are considered suitable for permeation experiments.

4.6 Experimental section

4.6.1 General experimental conditions

Commercially available chemicals and reagents were purchased from Acros Organics (Geel, Belgium), Merck KGaA (Darmstadt, Germany) or Sigma-Aldrich Chemie GmbH (München, Germany). All solvents used were of analytical grade or HPLC grade. Analytical HPLC analysis was performed on a system from Thermo Separation Products (Thermo Scientific) consisting of a SN400 controller, a P4000 pump, an AS3000 autosampler, a Spectra Focus UV-VIS detector and a RP-column (Luna C18-2, 150 x 4.6 mm, 3 µm; Phenomenex, Aschaffenburg, Germany) at a flow rate of 0.75 mL/min and a column temperature varying between 45 to 60 °C. Absorbance was detected at 210 nm. The mobile phase consisted of MeCN and 0.05 % trifluoroacetic acid (TFA) in Millipore water. All samples were filtered prior to injection using 0.2 µm Phenex-NY Syringe Filters (0.2 µm pore size, 4 mm diameter) (Phenomenex, Aschaffenburg, Germany). TTS manufacturing was performed at Hexal AG (Holzkirchen, Germany) in a separate laboratory area ("Technikum", part of the GMP area). Microscopic images were taken by means of a Leitz Laborlux S microscope (Leitz, Stuttgart, Germany) equipped with a SIS ColorView12 CCD camera (Soft Imaging System GmbH, Münster, Germany) or an Olympus BH-2 microscope (Olympus, Tokyo, Japan) equipped with a Digital Mikroskop DCM-500 Ocular microscope camera.

4.6.2 Production of transdermal therapeutic systems

4.6.2.1 General procedure for manufacturing transdermal therapeutic systems

Exact amounts of drug and ethyl acetate were weighed into a small glass vessel and mixed by stirring until, if possible, a clear stock solution was obtained. The required amount of silicone PSA (Bio PSA 4302, Dow Corning, Wiesbaden, Germany, solids content: 71.13 %, solvent: ethyl acetate) was added and the mixture was homogenized by stirring. The resulting coating mass was distributed on a release liner (PET-foil, fluorosiliconized, transparent, thickness: 75 µM Scotchpak 3M 1022, 3M Drug Delivery Systems, St. Paul, USA) by means of an motorized film applicator (Coatmaster 509/MC-I, Erichsen, Hemer, Germany) with adjusted gap width and coating speed followed by successively drying at ambient temperature and in a drying cabinet. Subsequently, the coating was laminated with PET backing foil (thickness: 15 µM, Hostaphan RN 15, Mitsubishi Polyester Film GmbH, Wiesbaden, Germany) and round patches with an area of 10 cm^2 or 2.5 cm^2 were cut out by means of a circle cutter. The TTS were separately packed in sachets, vacuum sealed and stored.

Manufacturing of candesartan prodrug containing TTS batches

PCAN0004TTS: The TTS batch was prepared according to the general procedure 4.6.2.1, using 0.4006 g of **3.31** and 3.57 g of ethyl acetate. To the resulting clear solution 5.1729 g of silicone PSA were added yielding a slightly turbid, homogeneous coating mixture, which was distributed with a gap width of 320 µm and a coating speed of 10 mm/s on the release liner. After drying for 5 min at ambient temperature and for 60 min at 60 °C the matrix was laminated and TTS were cut out and stored.

PCAN0005TTS: The TTS batch was prepared according to the general procedure 4.6.2.1, using 0.3999 g of **3.32** and 3.50 g of ethyl acetate. To the resulting clear solution 5.0935 g of silicone PSA were added yielding a slightly turbid, homogeneous coating mixture. The release liner was coated adjusting the gap width to 320 µm and the coating speed to 10 mm/s. After drying for 5 min at ambient temperature and for 60 min at 60 °C the matrix was laminated and TTS were cut out and stored.

PCAN0006TTS: The TTS batch was manufactured according to the general procedure 4.6.2.1, using 0.3998 g of **3.35** and 3.51 g of ethyl acetate. Despite extensive stirring and slight heating **3.35** remained undissolved. To the suspension 5.4072 g of silicone PSA were added yielding a clear mass with homogeneously distributed drug particles. The release liner was coated adjusting the gap width to 320 µm and the coating speed to 10 mm/s. After drying for 5 min at ambient temperature and for 60 min at 60 °C the matrix was laminated and TTS were cut out and stored.

PCAN0009TTS: According to the general procedure 4.6.2.1, 0.30 g of **3.31** were suspended in 2.23 g of ethyl acetate. To the suspension 4.39 g of silicone PSA were added and the coating mixture was distributed on the release liner using a gap width of 180 µm and a coating speed of 10 mm/s. After drying for 5 min at ambient temperature and for 60 min at 60 °C the matrix was laminated and TTS were cut out and stored.

PCAN0010TTS: The TTS batch was prepared according to the general procedure 4.6.2.1, using 0.297 g of **3.32** and 2.15 g of ethyl acetate. To the resulting clear solution 4.51 g of silicone PSA were added. The release liner was coated adjusting the gap width to 180 µm and the coating speed to 10 mm/s. After drying for 5 min at ambient temperature and for 60 min at 60 °C the matrix was laminated and TTS were cut out and stored.

PCAN0011TTS: The TTS batch was manufactured according to the general procedure 4.6.2.1, using 0.301 g of **3.35** as a suspension in 2.14 g of ethyl acetate. To the resulting suspension 4.41 g of silicone PSA were added. The release liner was coated adjusting the gap width to 180 µm and the coating speed to 10 mm/s. After drying for 5 min at ambient temperature and for 60 min at 60 °C the matrix was laminated and TTS were cut out and stored.

CAN0043TTS: The TTS batch was prepared according to the general procedure 4.6.2.1, using 0.4021 g of candesartan cilexetil and 3.50 g of ethyl acetate. To the resulting clear solution 5.3367 g of silicone PSA were added yielding a slightly turbid, homogeneous

coating mixture, which was distributed with a gap width of 320 µm and a coating speed of 10 mm/s on the release liner. After drying for 5 min at ambient temperature and for 60 min at 60 °C the matrix was laminated and TTS were cut out and stored.

CAN0044TTS: According to the general procedure 4.6.2.1, 0.303 g of candesartan cilexetil were suspended in 2.11 g of ethyl acetate. 4.51 g of silicone PSA were added and the coating mixture was distributed on the release liner using a gap width of 180 µm and a coating speed of 10 mm/s. After drying for 5 min at ambient temperature and for 60 min at 60 °C the matrix was laminated and TTS were cut out and stored.

Manufacture of cilazapril or cilazapril prodrug containing TTS batches

PCIL0002TTS: The TTS batch was prepared according to the general procedure 4.6.2.1 using 0.329 g of **3.1** and 2.06 g of ethyl acetate. To the resulting clear solution 4.11 g of silicone PSA were added yielding a clear coating mixture. The release liner was coated adjusting the gap width to 235 µm and the coating speed to 10 mm/s. After drying for 5 min at ambient temperature and for 90 min at 60 °C the matrix was laminated and TTS were cut out and stored.

PCIL0003TTS: The TTS batch was manufactured according to the general procedure 4.6.2.1 using 0.347 g of **3.2** and 2.18 g of ethyl acetate. To the resulting clear stock solution 4.07 g of silicone PSA were added yielding a clear coating mixture, which was distributed on the release liner with a gap width of 235 µm and a coating speed of 10 mm/s. After drying for 5 min at ambient temperature and for 90 min at 60 °C the matrix was laminated and TTS were cut out and stored.

PCIL0004TTS: The TTS batch was manufactured according to the general procedure 4.6.2.1 using 0.338 g of **3.14** and 2.20 g of ethyl acetate. To the resulting clear solution 4.38 g of silicone PSA were added yielding a clear coating mixture. The release liner was coated adjusting the gap width to 235 µm and the coating speed to 10 mm/s. After drying for 5 min at ambient temperature and for 90 min at 60 °C the matrix was laminated and TTS were cut out and stored.

PCIL0011TTS: The TTS batch was manufactured according to the general procedure 4.6.2.1 using 0.281 g of **3.1** and 2.01 g of ethyl acetate. To the resulting clear solution 4.29 g of silicone PSA were added yielding a clear coating mixture. The release liner was coated adjusting the gap width to 185 µm and the coating speed to 10 mm/s. After drying for 5 min at ambient temperature and for 60 min at 60 °C the matrix was laminated and TTS were cut out and stored.

PCIL0012TTS: The TTS batch was manufactured according to the general procedure 4.6.2.1 using 0.293 g of **3.2** and 2.00 g of ethyl acetate. After addition of 4.15 g of silicone PSA and homogenizing the clear coating mass was distributed on the release liner adjusting the gap width to 185 µm and the coating speed to 10 mm/s. After drying for 5 min at ambient temperature and for 60 min at 60 °C the matrix was laminated and TTS were cut out and stored.

PCIL0013TTS: The TTS batch was manufactured according to the general procedure 4.6.2.1 using 0.293 g of **3.14** and 1.99 g of ethyl acetate. After addition of 4.20 g of silicone PSA and homogenizing the clear coating mass was distributed on the release liner adjusting the gap width to 185 µm and the coating speed to 10 mm/s. After drying for 5 min at ambient temperature and for 60 min at 60 °C the matrix was laminated and TTS were cut out and stored.

CIL0025TTS: The TTS batch was manufactured according to the general procedure 4.6.2.1 using 0.529 g of cilazapril and 3.52 g of ethyl acetate. Because only little amounts of cilazapril could be dissolved after 2 h of stirring additional 0.97 g of ethyl acetate were added. As most of the compound remained undissolved 6.84 g of silicone PSA were added and 0.60 g of ethyl acetate were removed under a stream of nitrogen. The resulting crystals-containing, homogeneous coating mixture was distributed on the release liner using a gap width of 310 µm and the coating speed to 10 mm/s. After drying for 5 min at ambient temperature and for 120 min at 60 °C the matrix was laminated and TTS were cut out and stored.

CIL0027TTS: The TTS batch was manufactured according to the general procedure 4.6.2.1 using 0.354 g of cilazapril suspended in 2.69 g of ethyl acetate. To the suspension 5.11 g of silicone PSA were added and the coating mixture was distributed on the release liner using a gap width of 190 µm and a coating speed of 10 mm/s. After drying for 5 min at ambient temperature and for 60 min at 60 °C the matrix was laminated and TTS were cut out and stored.

4.6.3 Determination of TTS stability

The stability of the candesartan prodrugs **3.31**, **3.32**, **3.35** and candesartan cilexetil in a silicone adhesive layer after various storage periods under different storage conditions was studied in our laboratory. The analytical investigation of cilazapril and cilazapril prodrug (**3.1**, **3.2**, **3.14**) containing TTS was performed at Hexal AG (Holzkirchen, Germany).

4.6.3.1 Procedure for the determination of the stability of candesartan prodrug containing TTS by HPLC

For determination of stability two TTS each (2 x 10 cm^2 or 2 x 2.5 cm^2) of the candesartan prodrug containing TTS batches PCAN0004TTS, PCAN0005TTS, PCAN0006TTS and CAN0043TTS were analyzed promptly after manufacturing as well as after storage for two and eight months, respectively, at 5 °C/ 65 % rel. h., 25 °C/ 60 % rel. h. and 40 °C/ 75 % rel. h. The release liner was removed and each patch was put into a small glass vessel. After addition of THF (10 cm^2: 10.0 ml, 2.5 cm^2: 5.0 ml) the adhesive matrix was dissolved by sonication (15 min) and mixing on a shaker (30 min). The samples were diluted with mobile phase (10 cm^2: 1:10, 2.5 cm^2: 1:5) and filtrated. For HPLC analysis 25 µl of each sample were injected using the following gradient: 0 min: MeCN/0.05% TFA/aq 30/70, 20 min: 85/15, 21-26 min: 95/5, 27-35 min: 30/70.

4.7 References

1. Wokovich, A. M.; Prodduturi, S.; Doub, W. H.; Hussain, A. S.; Buhse, L. F. Transdermal drug delivery system (TDDS) adhesion as a critical safety, efficacy and quality attribute. *Eur. J. Pharm. Biopharm.* **2006,** 64, 1-8.
2. Tan, H. S.; Pfister, W. R. Pressure-sensitive adhesives for transdermal drug delivery systems. *Pharm. Sci. Technol. Today* **1999,** 2, 60-69.
3. Prausnitz, M. R.; Langer, R. Transdermal drug delivery. *Nat. Biotechnol.* **2008,** 26, 1261-8.
4. Wokovich, A. M.; Shen, M.; Doub, W. H.; Machado, S. G.; Buhse, L. F. Release liner removal method for transdermal drug delivery systems (TDDS). *J. Pharm. Sci.* **2010,** 99, 3177-87.
5. Farahmand, S.; Maibach, H. I. Transdermal drug pharmacokinetics in man: Interindividual variability and partial prediction. *Int. J. Pharm.* **2009,** 367, 1-15.
6. Colas, A.; Aguadisch, L. Silicones in Pharmaceutical Applications. *Chimie Nouvelle* **1997,** 58, 1779.
7. Meyer, W.; Neurand, K. The distribution of enzymes in the skin of the domestic pig. *Lab. Anim.* **1976,** 10, 237-47.

Chapter 5
Permeation of Prodrugs of Candesartan and Cilazapril Through Animal and Human Skin

5.1 Introduction

In order to exert a therapeutic effect, a dermally administered antihypertensive drug must overcome the various layers of the skin and reach the systemic circulation. This absorption process can be divided into three steps:

- penetration, which is the entry of a substance into a particular layer or structure such as the entrance of a compound into the stratum corneum;
- permeation, which is the penetration through one layer into another, where both layers are functionally and structurally different from each other;
- resorption, which is the uptake of a substance into the vascular system, which acts as the central compartment.[1]

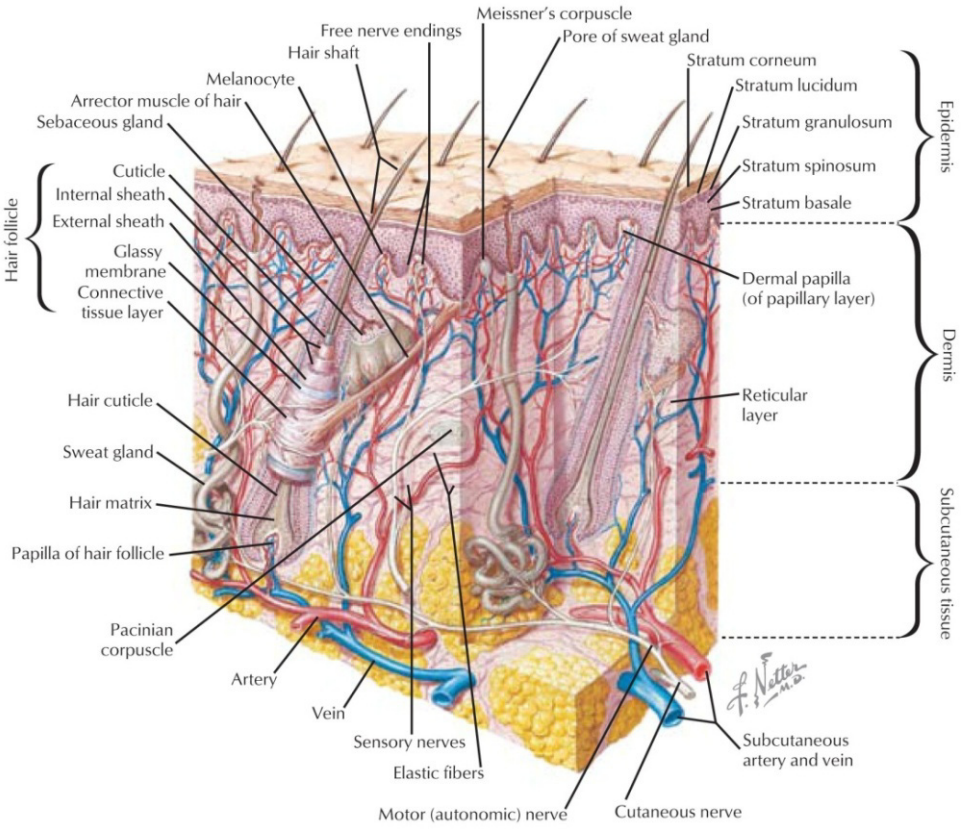

Figure 5.1. Schematic of skin and its appendages that shows the epidermis, dermis, and subcutaneous tissue. Netter illustration from www.netterimages.com. © Elsevier Inc. All rights reserved.

As interface between the body and the environment one of the most important functions of the skin is its ability to act as a protective barrier against noxious physical, chemical and mechanical harm and the loss of excessive endogenous material such as water. Basically, the skin can be divided into three layers: epidermis, dermis and hypodermis (cf. Figure 5.1). Whereas the hypodermis mainly comprises fatty tissue, the dermis is composed of collagen, elastin, salts, water, and a gel of glycosaminoglycans. The dermis is highly vascularized and also includes skin appendages as eccrine and apocrine sweat glands, sebaceous glands and hair follicles.[2-3] The upper part of the dermis, which is referred to as papillary dermis, is characterized by ridges and folds of papillae and a more widely dispersed arrangement of elastin and collagen fibers. In the reticular dermis, the subjacent thicker counterpart of the papillary dermis, the collagen fibers are arranged in an interwoven, crisscross pattern in a plane parallel with the skin.[3]

The uppermost part of the skin, the epidermis, can be divided into 4 to 5 distinct layers, which are (from deep to superficial) the stratum basale, stratum spinosum, stratum granulosum, stratum lucidum (only apparent at palms and soles of the feet) and the stratum corneum (Figure 5.2). The stratum basale is composed of a single layer of epidermal stem cells having the ability to undergo mitosis and thus, regenerating the epidermal tissue. Cells deriving from dividing cells of the stratum basale, the keratinocytes, migrate superficially into the stratum spinosum, where they begin to differentiate. They flatten and elongate, while a formation of lipid-enriched lamellar bodies and an increase in intracellular keratin filaments is noticeable. The stratum granulosum consists of 2-5 layers of cells containing keratohyalin granules. While these granules are released by exocytosis, the keratinocytes face cell death, turn into corneocytes and move to the surface, where they get sloughed by abrasion. The uppermost layer, the stratum corneum, consists of 18-21 layers of corneocytes.[2] Its architecture is probably best described by the 'brick and mortar' model by Elias suggesting that the keratin-enriched corneocytes resemble the bricks and are embedded in the mortar consisting of extracellular hydrophobic lipids.[5] According to an improved

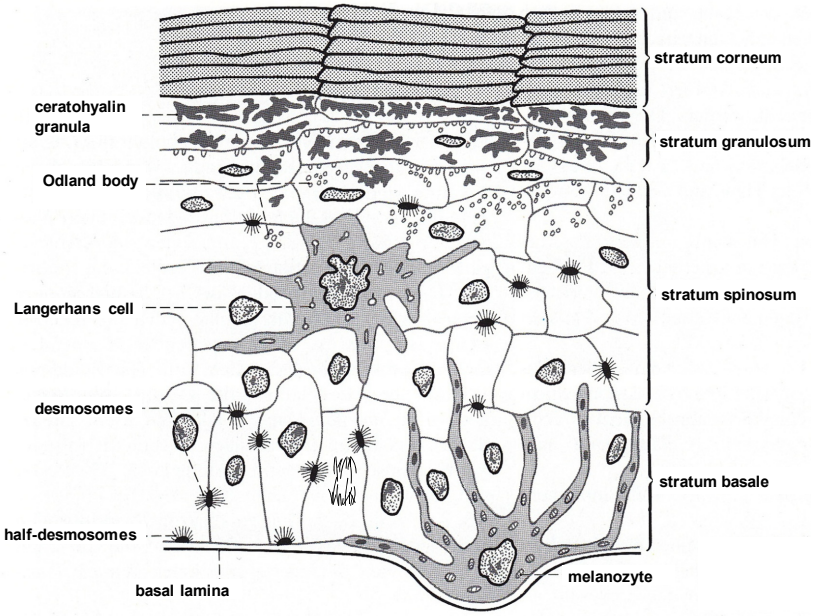

Figure 5.2. Schematic representation of the epidermis. Modified from Benninghoff.[4]

model proposed by Barry, the intercellular "mortar" is considered as stacks of intercellular lipid bilayers with an aqueous phase in between (cf. section 3.4).[6]

The average overall thickness of human skin is between 2-3 mm.[3] However, depending on the body part, the thickness varies considerably. The average diameter of the epidermis is indicated as 100-150 µm, of which 20-40 µm are attributed to the stratum corneum.[2]

To reach the viable cells, three different diffusion pathways for a permeant through the stratum corneum are discussed: a tortuous intercellular pathway through the extracellular lipids, a transcellular pathway through the corneocytes and the extracellular lipids and an appendageal pathway along sweat ducts or hair follicles. As the appendages cover only 0.1 % of the surface area of the skin, this route contributes negligibly to permeation, but may be important for ions and large polar molecules.[6] Due to the relative impermeability of the corneocytes, the major pathway for permeation through the stratum corneum is assumed to be the intercellular route (cf. section 3.4).[7]

As drug transport across the stratum corneum is a passive diffusion process, it can be described by Fick's Law[8] (Equation 5.1), stating that the flux of a compound (J) per unit path length (δx) is proportional to the concentration gradient (δc) and the diffusion coefficient or diffusivity (D).

$$J = -D \cdot \frac{\delta c}{\delta x}$$

Equation 5.1. Fick's Law. J = flux [mol·cm^{-2}·s^{-1}], D = diffusivity [cm^2·s^{-1}], δc = concentration gradient [mol·cm^{-3}], δx = path length [cm].

The steady-state flux J_{ss} results from the integrated form of Equation 5.1 according to Equation 5.2.

$$J_{ss} = \frac{K_m \cdot D \cdot \Delta c}{x} = K_p \cdot \Delta c$$

Equation 5.2. J_{ss} = steady-state flux [mol·cm^{-2}·s^{-1}], K_m = partition or distribution coefficient between the stratum corneum and the vehicle, D = diffusivity [cm^2·s^{-1}], Δc = concentration difference [mol·cm^{-3}], x = path length [cm], K_p = permeability constant [cm·s^{-1}].

Typically, the steady-state flux J_{ss} is assessed from an *in vitro* permeation experiment, in which the donor concentration of the permeant is kept (more or less) constant (infinite dose conditions), while the receiver phase provides sink conditions and is calculated from the slope of the linear portion of the graph of the cumulative amount permeated *vs*. time. Back-extrapolation of the latter plot to the x-axis yields the so-called lag time t_{lag}, which designates the time needed for the permeated compound to reach steady-state.

For the development of a novel transdermal therapeutic system the assessment of reliable skin absorption data is indispensable. Usually, percutaneous absorption is studied *in vivo* by means of various animal models or by different *in vitro* methods. In 2004 a guideline for *in vitro* skin absorption methods was designed by the OECD (Organisation for Economic Co-operation and Development) describing procedures and methods with the objective of ensuring the reliability of obtained skin absorption results.[9]

The principle of the described method comprises the application of a test substance to the surface of a skin sample, separating the donor and receptor reservoir of a diffusion cell. At appropriate periods of time the receptor fluid is sampled and analyzed for the test compound and/or metabolites. Two different designs of diffusion cells are used – the static cell (usually a Franz cell[10]) and the flow-through design[11]. Conventionally, the test substance is applied to the skin on the donor side as a reservoir solution or as a suitable formulation (e.g. a TTS). For transdermal *in vitro* absorption studies the most relevant barrier is of course human skin. However, since its availability is limited, a multitude of animal substitutes, ranging from snake, mouse, rat, guinea pig over pig to primates is used. Especially, porcine ear skin, which is readily obtainable from abattoirs and which has similar biochemical properties as human skin, is accepted to be particularly well-suited for permeation studies and to give results comparable to human skin.[12] Furthermore, the use of artificial skin such as Testskin™, Epiderm™ or Skinethic™ has been described.[13-15] However, due to rather constricted barrier function of these model systems, the use of artificial membranes is not recommended for *in vitro* permeation studies.[16] The OECD suggests the use of epidermal membranes (separated by heat, chemically or enzymatically), full-thickness skin or split-thickness skin (typically 200-400 µm) prepared with a dermatome.[9] Regarding the comparability of permeation results, particularly the anatomical site should be taken into consideration due to varying thickness of the epidermis depending on the body part. The age of the skin donors is known to affect skin permeation.[17] Furthermore, gender-related differences in skin physiology were reported. [18] By contrast, no statistical difference in percutaneous absorption was found between different human ethnicities (Caucasian, Asian, black).[19]

5.2 Selection of experimental design and conditions for in vitro permeation studies

As a suitable test system for permeation studies with candesartan and cilazapril prodrugs a static Franz diffusion cell system was chosen (cf. Figure 5.3). With this system, both, the permeation of substances from a reservoir solution, filled into the donor chamber, and from transdermal therapeutic systems directly stuck on top of the membrane, clamped between donor and receptor chamber, can be investigated. Each Franz cell has a donor chamber volume of 12.5 ml and a permeation area of 1.77 cm^2.

Figure 5.3. Assembly of a vertically arranged Franz diffusion cell. 1: donor chamber, 2: plug for donor chamber, 3: clamp for fixing donor and receptor chamber, 4: membrane contact surface, 5: sampling port, 6: receptor chamber, 7: water jacket, 8: connection to a thermostat.

The use of a Franz cell stirrer (Figure 5.4) allows parallel measurement of nine permeation samples. Each diffusion chamber is connected to a thermostat ensuring a constant receptor fluid and membrane temperature of 32 °C in accordance with the physiological skin temperature.

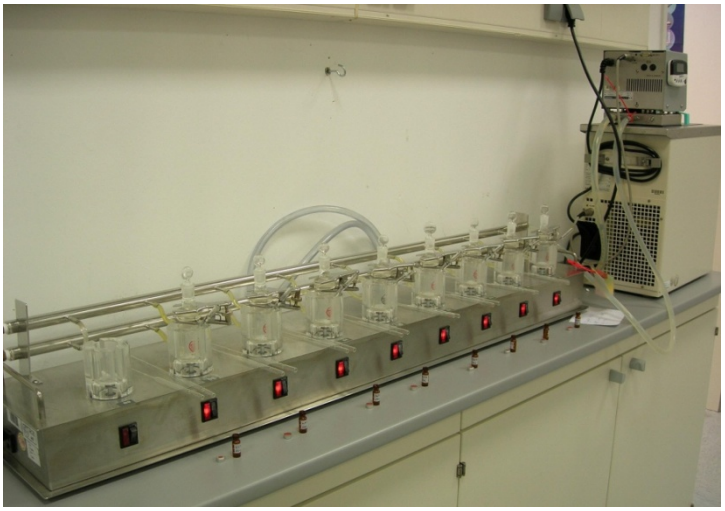

Figure 5.4. Nine-station Franz cell stirrer connected to a thermostat.

A prerequisite for the correct determination of dermal permeation is an adequate solubility of the permeant and its metabolites in the receptor fluid. In case of poor solubility, the receptor fluid acts as a barrier to permeation by inhibiting steady-state fluxes, when the permeant reaches its saturation concentration. Thus, it is necessary to make sure that the sink conditions are fulfilled. Normally, this is guaranteed in a volume of receptor fluid amounting to at least the 3-10-fold of the saturation volume.[20]

In addition, the receptor fluid should not affect skin integrity and the enzymatic activity in the skin should be maintained. Thus, the use of buffered aqueous solutions seems obvious. If maintenance of the viability of the skin is needed, solutions of "physiological" buffers are commonly used. In case of low aqueous solubility, compounds enhancing solubility should be added in order to provide sink conditions. As these additives should not affect skin integrity, high amounts of organic solvents like ethanol are unsuited. However, as an alternative, the usage of aqueous solutions containing cyclodextrins as solubility enhancers appeared to be favorable. Cyclodextrins consist of cyclic (α-1,4-)-linked α-D-glycopyranose units with a hydrophilic outer surface forming a central cavity, the lipophilicity of which is comparable to an aqueous ethanolic solution.[21] Substituted cyclodextrins such as 2-hydroxypropyl-β-cyclodextrin (HP-β-CD) are highly soluble in water and are able to form non-covalent inclusion complexes with rather lipophilic moieties of molecules, leading to an increase in the aqueous solubility of the guest molecules.[22]

Since the skin is capable of metabolic reactions like ester hydrolysis, not only the solubility of the candesartan and cilazapril prodrugs, but also that of the reaction products (candesartan and cilazapril/cilazaprilat) should be taken into account. In view of an appropriate receptor fluid for permeation studies, the equilibrium solubility (i.e. the concentration of a compound in saturated solution when excess of solid is present and solution and solid are at equilibrium)[23] of all relevant species was determined by means of HPLC.

As an appropriate receptor fluid for the rather lipophilic candesartan prodrugs an aqueous solution containing 10 % (w/v) HP-β-CD was considered. From Table 5.1 it is obvious that the equilibrium solubility of the prodrugs candesartan cilexetil, **3.31**, **3.32** and **3.35** was satisfactory with values between 0.16 mg/ml and 0.76 mg/ml. Although a rather low (0.02 mg/ml) equilibrium solubility of candesartan was determined, overall, 10 % HP-β-CD solution was regarded a promising receptor fluid.

Table 5.1. Equilibrium solubility of candesartan and candesartan prodrugs in 10 % HP-β-CD.

equilibrium solubility [mg/ml]				
candesartan	**CAN-CIL**	**3.31**	**3.32**	**3.35**
0.02	0.23	0.16	0.22	0.76

The experimentally determined log P_{oct/H_2O} values of all cilazapril prodrugs indicate a lower lipophilicity with respect to their candesartan analogues (cf. section 3.4). Hence, sufficient solubility in buffer solution devoid of solubility enhancers was assumed.

Table 5.2 shows the equilibrium solubility values of cilazapril and of the cilazapril prodrugs **3.1**, **3.2** and **3.14** in 50 mM phosphate buffer, pH 7.4. Whereas the equilibrium solubility of **3.14**, due to its protonatable morpholine, was convincing, only moderate to low values for **3.1** and **3.2** were determined. Nevertheless, taking into account that equilibrium solubility is known to be strongly influenced by parameters such as temperature or sedimentation time, 50 mM phosphate buffer, pH 7.4 was considered an acceptable receptor fluid particularly due to its low costs and compatibility with HPLC analysis. Furthermore, a fast enzymatic degradation of the cilazapril prodrugs in the skin, leading to the formation of the highly hydrophilic and therefore well water-soluble species cilazapril and cilazaprilat, was expected. The equilibrium solubility of cilazapril amounted to 15.43 mg/ml and the value for cilazaprilat was assumed to be even higher.

Table 5.2. Equilibrium solubility of cilazapril and cilazapril prodrugs in 50 mM phosphate buffer, pH 7.4.

equilibrium solubility [mg/ml]			
cilazapril	**3.1**	**3.2**	**3.14**
15.43	0.06	0.00	2.75

In order to determine steady-state fluxes, all permeation experiments were performed under conditions enabling the donor concentration of the permeant to be maintained more or less constant (infinite dose conditions). In an OECD guideline for the testing of chemicals *via* an *in vitro* skin absorption method[9] a duration of 24 h is recommended for adequate characterization of the absorption profile. Longer sampling periods lead to increasing deterioration of skin integrity, but are required for slowly permeating substances with high lag times.[9] In the present work, the permeation experiments were stopped after a period of at most 72 h independent of the permeated amount of drug.

5.2.1 Choice of skin

Due to the aforementioned similarities between porcine and human skin and its ready availability, dermatomized (500-800 µm) or full-thickness skin from pig ears was used for the majority of permeation experiments. Since excised human skin gives results more similar to the human *in vivo* situation, full- or split-thickness human skin was also used in exemplary permeation studies. In addition, permeability of selected compounds was investigated on nude mouse skin.

5.3 Permeation studies with candesartan prodrugs

The permeability of the novel candesartan prodrugs **3.31**, **3.32** and **3.35** as well as the standard reference candesartan cilexetil through porcine and human skin was investigated. Permeation studies of compounds with unknown permeability profile are usually performed with compound solutions under infinite dose conditions before applying the relevant formulation, in this case a transdermal therapeutic system. Thus, the permeability of the candesartan prodrugs through porcine ear skin was at first investigated using reservoir solutions, i.e. concentrated stock solutions of the respective prodrug, to avoid potential limitations of permeability by the dosage form. Subsequently, permeation experiments with prodrug containing TTS were performed.
For oral application, the recommended starting dose and maintenance dose of candesartan cilexetil amount to 8-16 mg.[24] The oral bioavailability has been cited as approximately 15 %.[25] Thus, a resorbed amount of 1.2-2.4 mg daily would be necessary to achieve a therapeutic effect by transdermal application.

5.3.1 Procedure

Permeation from reservoir solution. Into the donor chambers of thermostated Franz cells, equipped with dermatomized porcine ear skin (provided by Hexal AG) and a stirred 10 % HP-β-cyclodextrin solution serving as receptor fluid, solutions of the respective prodrugs in ethanol/propylene glycol 70/30 (v/v) were filled, at concentrations amounting to 90 % of the saturation concentration of the respective prodrug. At appropriate time periods, samples of 0.5 ml were withdrawn from the receptor chamber and directly analyzed by HPLC. The volume was replaced by fresh receptor fluid.
Permeation from TTS. Permeation through dermatomized porcine ear skin (provided by Hexal AG) and full-thickness porcine and human skin from TTS was measured in Franz cells, equipped with a stirred 10 % HP-β-cyclodextrin solution serving as receptor fluid. A 10-cm^2 or 2.5-cm^2 TTS was directly stuck on the epidermal side of a piece of thawed porcine ear or human skin, before a circle with a diameter of 27 mm was punched out, by which the area of the 10-cm^2 TTs was reduced to 5.7 cm^2. Skin and TTS were clamped between donor and receptor chamber. Essentially, the rest of the procedure was analogous to that described for the permeation from reservoir solution (see above).

The cumulative permeated amount (sum of intact prodrug and metabolites) was plotted against time. The steady-state flux (J_{ss}) was obtained from the slope of the linear regression line of this plot. The x-axis intercept of this regression line provided the corresponding lag time (t_{lag}), which is the time needed for the permeated compound to reach the steady-state.

5.3.2 Permeation of candesartan prodrugs through dermatomized porcine skin from reservoir solution

Permeation experiments using compound reservoir solutions were performed according to the procedure described in 5.3.1.

Shortly after applying the prodrug reservoir solutions (11 mg/ml in ethanol/propylene glycol 70/30 (v/v)) on the dermatomized porcine ear skin surfaces, streaks of donor solvent in the receptor chambers and an increasing turbidity of the receptor fluids could were observed. The permeation experiment was aborted after 6 h due to obvious leakage of the membranes.

Figure 5.5 depicts the cumulative permeated amount of each candesartan prodrug against time. The permeated amounts were found to increase very fast to approach saturation concentrations. Thus, sink conditions were not fulfilled, and steady-state fluxes could not be determined.Due to these unsatisfactory results, the approach studying permeation from prodrug reservoir solutions was not pursued any longer.

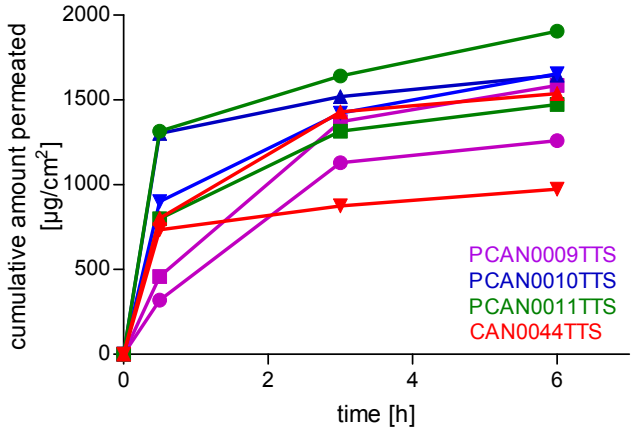

Figure 5.5. Skin permeation profile of candesartan prodrugs across dermatomized porcine skin from reservoir solutions. Depicted are individual values from two independent experiments.

5.3.3 Permeation of candesartan prodrugs through dermatomized porcine skin from TTS

The permeation of candesartan prodrugs from TTS across dermatomized porcine ear skin was studied following the procedure described in 5.3.1.

In Figure 5.6 and Figure 5.7 results from permeation experiments carried out with two differently sized patches (5.7-cm^2 and 2.5-cm^2 TTS) of the candesartan prodrug TTS batches PCAN0009TTS, PCAN0010TTS, PCAN0011TTS and CAN0043TTS are shown. Regarding the cumulative amount permeated, which was calculated as the sum of the respective prodrug and the parent drug candesartan, striking differences became obvious. Whereas the batches PCAN0009TTS and PCAN0011TTS containing the candesartan prodrugs candesartan 1-(isopropyloxycarbonyloxy)ethyl ester (**3.31**) and candesartan morpholinoethyl ester (**3.35**) show only moderate skin permeation (~ 40-73 µg/cm^2), the values for the TTS batch PCAN0010TTS (**3.32**) containing candesartan 1-(2,2-dimethylpropanoyloxy)ethyl ester were found to be approx.

5 to 14-fold higher (388-559 µg/cm^2). The reference compound, candesartan cilexetil (CAN0044TTS), showed rather low skin permeation (1-2 µg/cm^2).

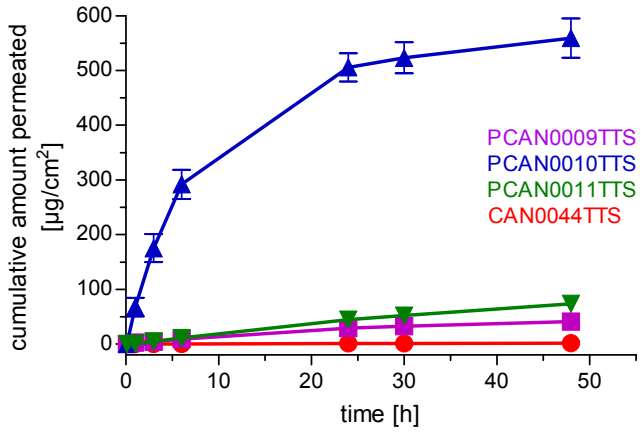

Figure 5.6. Skin permeation profile of candesartan prodrugs across dermatomized porcine skin from 5.7-cm^2 TTS. The data represent the sum of candesartan prodrug and candesartan and is depicted as mean ± SEM values (n=4).

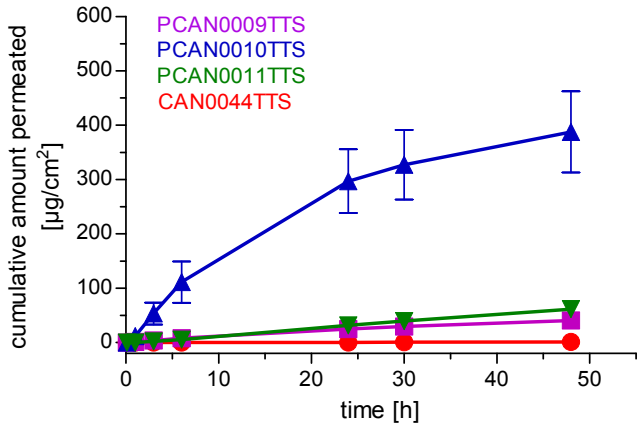

Figure 5.7. Skin permeation profile of candesartan prodrugs across dermatomized porcine skin from 2.5-cm^2 TTS. The data represent the sum of candesartan prodrug and candesartan and is depicted as mean ± SEM values (n=4).

As sink conditions for **3.32** were not fulfilled, steady-state fluxes were only calculated for **3.31**, **3.35** and candesartan cilexetil (cf. Figure 5.8 A+B).

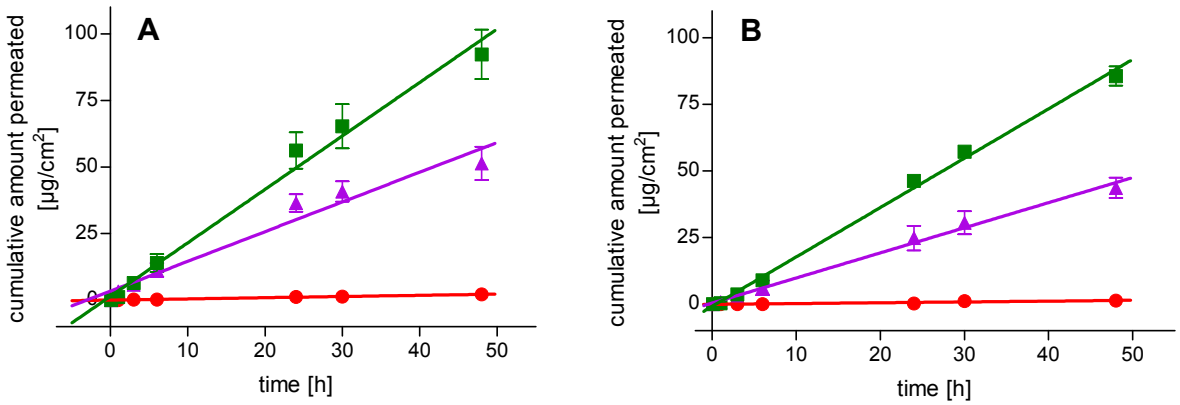

Figure 5.8. Permeation profiles (mean ± SEM, n = 3-6) for candesartan prodrugs **3.35** (■), **3.31** (▲) and candesartan cilexetil (●) through dermatomized porcine ear skin from 5.7-cm^2 (**A**) and 2.5-cm^2 (**B**) TTS.

The novel candesartan prodrugs **3.31** and **3.35** showed a 30 to 60-fold higher flux through porcine ear skin than candesartan cilexetil (Table 5.3). Although the permeation

area for each experiment was the same (1.77 cm^2), the use of 2.5-cm^2 patches led to a slight decrease in flux compared to 5.7-cm^2 TTS, suggesting that diffusion processes from parts of the TTS outside of the permeation area play a role by increasing the concentration gradient and thus, directly leading to higher fluxes. Intersection of the linear regression line with the x-axis gave the corresponding lag times (Table 5.3), indicating almost instantaneous permeation of all prodrugs.

Table 5.3. Steady-state fluxes and lag times (mean ± SEM, n = 3-6) of candesartan prodrugs from 5.7-cm^2 and 2.5-cm^2 TTS through dermatomized porcine ear skin.

compound	TTS batch	J_{ss} [µg·cm^{-2}·h^{-1}]		t_{lag} [h]	
		5.7-cm^2	2.5-cm^2	5.7-cm^2	2.5-cm^2
3.31	PCAN0009TTS	1.12 ± 0.14	1.08 ± 0.13	-3.94 ± 1.88	-1.39 ± 1.26
3.35	PCAN0011TTS	2.01 ± 0.18	1.86 ± 0.05	-0.73 ± 0.61	1.01 ± 0.51
CAN-CIL	CAN0044TTS	0.04 ± 0.01	0.03 ± 0.01	-0.05 ± 1.63	3.51 ± 0.58

In case of compound **3.35,** mostly intact prodrug was found in the receptor fluid, whereas for the double esters **3.31**, **3.32** and candesartan cilexetil prodrug as well as increasing amounts of candesartan were determined. Surprisingly, all novel candesartan prodrugs permeated porcine ear skin very quickly.

The enormous difference in skin permeation of **3.32** compared to **3.31**, **3.35** and candesartan cilexetil, could presumably be explained by the different state of the prodrugs in the TTS matrix. In case of PCAN0010TTS, the prodrug **3.32** is present in dissolved form in individual emulsion droplets, whereas **3.31**, **3.35** and candesartan cilexetil prevail as suspended crystals and agglomerates. Therefore, skin permeation seems to be favored, when dissolved drug is available in the TTS matrix.

These findings were corroborated by results from permeation experiments with the TTS batches PCAN0004TTS, PCAN0005TTS, PCAN0006TTS and CAN0043TTS performed by Hexal AG (Figure 5.9), using automated sampling (AutoPlus MultiFill, Hanson Research, Chatsworth, USA).

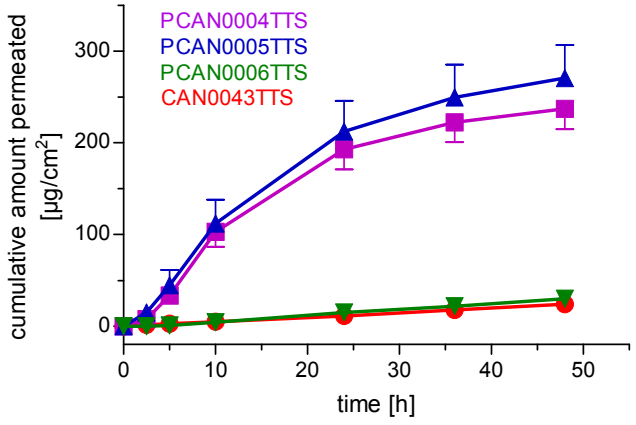

Figure 5.9. Skin permeation profile of candesartan prodrugs across dermatomized porcine skin from TTS. The data represent the sum of candesartan prodrug and candesartan and is given mean values ± SEM (n=6).

Again, reliable steady-state fluxes could only be determined for **3.35** (PCAN0006TTS) and candesartan cilexetil (CAN0043TTS), due to the lack of sink conditions for **3.31** (PCAN0004TTS) and **3.32** (PCAN0005TTS). In accordance with aforementioned results, the diffusion from TTS, in which the drug prevails as suspension in the PSA matrix (PCAN0006TTS, CAN0043TTS) rather than as a solution (PCAN0004TTS, PCAN0005TTS), appears to be hindered. The steady-state fluxes (Table 5.4) were determined to be between those obtained for the TTS batches PCAN0009TTS, PCAN0011TTS and CAN0044TTS. The lag times were rather short.

Table 5.4. Steady-state fluxes and lag times (mean ± SEM, n = 6) of candesartan prodrugs from TTS through dermatomized porcine ear skin.

compound	TTS batch	J_{ss} [µg·cm^{-2}·h^{-1}]	t_{lag} [h]
3.35	PCAN0006TTS	0.65 ± 0.11	0.57 ± 0.75
CAN-CIL	CAN0043TTS	0.50 ± 0.08	2.55 ± 0.54

Overall, the unsatisfactory results from the permeation experiments using reservoir solutions, the extraordinarily high skin permeation of some candesartan prodrug containing TTS lots as well as the short lag times prompted us to examine the used porcine ear skin in detail.

5.3.4 Histological studies on porcine ear skin

In order to gain deeper insight in the status of the porcine skin used, histological studies were performed. Thin slices of tissue, embedded in paraffin, were prepared and studied by light microscopy. In brief, small pieces of the tissue were fixated, dehydrated, embedded in paraffin and cut into 6 µm thin slices by means of a microtome. Then, the sections were stained according to a Masson-Goldner trichrome protocol, modified by Jerusalem. As a result nuclei appear dark brown to black, collagen green and cytoplasm, muscle, fibrin and keratin red.

When comparing images of thawed dermatomized porcine ear skin, which was stored at -20 °C, used for the past permeation experiments (Figure 5.10 A, C, E) and a reference section from fresh porcine skin (Figure 5.10 B, D, F), it became obvious that surprisingly, the whole epidermis of the experimentally used specimens was missing. Furthermore, dermis volume was apparently increased and the collagen matrix appeared swollen, allegedly a result of the process of freezing and thawing.

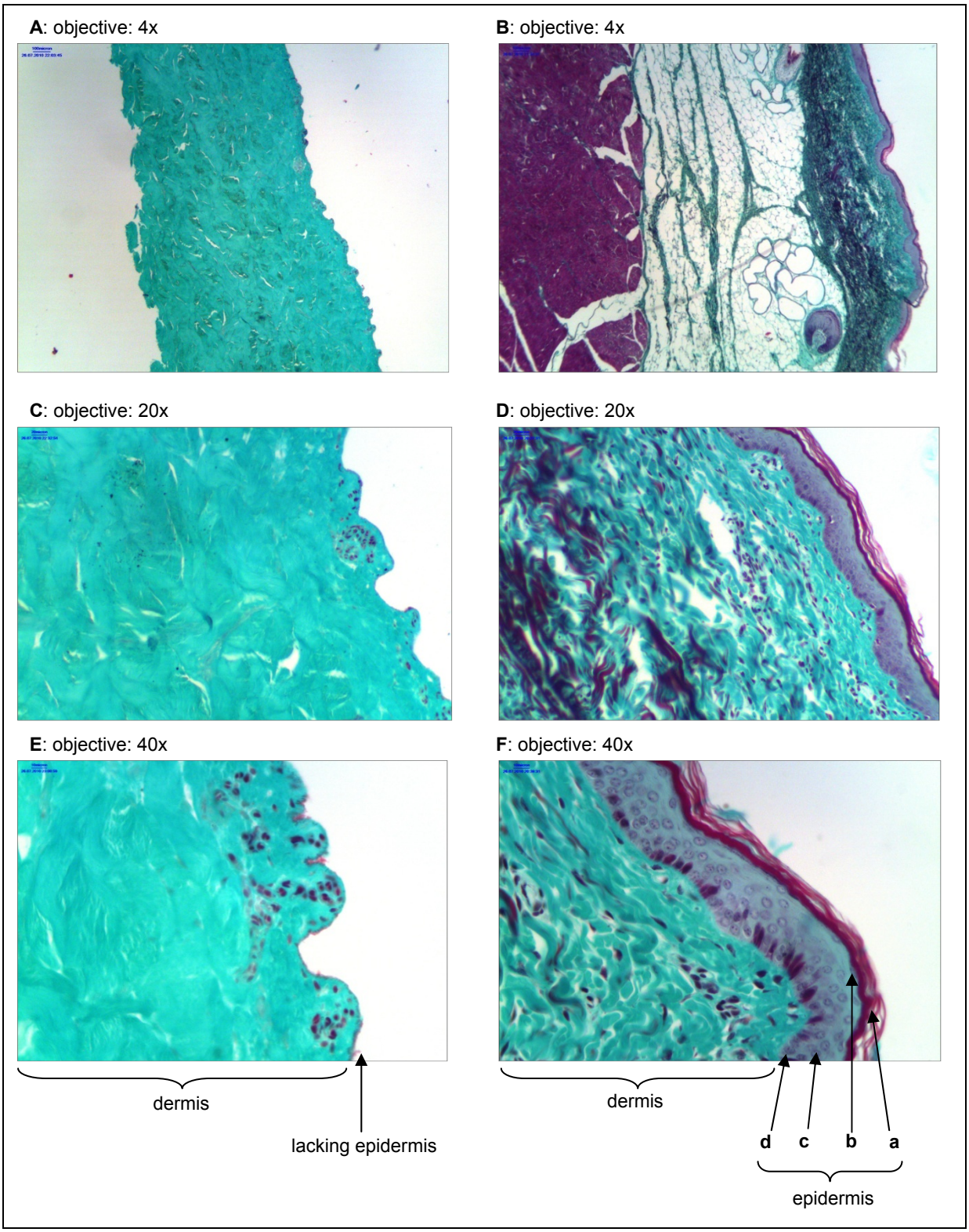

Figure 5.10. Micrographs of Masson-Goldner trichrome stained paraffin sections of dermatomized porcine ear skin (skin provided by Hexal AG) (**A**, **C**, **E**) and of intact porcine reference skin (**B**, **D**, **F**). The dermatomized porcine ear skin was stored at -20 °C and thawed prior to fixation in Bouin's solution. **a**: stratum corneum, **b**: stratum granulosum, **c**: stratum spinosum, **d**: stratum basale.

The lack of epidermis seemed neither result from freezing and thawing nor from processing with a dermatome, as fresh, non-processed skin samples from the same source showed the same results (Figure 5.11 A+B).

A: objective: 4x

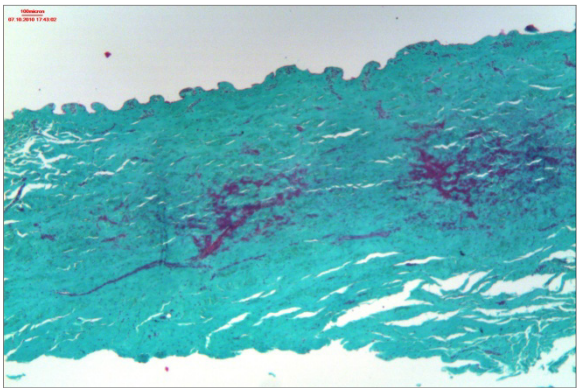

B: objective: 10x

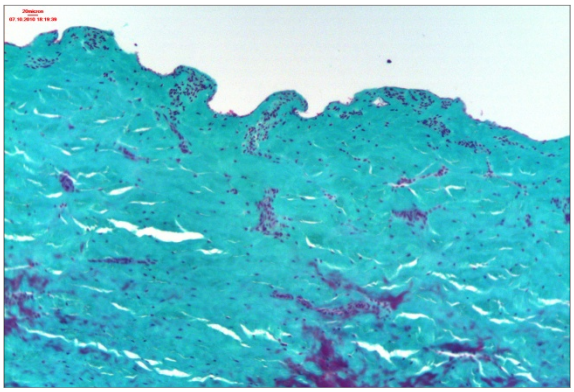

Figure 5.11 A+B. Masson-Goldner trichrome stained paraffin sections of fresh, dermatomized porcine ear skin (skin provided by Hexal AG).

Consequentially, porcine ears obtained from the respective slaughterhouse were inspected under a stereo microscope and photographed using a macro lens. It became obvious that the slaughtered pigs were presumably treated in a way to deprive them of the epidermis. Pictures taken with a digital camera (Figure 5.12 A+B) and by means of a stereo microscope (Figure 5.13 A+B) revealed almost hairless skin with only residual pieces of epidermis. This gave rise to the presumption that the pigs went through a routine slaughter process with scalding and scraping, before their ears were resected. Residual hairs are commonly removed by singeing.

A

B

Figure 5.12. Pictures from porcine ears (material provided by Hexal AG) taken with a digital camera (Nikon, Tokyo, Japan). **A**: upper side, **B**: lower side.

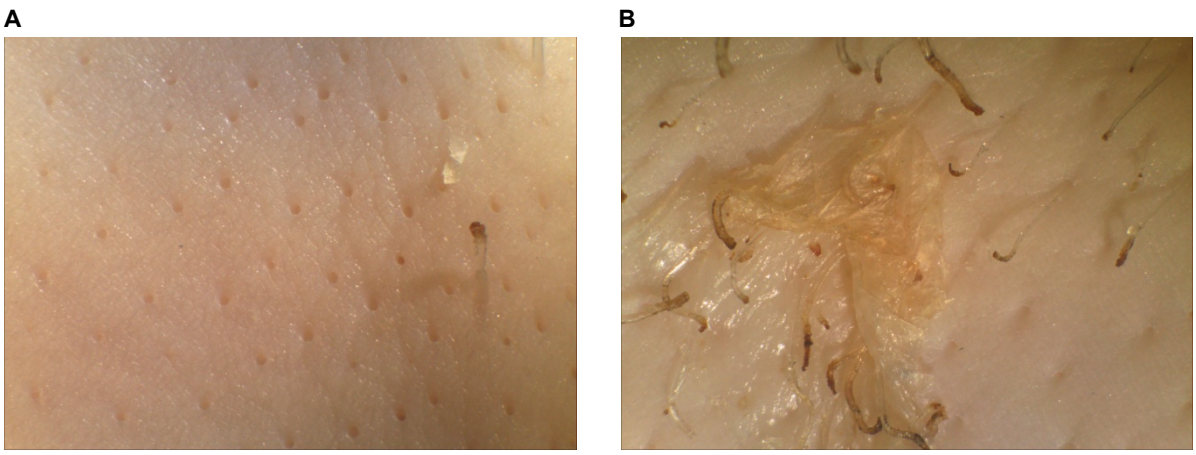

Figure 5.13 A+B. Images of the dorsal side of porcine ears (material provided by Hexal AG) taken with a stereo microscope.

These findings prompted us to find a new source of untreated porcine ear skin with intact anatomy. A local butcher supplied porcine ears, of which the skin was carefully excised. Histological studies proved the flawless structure of epidermis and dermis (Figure 5.14 A-C). The overall thickness was variable and estimated to be 1.0 – 1.7 mm, whereas the thickness of the epidermis amounted to 70 – 230 µm.

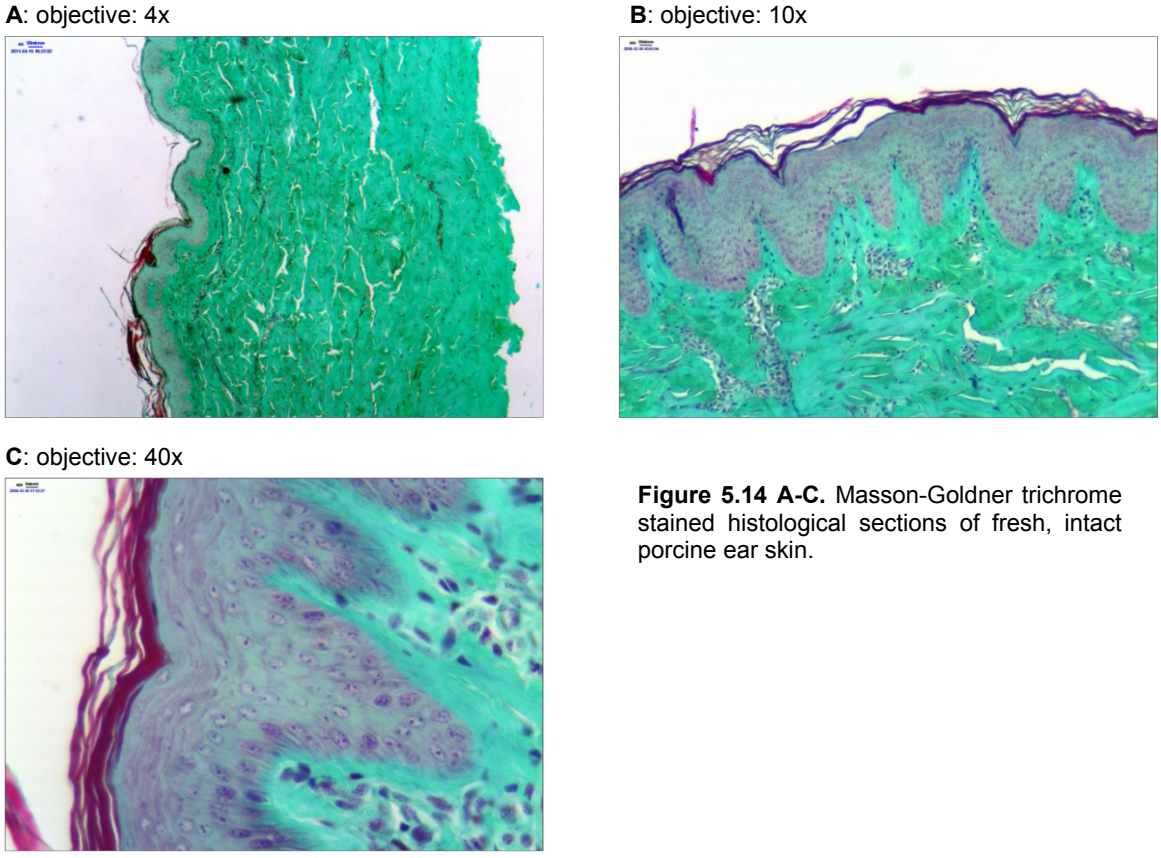

Figure 5.14 A-C. Masson-Goldner trichrome stained histological sections of fresh, intact porcine ear skin.

5.3.5 Permeation of candesartan prodrugs through full-thickness porcine skin

According to the procedure 5.3.1 permeation of candesartan prodrugs through full-thickness porcine ear skin was studied using the candesartan prodrug TTS batches PCAN0009TTS, PCAN0010TTS, PCAN0011TTS and CAN0044TTS. Skin specimens were obtained from two female, 6-7 months old animals (crossbred Deutsche Landrasse x Pietrain). Shortly after slaughtering, skin samples were prepared and immediately stored at -20 °C. For permeation studies freshly thawed pieces of skin were used.

Compared to the results obtained with epidermis-free (scalded and scraped) porcine skin a striking decrease in skin permeation was observed (Figure 5.15). Thus, the sampling-time was extended to 72 h. Nevertheless, for the prodrugs **3.35** (PCAN0011TTS) and candesartan cilexetil (CAN0044TTS) no skin permeation over a period of 72 h was detectable. Still, **3.32** appeared to be the most permeable compound, but was only reaching at the best 1/30 (~ 19 µg/cm^2 after 72 h) of the skin permeation obtained with epidermis-free skin. The skin permeation of **3.31** was low. Determination of the steady-state flux was possible for **3.31** (PCAN0009TTS) and **3.32** (PCAN0010TTS), respectively, for one of two experiments each. **3.31** revealed a very low flux of 0.12 µg·cm^{-2}·h^{-1} and a long lag time (44.68 h), whereas the flux of **3.32** was found to be nearly 3-fold higher (0.29 µg·cm^{-2}·h^{-1}) corresponding to a 3.5-fold shorter lag time of 12.62 h.

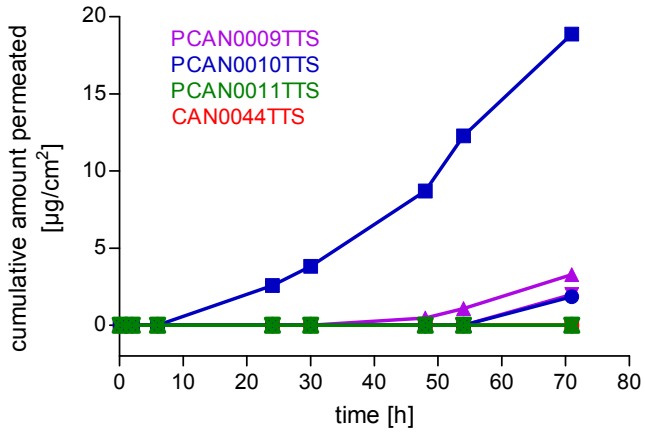

Figure 5.15. Skin permeation profile of candesartan prodrugs across full-thickness porcine skin from TTS (n = 2) depicted as the sum of candesartan prodrug and candesartan.

Obviously, the presence of an intact epidermis with the stratum corneum serving as a lipophilic barrier is the decisive factor for the low permeability. Presumably, only low amounts of the candesartan prodrugs are able to penetrate into the epidermis. Thereby, also the prodrug formulation (prodrug dissolved/ suspended) may influence the extent of drug penetration. However, the formation of a drug reservoir in the skin, presumably in the epidermis, leading to low receptor fluid levels should be taken into account, as this is postulated especially for compounds having low solubility in water and oil as well as a log P_{oct/H_2O} greater than 1.[26-27] Furthermore, the influence of the absence of physiological blood circulation and drug distribution should be considered, since this may lead to underestimation of the permeability.

5.3.6 Permeation of candesartan prodrugs through dermatomized and full-thickness human skin

In the following, results from permeation experiments with candesartan prodrug containing TTS batches using dermatomized or full-thickness human skin as *in vitro* model are shown. Excised human skin samples were obtained according to the guidelines of the charitable state controlled foundation HTCR, with the informed patient's consent. Dermatomized skin was prepared from male (51 years) abdominal tissue. Full-thickness skin was obtained from femoral or abdominal regions of two female patients (75 and 47 years). Appropriately sized skin samples were prepared as soon as possible after surgery and were immediately stored at -20 °C. For permeation experiments freshly thawed skin samples were used.

5.3.6.1 Histological studies of full-thickness human skin

Prior to permeation experiments, histological analysis of the used full-thickness human skin before storage at -20 °C and after thawing was performed in order to verify the anatomical integrity. Figure 5.16 A-C confirm the intactness of epidermis and dermis of fresh skin before freezing as well as the nearly complete removal of the subcutaneous fat (Figure 5.16 A). The overall thickness of the skin was found to be quite varying and was estimated between 1.4-2.3 mm, of which approx. 30-90 µm are related to the epidermis. Furthermore, the process of freezing and thawing seems to lead to partly severing the stratum corneum (Figure 5.16 D). Notwithstanding, the residual epidermis appeared to be intact.

A: objective: 4x

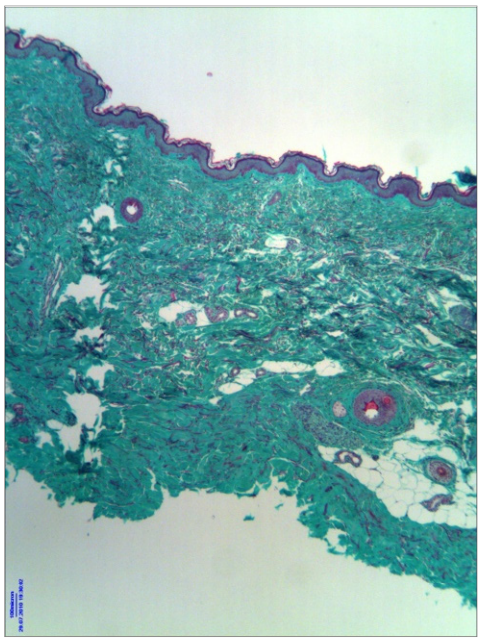

B: objective: 20x

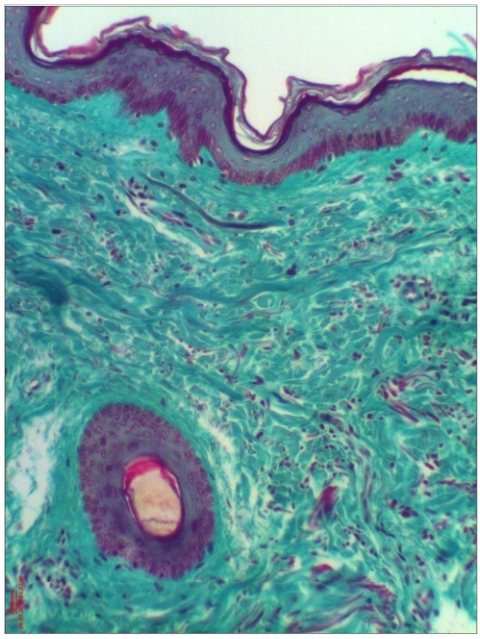

C: objective: 40x

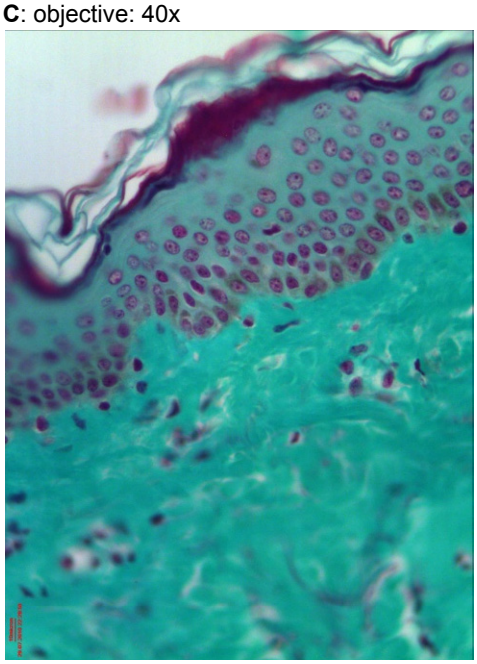

D: objective: 20x

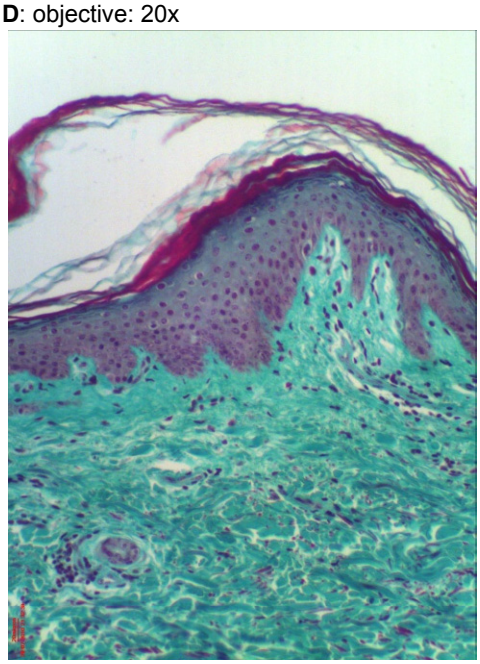

Figure 5.16 A-D. Masson-Goldner trichrome stained histological sections of full-thickness human femoral skin. **A**-**C**: prior to freezing, **D**: thawed.

5.3.6.2 Permeation of candesartan prodrugs through dermatomized human skin

The following results were obtained from permeation experiments performed by Hexal AG (Holzkirchen, Germany) with dermatomized (500-800 µm) human abdominal skin, using the candesartan prodrug containing TTS batches PCAN0004TTS, PCAN0005TTS, PCAN0006TTS and CAN0043TTS by means of automated sampling (AutoPlus MultiFill, Hanson Research, Chatsworth, USA) and illustrated in Figure 5.17. In accordance with permeation results obtained with full-thickness porcine ear skin, very low fluxes between 0.04 and 0.09 $\mu g \cdot cm^{-2} \cdot h^{-1}$ were determined for all candesartan prodrugs (Table 5.5). However, a significantly improved permeability compared to candesartan cilexetil was achieved by variation of the pro-moiety.

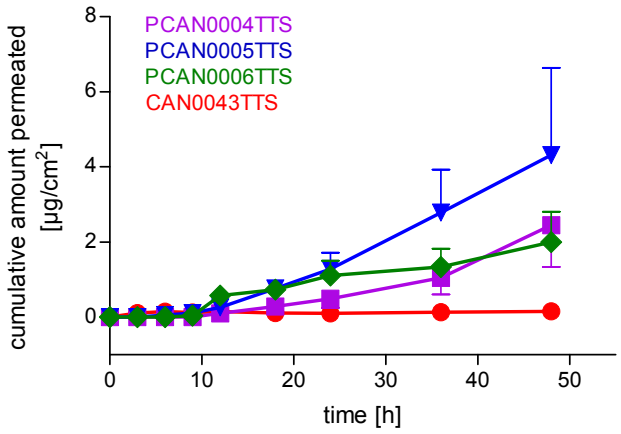

Figure 5.17. Skin permeation profile of candesartan prodrugs across dermatomized human skin from TTS. Data represent mean values ± SEM of 3-4 individual experiments.

Table 5.5. Steady-state fluxes and lag times (mean ± SEM, n = 3-4) of candesartan prodrugs from TTS through dermatomized human skin.

compound	TTS batch	J_{ss} [$\mu g \cdot cm^{-2} \cdot h^{-1}$]	t_{lag} [h]
3.31	PCAN0004TTS	0.05 ± 0.02	5.63 ± 1.78
3.32	PCAN0005TTS	0.09 ± 0.05	4.04 ± 1.48
3.35	PCAN0006TTS	0.04 ± 0.02	0.90 ± 2.21
CAN-CIL	CAN0043TTS	0.00	-

5.3.6.3 Permeation of candesartan prodrugs through full-thickness human skin

Using full-thickness human femoral skin very low skin permeation was observed for all candesartan prodrugs over a sampling period of 72 h (Figure 5.18). Thereby, only the active principle candesartan but no intact prodrug was detected. Due to the variations of the single permeation values and the limited number of experiments due to shortage of human skin reliable steady-state fluxes and lag times could not be generated.

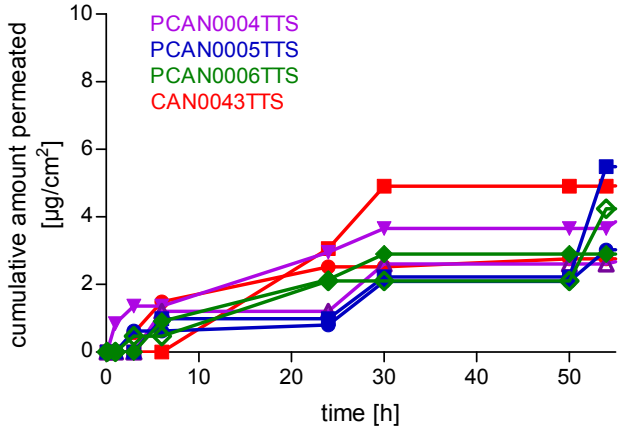

Figure 5.18. Skin permeation profile of candesartan prodrugs across full-thickness human skin from TTS referring to two individual experiments.

In order to investigate, if the prodrugs penetrated into the skin at all or if they were subjected to reservoir formation, concentrations of the prodrugs in the skin samples and in the TTS were determined. After termination of the permeation experiment, skin samples and TTS were removed from the Franz cells, separately extracted with organic solvent and analyzed by HPLC. In Table 5.6 absolute amounts of the candesartan prodrugs, extracted from the TTS and skin samples, and corresponding recoveries are summarized. Amounts between 35 µg and 353 µg were determined in the skin samples. The high value found for PCAN0011TTS in the skin (1063 µg) presumably results from residual matrix sticking to the skin after removal of the patch. The overall recovery values of the prodrugs range between 76 % and 106 %. In conclusion, these results indicate unequivocally that all candesartan prodrugs penetrate into the skin. It may be speculated that diffusion from the epidermis into the dermis is the permeation-limiting factor.

Table 5.6. Mean recovery of candesartan prodrugs in skin and TTS (n = 2) after 72 h.

	recovered amounts [µg]		**sum of recovered amounts [µg]**	**theoretical amount [µg]**	**recovery [%]**
prodrug/ batch	TTS	skin	TTS + skin		
3.31/	4502	60	4562	5642	81
PCAN0009TTS	4271	35	4306		76
3.32/	4742	79	4821	5049	95
PCAN0010TTS	4961	62	5023		99
3.35/	5865	276	6141	5984	103
PCAN0011TTS	4480	*1063* [a]	5543		93
CANCIL[b]/	4288	353	4641	4393	106
CAN0044TTS	4381	114	4495		102

[a]: This value was considered an outlier with reference to the observed values. [b] **CANCIL** = candesartan cilexetil.

5.4 Permeation studies with cilazapril and cilazapril prodrugs

The permeability of the novel cilazapril prodrugs **3.1**, **3.2** and **3.14** as well as the reference standard cilazapril was investigated using nude mouse, porcine and human skin. The experiments were performed according to the procedure described in 5.3.1 using 50 mM phosphate buffer pH 7.4 as receptor fluid. For permeation studies with nude mouse skin, dermatomized and full-thickness porcine skin as well as full-thickness human skin the following TTS batches were used: PCIL0011TTS, PCIL0012TTS, PCIL0013TTS and CIL0027TTS. Permeation studies with dermatomized human skin were performed with PCIL0002TTS, PCIL0003TTS, PCIL0004TTS and CIL0025TTS.
For oral application the recommended starting dose and maintenance dose of cilazapril amount to 1.25 mg and 2.5 mg, respectively.[24] The oral bioavailability of cilazapril is indicated as 57 % (range 45-75 %) and that of cilazaprilat as 19 % (range 8-40 %).[28] Hence, transdermal delivery of 0.7 mg would be sufficient as starting dose and 1.4 mg daily would be necessary to maintain the antihypertensive effect.

5.4.1 Permeation of cilazapril and cilazapril prodrugs through nude mouse skin

The suitability of nude (thymusaplastic) mice as a model of percutaneous penetration in man is discussed controversially.[29] Transdermal delivery is highly dependent on the physicochemical properties of the investigated compound, but nude mouse skin shows generally higher permeation than human skin.[12, 29] This could presumably be associated with the reduced thickness of the stratum corneum of nude mice, which is less than half as thick as that of the human integument.[29] However, by the lack of a fur coat nude mouse skin better resembles human skin than that of furred animals.[12] For the purpose of comparison and due to ready availability, the permeability of cilazapril and selected cilazapril prodrugs was studied on freshly excised full-thickness skin of nude (NMRI (nu/nu)) mice.

5.4.1.1 Histological studies on nude mouse skin

Histological studies of freshly excised nude mouse skin proved the integrity of the skin consisting of epidermis, dermis and subcutis (Figure 5.19 A-C). The overall thickness was estimated to be approximately 800-1000 µm, the epidermis to be 15-30 µm, rendering the full skin and the epidermis markedly thinner than pig or human tissue.

A: objective: 4x

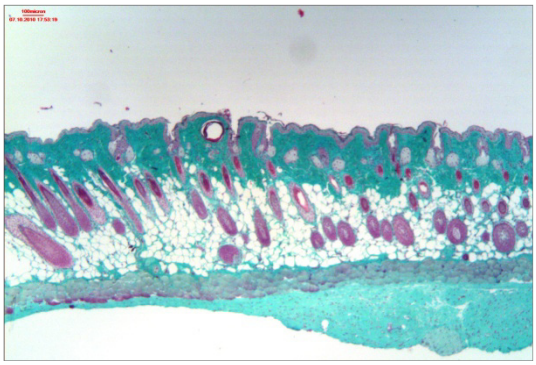

B: objective: 20x

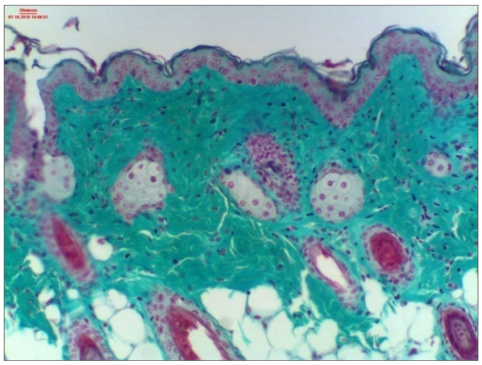

C: objective: 40x

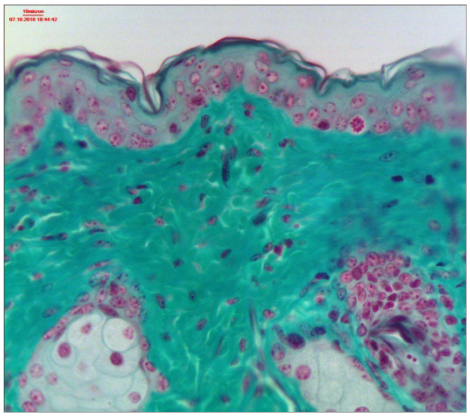

Figure 5.19 A-C. Masson-Goldner trichrome stained histological sections of full-thickness nude mouse skin.

5.4.1.2 Results from permeation experiments with nude mouse skin

The permeability of cilazapril and the cilazapril prodrugs **3.1**, **3.2** and **3.14** through full-thickness nude mouse skin was investigated using patches of the corresponding TTS batches CIL0027TTS, PCIL0011TTS, PCIL0012TTS and PCIL0013TTS as donor vehicle applied on the epidermal side of the skin samples (Figure 5.20). In the receptor fluid mainly cilazapril and cilazaprilat were detected. No intact prodrug was found for **3.1**, **3.2** and **3.14**, but for **3.14** a metabolite resulting from the hydrolysis of the homophenylalanine ethyl ester group could be observed. The sink conditions were fulfilled over the entire sampling period of 72 h. The resulting skin permeation profile of all cilazapril prodrugs was quite promising.

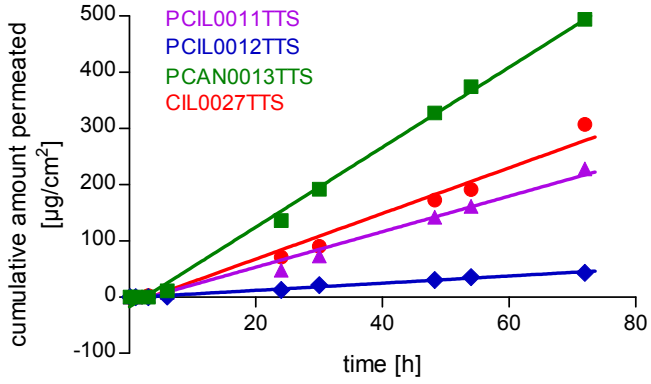

Figure 5.20. Permeation profiles for cilazapril and cilazapril prodrugs through full-thickness nude mouse skin from TTS depicted as the sum of all compound related metabolites.

As depicted in Table 5.7 the highest steady-state flux was detected for the morpholino-ethyl ester of cilazapril (**3.14**) (7.10 µg·cm^{-2}·h^{-1}). Cilazapril and **3.1** showed a similar, moderate flux (4.05 and 3.16 µg·cm^{-2}·h^{-1}), whereas the skin permeation of **3.2** was rather low (0.64 µg·cm^{-2}·h^{-1}). The corresponding lag times varied between ~ 1.6 and 3.3 h.

Table 5.7. Steady-state fluxes of cilazapril and cilazapril prodrugs from TTS through nude mouse skin.

compound	TTS batch	J_{ss} [µg·cm^{-2}·h^{-1}]	t_{lag} [h]
3.1	PCIL0011TTS	3.16	3.21
3.2	PCIL0012TTS	0.64	1.61
3.14	PCIL0013TTS	7.10	2.47
cilazapril	CIL0027TTS	4.05	3.31

For reasons of practicability, data were obtained from a single experiment. However, the results are considered plausible and reliable, because reproducibility is usually high, when data are acquired from tissues of animals of identical genetic background. As the skin of nude mice is thinner and generally more permeable than human skin, the obtained results must not be overestimated and may be considered at most “best case” results.

5.4.2 Permeation of cilazapril and cilazapril prodrugs through dermatomized, scalded and scraped porcine skin

Dermatomized, scalded and scraped porcine ear skin (provided by Hexal AG) was found to be permeable for cilazapril and the cilazapril prodrugs **3.1**, **3.2** and **3.14**. The most hydrophilic compounds, cilazapril and cilazapril morpholinoethyl ester (**3.14**), showed highest skin permeation (Figure 5.21 and Figure 5.22). In the receptor fluid mainly cilazapril and cilazaprilat were detected. Furthermore, regarding the cilazapril prodrugs **3.1**, **3.2** and **3.14** both intact prodrug and molecular species resulting from the hydrolysis of the homophenylalanine ethyl ester group were found. Thus, both findings led to the conclusion that the used porcine skin, despite the lack of the epidermis, was still capable of enzymatically hydrolyzing the present ester moieties.

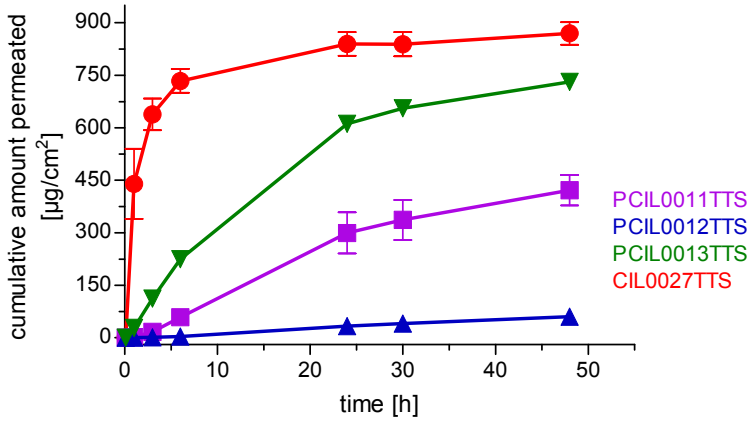

Figure 5.21. Permeation profiles for cilazapril and cilazapril prodrugs through dermatomized, scalded and scraped porcine ear skin from 5.7-cm^2 TTS (mean ± SEM, n=3-4). The data represent the sum of parent drug and detected metabolites.

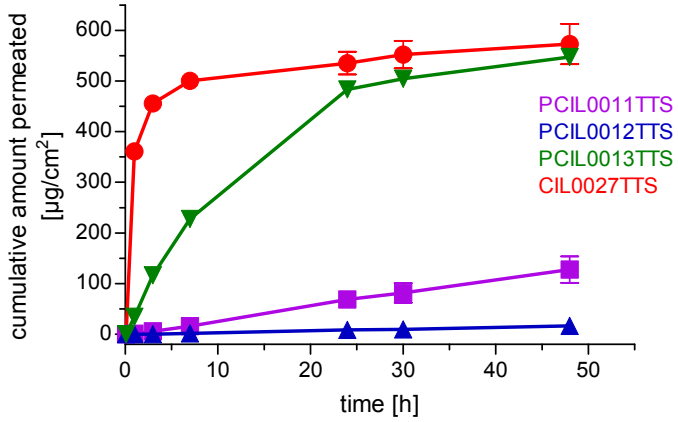

Figure 5.22. Permeation profiles for cilazapril and cilazapril prodrugs through dermatomized, scalded and scraped porcine ear skin from 2.5-cm^2 TTS (mean ± SEM, n=4). The data represent the sum of parent drug and detected metabolites.

In general, the use of 5.7-cm^2 TTS led to higher permeation values compared to 2.5-cm^2 TTS (Table 5.8) indicating diffusion processes from outer parts of the TTS to the actual permeation area as suggested for 5.7-cm^2 and 2.5-cm^2 patches of candesartan prodrug TTS batches (cf. 5.3.3).

Table 5.8. Skin permeation (sum of parent compound and metabolites) of cilazapril prodrugs and cilazapril after a period of 48 h (mean ± SEM, n = 3-4).

		skin permeation µg/cm^2	
compound	**TTS batch**	2.5-cm^2	5.7-cm^2
3.1	PCIL0011TTS	128 ± 22	383 ± 25
3.2	PCIL0012TTS	17 ± 4	61 ± 7
3.14	PCIL0013TTS	548 ± 12	803 ± 23
cilazapril	CIL0027TTS	573 ± 8	877 ± 36

Steady-state fluxes were determined by linear regression of the permeation data obtained with 5.7-cm^2 (Figure 5.23 A) and 2.5-cm^2 (Figure 5.23 B) patches for **3.1** (PCIL0011TTS) and **3.2** (PCIL0012TTS) and amounted to 8.63 ± 0.69 µg·cm^{-2}·h^{-1} (5.7-cm^2) *vs.* 2.73 ± 0.49 µg·cm^{-2}·h^{-1} (2.5 cm^2), respectively for **3.1** and 1.34 ± 0.15 µg·cm^{-2}·h^{-1} (10 cm^2) *vs.* 0.36 ± 0.09 µg·cm^{-2}·h^{-1} (2.5 cm^2), respectively for **3.2** (Table 5.9). In addition, the lag times were found to be short. Despite the lack of epidermis, the permeation of **3.2** was surprisingly low. This was presumably caused by inappropriate physicochemical properties such as an unsuitably high lipophilicity, which decelerated the penetration into the dermis.

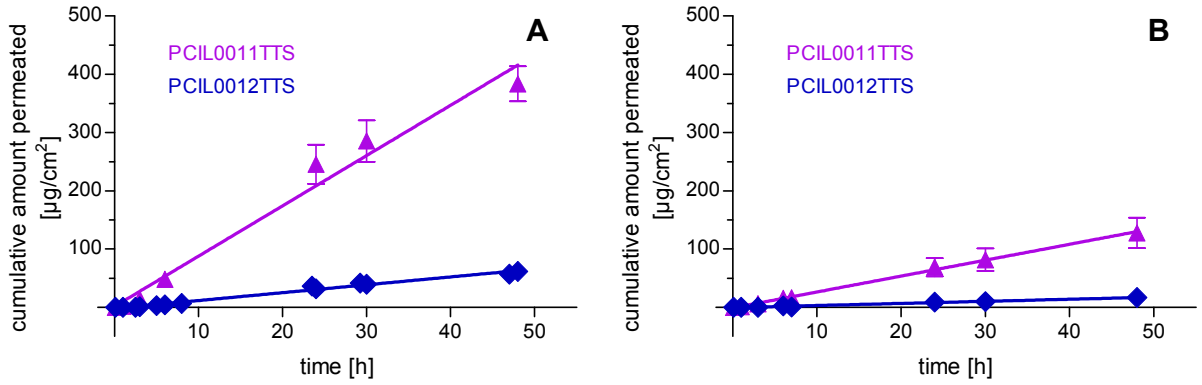

Figure 5.23 A+B. Permeation profiles (mean ± SEM, n = 3-4) for cilazapril prodrugs **3.1** (PCIL0011TTS) and **3.2** (PCIL0012TTS) through dermatomized, scalded and scraped porcine ear skin from 5.7-cm^2 (**A**) and 2.5-cm^2 (**B**) TTS.

Table 5.9. Steady-state fluxes (mean ± SEM, n = 3-4) of cilazapril and cilazapril prodrugs from TTS through dermatomized, scalded and scraped porcine ear skin.

compound	TTS batch	J_{ss} [µg·cm^{-2}·h^{-1}]		t_{lag} [h]	
		5.7-cm^2	2.5-cm^2	5.7-cm^2	2.5-cm^2
3.1	PCIL0011TTS	8.63 ± 0.69	2.73 ± 0.49	-0.28 ± 0.13	0.48 ± 0.28
3.2	PCIL0012TTS	1.34 ± 0.15	0.36 ± 0.09	1.25 ± 0.08	1.17 ± 0.65

In summary, the lack of epidermis resulted in a drastic decrease of the barrier function of the skin. This was noticeable by high and fast skin permeation of cilazapril and **3.14**. The compounds **3.1** and **3.2** showed lower but also almost immediate permeation.

5.4.3 Permeation of cilazapril and cilazapril prodrugs through full-thickness porcine skin

The following results were obtained from skin permeation studies using intact full-thickness porcine ear skin of two female, 6-7 months old animals (crossbred Deutsche Landrasse x Pietrain) (cf. 5.3.5). In Figure 5.24 A+B the cumulative permeated amounts as a sum of all detected metabolites of cilazapril, **3.1** (PCIL0011TTS), **3.2** (PCIL0012TTS) and **3.14** (PCIL0013TTS) are depicted for two different porcine skin specimens. Mainly cilazapril and cilazaprilat were detected in the receptor fluid but no intact prodrug (**3.1**, **3.2**, **3.14**). Furthermore, in the case of **3.14** a metabolite resulting from the hydrolysis of the homophenylalanine ethyl ester group was observed. The sink conditions were fulfilled over the entire sampling period of 72 h.

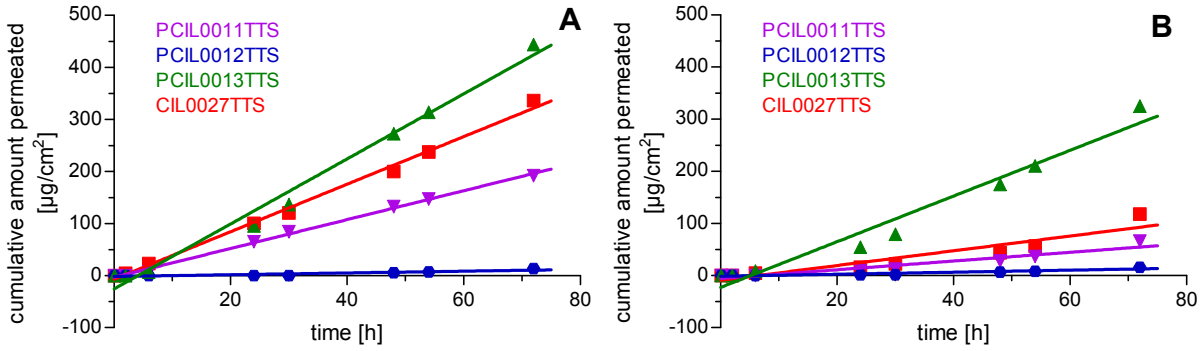

Figure 5.24. A+B. Permeation profiles from TTS of **3.1** (PCIL0011TTS), **3.2** (PCIL0012TTS), **3.14** (PCIL0013TTS) and cilazapril (CIL0027TTS) through full-thickness porcine ear skin prepared from two different animals (**A** and **B**). The cumulative amount permeated is depicted as a sum of all compound related detected metabolites.

In Table 5.10 steady-state fluxes and lag times for the cilazapril prodrugs **3.1**, **3.2** and **3.14** and for cilazapril are summarized. Although skin samples of two female pigs of the same race with similar age and body weight were used, the results for **3.1**, **3.14** and cilazapril differ significantly, showing 1.4 to 3.3 fold higher skin permeation through skin sample A. In addition, except for **3.2,** shorter lag times were found for skin sample A. Compared to scalded and scraped porcine skin, the skin permeation of all compounds was markedly decreased. The steady-state fluxes of **3.1** and **3.2** were reduced by a factor of approx. 5 to 7. Furthermore, lag times were notably increased. With respect to nude mouse skin, lower mean steady-state fluxes and higher lag times were observed, but the rank orders of the compounds were consistent. Concerning the thickness of porcine skin compared to that of nude mouse skin, the decrease in permeability (factor 1.5 – 3.5) through full-thickness porcine skin was less pronounced than expected.

Table 5.10. Steady-state fluxes of cilazapril and cilazapril prodrugs from 5.7-cm^2 TTS through intact porcine ear skin (two different skin specimens used (A+B, referring to Figure 5.24 A+B)).

compound	**TTS batch**	**J_{ss} [µg·cm^{-2}·h^{-1}]**			**t_{lag} [h]**		
		A	B	mean	A	B	mean
3.1	PCIL0011TTS	2.77	0.84	1.81	1.26	7.05	4.16
3.2	PCIL0012TTS	0.17	0.20	0.19	10.52	8.35	9.44
3.14	PCIL0013TTS	6.25	4.39	5.32	4.14	5.26	4.70
cilazapril	CIL0027TTS	4.57	1.41	2.99	1.56	6.53	4.05

With regard to transdermal delivery of cilazapril, therapeutic doses of approximately 1.3 mg could be reached within 24 h, assuming the application of a 10-cm^2 TTS, containing prodrug **3.14**. In the case of cilazapril, **3.1** and **3.2**, possibly, either enlarged size or higher drug dose of the TTS would be needed to reach the desired effect.

5.4.4 Permeation of cilazapril and cilazapril prodrugs through human skin

In the following, results obtained from Franz cell permeation experiments with human skin are depicted and discussed. As *in vitro* skin absorption studies with human tissue are regarded to have the highest predictive value, they should be considered as most relevant.

5.4.4.1 Permeation of cilazapril and cilazapril prodrugs through dermatomized human skin

The following permeation experiments were performed by Hexal AG (Holzkirchen, Germany) with dermatomized (500-800 µm) human abdominal skin using the cilazapril or cilazapril prodrug containing TTS batches PCIL0002TTS, PCIL0003TTS, PCIL0004TTS and CIL0025TTS by means of automated sampling (AutoPlus MultiFill, Hanson Research, Chatsworth, USA) The obtained results (personal communication) are shown in Table 5.11. The highest steady-state flux (3.32 ± 0.12 $\mu g \cdot cm^{-2} \cdot h^{-1}$) was observed for the cilazapril morpholinoethyl ester **3.14** (PCIL0004TTS). The double ester prodrugs **3.1** (PCIL0002TTS) and **3.2** (PCIL0003TTS) showed approx. 2.5 to 3 fold lower skin permeation (1.42 ± 0.31 $\mu g \cdot cm^{-2} \cdot h^{-1}$ and 1.07 ± 0.42 $\mu g \cdot cm^{-2} \cdot h^{-1}$, respectively) than **3.14**. Interestingly, the lowest flux was found for cilazapril (1.00 ± 0.39 $\mu g \cdot cm^{-2} \cdot h^{-1}$) confirming the working hypothesis that masking of the free carboxylic acid group in cilazapril with suitable prodrug moieties is key to improve skin permeation. Compared to the other investigated prodrugs, the introduction of the hydrophilic morpholinoethyl ester led to a lower log *D* value. This seems to be favorable for penetration into the epidermis and permeation across the dermis. The lag times of compounds **3.1**, **3.2**, **3.14** and cilazapril ranged from approximately 3 (**3.1, 3.2**) to 10 h. Remarkably, the prodrug **3.14** and cilazapril showed a big difference in skin permeation, regardless of similar lag times. Compared to the results obtained with porcine and nude mouse skin the permeability of cilazapril was significantly lower in human skin. It may me speculated that this is crucially depending on the different lipid composition of human, porcine and murine skin. Among all investigated cilazapril prodrugs compound **3.14** appeared most suitable for application by means of a TTS, since the achieved flux corresponds to an (estimated) transdermal resorption of 0.8 mg daily (assuming the use of a 10 cm^2 patch), which is in the desired therapeutic range.

Table 5.11. Steady-state fluxes (mean ± SEM, n = 2-4) of cilazapril and cilazapril prodrugs from TTS through dermatomized human skin (data provided from Hexal AG).

compound	TTS batch	J_{ss} [$\mu g \cdot cm^{-2} \cdot h^{-1}$]	t_{lag} [h]
3.1	PCIL0002TTS	1.42 ± 0.31	3.05 ± 2.49
3.2	PCIL0003TTS	1.07 ± 0.42	3.06 ± 0.26
3.14	PCIL0004TTS	3.32 ± 0.12	9.07 ± 0.01
cilazapril	CIL0025TTS	1.00 ± 0.39	10.65 ± 0.58

5.4.4.2 Permeation of cilazapril and cilazapril prodrugs through full-thickness human skin

For the permeation studies with full-thickness human skin, freshly thawed femoral or abdominal skin specimens from two female patients (75 and 47 years) were used (cf. 5.3.6). In Figure 5.25 A+B the skin permeation profiles of cilazapril and cilazapril prodrugs from TTS obtained from each donor are depicted as a sum of all detected metabolites.

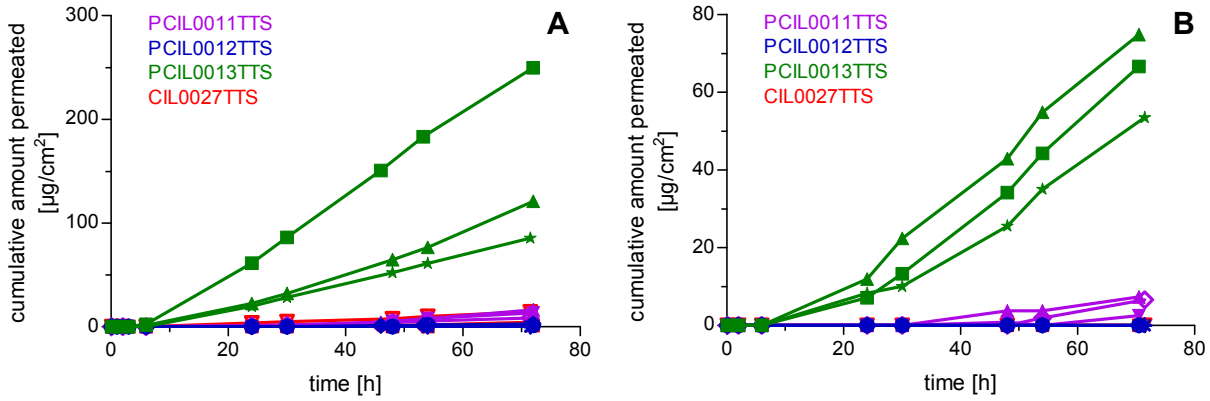

Figure 5.25 A+B. Permeation profiles (n = 3) from 5.7-cm^2 TTS of **3.1** (PCIL0011TTS), **3.2** (PCIL0012TTS), **3.14** (PCIL0013TTS) and **cilazapril** (CIL0027TTS) through two different full-thickness human skin specimens. A: femoral skin, B: abdominal skin. The cumulative amount permeated is depicted as a sum of all compound related detected metabolites.

Similar to the results obtained with dermatomized human skin, in both donor skin samples the highest permeability was found for prodrug **3.14** (PCIL0013TTS). However, markedly lower steady-state fluxes were estimated for compounds **3.1** (PCIL0011TTS), **3.2** (PCIL0012TTS) and cilazapril (CIL0027TTS) (cf. Table 5.12), and the absolute skin permeation appeared to be lower as well. Considerable differences between the two donor skin samples became obvious: **3.1** and **3.14** showed approx. 2.5-fold higher permeation through femoral than through abdominal skin. Whereas **3.2** and cilazapril yielded very small fluxes through femoral skin, no compound or corresponding metabolites were detected in the receptor fluid of the abdominal skin sample over a sampling period of 72 h. Again rather long lag times between 4 and 12 h were estimated, whereby the corresponding lag times referring to the femoral skin sample were found to be shorter. In conclusion, **3.14** and to a smaller degree also **3.1** turned out to exhibit clear advantages compared to cilazapril in terms of permeability through human skin, **3.14** being the most promising candidate.

Table 5.12. Steady-state fluxes (mean ± SEM, n = 3) of cilazapril and cilazapril prodrugs from 5.7-cm^2 TTS through full-thickness human skin.

compound	TTS batch	J_{ss} [µg·cm^{-2}·h^{-1}]		t_{lag} [h]	
		femoral skin	abdominal skin	femoral skin	abdominal skin
3.1	PCIL0011TTS	0.16 ± 0.02	0.06 ± 0.02	7.97 ± 0.40	11.91 ± 0.79
3.2	PCIL0012TTS	0.02 ± 0.01	0.00	8.84 ± 0.19	-
3.14	PCIL0013TTS	2.13 ± 0.59	0.91 ± 0.08	3.92 ± 0.30	6.21 ± 0.40
cilazapril	CIL0027TTS	0.09 ± 0.05	0.00	8.85 ± 2.13	-

The use of full-thickness skin resulted in rather high variance, probably, due to non-uniform skin samples. Thus, it appears reasonable to use dermatomized skin samples with more or less the same thickness. Moreover, factors such as anatomical, age and gender should be taken into consideration, when comparing results obtained with different skin specimens.

5.5 Summary

The permeability of the novel candesartan prodrugs candesartan 1-(isopropyloxycarbonyloxy)ethyl ester (**3.31**), candesartan 1-(2,2-dimethylpropanoyloxy)ethyl ester (**3.32**) and candesartan morpholinoethyl ester (**3.35**) as well as of the novel cilazapril prodrugs cilazapril 1-(ethoxycarbonyloxy)ethyl ester (**3.1**), cilazapril 1-(cyclohexyloxycarbonyloxy)-ethyl ester (**3.2**) and cilazapril morpholinoethyl ester (**3.14**) and the reference compounds candesartan cilexetil and cilazapril, released from various TTS batches, through porcine, murine and human skin was investigated *in vitro* using static Franz diffusion cells. In the "receptor fluids" exclusively the corresponding active principle or other prodrug related metabolites were analyzed, indicating effective metabolism of all applied prodrugs during permeation through intact skin.

The permeability of all candesartan prodrugs across full-thickness porcine ear skin as well as across dermatomized and full-thickness human skin was rather low. Nevertheless, modification of the pro-moiety improved the permeability with respect to candesartan cilexetil. Probably, the skin permeation is affected by the kind of formulation (prodrug dissolved or suspended) resulting in different penetration rates or reservoir formation in certain layers of the skin due to inappropriate physicochemical properties. Furthermore, the lack of the physiological blood microcirculation in the dermis and the high inter-individual variability of the used tissue in terms of thickness or age of donor should be taken into account when drawing conclusions from *in vitro* results with respect to *in vivo* conditions.

Permeability of the cilazapril prodrugs and cilazapril across nude mouse skin was comparably high, presumably due to the rather low barrier function of mouse epidermis. Compared to cilazapril the morpholinoethyl ester **3.14** showed clear advantages in terms of skin permeation, whereas the double ester prodrugs **3.1** and **3.2** were found to be less permeable. On full-thickness porcine ear skin reduced steady-state fluxes were obtained

for all compounds. Surprisingly, the rank order of permeability was changed, when using human tissue. Across dermatomized human skin the steady-state flux of cilazapril was found to be ~1.5 fold and ~3 fold, respectively, lower than the fluxes of **3.1** and **3.14**. Also with full-thickness human skin the best and most promising permeation profile was obtained for **3.14** (2.13 $\mu g \cdot cm^{-2} \cdot h^{-1}$, femoral skin) followed by **3.1** (0.16 $\mu g \cdot cm^{-2} \cdot h^{-1}$, femoral skin), whereas cilazapril and **3.2** appeared to be poorly permeable.
In addition, histological studies of all used skin species were performed by preparing paraffin sections stained according to Masson and Goldner. Thereby, a lack of the epidermis of certain dermatomized batches of porcine ear skin was detected, which was likely caused by a standard cleaning procedure in the slaughterhouse, before the ears were resected. Comparable permeation experiments with intact porcine ear skin illustrated the importance of the epidermis and especially of the stratum corneum to achieve the full permeation barrier effect, since the permeability of all investigated compounds was markedly decreased, when the epidermis was missing.

5.6 Perspectives

Compared to studies on isolated animal tissue, *in vitro* skin permeation data from human tissue is known to correlate much better with the *in vivo* profile of the TTS in humans. Therefore, the utmost importance was attached to the results obtained from dermatomized and full-thickness human skin. It should be noted, that a considerable variability of the used porcine and human skin specimens regarding permeability was observed, which can presumably be attributed to various factors as different age, gender, or varying thickness of the epidermis depending on the body part.
Candesartan prodrugs: Although an improved *in vitro* skin permeation for the novel candesartan prodrugs was observed, it is assumed that fluxes, required to produce therapeutic drug levels *in vivo*, are unlikely to be reached by application of present TTS. However, various approaches to the optimization of the formulation are conceivable, for instance, increase in drug loading of the TTS. Furthermore, a variation of the PSA should be considered. Optionally, the addition of drug solubilizers like polyvinylpyrrolidone (PVP) could be advantageous to prevent premature crystallization.[30] Moreover, the use of permeation enhancers could be taken into consideration to affect the diffusion across the stratum corneum or to alter the distribution into the stratum corneum.[31] A further approach could be the creation of a supersaturated system, i.e. a formulation containing a drug concentration higher than the saturation concentration, to improve the transdermal delivery.[32]
Cilazapril prodrugs: Regarding human skin permeation at least two of three studied novel cilazapril prodrugs turned out to be superior to cilazapril. These findings corroborate the assumption that masking of the free carboxylic acid of cilazapril by using pro-moieties with appropriate physicochemical properties leads to a considerable gain in permeability. So far, besides the (ethoxycarbonyloxy)ethyl ester (**3.1**) the morpholinoethyl ester of

cilazapril (**3.14**) turned out to be the most promising candidate for preclinical proof-of-concept studies. In addition, the (2-morpholinoacetoxy)ethyl ester (**3.18**) should be taken into consideration due to similar physicochemical properties of the promoiety. For further TTS development upscaling of the synthesis of the respective prodrugs in pharmaceutical quality is inevitable. Stability of the compounds as solids and after incorporation in the patch has to be determined again and a greater number of permeation experiments is required due to the high interindividual variations within the skin of donors to gain more reliable and predictive permeability data. In addition, the formulation should be optimized, and studies concerning the potential of the TTS for causing skin irritations should be carried out at an early stage.

5.7 Experimental section

5.7.1 General experimental conditions

Commercially available chemicals and reagents were purchased from Acros Organics (Geel, Belgium), Merck KGaA (Darmstadt, Germany) or Sigma-Aldrich Chemie GmbH (München, Germany). All solvents used were of analytical grade or HPLC grade. Analytical HPLC analysis was performed on a system from Thermo Separation Products (Thermo Scientific) consisting of a SN400 controller, a P4000 pump, an AS3000 autosampler, a Spectra Focus UV-VIS detector and a RP-column (Luna C18-2, 150 x 4.6 mm, 3 µm; Phenomenex, Aschaffenburg, Germany) at a flow rate of 0.75 mL/min and a column temperature varying between 45 to 60 °C. Absorbance was detected at 210 nm. The mobile phase consisted of MeCN and 0.05 % trifluoroacetic acid (TFA) in Millipore water. All samples were filtered prior to injection using 0.2 µm Phenex-NY Syringe Filters or 0.2 µm Phenex-RC Syringe Filters (each 0.2 µm pore size, 4 mm diameter) (Phenomenex, Aschaffenburg, Germany). Permeation experiments were performed, unless otherwise indicated, using customized Franz diffusion cells and a 9-station Franz cell stirrer (Crown Glass Company, Inc., Somerville, NJ, USA) equipped with a Lauda Ecoline 003/E100 heating water bath circulator (LAUDA DR. R. WOBSER GMBH & CO. KG, Lauda-Königshofen, Germany). Microscopic images were taken by means of an Olympus BH-2 microscope (Olympus, Tokyo, Japan) equipped with a Digital Mikroskop DCM-500 Ocular microscope camera.

5.7.2 Determination of equilibrium solubility

To a defined amount of substance in a small vessel a defined volume of receptor fluid was added resulting in a saturated solution with excess of solid present. The sample was stirred at room temperature for a specified time. After centrifugation the supernatant was collected and diluted with mobile starting phase to yield an appropriate concentration for HPLC analysis. The drug concentrations were determined on the analytical HPLC system described in the general experimental conditions (5.7.1) by applying following gradients: **3.31**: 0 min: MeCN/0.05% TFA/aq 20/80, 24 min: 73/27, 25-33 min: 95/5, 34-42 min: 20/80. **3.32, candesartan cilexetil**: 0 min: MeCN/0.05% TFA/aq 20/80, 24 min: 80/20, 25-33 min: 95/5, 34-42 min: 20/80. **3.35**: 0 min: MeCN/0.05% TFA/aq 20/80, 24 min: 43/57, 25-33 min: 95/5, 34-42 min: 20/80. **3.1, cilazapril**: 0 min: MeCN/0.05% TFA/aq 25/75, 23 min: 39/61, 27 min: 43/57, 28-34 min: 95/5, 35-43 min: 25/75. **3.2**: 0 min: MeCN/0.05% TFA/aq 25/75, 36 min: 47/53, 42 min: 53/47, 43-49 min: 95/5, 50-58 min: 25/75. **3.14**: 0 min: MeCN/0.05% TFA/aq 25/75, 23 min: 39/61, 27 min: 43/57, 28-34 min: 95/5, 35-43 min: 25/75. Determination of the corresponding equilibrium solubility was achieved by comparison with the respective calibration curve.

5.7.3 Preparation of skin membranes

Porcine skin. Dermatomized (500-800 µm) porcine ear skin specimens were prepared using a Nouvag TCM3000 dermatome (Nouvag, Konstanz, Germany) and were provided by Hexal AG. The cooled skin samples were stored at -20 °C immediately after receipt and thawed prior to permeation experiments.

Full-thickness porcine skin membranes were prepared from porcine ears, immediately obtained after slaughtering from a local abattoir. The ears were gently cleaned with water and the skin from the upper side was excised. The tissue was divided into several pieces of approximately 6-8 cm^2, humidified with PBS and stored at -20 °C.

Human skin. Tissue samples were obtained and experimental procedures were performed according to the guidelines of the charitable state controlled foundation HTCR, with the informed patient's consent.[33] Human femoral or abdominal skin specimens were obtained from two female patients (75 and 47 years). As soon as possible after surgery, subcutis and fatty tissue were removed and the skin was divided in appropriately sized pieces (6-8 cm^2), which were humidified with PBS and stored at -20 °C.

Nude mouse skin. After sacrifice the skin of two 74 d old NMRI (nu/nu) mice was excised and stored moistly on ice until prompt use.

5.7.4 General procedure for *in vitro* skin permeation

Reservoir solution. The receptor compartment of a Franz diffusion cell was filled with 12.5 ml of 10 % (w/v) HP-β-CD solution or 50 mM phosphate buffer pH 7.4, respectively. Whilst the constantly stirred receptor fluid was allowed to equilibrate at 32 °C, frozen porcine, murine or human skin was thawed on a soaked paper tissue. A circle with a diameter of 27 mm was punched out and mounted on the receptor compartment with the epidermal side facing upwards. After adjustment of the donor compartment, 2.0 ml of a solution of the test compound in ethanol/propylene glycol 70/30 (v/v) were filled into the chamber. The cell was occluded and gently turned upside down to remove bubbles. At appropriate intervals, 500 µl aliquots of the receptor fluid were withdrawn and immediately replaced with an equal volume of fresh solution. The samples were filtrated and analyzed by HPLC.

TTS. The receptor compartment of a Franz diffusion cell was filled with 12.5 ml of 10 % (w/v) HP-β-CD solution or 50 mM phosphate buffer pH 7.4, respectively. The receptor fluid was constantly stirred and allowed to equilibrate at 32 °C. A TTS was stuck on the epidermal side of a thawed animal or human skin sample, before a circle with a diameter of 27 mm was punched out and clamped between receptor and donor chamber. The cell was occluded and bubbles were removed by gently turning the cell upside down. Sampling and HPLC analysis were performed by analogy with the above described procedure.

The determination of drug concentrations in the receptor fluid samples was performed on the analytical HPLC system described in the general experimental conditions (5.7.1). The injection volume of each sample amounted to 25 µl. Candesartan prodrug containing samples were analyzed applying following gradient: 0 min: MeCN/0.05% TFA/aq 30/70, 20 min: 85/15, 21-26 min: 95/5, 27-35 min: 30/70. For analysis of cilazapril and cilazapril prodrug containing samples the HPLC gradient was as follows: 0 min: MeCN/0.05% TFA/aq 15/85, 16-20 min: 35/65, 26 min: 70/30, 27-32 min: 95/5, 33-41 min: 15/85.

5.7.4.1 Recovery

At the end of the permeation experiment TTS and skin membranes were separated and positioned in small glass vessels. To vessels containing TTS samples 5 ml THF were added. The vessels were sonicated for 3 min and subsequently treated with a shaker for 1 h. Skin samples were extracted with 10 ml MeOH by treatment in an ultrasonic bath for 1 h and by shaking for 1.5 h. Each sample was diluted with mobile phase (TTS: 1:10, skin: 1:5), filtrated and analyzed by HPLC according to the HPLC method described in 5.7.4.

5.7.5 Preparation of paraffin sections for histological studies of animal and human skin

Tissue samples (approx. 1x1 cm^2) were fixed in approx. 25 ml of Bouin's solution (300 ml sat. aq. picric acid solution, 100 ml formaldehyde 37 %, 20 ml glacial acetic acid) for at most 3 days, dehydrated, and embedded into paraffin. Serial 6-µm sections were prepared with a Leica RM2255 microtome (Leica, Bensheim, Germany), deparaffinated, and stained according to Masson and Goldner (modification by Jerusalem).[34]

5.8 References

1. Schaefer, H.; Redelmeier, T. E. *Skin barrier : principles of percutaneous absorption*. Karger: Basel [u.a.], 1996; p XVI, 310 S.
2. Menon, G. K. New insights into skin structure: scratching the surface. *Adv. Drug Del. Rev.* **2002**, 54 Suppl 1, S3-17.
3. Kusuma, S.; Vuthoori, R. K.; Piliang, M.; Zins, J. E. Skin Anatomy and Physiology. In *Plast. Reconstr. Surg.*, Siemionow, M. Z.; Eisenmann-Klein, M., Eds., Springer London: 2010; pp 161-171.
4. Benninghoff, A.; Fleischhauer, K.; Goerttler, K. *Makroskopische und mikroskopische Anatomie des Menschen*. [13./14. Aufl.] ed.; Urban & Schwarzenberg: München [u.a.], 1985.
5. Elias, P. E. The intercorneocyte space. In *Stratum corneum*, Marks, R.; Plewig, G., Eds., Springer: Berlin [u.a.], 1983; pp XI, 265 S.
6. Barry, B. W. Novel mechanisms and devices to enable successful transdermal drug delivery. *Eur. J. Pharm. Sci.* **2001**, 14, 101-114.
7. Bouwstra, J. A.; Honeywell-Nguyen, P. L.; Gooris, G. S.; Ponec, M. Structure of the skin barrier and its modulation by vesicular formulations. *Prog. Lipid Res.* **2003**, 42, 1-36.
8. Scheuplein, R. J.; Blank, I. H. Permeability of the skin. *Physiol. Rev.* **1971**, 51, 702-747.
9. OECD Guidelines for the Testing of Chemicals. In *Test No. 428: Skin Absorption: In Vitro Method*, Development, O. f. E. C.-o. a., Ed. 2010; Vol. 1, pp 1-8.
10. Franz, T. J. Percutaneous absorption on the relevance of in vitro data. *J. Invest. Dermatol.* **1975**, 64, 190-195.
11. Bronaugh, R. L.; Stewart, R. F. Methods for in vitro percutaneous absorption studies IV: The flow-through diffusion cell. *J. Pharm. Sci.* **1985**, 74, 64-67.
12. Godin, B.; Touitou, E. Transdermal skin delivery: predictions for humans from in vivo, ex vivo and animal models. *Adv. Drug Del. Rev.* **2007**, 59, 1152-1161.
13. Lotte, C.; Hinz, R. S.; Rougier, A.; Guy, R. H. A reconstructed skin model (Test-skin^{TM} LSE^{TM}) for permeation studies. In *Perspectives in percutaneous penetration*, Brain, K. R.; James, V. J.; Walters, K. A., Eds., STS Publishing: Cardiff, UK, 1997.
14. Marty, P.; Faure, C.; Laroche, F.; Farenc, C. Assessment of human skins obtained by in vitro culture as membrane models for cutaneous permeation tests. In *Perspectives in percutaneous penetration*, Brain, K. R.; James, V. J.; Walters, K. A., Eds., STS Publishing: Cardiff, UK, 1997.
15. Monteiro-Riviere, N. A.; Inman, A. O.; Snider, T. H.; Blank, J. A.; Hobson, D. W. Comparison of an in vitro skin model to normal human skin for dermatological research. *Microsc. Res. Tech.* **1997**, 37, 172-179.
16. Huong, S. P.; Bun, H.; Fourneron, J. D.; Reynier, J. P.; Andrieu, V. Use of various models for in vitro percutaneous absorption studies of ultraviolet filters. *Skin Res. Technol.* **2009**, 15, 253-261.
17. Roskos, K. V.; Maibach, H. I.; Guy, R. H. The effect of aging on percutaneous absorption in man. *J. Pharmacokinet. Biopharm.* **1989**, 17, 617-630.
18. Jacobi, U.; Gautier, J.; Sterry, W.; Lademann, J. Gender-related differences in the physiology of the stratum corneum. *Dermatology* **2005**, 211, 312-317.
19. Lotte, C.; Wester, R. C.; Rougier, A.; Maibach, H. I. Racial differences in the in vivo percutaneous absorption of some organic compounds: a comparison between black, Caucasian and Asian subjects. *Arch. Dermatol. Res.* **1993**, 284, 456-459.
20. *European Pharmacopoeia*. 7th ed.; Council of Europe: Strasbourg, 2011.
21. Frömming, K.-H.; Szejtli, J. *Cyclodextrins in pharmacy*. Kluwer Acad. Publ.: Dordrecht [u.a.], 1994; p VIII, 224 S.
22. Loftsson, T.; Jarho, P.; Masson, M.; Jarvinen, T. Cyclodextrins in drug delivery. *Expert Opin. Drug Deliv.* **2005**, 2, 335-351.
23. Baka, E.; Comer, J. E.; Takacs-Novak, K. Study of equilibrium solubility measurement by saturation shake-flask method using hydrochlorothiazide as model compound. *J. Pharm. Biomed. Anal.* **2008**, 46, 335-341.
24. Rote-Liste-Service; Bundesverband der Pharmazeutischen Industrie. *ROTE LISTE® 2009 : Arzneimittelverzeichnis für Deutschland (einschließlich EU-Zulassungen und bestimmter Medizinprodukte)*. Verl. Rote Liste: Frankfur/Main, 2009; p Getr. Zählung +.
25. Easthope, S. E.; Jarvis, B. Candesartan cilexetil: an update of its use in essential hypertension. *Drugs* **2002**, 62, 1253-1287.

26. Chu, I.; Dick, D.; Bronaugh, R.; Tryphonas, L. Skin reservoir formation and bioavailability of dermally administered chemicals in hairless guinea pigs. *Food Chem. Toxicol.* **1996**, 34, 267-273, 275-276.
27. Miselnicky, S. R.; Lichtin, J. L.; Sakr, A.; Bronaugh, R. L. The Influence of Solubility, Protein-Binding, and Percutaneous-Absorption on Reservoir Formation in Skin. *J. Soc. Cosmet. Chem.* **1988**, 39, 169-177.
28. Williams, P. E.; Brown, A. N.; Rajaguru, S.; Francis, R. J.; Walters, G. E.; McEwen, J.; Durnin, C. The pharmacokinetics and bioavailability of cilazapril in normal man. *Br. J. Clin. Pharmacol.* **1989**, 27 Suppl 2, 181S-188S.
29. Simon, G. A.; Maibach, H. I. Relevance of Hairless Mouse as an Experimental Model of Percutaneous Penetration in Man. *Skin Pharmacol. Physiol.* **1998**, 11, 80-86.
30. Jain, P.; Banga, A. K. Inhibition of crystallization in drug-in-adhesive-type transdermal patches. *Int. J. Pharm.* **2010**, 394, 68-74.
31. Thomas, B. J.; Finnin, B. C. The transdermal revolution. *Drug Discov. Today* **2004**, 9, 697-703.
32. Leichtnam, M. L.; Rolland, H.; Wuthrich, P.; Guy, R. H. Enhancement of transdermal testosterone delivery by supersaturation. *J. Pharm. Sci.* **2006**, 95, 2373-2379.
33. Thasler, W. E.; Weiss, T. S.; Schillhorn, K.; Stoll, P. T.; Irrgang, B.; Jauch, K. W. Charitable State-Controlled Foundation Human Tissue and Cell Research: Ethic and Legal Aspects in the Supply of Surgically Removed Human Tissue For Research in the Academic and Commercial Sector in Germany. *Cell. Tissue. Bank.* **2003**, 4, 49-56.
34. Romeis, B.; Boeck, P. *Mikroskopische Technik*. 17., neubearb. Aufl. ed.; Urban & Schwarzenberg: Muenchen [u.a.], 1989; p 697 S.

Chapter 6
Exploring the Toxic Potential of N^G-Acylated Hetarylpropylguanidines – Trapping of Reactive Metabolites

6.1 Introduction

6.1.1 Trapping of reactive metabolites

Although the link between the formation of reactive drug metabolite-protein adducts and drug-induced toxicity is neither well-defined nor consistent, it is widely accepted that these processes may be causally related.[1-2] Thus, a few strategies have been established enabling the identification of compounds that bear the potential for bioactivation at an early stage of preclinical drug development to avoid economic risks associated with pursuing the development of a drug with apparent safety issues. Typically, these approaches involve the use of small molecule trapping agents capable of covalently binding to reactive metabolites generated by hepatic subcellular fractions in the presence of cytochrome P450 enzymes and cofactor NADPH. The resulting stable adduct should be amenable to analytical characterization.[2]

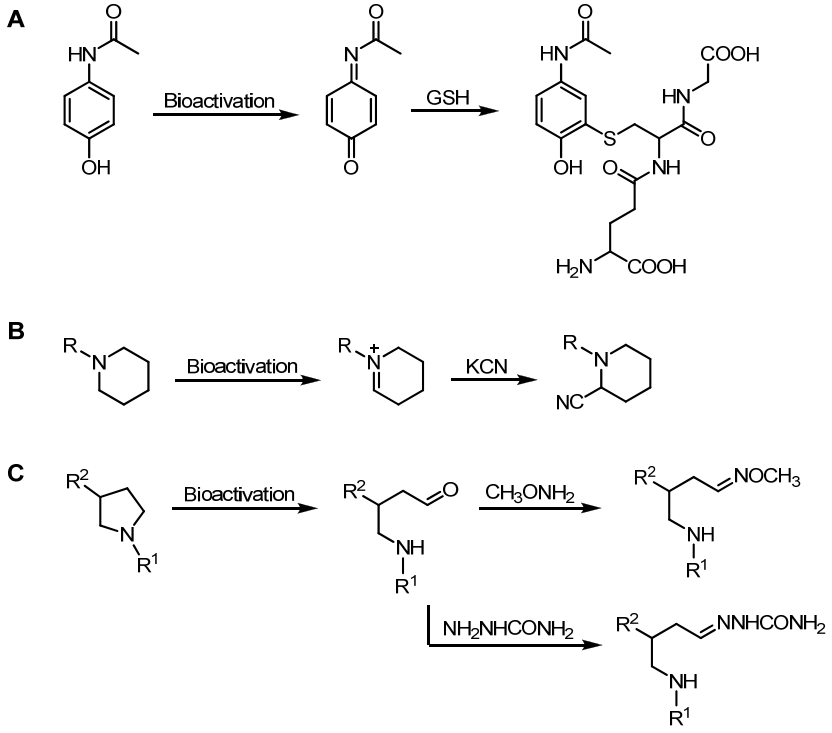

Scheme 6.1. Examples of reactions of trapping agents with reactive metabolites: trapping of a quinoneimine by glutathione (GSH) (**A**), of an iminium ion by cyanide (**B**) and of an aldehyde by methoxylamine or semicarbazide (**C**). Adapted from Ma[3] and Argikar[4].

Due to the electrophilic nature of most reactive metabolites, appropriate nucleophilic trapping agents, espacially thiol-containing nucleophiles, as the endogenous tripeptide glutathione (GSH) (Scheme 6.2), are most frequently used and commonly applied for early screening. GSH is particularly useful for the reaction with various soft electrophiles (e.g. Michael acceptors or epoxides) (Scheme 6.1 A), but for trapping of hard nucleophiles like iminium ions or nitrons a hard nucleophile, such as cyanide, is more effective (Scheme 6.1 B).[4-5] In addition, reactive aldehydes are capable of reacting with methoxylamine or semicarbazide *via* a Schiff base-reaction (Scheme 6.1 C).[2]

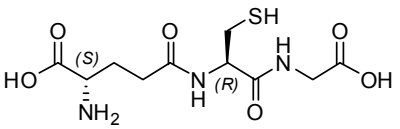

Scheme 6.2. Chemical structure of glutathione (GSH).

Further screening for reactive metabolites may include the synthesis of a radiolabeled analogue of the compound to perform *in vitro* covalent binding studies in liver microsomal or hepatocyte preparations from laboratory animals and humans, or also *in vivo*, typically in the rat.[2]

6.1.2 Glutathione (GSH)

The tripeptide glutathione (γ-glutamylcysteinylglycine) is the most abundant intracellular small molecule thiol, reaching concentrations up to 10 mM[6] in the liver.[7] It is kept in its reduced thiol form by glutathione disulfide (GSSG) reductase.[8] As a potent antioxidant it plays a major role in the maintenance of a reductive cellular environment. Furthermore, it is involved in the detoxification of a variety of endogenous and exogenous electrophilic compounds and peroxides. Its cysteine sulfhydryl group is capable of reacting with electrophilic species non-enzymatically or *via* catalysis by glutathione S-transferases (GST) and glutathione peroxidases (GPx). In addition, GSH is known to play a role in various cellular processes, including the regulation of protein and gene expression.[7]

6.1.3 LC/MS analysis of reactive metabolite-GSH adducts

The detection of reactive metabolite-GSH adducts is commonly based on the analysis by liquid chromatography/ tandem mass spectrometry (LC-MS). Traditionally, a triple quadrupole mass spectrometer is used, allowing the performance of several types of experiments (Figure 6.1). Besides, a full scan to search for putative glutathione adducts, a constant neutral loss (CNL) scanning for 129 mass units in the positive ion mode proved to be particularly useful, since glutathione conjugates, when frag-

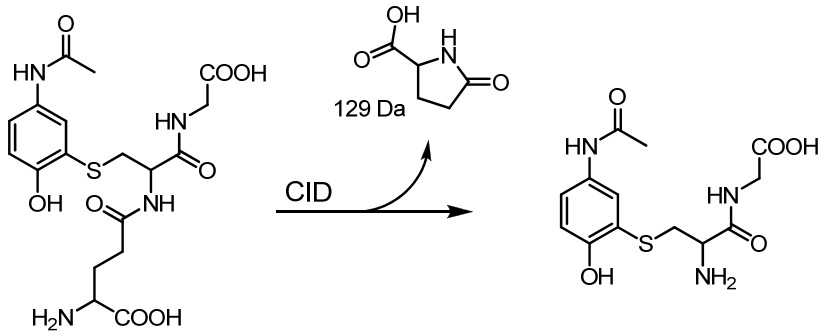

Scheme 6.3. Example of constant neutral loss for a glutathione conjugate of acetaminophene loosing a pyroglutamic acid moiety with the corresponding mass of 129 Da on CID.

mented under collision induced dissociation (CID), can give a characteristic loss of a neutral fragment of 129 Da corresponding to the pyroglutamic acid moiety (Scheme 6.3).[9] Nevertheless, one should be aware that this technique suffers from poor selectivity, as on CID endogenous compounds present in biological matrices may undergo a loss of 129 Da, which is not glutathione-conjugate related, resulting in the detection of false positive CNL signals.[3] To enhance selectivity, multiple reaction monitoring (MRM) can be performed to follow either one or usually more specific mass transitions of a putative adduct induced by CID. Furthermore, a characteristic product ion scan (MS/MS spectrum) can provide additional information about the molecular structure of the trapped reactive metabolite.

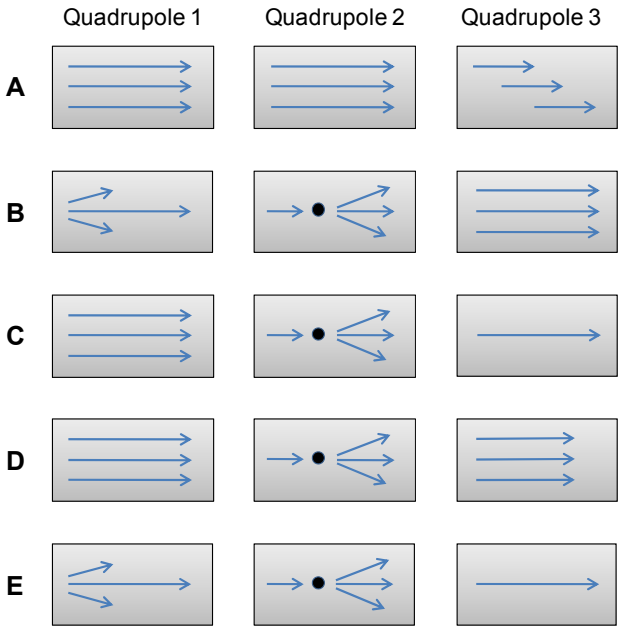

Figure 6.1. Schematic representation of common types of MS/MS experiments performed on a triple quadrupole (TQ) MS. **A**: full scan (Q1-Q3: scan), **B**: product ion scan = MS/MS (Q1: selecting m/z, Q2: CID, Q3: scanning), **C**: precursor ion scan (Q1: scanning, Q2: CID, Q3: scanning selected *m/z*), **D**: constant neutral loss (CNL) scan (Q1: scanning, Q2: CID, Q3: scanning neutral loss), **E**: multiple reaction monitoring (MRM) (Q1: selecting m/z, Q2: CID, Q3: scanning selected *m/z*).

Other LC-MS/MS-based techniques for the identification of GSH adducts include precursor ion scanning of an anion fragment at *m/z* 272 in the negative ionization mode[10], the use of stable isotope labeled GSH[11] and the use of high resolution mass spectrometry-based mass defect filtering[12].

6.2 Reactive metabolites of N^G-acylated hetarylpropylguanidines

N^G-acylated hetarylpropylguanidines as N^G-acylated imidazolylpropylguanidines and N^G-acylated 2-aminothiazolylpropylguanidines are potent histamine H_2 receptor agonists.

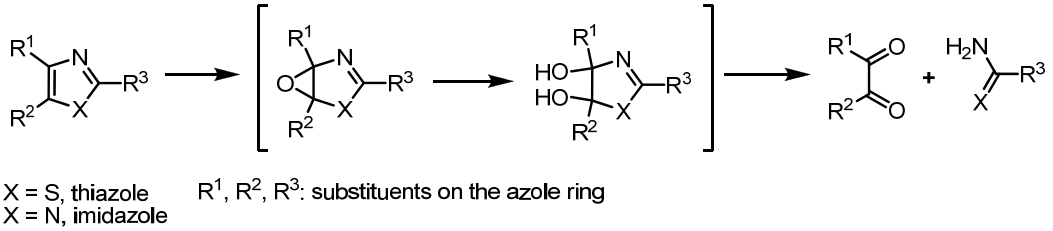

Scheme 6.4. General mechanism of oxidative ring opening of azoles. Adapted from Dalvie.[13]

Due to their improved pharmacokinetic properties (oral bioavailability, CNS penetration) relative to the corresponding strongly basic N^G-alkylated analogues the acylguanidines are valuable pharmacological tools for *in vitro* and potential *in vivo* studies.[14] Hence, the identification of their toxic potential is obvious. It is known that biotransformation of heterocycles such as imidazole and thiazole through cytochrome P450-mediated oxidative ring opening can result in toxic metabolites (e.g. thioamide) and compounds capable of generating covalent adducts with biological nucleophiles (Scheme 6.4).[13] Furthermore, there is strong evidence that the bioactivation of the 2-aminothiazole ring results in highly reactive intermediates capable of forming adducts with critical biomacromolecules (Scheme 6.5).[15]

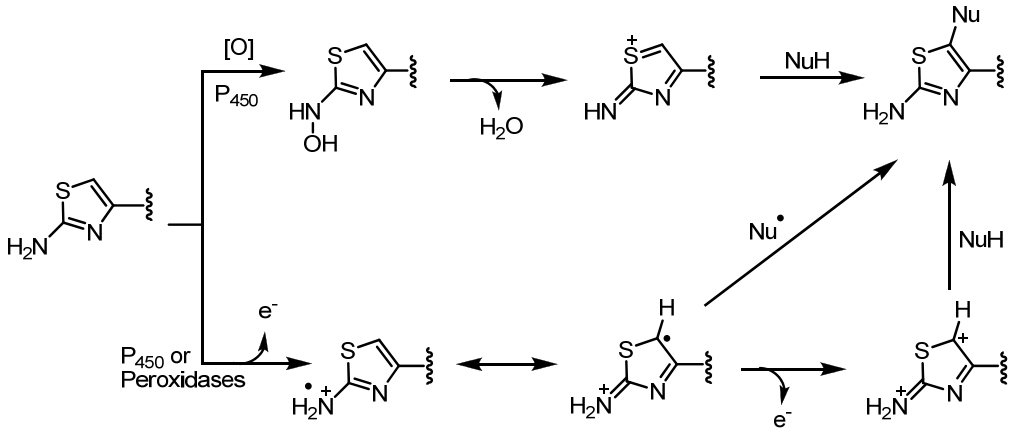

Scheme 6.5. Proposed mechanism for the bioactivation of the 2-aminothiazole motif. NuH refers to e.g. a protein nucleophile or GSH. Adapted from Kalgutkar.[15]

In view of the great potential of N^G-acylated hetarylpropylguanidines with regard to pharmacological studies and potential therapeutic use, representative N^G-acylated 2-aminothiazol-5-ylpropylguanidines are studied with respect to the formation of reactive intermediates by incubation of the respective substance with rat liver microsomes in the presence of GSH as a trapping agent for electrophilic reactive metabolites. Subsequently, putative covalent GSH adducts are analyzed by appropriate LC-MS/MS experiments such as CNL scanning, MRM and product ion scanning.

In order to explore the suitability of this method for determination of unknown GSH adducts a proof of concept study was performed using diclofenac as model substrate.

6.2.1 Proof of concept study – Determination of reactive metabolites of diclofenac by GSH trapping and LC-MS/MS analysis

Diclofenac, a non-steroidal anti-inflammatory drug, causes rare, but severe cases of hepatotoxicity. It is known that P450-mediated oxidative metabolism of diclofenac leads to the formation of highly reactive 1',4'-quinone imine and 2,5-quinone imine intermediates capable of covalently binding to proteins causing liver injury.[16]

The purpose of this study was to detect reactive metabolites from a GSH trapping assay in rat liver microsomes by applying a triple quadrupole LC-MS/MS system. So far, four GSH adducts from diclofenac are reported in the literature (Scheme 6.6).[16-17]

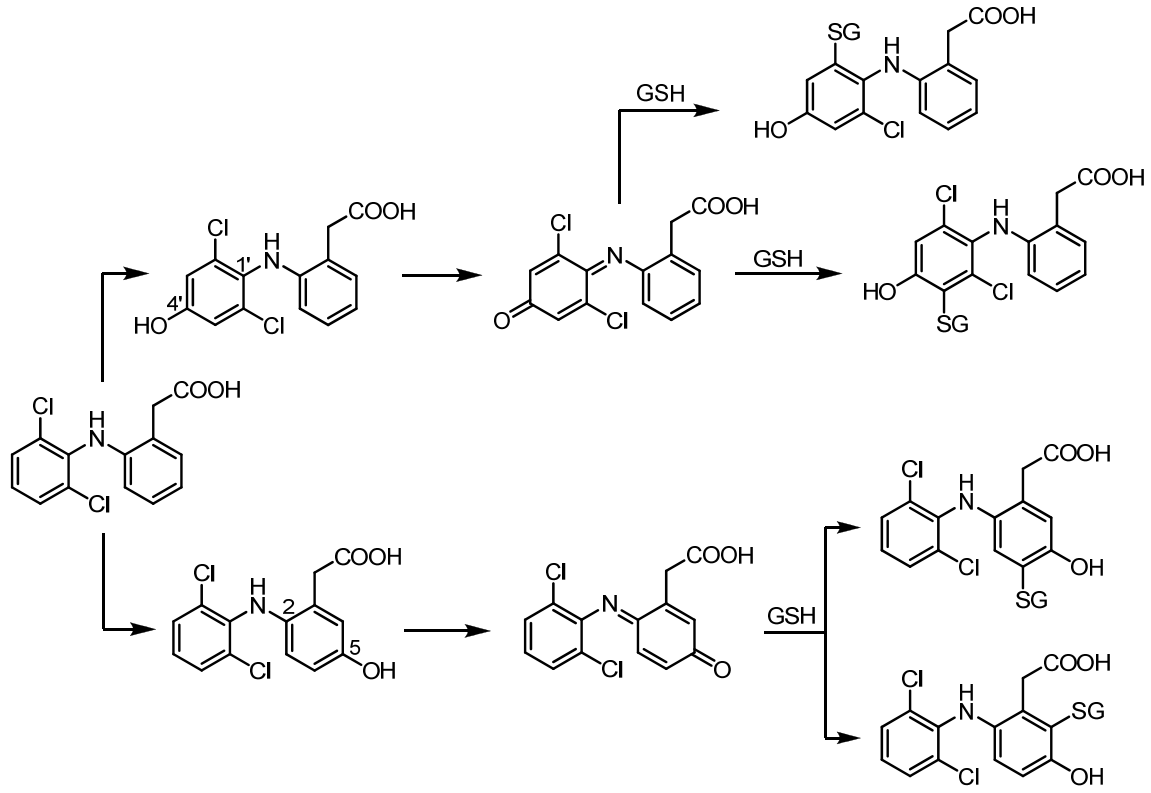

Scheme 6.6. Proposed bioactivation pathway of diclofenac, showing the formation of reactive quinone imine intermediates and GSH conjugates.

6.2.1.1 Method

In brief, diclofenac was incubated in 0.1 M potassium phosphate buffer, pH 7.4, in the presence of rat liver microsomes, GSH and a NADPH regenerating system for 17 h at 37 °C. After quenching of the reaction with ice cold acetonitrile, precipitated proteins were removed by centrifugation. The supernatant was concentrated, reconstituted in mobile LC phase and analyzed by LC-MS/MS.

6.2.1.2 Results

Four GSH-containing adducts of diclofenac are reported in the literature: 4'-OH-2'-glutathion-deschloro-diclofenac (4'-OH-2'-GS-DDF, exact mass: 582)[16] as well as three constitutional isomers 5-OH-4-GS-DF, 5-OH-6-GS-DF and 4'-OH-3'-GS-DF (exact mass: 616)[18] (cf. Scheme 6.6). Figure 6.2 shows a full scan of a microsomal incubation mixture containing diclofenac. In accordance with the literature, the extracted ion chromatograms at *m/z* 583 and *m/z* 617 revealed the presence of four distinct GSH adducts (A1-A4), all of them exhibiting the characteristic one-chlorine or two-chlorine isotope cluster (MS not shown). Furthermore, a potential diclofenac phase-I metabolite (A5), presumably derived from ring oxidation in 5 or 4'-position, was detected showing a corresponding *m/z* 312 (Figure 6.2 D). Unfortunately, CNL scanning at *m/z* 129 for the characteristic loss of pyroglutamic acid failed to yield the expected corroboration of the full scan results (cf. Figure 6.3), as the intensity of the obtained CNL signals was too weak to selectively detect all proposed GSH-containing adducts A1-A4. However, selectivity as well as sensitivity could be remarkably increased by an LC-MRM/MS experiment monitoring specific mass transitions of putative GSH adducts (Figure 6.4). Besides the observation of the loss of pyroglutamic acid (-129 Da), CID induced fragmentation of glycine from the GSH residue corresponding to a loss of 75 Da turned out to be a useful marker of GSH-containing adducts. Thus, by monitoring two discrete mass transitions characteristic of GSH-derived metabolites the presence of the glutathionyl moiety in A1 to A4 becomes very likely.

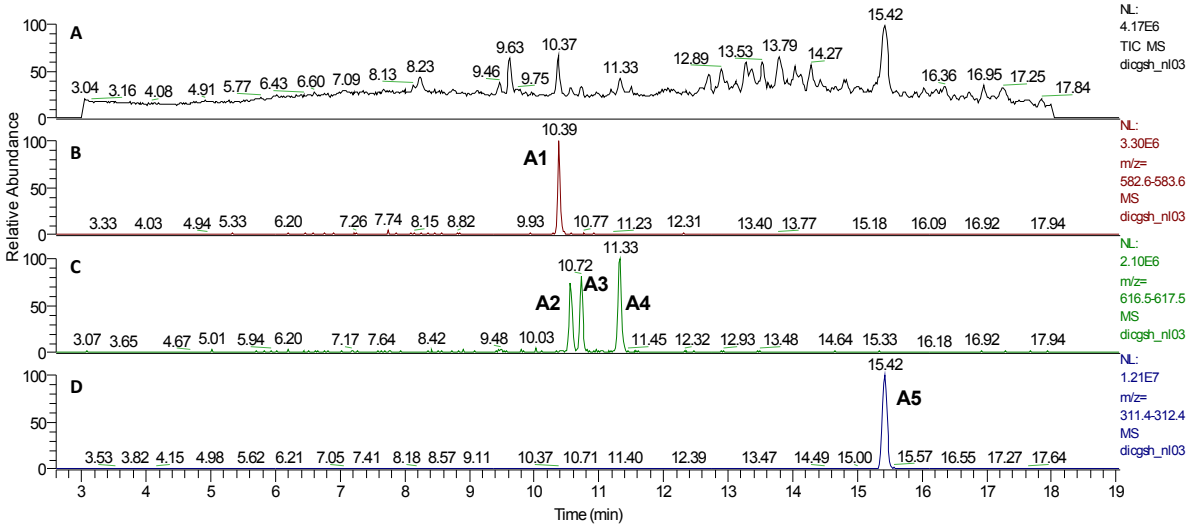

Figure 6.2. Full scan TIC of a microsomal incubation mixture containing diclofenac, GSH and a NADPH-regenerating system (**A**). Extracted ion chromatograms (MH^+) of GSH-containing adducts A1 at *m/z* 583 (**B**) and of A2, A3 and A4 at *m/z* 617 (**C**) and of the oxidized diclofenac metabolite A5 at *m/z* 312 (**D**).

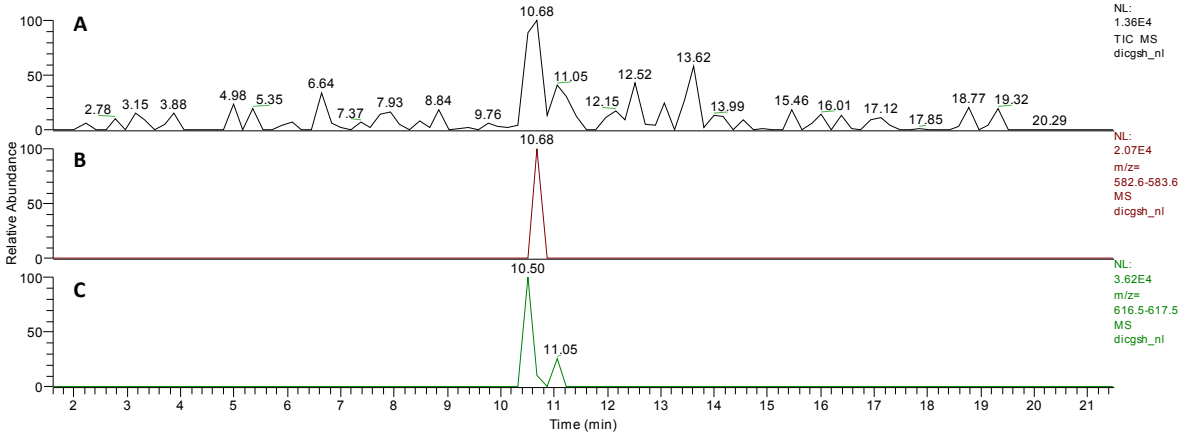

Figure 6.3. CNL scanning (129 Da) of GSH adducts generated by microsomal incubation of diclofenac with GSH and a NADPH-generating system on a triple quadrupole instrument. **A**: TIC of the CNL scanning of a diclofenac incubation sample. **B**, **C**: Extracted ion chromatograms (MH^+) at *m/z* 583 and 617, respectively.

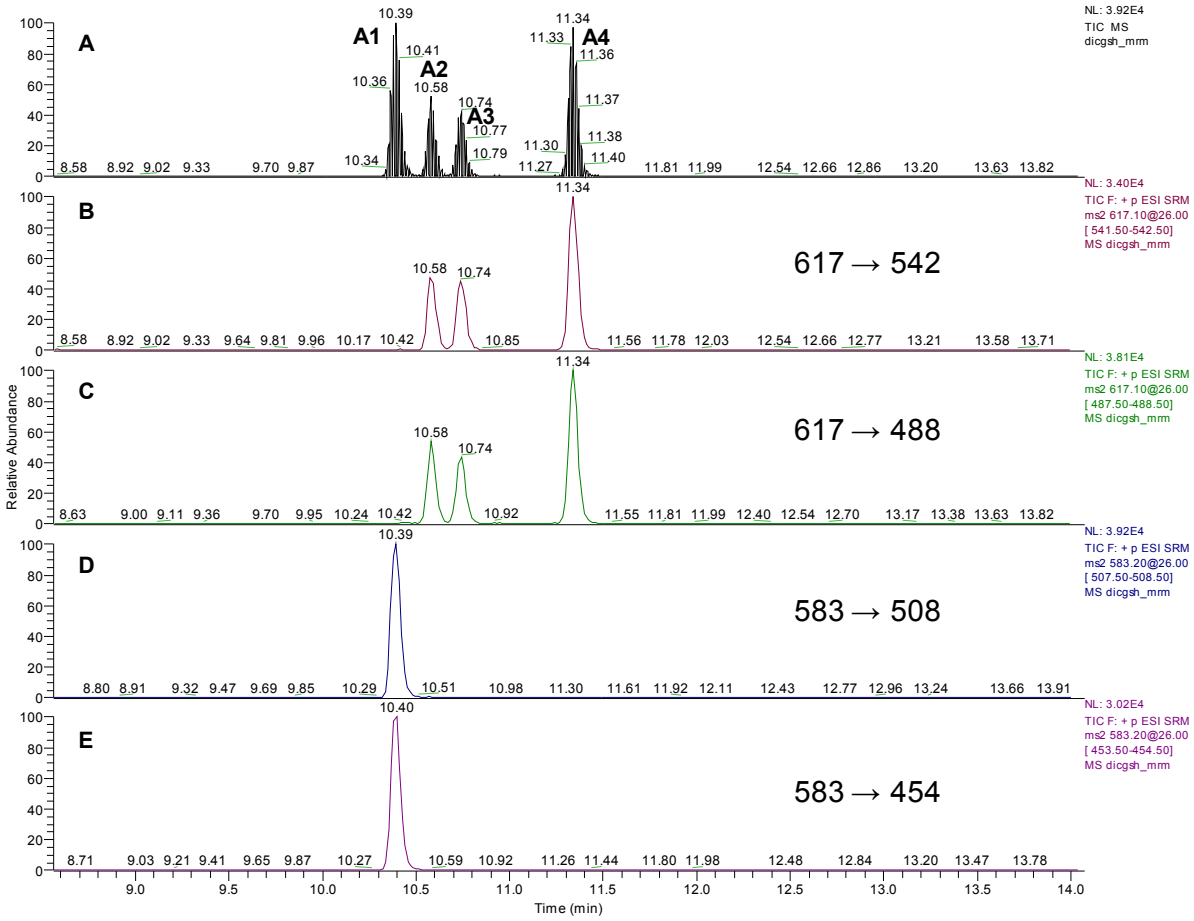

Figure 6.4. TIC of the LC-MRM/MS of four GSH-containing metabolites of diclofenac (A1-A4) generated by microsomal incubation with GSH and a NADPH-generating system (**A**). MRM chromatograms for *m/z* 617→542 (**B**), *m/z* 617→488 (**C**), *m/z* 583→508 (**D**) and *m/z* 583→454 (**E**).

Further confirmation of the proposed reactive metabolites trapped by glutathione could be achieved by product ion scans. Thus, CID of A1 produced product ions at *m/z* 508 by loss of glycine, at *m/z* 454 by fragmentation of pyroglutamate and *m/z* 436 by subsequent loss of water (Figure 6.5 A). Beside the characteristic elimination of glycine

and pyroglutamate the MS/MS spectrum of A4 showed product ions at *m/z* 313 and 342, respectively, derived from the fragmentation of the complete glutathionyl moiety and γ-glutamyl-dehydroalanyl-glycine, respectively (Figure 6.5 B).

6.2.1.3 Conclusion

In summary, four GSH adducts of diclofenac formed, in a rat microsomal incubation mixture *in vitro,* were identified by triple quadrupole LC-MS/MS. The combination of full scan, constant neutral loss scanning, multiple reaction monitoring and product ion scanning proved to be a successful strategy for the identification of GSH adducts. Thus, the method is considered appropriate for detection of GSH adducts formed by trapping of potential reactive intermediates of N^G-acylated 2-aminothiazolylpropylguanidines.

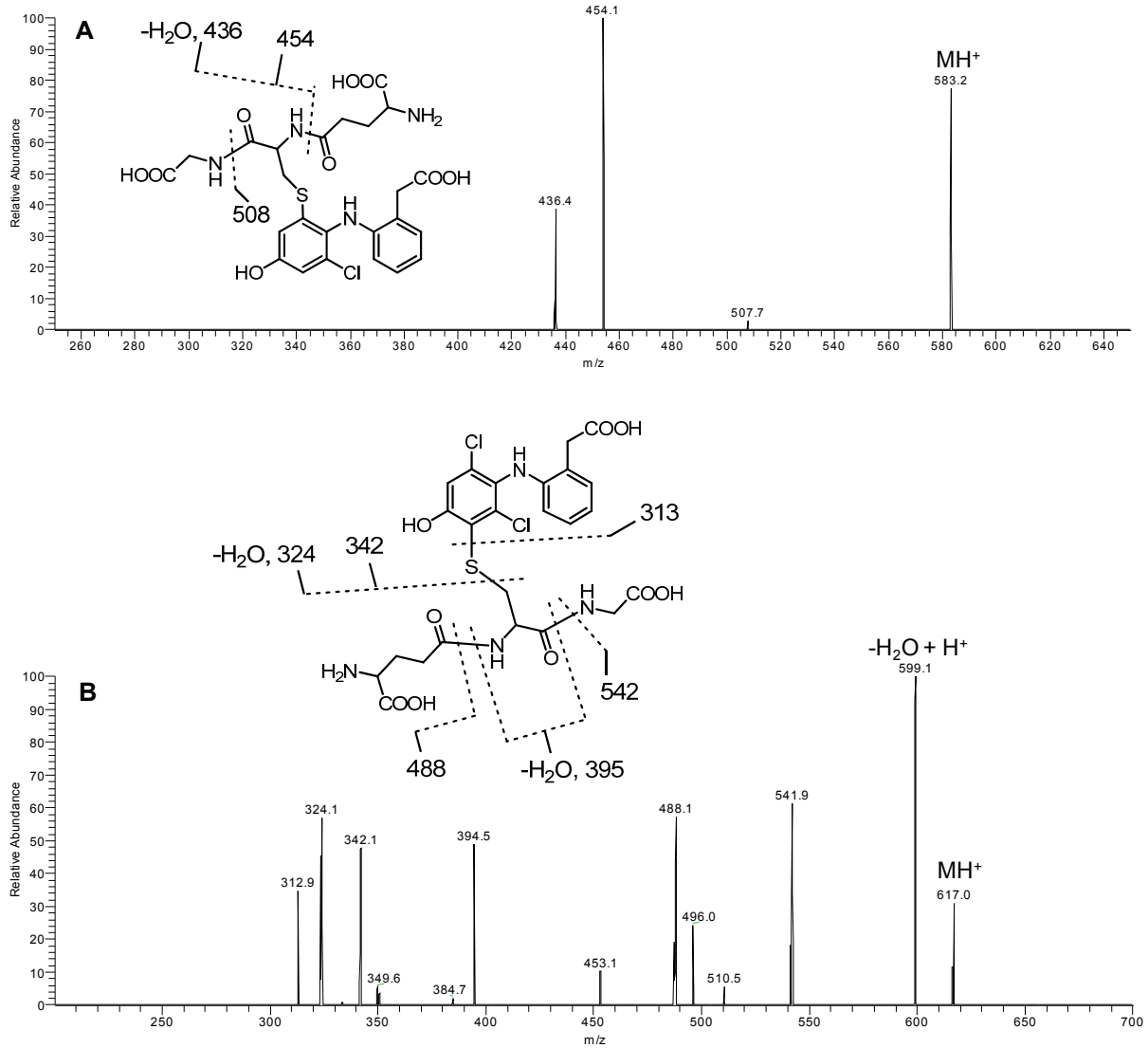

Figure 6.5. TQ LC-MS/MS product ion spectra of GSH adducts A1 (**A**) and A4 (**B**) detected in microsomal incubation mixture of diclofenac supplemented with GSH. The proposed origins of key fragment ions are indicated and refer to monoprotonated species.

6.2.2 Determination of reactive metabolites of 3-(2-aminothiazol-5-yl)-propylguanidines and 3-(2-amino-4-methylthiazol-5-yl)propylguanidines by GSH trapping and LC-MS/MS analysis

6.2.2.1 Aminothiazolylpropylguanidines

For the investigation of the potential bioactivation of 2-aminothiazolylpropylguanidines two compounds of rather "simple" chemical structures (**6.1** and **6.2**, synthesized in our laboratory by Dr. A. Kraus[19]) were chosen as examples to minimize the probability of metabolic attacks at moieties other than the heterocycle (Scheme 6.7). The initial consideration to use the free guanidine (1-[3-(2-aminothiazol-5-yl)propyl]guanidine) as a model substrate for microsomal incubation was not pursued, since the lower polarity of acylguanidines entailed marked advantages in terms of analyzability on a RP-LC column. The analyte is detected at longer retention times, where less noise (e.g. caused by buffer salts) is present.

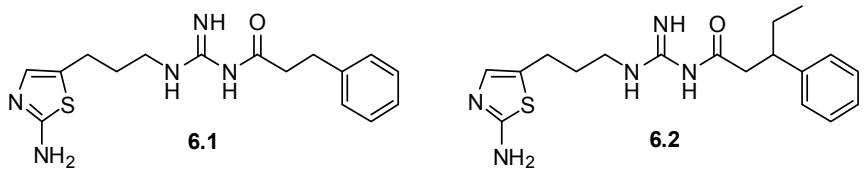

Scheme 6.7. Structures of two 2-aminothiazolylpropylguanidines used for bioactivation studies.

Method

The incubation of the substances **6.1** and **6.2** was carried out according to procedure 6.2.1.1, but the incubation period was reduced to 2 h.

Results

Figure 6.6 A displays the full scan base peak chromatogram of the supernatant of a microsomal incubation of **6.1** containing GSH and a NADPH-regenerating system. A recorded UV profile at 210 nm did not provide any additional information due to insufficient sensitivity, and is therefore not shown. Interestingly, no parent compound was detected after 2h of microsomal incubation. LC-MS/MS screening for potential GSH-containing adducts was performed by CNL scanning for the loss of 129 Da upon CID and in fact, led to the detection of a putative GSH adduct (B1, t_R ~ 24.9 min) at *m/z* 637 (MH^+) (Figure 6.6 B+C). Besides B1 a second CNL signal was detected at t_R ~ 11.1 min corresponding to oxidized glutathione (glutathione disulfide, GSSG, *m/z* 613 (MH^+)), which derived from GSH during incubation and/or sample preparation.

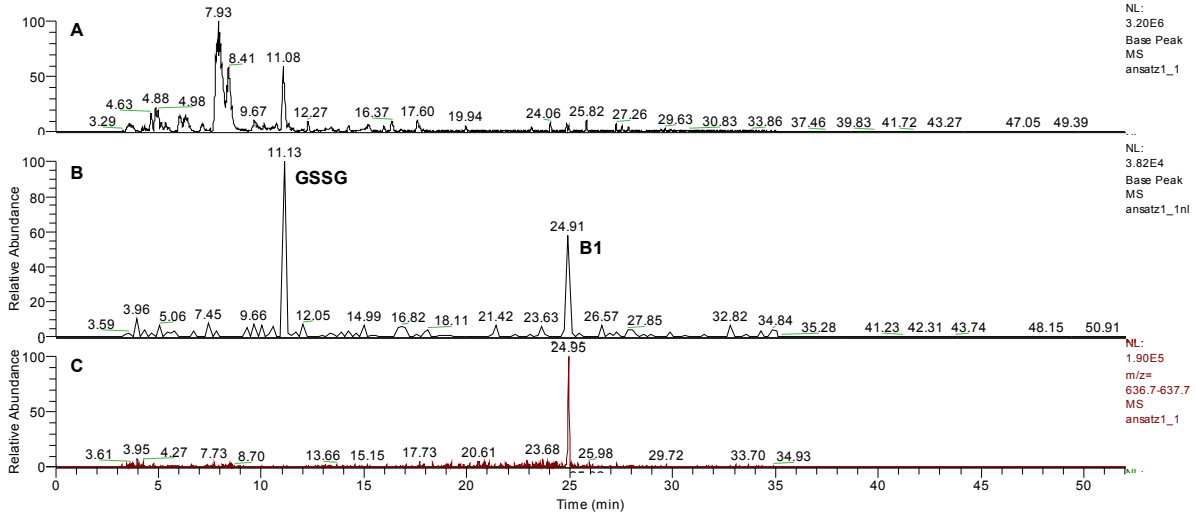

Figure 6.6. TQ LC-MS/MS analysis of a microsomal incubation mixture containing **6.1**, GSH and a NADPH-regenerating system. **A**: Full scan base peak chromatogram. **B**: CNL scanning of *m/z* 129. **C**: Full scan extracted ion chromatogram of B1 at *m/z* 637 (MH^+).

The susceptibility of the 2-aminothiazole ring to bioactivation and subsequent GSH addition is known from the literature.[15, 20] Therefore, in case of the bioactivated histamine H_2 receptor agonists, the GSH moiety is most likely attached to the aminothiazole, although the exact regiochemistry of the addition is unknown. The proposed bioactivation pathway for **6.1** is shown in Scheme 6.8 and is assumed to involve either a cytochrome P450-mediated epoxidation (A) or a ring oxidation resulting in an electrophilic reactive intermediate (B). Both intermediates are assumed to readily undergo nucleophilic trapping reactions with glutathione. Epoxide ring opening by GSH in 4-position of the aminothiazole is supposed to be preferred, since nucleophilic attack in 5-position is sterically hindered and does not lead to an energetically favored aromatic ring system. Thus, pathway B is also assumed to be rather unlikely.

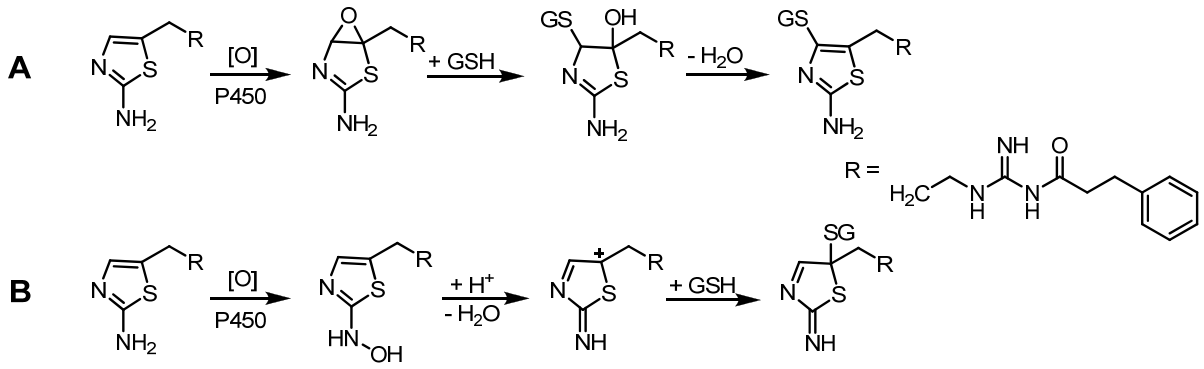

Scheme 6.8. Proposed bioactivation pathway of the 2-aminothiazolylpropylguanidine **6.1**.

Further characterization of the proposed GSH adduct B1 was achieved by subsequent product ion scanning of the MH^+ ion at *m/z* 637 and revealed two major fragment ions at *m/z* 508 and 364 corresponding to a neutral loss of 129 Da, consistent with the loss of pyroglutamic acid, and to the fragmentation of γ-glutamyl-dehydroalanyl-glycine, respectively (Figure 6.7).

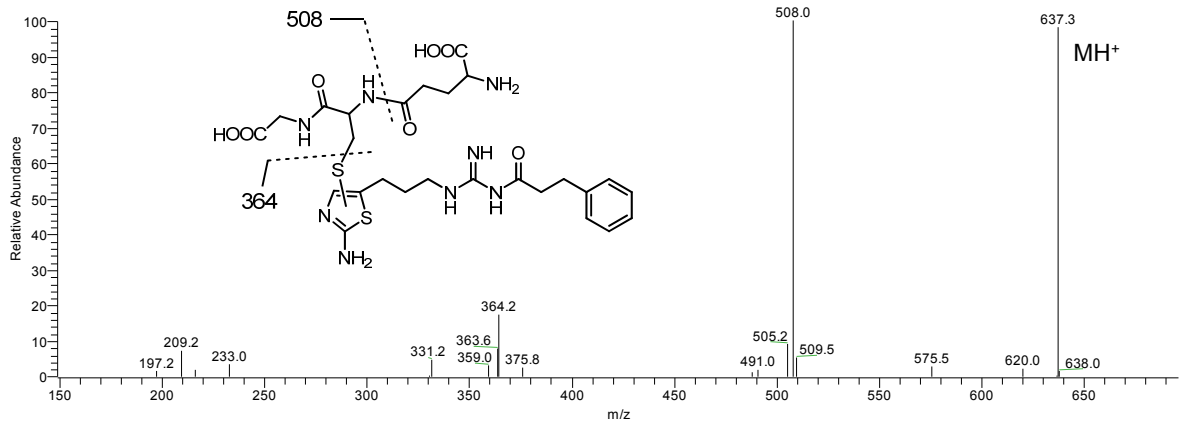

Figure 6.7. TQ LC-MS/MS product ion spectrum of the proposed GSH adduct B1 derived from a microsomal incubation of **6.1** supplemented with GSH. The proposed origins of key fragment ions are as indicated and refer to monoprotonated species. The exact regiochemistry of the GSH addition is unknown.

Additionally, four potential phase I metabolites (B2-B5) were detected with ions at *m/z* 348 consistent with monohydroxylated metabolites of **6.1** (cf. Figure 6.8). Unfortunately, product ion scans of B2-B5 did not provide more detailed information about the attachment site of the OH group. However, oxidation in various positions of the phenyl ring seems plausible.

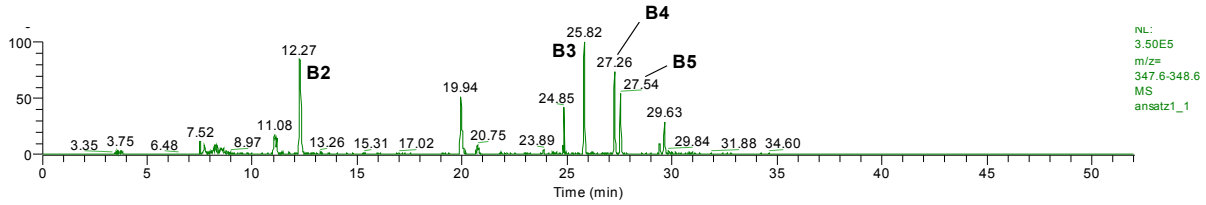

Figure 6.8. Full scan extracted ion chromatogram of a microsomal incubation mixture containing **6.1**, GSH and a NADPH-regenerating system at *m/z* 348 (MH^+) depicting four potential oxidized metabolites (B2-B5) of **6.1**. Unlabeled peaks do not exhibit a molecular ion at *m/z* 348.

To explore the dependence of bioactivation on the presence of cytochrome P450 enzymes, an incubation sample of **6.1** was analyzed, in which rat liver microsomes were replaced with a respective volume of phosphate buffer (Figure 6.9). In fact, in the absence of rat liver microsomes biotransformation of **6.1** (t_R ~ 24.3 min) was not observed. Hence, neither the GSH adduct B1 nor the putative hydroxylated metabolites B2-B5 were detected, suggesting that their formation is P450-dependent.

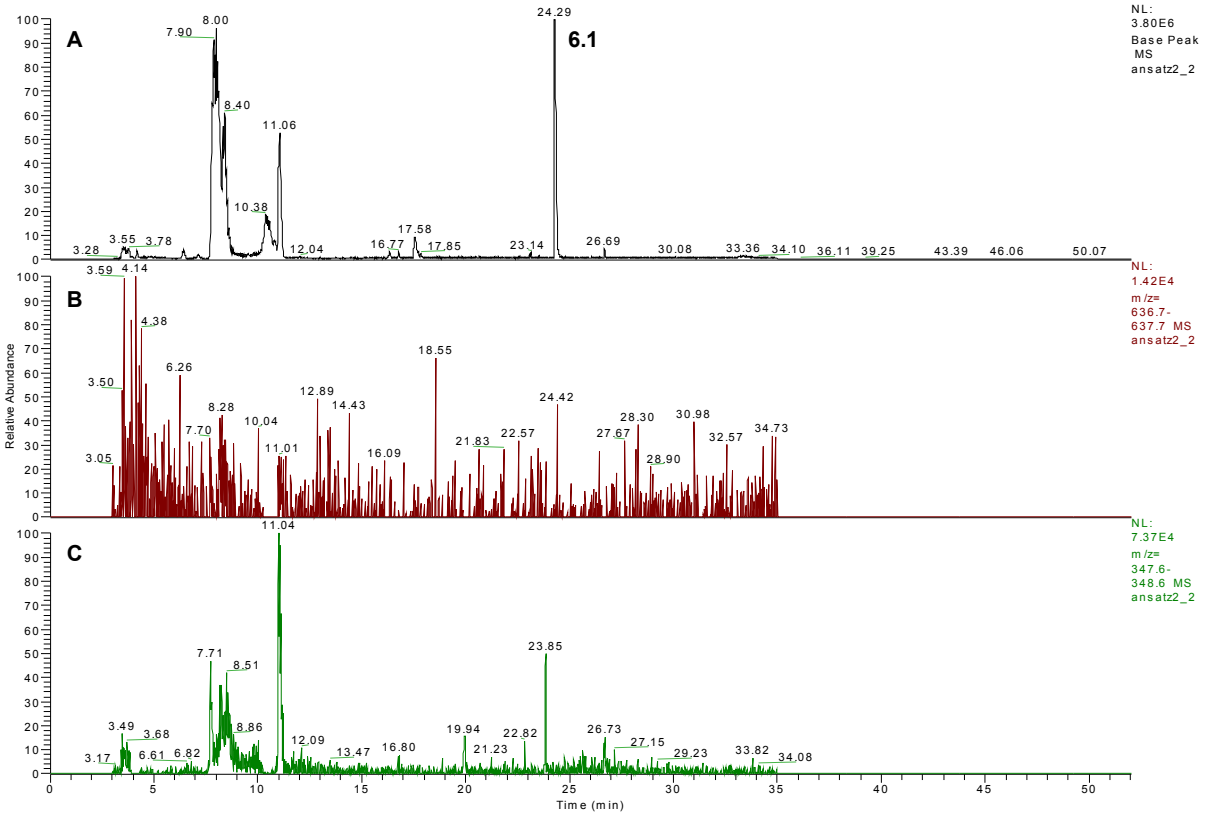

Figure 6.9. TQ LC-MS/MS analysis of an incubation mixture of **6.1** devoid of rat liver microsomes, supplemented with GSH and a NADPH-regenerating system. **A**: Full scan base peak chromatogram showing the parent compound **6.1** at t_R ~ 24.3 min. **B**, **C**: Full scan extracted ion chromatograms at *m/z* 637 and 348, respectively confirming the absence of B1-B5.

Strikingly, the sum of the peak areas of all potential **6.1**-derived metabolites in Figure 6.6 A turned out to be considerably smaller than the peak area of **6.1** detected in an incubation sample devoid of microsomes (Figure 6.9 A). This may be caused by high unspecific or covalent protein binding of **6.1** and/or **6.1**-derived metabolites, presumably resulting in a loss of (detectable) substance during protein precipitation and separation. Plasma protein binding (PPB) studies with various N^G-acylated hetarylpropylguanidines using bovine serum albumin indeed indicated a high unspecific PPB, which amounted to 79 % for **6.1** (in-house communication).

In Figure 6.10 the base peak chromatogram of a microsomal incubation sample of **6.2** containing GSH and a NADPH-regenerating system (**A**) as well as the TIC of a control sample devoid of microsomes (**B**) are shown. Apparently, the recovery of **6.2** compared to **6.1** was higher, although the experimentally determined PPB was actually increased (87 %, in-house communication).

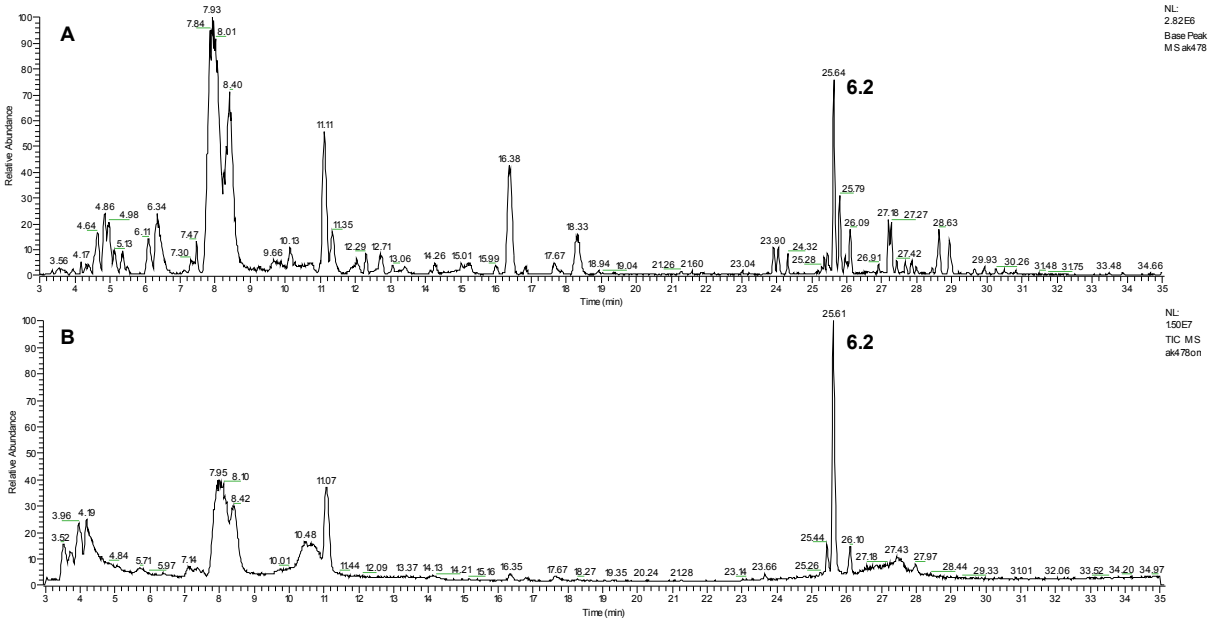

Figure 6.10. A: Full scan base peak chromatogram of **6.2** coincubated with GSH and a NADPH-regenerating system in rat liver microsomes. **B**: Full scan TIC of the negative control sample devoid of rat liver microsomes.

Screening of the full scan data set of the **6.2**-containing microsomal incubation mixture for trapping of reactive intermediates by GSH revealed the presence of a potential GSH adduct (C1) at t_R ~ 26.0 min with a pseudomolecular ion (MH^+) at *m/z* 665, which is consistent with the addition of one molecule of GSH to **6.2** (Figure 6.11 A, B, D). This addition is assumed to take place by analogy with the formation of the **6.1**-derived GSH adduct B1.

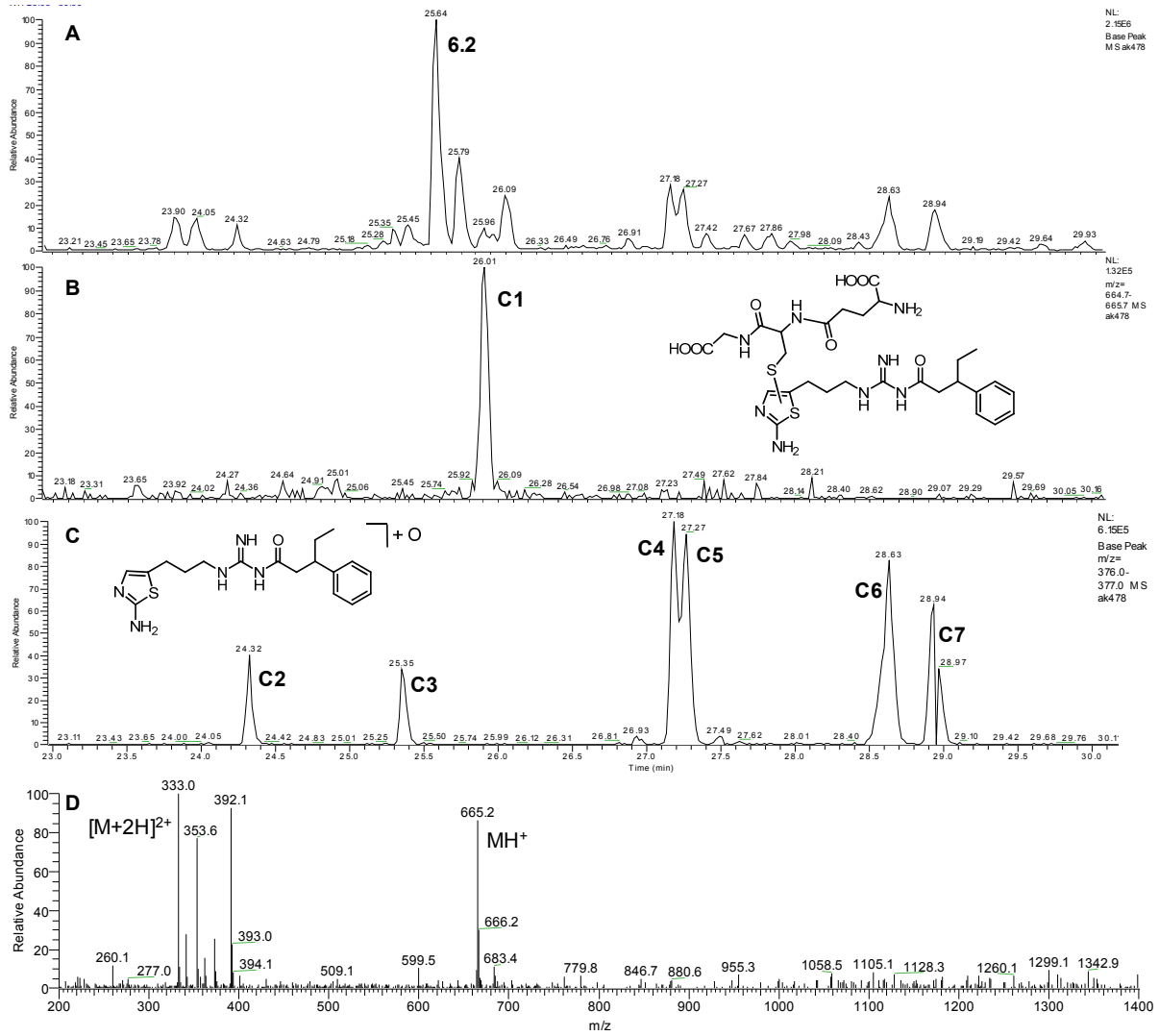

Figure 6.11. TQ LC-MS/MS analysis of a microsomal incubation mixture of **6.2** supplemented with GSH and a NADPH-regenerating system. **A**: Detailed representation of a full scan base peak chromatogram of the **6.2**-containing microsomal incubation mixture. **B**: Extracted ion chromatogram at *m/z* 665 showing the proposed structure of the GSH adduct C1 eluting at t_R ~ 26.0 min. **C**: Extracted ion chromatogram at m/z 376 depicting the presence of six potential monohydroxylated metabolites of **6.2** (C2-C7). **D**: Full scan mass spectrum of C1 at t_R ~26.0 min. As the exact regiochemistry of hydroxylation and the attachment point of the glutathionyl moiety are not known, the structures are only drawn for illustrative purpose.

More detailed information on the proposed structure of C1 was obtained by using the MRM mode to follow specific fragmentation pathways known for the glutathionyl moiety. Moreover, the MRM mode is superior to CNL scanning in terms of sensitivity, which is of particular interest in cases of low analyte levels. Three distinct mass transitions were chosen as criteria for the presence of a glutathionyl moiety in C1: the loss of pyroglutamic acid (-129 Da), glycine (-75 Da) and γ-glutamyl-dehydroalanyl-glycine (-273 Da). As depicted in Figure 6.12, C1 showed corresponding MRM signals for all three characteristic mass transitions and is therefore suggested to be a GSH adduct of **6.2**.

Analogously to **6.1**, various species with a mass difference of +16 Da, consistent with monohydroxylation, were detected after microsomal incubation showing corresponding ions at *m/z* 376 (cf. Figure 6.11 C). The appearance of an enlarged number of proposed hydroxylated species (C2-C7) compared to **6.1** (B2-B5) could be due to the introduction

of an additional ethyl group, which may also serve as potential point of attack in phase I oxidation. The seemingly increased amount of monohydroxylated species gives rise to the speculation that the ethyl substitution shifts the metabolic pathway to enhanced alkyl and aryl oxidation instead of formation of reactive intermediates by bioactivation of the aminothiazole ring. This could lead to less protein binding and hence, to higher recovery.
LC-MS/MS analysis of a control sample of **6.1** containing GSH and a NADPH-regenerating system incubated in the absence of rat liver microsomes revealed neither the formation of the GSH adduct C1 nor of the hydroxylated metabolites C2-C7. This corroborates the P450 dependence of these reactions.

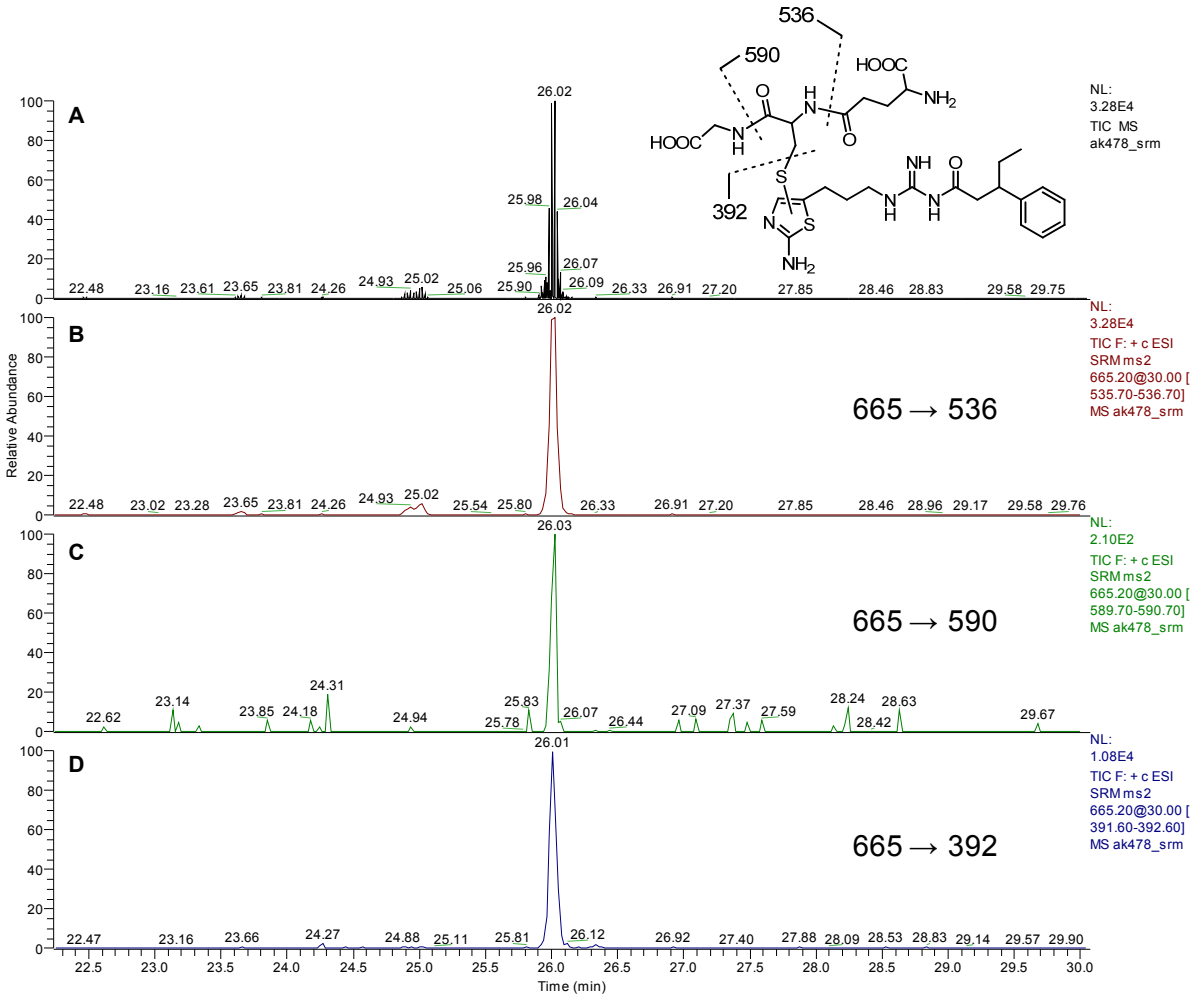

Figure 6.12. TIC of the LC-MRM/MS of the **6.2**-derived GSH-containing metabolite C1 generated by microsomal incubation with GSH and a NADPH-generating system (**A**). MRM chromatograms for *m/z* 665→536 (**B**), *m/z* 665→590 (**C**) and *m/z* 665→392 (**D**). All mass transitions are assumed to take place as indicated in the drawn structure.

6.2.2.2 N^G-Acylated 3-(2-amino-4-methylthiazol-5-yl)propylguanidines

Recently, Kalgutkar et al. published a chemical intervention strategy to reduce the bioactivation liability of the 2-amino-4-arylthiazole motif.[15] The authors showed that replacement of the thiazole against a 1,2,4-thiadiazole analogue or blocking of the C5-position by introduction of a fluorine atom abolished the liability for GSH adduct formation. Based on a predictive *in silico* model and subsequent screening for GSH adducts, Subramanian et al. observed that introduction of a methyl substituent in C4-position of a 5-(2-aminothiazol-5-yl)indolin-2-one motif prevented GSH conjugation.[20] In our workgroup the introduction of a methyl group in position 4 of the thiazole ring as in the H_2R agonist amthamine (2-amino-4-methylthiazol-5-ethanamine) was investigated in the course of structure-activity studies of H_2R agonists.[21] Considering these results, it seems reasonable to investigate the role of 4-methyl substitution with regard to GSH adduct formation. Thus, the bioactivation potential of the 4-methyl analogues **6.3** and **6.4** (Scheme 6.9, synthesized in our laboratory by Dr. A. Kraus[19, 21]) of the 2-aminothiazolylpropylguanidines **6.1** and **6.2** was explored in a GSH trapping assay using rat liver microsomes.

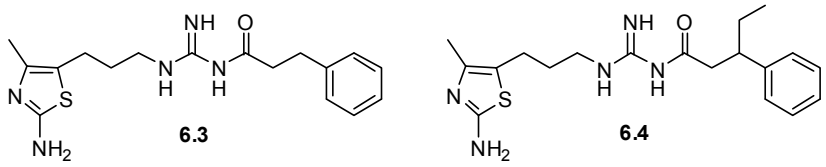

Scheme 6.9. Structure of two 2-amino-4-methylthiazolylpropylguanidines used for bioactivation studies.

Method

The incubation of the substances **6.3** and **6.4** was carried out according to the procedure described in section 6.2.2.1 for the incubation of 2-aminothiazolylpropylguanidines.

Results

There is evidence from the literature that by introduction of a methyl group in 4-position of the 2-aminothiazole epoxidation and subsequent GSH conjugation becomes unlikely due to sterical hindrance.[20] However, GSH addition after ring oxidation according to Scheme 6.8, pathway B seems theoretically possible (Scheme 6.10). Thereby, the addition is assumed to take place in 5-position in structure (I), as the contribution of structure (II) to resonance is negligible due to highly unfavorable distribution of charges.

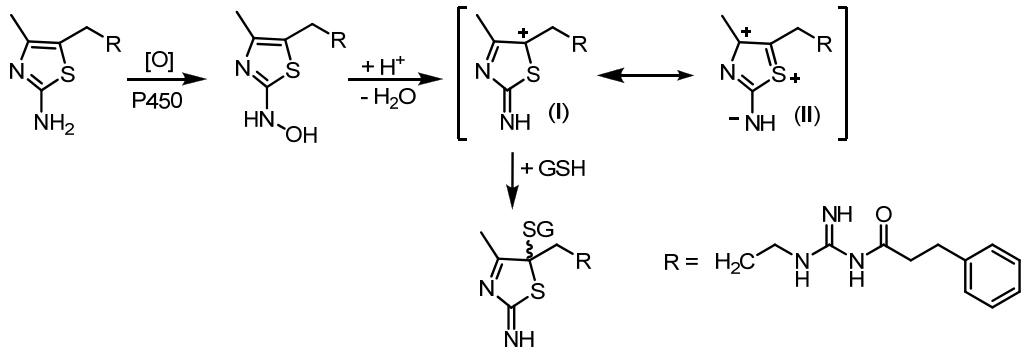

Scheme 6.10. Proposed mechanism for GSH conjugation at the 2-amino-4-methylthiazolylpropylguanidine **6.3**.

Full scan LC-MS/MS analysis of the supernatants of an incubation mixture containing **6.3**, GSH, NADPH-regenerating system and rat liver microsomes as well as of the control sample devoid of microsomes revealed a very low recovery of the parent compound **6.3** after microsomal incubation (Figure 6.13). According to the results for the demethylated analogue **6.1** this finding is in agreement with a high degree of unspecific protein binding.

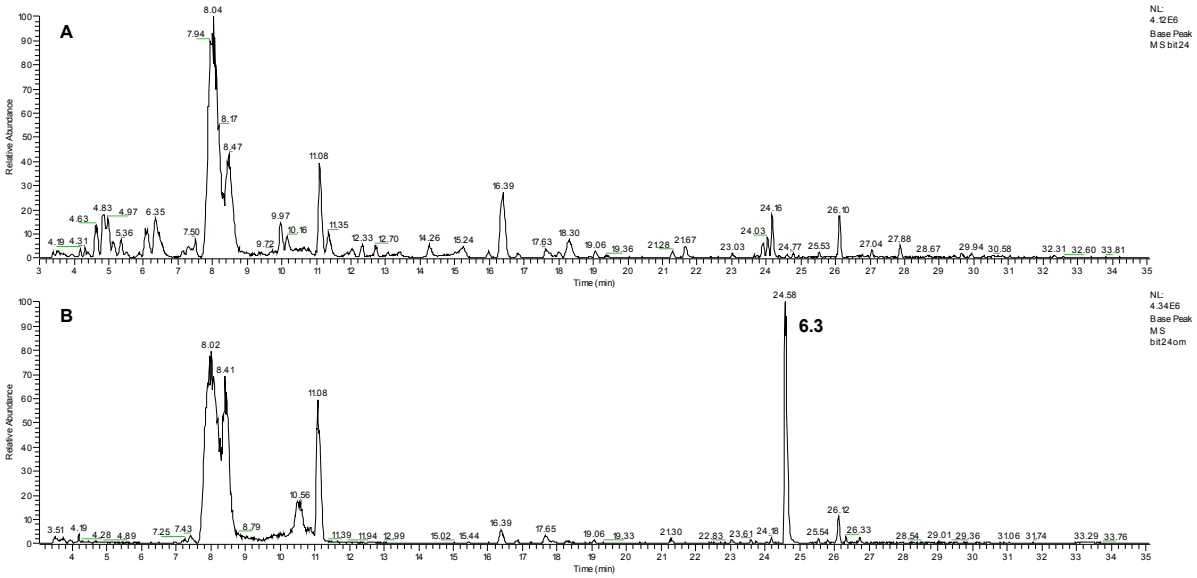

Figure 6.13. A: Full scan base peak chromatogram of **6.3** coincubated with GSH and a NADPH-regenerating system in rat liver microsomes. **B**: Full scan base peak chromatogram of a control sample without microsomes.

Screening of the full scan data set of a **6.3**-containing microsomal incubation mixture supplemented with GSH and a NADPH-regenerating system for potential GSH adducts of **6.3,** formed by the bioactivation pathway proposed in Scheme 6.10, yielded two separate signals at t_R ~ 23.7 min (D1) and 23.8 min (D2), respectively, both showing a corresponding pseudomolecular ion (MH^+) at *m/z* 651 (Figure 6.14). D1 and D2 are considered potential diastereomers derived from GSH addition in C5-position, which could yield the *(R)* or *(S)*-configured stereocenter. However, relative abundance of both putative GSH adducts was very low. Thus, CNL scanning of 129 Da gave no corresponding CNL signals. Furthermore, two potentially monohydroxylated species with ions at *m/z* 362 were detected at t_R ~ 21.7 min and 22.4 min, respectively, that have apparent masses consistent with the formal addition of an oxygen atom (Figure 6.15).

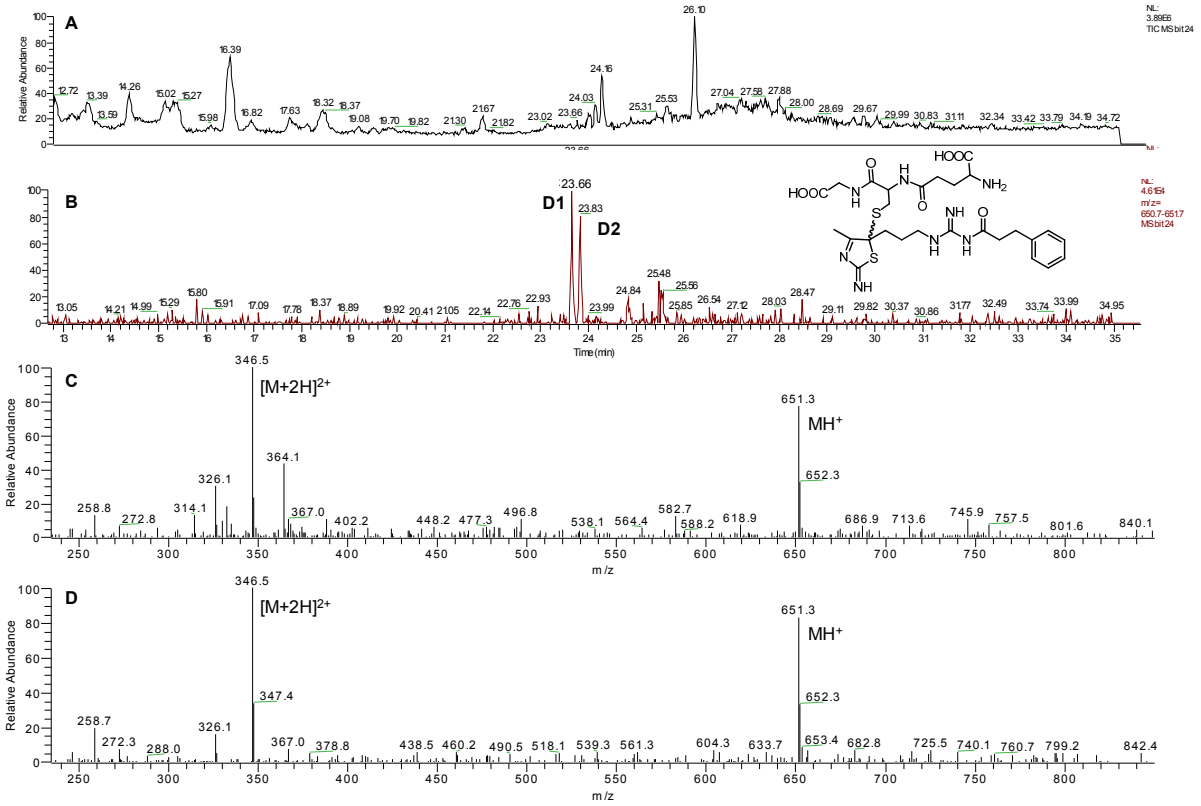

Figure 6.14. A: Detailed representation of a full scan TIC chromatogram of a microsomal incubation mixture containing **6.3**, GSH and a NADPH-regenerating system. **B**: Extracted ion chromatogram at *m/z* 651 showing two potential diastereomeric GSH adducts (D1, D2) and their corresponding proposed structure with undefined stereochemistry at C5. **C**, **D**: Full scan mass spectra of the MH^+ ions at 651 Da of D1 and D2 at t_R ~23.7 min and t_R ~ 23.8 min.

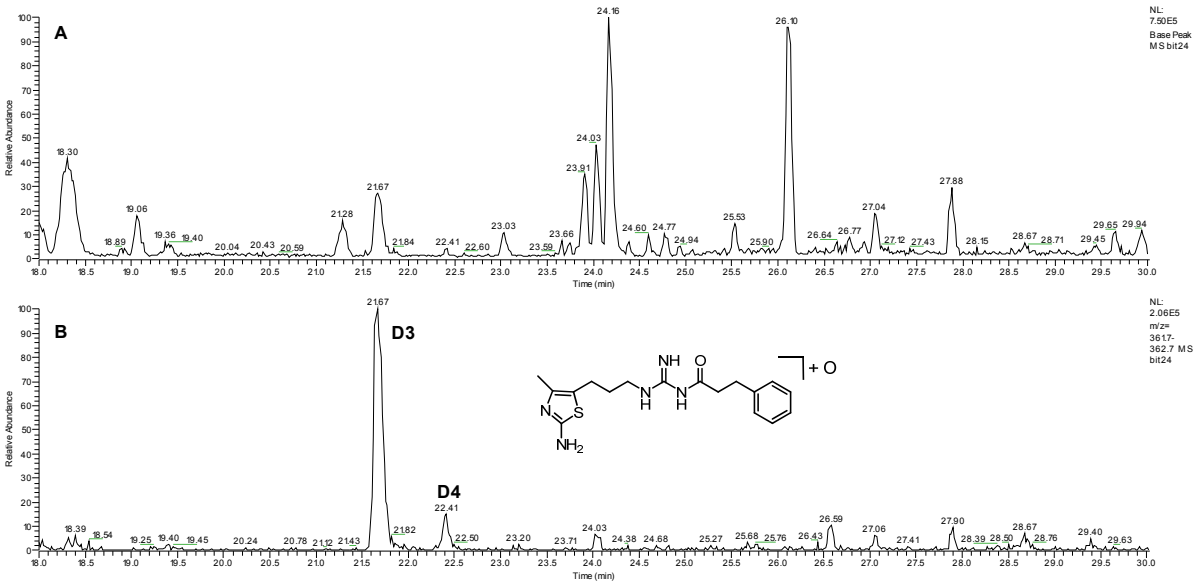

Figure 6.15. A: Detailed representation of a full scan base peak chromatogram of a microsomal incubation mixture containing **6.3**, GSH and a NADPH-regenerating system. **B**: Extracted ion chromatogram at *m/z* 362 showing two potential monohydroxylated metabolites (D3, D4) of **6.3**.

In Figure 6.16 the results of full scan analyses of incubation mixtures containing **6.4**, GSH and a NADPH-regenerating system in the absence (A) and in the presence (B) of rat liver microsomes are depicted. In accordance with the results for the demethylated analogue **6.2** the recovery of **6.4** after microsomal incubation was higher than for compound **6.3** lacking the ethyl substituent in the acyl part.

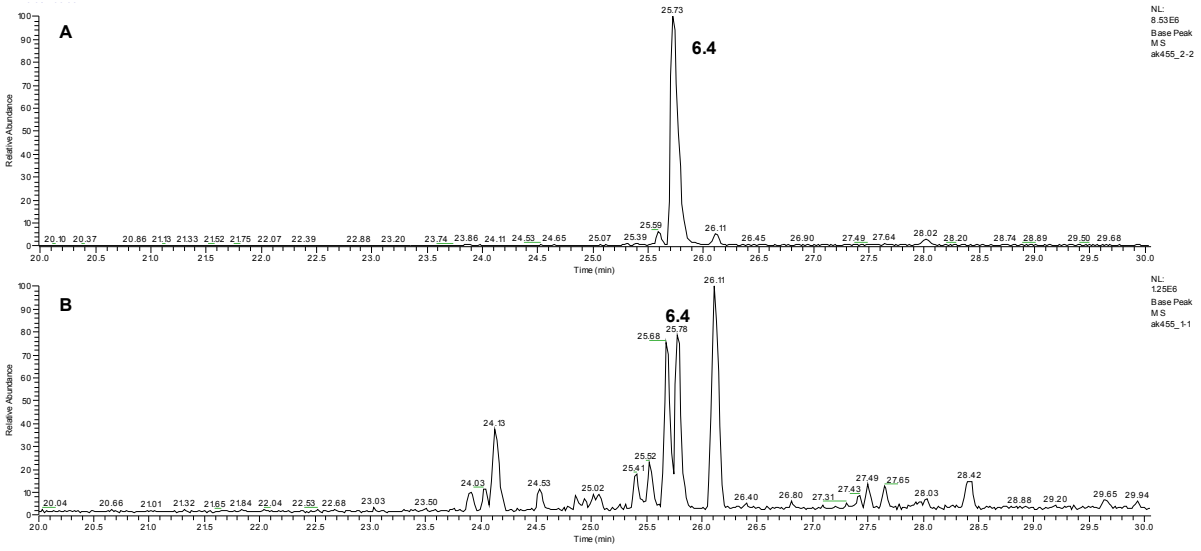

Figure 6.16. A: Full scan base peak chromatogram of a **6.4**-containing incubation mixture co-incubated with GSH and a NADPH-regenerating system in the absence of rat liver microsomes. **B**: Full scan base peak chromatogram of an analogous incubation mixture with rat liver microsomes.

By analogy with the analysis of **6.3**, the full scan data set of the microsomal incubation sample was scanned for a GSH adduct, formed by the postulated bioactivation pathway depicted in Scheme 6.10, having a molecular weight, which is consistent with the proposed structure shown in Figure 6.17 A. Apparently, compound E1, detected at t_R ~ 26.1 min, suggests the addition of a GSH molecule, as it shows a corresponding pseudomolecular ion at *m/z* 679. However, beside the pseudomolecular ion MH^+ at *m/z* 679 a sodium adduct ion ($[M+Na]^+$) at *m/z* 701 and a potassium adduct ion ($[M+K]^+$) at *m/z* 717 were detected, which were not observed with other GSH adducts. Moreover, the CID fragmentation pattern obtained by a product ion scan of the MH^+ ion at *m/z* 679 did not confirm the formation of an GSH adduct, as characteristic fragment ions of the glutathionyl moiety due to the loss of glycine (-75 Da) or γ-glutamyl-dehydroalanyl-glycine (-273 Da) were missing. In addition, the required collision energy (45 eV) for adequate fragmentation was unusually high in contrast to product ion scans of other GSH adducts, which only required 22-30 eV. Furthermore, in incubation mixtures containing **6.2** and **6.3**, respectively, corresponding peaks at t_R ~ 26.1 min were detected. Thus, the formation of a specific **6.4**-derived GSH adduct seems rather unlikely.

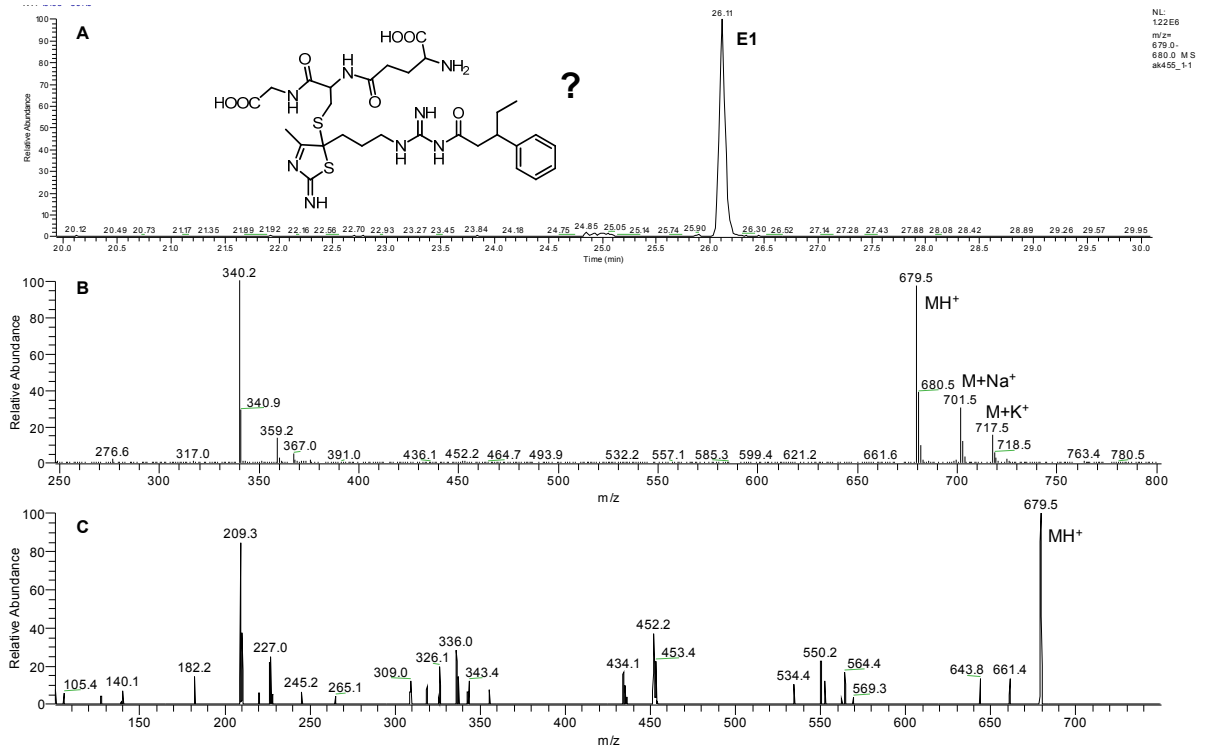

Figure 6.17. A: Extracted ion chromatogram at *m/z* 679 showing the presence of a putative GSH adduct of **6.4** (E1) with corresponding possible structure. **B**: Mass spectrum of E1 (t_R ~ 26.1 min). **C**: Product ion scan of E1 at t_R ~ 26.1 min.

However, the generation of monohydroxylated metabolites of **6.4** seemed possible, as the extracted ion chromatogram for *m/z* 390 revealed two species at t_R ~ 24.5 min and 25.4 min, respectively, consistent with the formal addition of one oxygen atom (Figure 6.18).

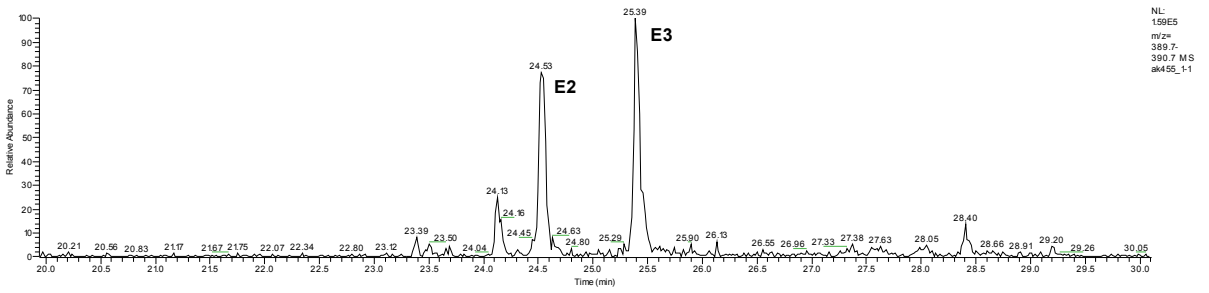

Figure 6.18. Extracted ion chromatogram at *m/z* 390 showing the presence of two putative monohydroxylated metabolites of **6.4** (E2, E3).

6.2.2.3 Metabolite identification

In order to gain further information about the metabolic fate of N^G-acylated hetarylpropyl-guanidines the metabolite profiles of compounds **6.1** and **6.3** were investigated. The studies were carried out in cooperation with Dr. A. Rottmann and coworkers at the department of Drug Metabolism and Pharmacokinetics at Bayer Schering Pharma AG (Berlin, Germany). The substances were incubated in the presence of rat and human liver microsomes as well as rat hepatocytes. For microsomal incubations a NADPH-

regenerating system was added or omitted (negative control sample). Furthermore, the incubation samples were not supplemented with GSH.
Subsequent LC-MS analysis yielded poor recoveries for both substances possibly due to high unspecific or covalent protein binding. Incubation of **6.1** and **6.3** in the presence of rat hepatocytes led to the detection of 1-[3-(2-aminothiazol-5-yl)propyl]guanidine and 1-[3-(2-amino-4-methylthiazol-5-yl)propyl]guanidine, respectively by cleavage of the amide bond. However, no GSH adducts were detected. Thus, bioactivation of **6.1** and **6.3** to reactive intermediates could not be verified. Furthermore, in all incubation samples various potential mono- as well as dihydroxylated metabolites of **6.1** and **6.3** were detected, but not further characterized.

6.3 Modification of the trapping agent – fluorescence-labeled GSH

In order to increase the sensitivity of GSH adduct detection and to improve specificity, the possibility of using a fluorescence-based detection method was explored. Gan et al. reported a LC-MS/MS method that exploits the fluorescent signal of a dansylated glutathione derivative.[22] Dansyl chloride is a widely applied derivatizing agent for compounds bearing hydroxyl or amino groups. Thus, it is applied especially for amino acid and peptide analysis[23-24], but also for the determination of pharmaceutical compounds in pharmaceutical preparations and biological fluids[25]. In the following the synthesis of dansylated glutathione (dGSH) and its use for trapping of reactive intermediates is presented.

6.3.1 Chemistry

The synthesis of dansylated glutathione (dGSH) was performed according to described procedures[22, 26] with several modifications. Since reaction of dansyl chloride with the free thiol group in GSH must be avoided, oxidized glutathione (glutathione disulfide, GSSG) was used as starting material. Derivatization of the γ-glutamyl amino moieties was accomplished under basic reaction conditions in a mixture of carbonate buffer, pH 9.0, and acetone. Subsequent reduction of the disulfide bond of double dansylated GSSG (ddGSSG) was achieved by addition of dithiothreitol (DTT) to yield dGSH (Figure 6.19).

6.3.2 Trapping reactions with test substances

To prove the trapping efficiency of dGSH towards reactive intermediates, adduct formation was investigated using test compounds exhibiting an intrinsic tendency for reaction with nucleophiles like thiols. As an indicative model reaction, the addition of dGSH to acrolein and *N*-ethylmaleimide, respectively (Figure 6.20), was followed by means of HPLC using fluorescence detection. Dansyl-related fluorescence was monitored at 525 nm after excitation at 340 nm.

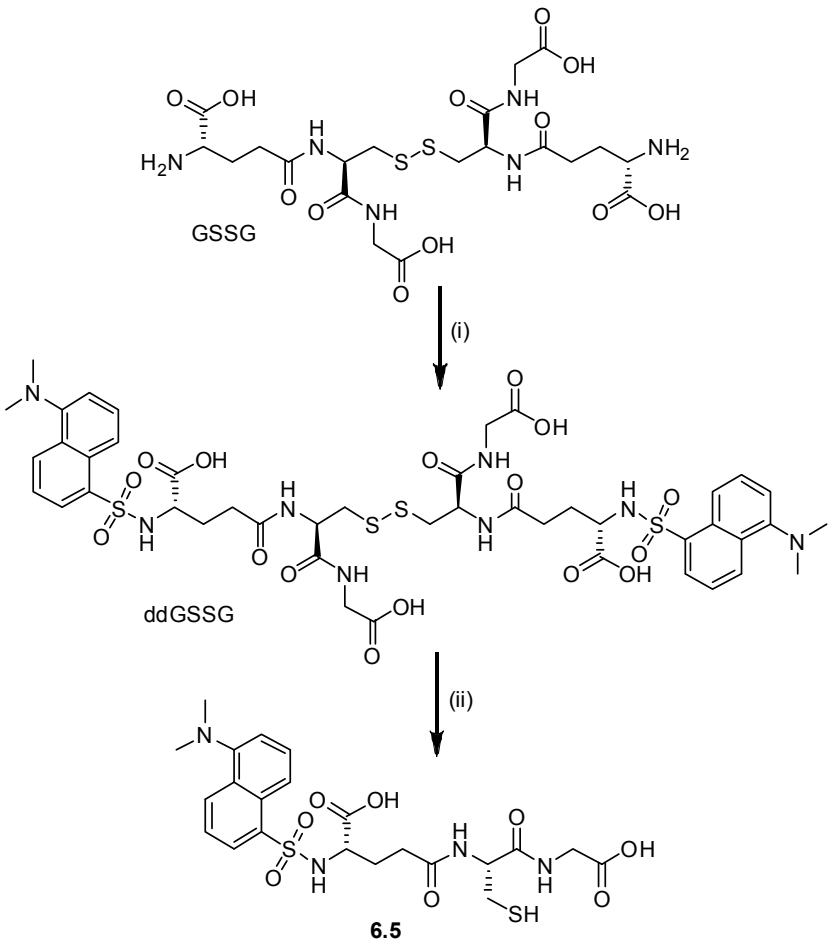

Figure 6.19. Synthesis of dansylated glutathione (**6.5**). Reagents and conditions: (i) dansyl chloride (3 eq), sodium carbonate buffer pH 9/ acetone, rt, 3 h, protection from light (ii) dithiothreitol (5 eq), 0.1 M TRIS buffer pH 8, rt, 1.5 h protection from light.

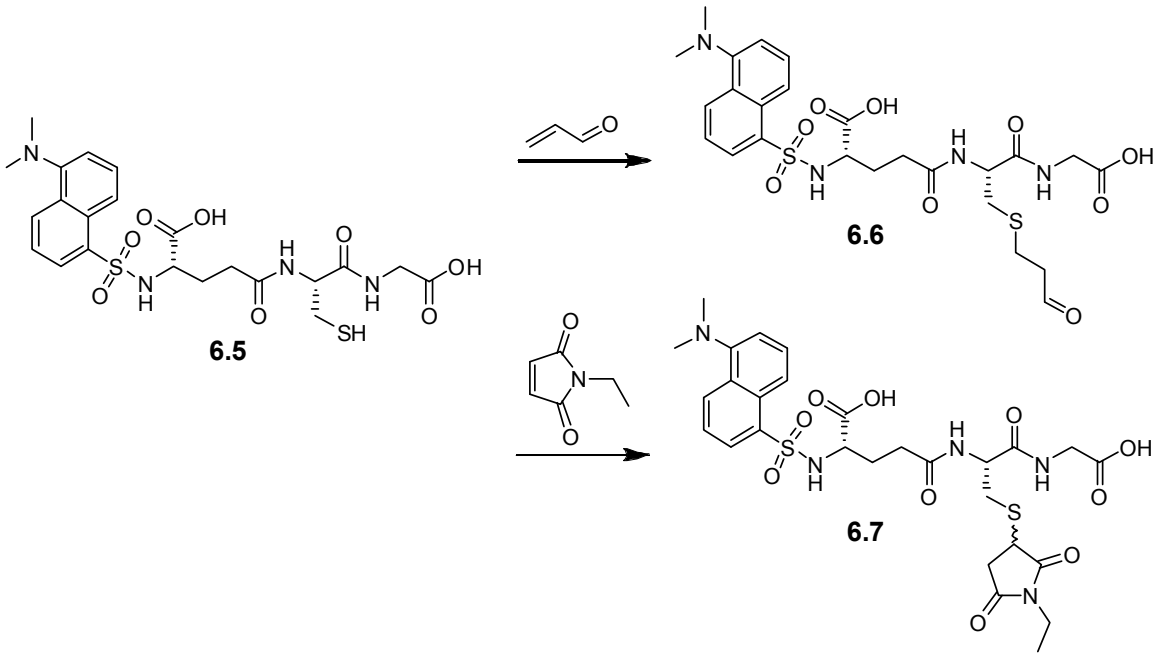

Figure 6.20. Examples of trapping reactions with dGSH using acrolein and *N*-ethylmaleimide.

Michael addition of dGSH (**6.5**) to acrolein yielded the fluorescent adduct **6.6** (cf. Figure 6.20). Apparently, **6.5** and **6.6** showed overlapping retention times under chosen chromatographic conditions resulting in the detection of one broad fluorescence signal for **6.5** and **6.6** (Figure 6.21). Nevertheless, LC-MS analysis of the reaction mixture yielded sufficient separation of both species to determine a clean mass spectrum for **6.6**, which corroborates the formation of the acrolein-dGSH adduct consistent with the pseudomolecular ion (MH^+) at *m/z* 597 (Figure 6.22). A second distinct fluorescence signal at t_R ~ 18.9 min (Figure 6.21) was observed, which was identified by LC-MS as double dansylated glutathione disulfide (ddGSSG) (Figure 6.22) formed by oxidation of excess dGSH.

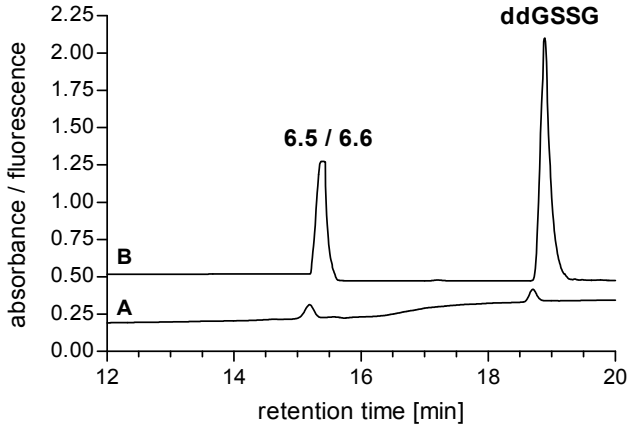

Figure 6.21. Chromatograms of a reaction mixture of acrolein and dGSH. The fluorescent acrolein-dGSH adduct (**6.6**) and residual dGSH (**6.5**) appear to overlap. **A**: fluorescence trace. **B**: UV trace (210 nm).

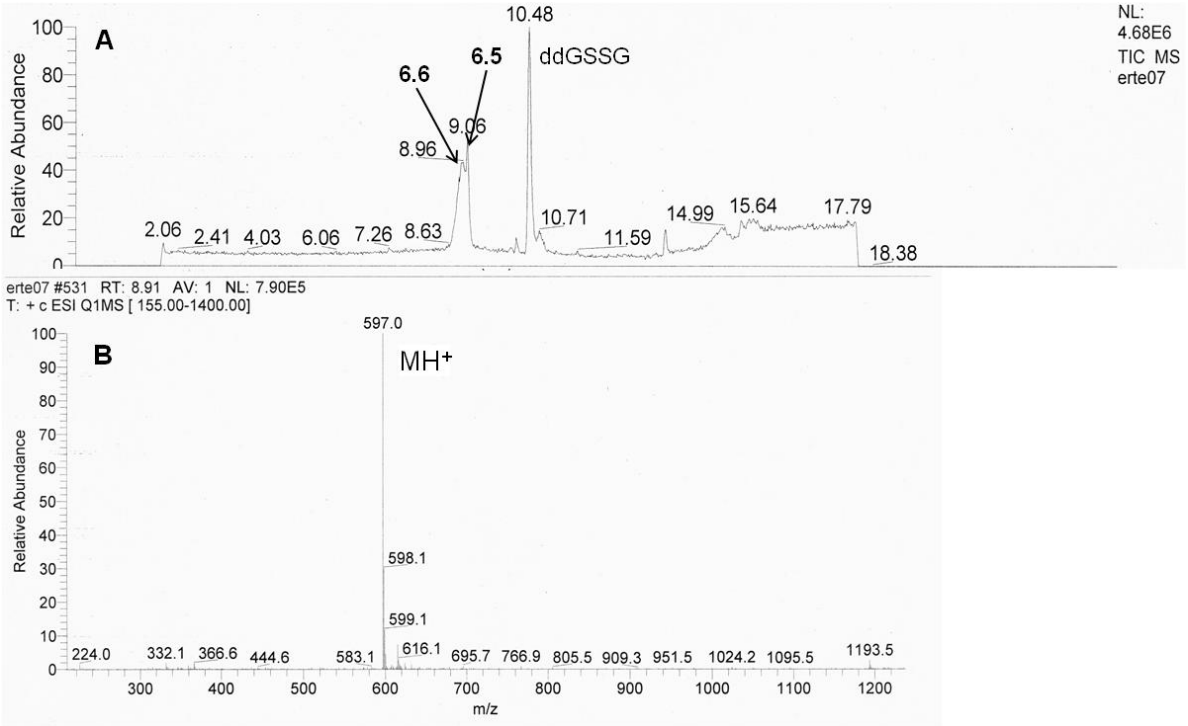

Figure 6.22. A: Full scan TIC chromatogram of a reaction mixture containing acrolein and dGSH. The trapped acrolein-dGSH adduct (**6.6**, t_R = 8.96 min) and dGSH (**6.5**, t_R = 9.06 min) was not completely resolved under present chromatographic conditions. **B**: Mass spectrum of **6.6** at t_R = 8.91 min.

By analogy with acrolein the reaction of dGSH with an excess of *N*-ethylmaleimide (NEM) led to the formation of adduct **6.7**. However, since dGSH is a chiral compound Michael addition to NEM yielded two diastereomers, which could be resolved with the applied chromatographic method and showed two distinct fluorescence signals (Figure 6.23). A faster HPLC gradient used for LC-MS resulted in merging of the two diastereomers of **6.7** (Figure 6.24 A). Nevertheless, a mass spectrum of **6.7** recorded at t_R = 9.56 min revealed the presence of a pseudomolecular ion (MH^+) at *m/z* 666 and a monoprotonated cluster ion ($2M+H^+$) at *m/z* 1331 consistent with the addition of one molecule of dGSH to NEM (Figure 6.24 B).

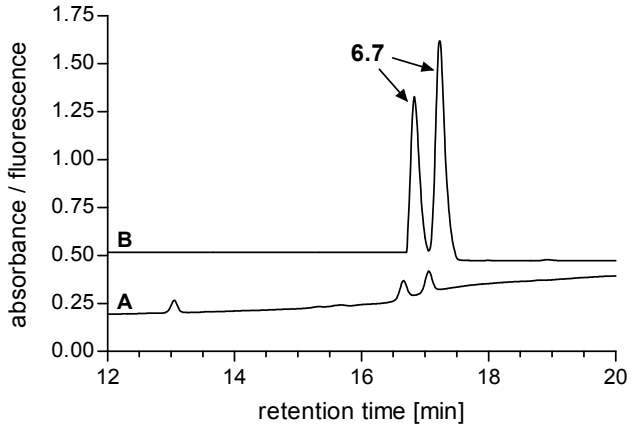

Figure 6.23. Chromatograms of a reaction mixture of *N*-ethylmaleimide (NEM) and dGSH depicting the formation of two diastereomeric NEM-dGSH adducts (**6.7**). **A**: fluorescence trace. **B**: UV trace (210 nm).

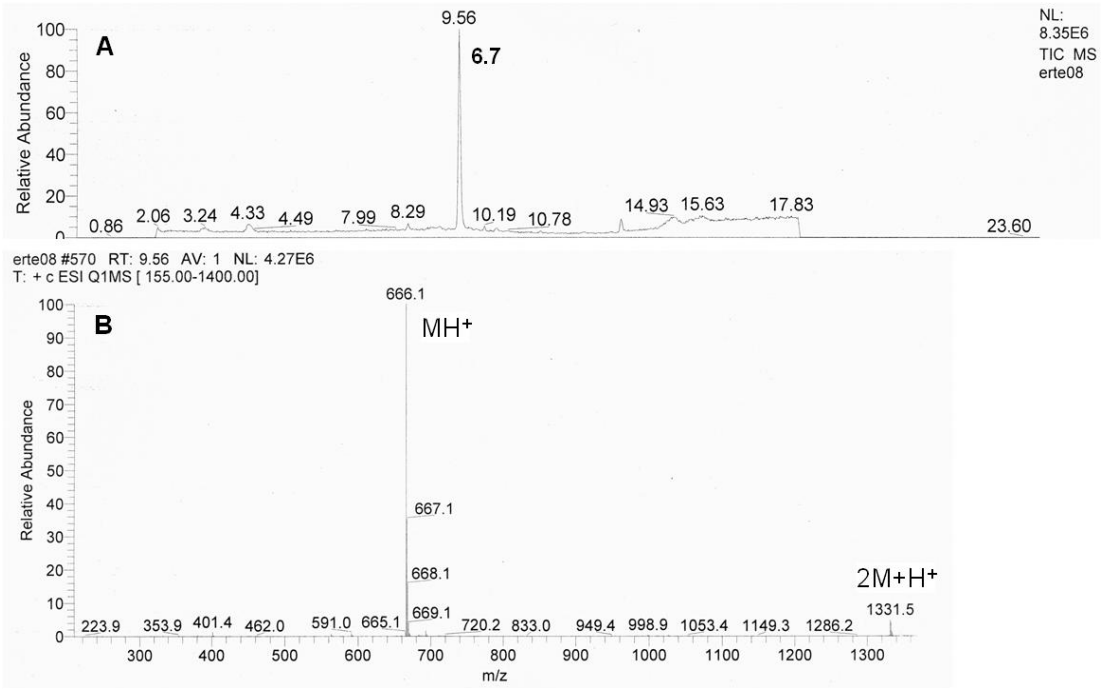

Figure 6.24. A: Full scan TIC chromatogram of a reaction mixture containing *N*-ethylmaleimide and dGSH. Diastereomeric separation of the dGSH adduct **6.7** (t_R = 9.56 min) was not achieved under present chromatographic conditions. **B**: Mass spectrum of **6.7** at t_R = 9.56 min.

In summary, dansylated glutathione reacted with the chosen Michael acceptors to give adducts, which could be identified by HPLC using fluorescence detection. Thus, dGSH could be a suitable trapping reagent for the identification of unknown reactive intermediates.

6.3.3 Trapping of reactive metabolites of N^G-acylated hetarylpropylguanidines with dGSH

The suitability of dansylated glutathione (**6.5**) for trapping of reactive metabolites was studied using the 2-aminothiazolylpropylguanidine **6.1**, which had already provided evidence of being bioactivated to reactive intermediates on incubation with rat liver microsomes.

Method

6.1 was co-incubated with rat liver microsomes, dGSH and a NADPH regenerating system in 0.1 M potassium phosphate buffer, pH 7.4, for 2 h at 37 °C. After quenching of the reaction with ice cold acetonitrile, precipitated proteins were removed by centrifugation. The supernatant was concentrated, reconstituted in mobile LC phase and analyzed by LC-MS/MS. Unfortunately, simultaneous fluorescence detection could not be carried out with the available LC-MS/MS system.

Results

Derivatization of GSH with the dansyl fluorophore enabled sensitive fluorescence detection, but also improved the signal to noise ratio using UV detection. In Figure 6.25 the UV trace as well as the base peak chromatogram of a microsomal incubation mixture of **6.1** coincubated with **6.5** and a NADPH-regenerating system is depicted revealing a very prominent and sharp eluting signal of **6.5** at t_R ~ 13.3 min and a smaller peak referring to ddGSSG formed by oxidation of **6.5**. A product ion scan of **6.5** at t_R ~ 13.3 min was performed to assess the typical CID-induced fragmentation pattern of **6.5** (Figure 6.25 C). Besides the loss of glycine, fragmentation of the dansylated γ-glutamyl moiety as well as dissociation of the sulfonamide bond between GSH and the dansyl moiety was observed. Therefore, fragmentation of dGSH appeared to proceed by analogy with the fragmentation of GSH. Scanning of the full scan data set for potential dGSH adducts of **6.1** led to the detection of the species F1 (t_R ~ 14.6 min) at *m/z* 870 (MH^+) (Figure 6.26). The corresponding molecular weight of 869 Da suggests the addition of one molecule of dGSH to **6.1**. However, F1 showed only a very low relative abundance. Hence, product ion scan and CNL scanning failed due to insufficient sensitivity. Though, using the MRM mode the characteristic loss of glycine (*m/z* 870 → 795) as well as the dansylated γ-glutamyl fragment (*m/z* 870 → 363) could be monitored corroborating the formation of a dGSH adduct of **6.1** (Figure 6.27).

Generally, dGSH can be considered a useful alternative trapping agent for the screening of compounds for reactive intermediate formation, especially because it allows sensitive and quantitative analysis. However, by introduction of the rather bulky dansyl group to

GSH the recognition of the (modified) cofactor by glutathione S-transferases (GST) could be impaired. This, in turn, might increase the percentage of non-enzymatic adduct formation.[22]

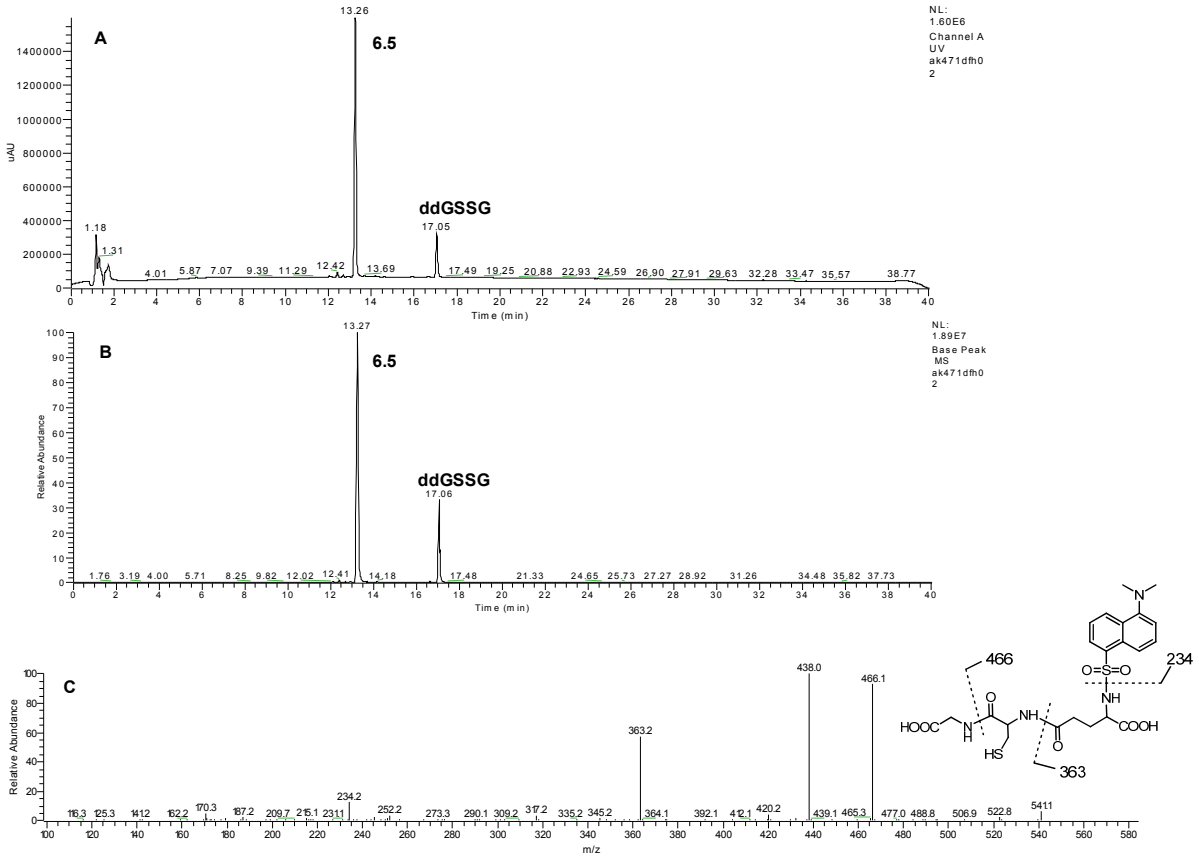

Figure 6.25. Triple quadrupole LC-MS/MS analysis of **6.1** coincubated with dGSH (**6.5**) and a NADPH-regenerating system in rat liver microsomes. **A**: UV trace recorded at 210 nm. **B**: Full scan base peak chromatogram. **C**: Product ion spectrum of **6.5** at t_R = 13.27 min. The proposed origins of key fragment ions are as indicated.

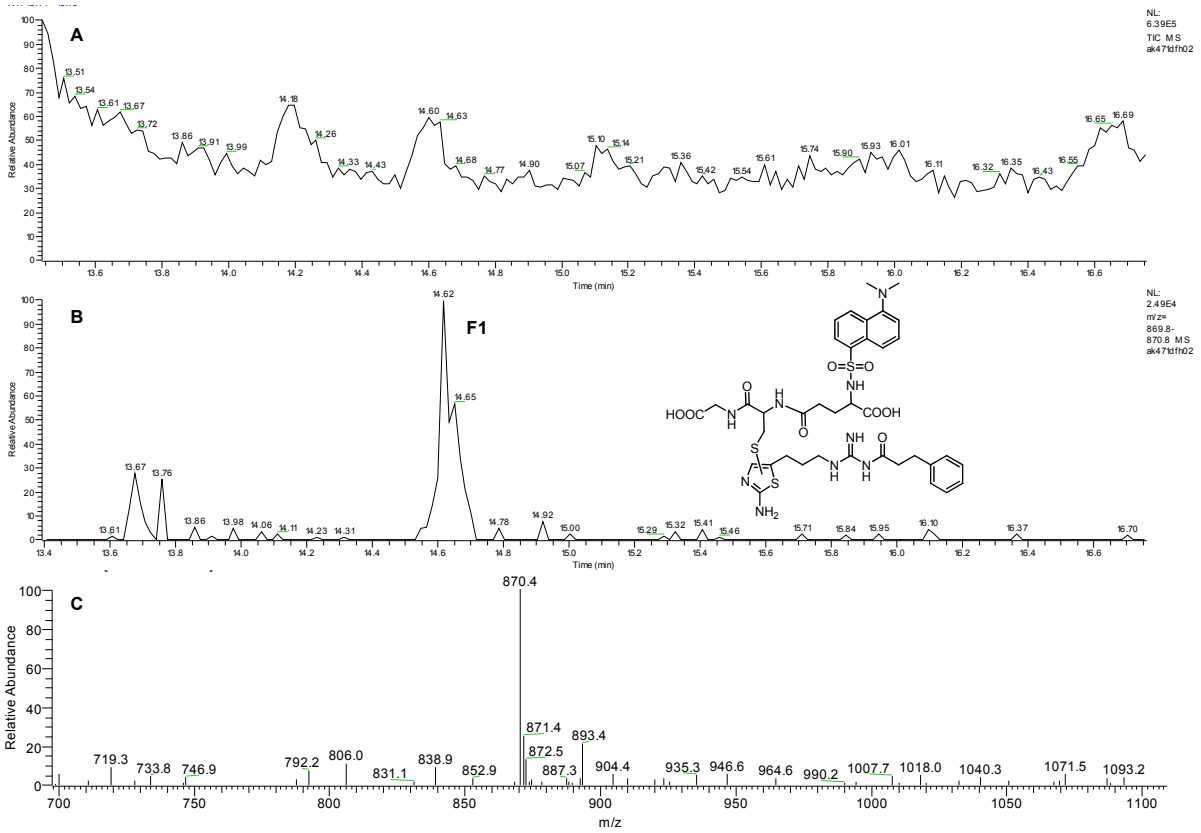

Figure 6.26. A: Detailed representation of a TIC chromatogram of a microsomal incubation mixture containing **6.1**, dGSH (**6.5**) and a NADPH-regenerating system. **B**: Extracted ion chromatogram at *m/z* 870 showing a potential dGSH adduct (F1) of **6.3** with proposed structure. **C**: Mass spectrum of F1 at t_R = 14.62 min.

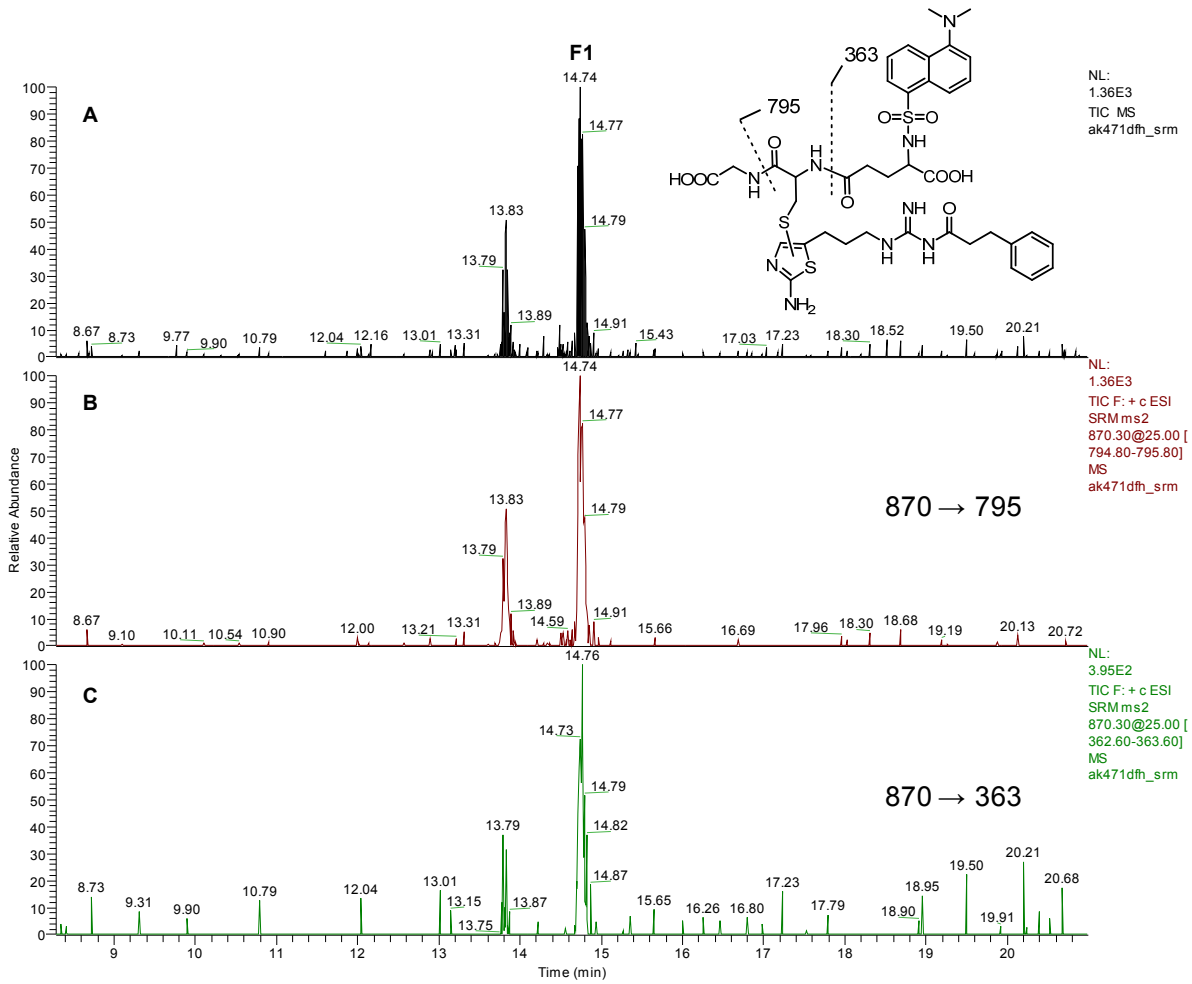

Figure 6.27. TIC of the LC-MRM/MS of the **6.1**-derived dGSH-containing metabolite F1 generated by microsomal incubation with dGSH and a NADPH-generating system (**A**). MRM chromatograms for *m/z* 870→795 (**B**) and *m/z* 870→363 (**C**). All mass transitions are assumed to take place as indicated in the drawn structure. The signal at t_R ~ 13.8 min does not correspond to a pseudomolecular ion at *m/z* 870, but indicates an isotope peak of a different molecular species.

6.4 Summary

Previously, strong evidence was arising concerning a toxic potential of 2-aminothiazoles due to bioactivation of the heterocycle resulting in electrophilic intermediates capable of covalently binding to proteins.[15, 20] In view of future pharmacological *in vivo* investigations of N^G-acylated 2-aminothiazol-5-ylpropylguanidines, developed in our workgroup as highly potent and selective H_2 agonists[19], the bioactivation potential of examples of N^G-acylated 3-(2-aminothiazol-5-yl)propylguanidines and N^G-acylated 3-(2-amino-4-methylthiazol-5-yl)propylguanidines was investigated *in vitro* by coincubation with rat liver microsomes and glutathione to trap putative reactive intermediates. A suitable method for the detection of GSH adducts based on liquid chromatography/tandem mass spectrometry (LC-MS) was developed, which was successfully applied for identification of GSH-containing metabolites of the model compound diclofenac by combination of appropriate MS/MS experiments as full scan, constant neutral loss scanning, multiple reaction monitoring and product ion scanning. Application of this method to bioactivation studies with N^G-acylated 3-(2-aminothiazol-5-yl)propylguanidines revealed P450-mediated formation of putative GSH adducts, presumably generated by oxidation or epoxidation of the heterocycle followed by trapping with GSH. Concerning the bioactivation of N^G-acylated (2-amino-4-methylthiazol-5-yl)propylguanidines the epoxidation pathway was assumed to be rather unlikely due to steric hindrance by the 4-methyl group. The addition of GSH in 5-position of the 2-aminothiazole was still conceivable, but could not be unequivocally confirmed by LC-MS/MS analysis. Further metabolic investigations with human liver microsomes and rat hepatocytes suggested that cleavage of the amide bond resulting in the free guanidine and oxidation of phenyl and alkyl substituents were the preferred metabolic pathways for N^G-acylated 3-(2-aminothiazol-5-ylpropyl)guanidines and 3-(2-amino-4-methylthiazol-5-yl)propylguanidines. Aiming at increased sensitivity of GSH adduct detection and improved selectivity, dansyl glutathione (dGSH), a fluorescence-labeled glutathione derivative, was synthesized. Its benefit in terms of trapping of reactive species was demonstrated using the Michael acceptors acrolein and *N*-ethylmaleimide as examples. The reaction was investigated by HPLC-fluorescence detection and LC-MS analysis of resulting dGSH adducts. Indeed, also dansylated glutathione proved to be suitable for detecting trapped reactive intermediates derived from bioactivation of 2-aminothiazolylpropylguanidines, since a dGSH adduct of **6.1** was identified by LC-MS/MS.

6.5 Discussion and outlook

Apparently, the detection of GSH adducts of N^G-acylated 2-aminothiazolylpropylguanidines indicates a certain potential of 2-aminothiazoles for bioactivation resulting in reactive intermediates. Although these GSH adducts appeared to be rather low level metabolites, the possibility of their formation should not be neglected, but the 2-aminothiazole ring should rather be considered a structural alert. As it is extremely difficult to predict a correlation between formation of reactive intermediates and the incidence of adverse drug reactions, a lot more information about the proposed GSH adducts should be collected. Firstly, structural elucidation is required to identify the exact point of attachment of the glutathionyl moiety and to allow conclusions on the pathway of bioactivation. This could be achieved by means of LC-NMR analysis. However, as the NMR technique suffers from relatively low sensitivity[27], the amounts of putative GSH adducts will have to be increased. Thus, upscaling of the microsomal incubation samples followed by solid phase extraction should be considered. Furthermore, more sophisticated MS techniques, especially high resolution mass spectrometry (HR-MS), could provide more detailed structural information and help to exclude false positives.[9] If the suspicion of reactive intermediate formation was confirmed, the synthesis of a radiolabeled test compound would be reasonable to investigate covalent protein binding by means of liquid scintillation counting.[2] Moreover, a radiolabeled compound might help to enlighten the phenomenon of low recovery of all tested N^G-acylated hetarylpropylguanidines, which was assumed to be caused by high unspecific protein binding. Thereby, also the possibility of an increased binding affinity to precipitated protein (occurring during sample preparation) should be taken into account.

Based on the results obtained from GSH trapping assays with N^G-acylated 2-amino-4-methylthiazolylpropylguanidines, blocking of the 4-position of the 2-aminothiazole by methyl substitution seems to be a successful chemical intervention strategy to prevent bioactivation of the heterocycle by epoxidation. Thus, the 2-amino-4-methylthiazole moiety presents a safer alternative to the non-methylated 2-aminothiazole in terms of potential bioactivation. Hence, it should be taken into consideration as a suitable structural replacement, as long as desired pharmacological and pharmacokinetic properties can be retained.

6.6 Experimental section

6.6.1 General experimental conditions

Commercially available chemicals and reagents were purchased from Acros Organics (Geel, Belgium), Alfa Aesar GmbH & Co. KG (Karlsruhe, Germany), Merck KGaA (Darmstadt, Germany) or Sigma-Aldrich Chemie GmbH (München, Germany). All solvents used were of analytical grade or distilled before use. Melting points (mp) were determined with a Büchi 510 melting point apparatus and are uncorrected. Nuclear Magnetic Resonance (^{1}H-NMR and ^{13}C-NMR) spectra were recorded on an Avance 300 (^{1}H: 300 MHz) or an Avance 600 (^{1}H: 600 MHz) (Bruker BioSpin GmbH, Rheinstetten, Germany) with per-deuterated solvents (Deutero GmbH, Kastellaun, Germany). The chemical shift δ is given in parts per million (ppm) with reference to the chemical shift of the residual protic solvent compared to tetramethylsilane (δ = 0). Multiplicities are specified with the following abbreviations: s (singlet), d (doublet), t (triplet), q (quartet), sept (septet), m (multiplet) and bs (broad singlet). The multiplicity of carbon atoms was determined by DEPT 135 (distortionless enhancement by polarization transfer) and is indicated as follows: “+” for primary and tertiary carbon atoms (positive DEPT 135 signal), “-“ for secondary carbon atoms (negative DEPT 135 signal), “quat” for quaternary carbon atoms. 2D-NMR techniques (COSY, TOCSY, HSQC, HMBC) were performed to support interpretation of 1D spectra. Mass spectrometry analysis (MS) was performed on a Finnigan MAT 95 (EI-MS 70eV, HR-MS) and on a Finnigan ThermoQuest TSQ 7000 (ES-MS) spectrometer. The peak-intensity in % relative to the strongest signal is given in parenthesis. Purification by preparative HPLC was performed on a RP-column (Nucleodur 100-5 C18 ec, 250 x 21 mm, 5 µm; Machery-Nagel, Düren, Germany) with a system consisting of two K-1800 pumps (Knauer, Berlin, Germany) and a UV-VIS detector model K-2000 (Knauer). UV-detection was done at 220 nm, the temperature was 30 °C and the flow rate 20 ml/min. Analytical HPLC analysis was performed on a system from Thermo Separation Products or a system from Merck Hitachi. The Thermo Separation Products system consisted of a SN400 controller, a P4000 pump, an AS3000 autosampler, a Spectra Focus UV-VIS detector and a RP-column (Luna C18-2, 150 x 4.6 mm, 3 µm; Phenomenex, Aschaffenburg, Germany) at a flow rate of 0.75 mL/min and a column temperature of 30 °C. Absorbance was detected at 210 nm. The retention (capacity) factor k was calculated from the retention time t_R and the hold-up time t_0 according to $k = (t_R - t_0)/t_0$ with t_0 = 2.88 min for Luna C18-2, 150 x 4.6 mm, 3 µm. The Merck Hitachi system consisted of a 655A-12 pump, a 655A-40 autosampler, a 655A-52 column oven, a L-4250 UV-VIS detector, a F1000 Fluorescence Spectrophotometer and a RP-column (Eurosphere C18, 250mm, 4.6 mm, 5 µm; Knauer, Berlin, Germany). The system was operated at a flow rate of 0.7 ml/min and a column temperature of 30 °C. UV-absorbance was detected at 210 nm and fluorescence emission was monitored at 525 nm after excitation at 340 nm. The mobile phases were MeCN and 0.05 % trifluoroacetic acid (TFA) in Millipore water (Thermo Scientific system) or MeOH + 0.05 %

TFA and 0.05 % TFA in Millipore water (Merck system). All samples were filtered prior to injection using 0.2-µm Phenex-NY Syringe Filters (0.2 µm pore size, 4 mm diameter) (Phenomenex, Aschaffenburg, Germany). Millipore water was used throughout for the preparation of buffers and HPLC eluents. The NADPH regenerating system used for *in vitro* microsomal incubations was purchased from Promega (Madison, USA) consisted of two separate solutions (A + B). Solution A contained 26 mM NADP+, 66 mM glucose-6-phosphate and 66 mM $MgCl_2$. Solution B contained 40 U/ml glucose-6-phophate dehydrogenase in 5 mM sodium citrate (pH 5.5). Liquid chromatography-tandem mass spectrometry (LC-MS/MS) was carried out on a Finnigan ThermoQuest TSQ 7000 (Thermo Scientific, Waltham, USA) mass spectrometer interfaced to an Agilent HP1100 (Santa Clara, USA) HPLC system consisting of autosampler, binary pump, DAD and heater. The mobile phases consisted of 0.1 % formic acid in Millipore water (A) and MeCN + 0.1 % formic acid (B). The column temperature was 25 °C and UV-detection was performed at 210 nm. LC-MS/MS analyses were operated in the positive ion electrospray mode. The spray voltage was set at 4.0 kV, and the capillary temperature was set at 300 °C. Argon was used as the collision gas with a pressure of approximately 2 mtorr in the collision cell.

6.6.2 Chemistry: Experimental protocols and analytical data

6.6.2.1 N^G-acylated hetarylpropylguanidines

Used 2-aminothiazolylpropylguanidines (**6.1**, **6.2**) and 2-amino-4-methylthiazolylpropyl-guanidines (**6.3**, **6.4**) were synthesized by Dr. A. Kraus and T. Birnkammer as reported elsewhere and kindly provided.[19, 21]

6.6.2.2 Synthesis and analytical data of (*S*)-5-[(*R*)-1-(carboxymethylamino)-3-mercapto-1-oxopropan-2-ylamino]-2-[5-(dimethylamino)naphthalene-1-sulfonamido]-5-oxopentanoic acid (6.5)[22]

A solution of dansyl chloride (3 eq, 1.01 mmol, 0.28 g) in acetone (3.5 ml) was added dropwise to a solution of glutathione disulfide (1 eq, 0.34 mmol, 0.21 g) in 4 ml of sodium carbonate buffer pH 9. The reaction mixture was stirred for 3 h at room temperature under exclusion of light and was extracted with diethylether twice. The aqueous layer was separated and lyophilized. The resulting crude solid was resolved in 0.1 M TRIS buffer pH 8 (15 ml) followed by addition of dithiothreitol (5 eq, 1.72 mmol, 0.27 g). The reaction mixture was stirred for 1.5 h at room temperature under protection from light and lyophilized. The title compound was obtained as a white powder after purification by preparative HPLC (73 mg, 20 %). Mp.: 112-113 °C. ^{1}H-NMR (D_2O) δ ppm: 1.70 and 1.89 (m, 2H, γ-Glu-C^β-H_2), 2.24 (m, 2H, γ-Glu-C^γ-H_2), 2.76 (m, 2H, Cys-C^β-H_2), 3.40 (s, 6H, dimethylamino), 3.76 (m, 1 H, γ-Glu-C^α-H), 3.87 (s, 2H, Gly-CH_2), 4.37 (t, 1H, ^3J = 6.0 Hz, Cys-C^α-H), 7.77 (m, 2H, naphthalene-H), 7.98 (m, 1H, naphthalene-H), 8.25 (m, 1H, naphthalene-H), 8.32 (m, 1H, naphthalene-H), 8.68 (m, 1H, naphthalene-H). ^{13}C-NMR (D_2O) δ ppm: 25.41 (-, Cys-C^β), 27.37 (-, γ-Glu-C^β), 30.85 (-, γ-Glu-C^γ), 41.07 (-, Gly-

CH_2), 46.79 (2C, +, dimethylamino), 55.17 (+, γ-Glu-C^α), 55.30 (+, Cys-C^α), 119.44 (+, naphthalene-C), 125.41 (quat, naphthalene-C), 125.85 (+, naphthalene-C), 126.58 (+, naphthalene-C), 126.85 (+, naphthalene-C), 127.99 (+, naphthalene-C), 128.70 (quat, naphthalene-C), 130.87 (+, naphthalene-C), 134.94 (quat, naphthalene-C), 138.37 (quat, naphthalene-C), 172.29 (quat, Cys-CO), 172.92 (quat, Gly-COOH), 174.16 (quat, γ-Glu-COOH), 174.67 (γ-Glu-CO). HRMS: EI-MS: *m/z* for ($C_{22}H_{28}N_4O_8S_2$) calcd. 541.1427, found: 541.14255. Prep. HPLC: 0 min: MeCN/0.05% TFA/aq 5/95, 20 min: 50/50, 20.1-30 min: 95/5. Analytical HPLC (Thermo Scientific system): 0 min: MeCN/0.05% TFA/aq 10/90, 25 min: 40/60, 35 min: 10/90, 36-42 min: 95/5, purity 99 %, t_R = 11.93 min, k = 3.14. Anal. ($C_{22}H_{28}N_4O_8S_2 \cdot C_2HF_3O_2 \cdot 2\ H_2O$) C, H, N, S. $C_{22}H_{28}N_4O_8S_2 \cdot 1$ TFA (654.63).

6.6.2.3 Preparation and HPCL-fluorescence detection of (*S*)-5-[(*R*)-1-(carboxymethylamino)-1-oxo-3-(3-oxopropylthio)propan-2-ylamino]-2-[5-(dimethylamino)naphthalene-1-sulfonamido]-5-oxopentanoic acid (6.6)

A reaction mixture containing **6.5** (1 mM) and acrolein (5 mM) in 200 µl 0.1 M potassium phosphate buffer pH 7.4 was stirred for 1 h at room temperature. The reaction was monitored by analytical HPLC with fluorescence detection (Merck system) after dilution (1:10) with mobile phase (MeOH+0.05 % TFA / 0.05 % TFA/aq 20/80). Following gradient was applied: 0 min: MeOH+0.05 % TFA / 0.05 % TFA/aq 20/80, 20-30 min 80/20; t_R (**6.6**) ~ 15.4 min. ES-MS (DCM/MEOH + 10 mM NH_4OAc) *m/z* (%): 597 (100) $[M+H]^+$.

6.6.2.4 Preparation and HPCL-fluorescence detection of (*S*)-5-[(*R*)-1-(carboxymethylamino)-3-(1-ethyl-2,5-dioxopyrrolidin-3-ylthio)-1-oxopropan-2-ylamino]-2-[5-(dimethylamino)naphthalene-1-sulfonamido]-5-oxopentanoic acid (6.7)

A solution of **6.5** (1 mM) and *N*-ethylmaleimide (2 mM) in 200 µl 0.1 M potassium phosphate buffer pH 7.4 was stirred for 1 h at room temperature. The reaction was monitored by analytical HPLC with fluorescence detection (Merck system) after dilution (1:10) with mobile phase (MeOH+0.05 % TFA / 0.05 % TFA/aq 20/80). Following gradient was applied: 0 min: MeOH+0.05 % TFA / 0.05 % TFA/aq 20/80, 20-30 min 98/2; t_R (**6.7**) ~ 16.8 min + 17.2 min (diasteromers). ES-MS (DCM/MEOH + 10 mM NH_4OAc) *m/z* (%): 666 (100) $[M+H]^+$.

6.6.3 Bioanalytics: Experimental protocols and instrument settings

6.6.3.1 Preparation of phenobarbital-induced rat liver microsomes

To obtain liver microsomes with metabolically activated CYP enzymes, a male Sprague Dawley rat received 50 mg/kg per day phenobarbital sodium (solution in 0.9 % NaCl solution) intraperitoneally over three days. Then the rat was killed, the liver was excised and immediately cooled on ice. The liver was cut into small pieces with scissors, divided onto two Potter-Elvehjem homogenizer tubes, each filled with 30 ml of cooled 0.15 M potassium phosphate buffer (pH 7.4) and homogenized under ice cooling by 25 heaves at 100 RPM. After every 5 heaves a break of 30 seconds was kept to avoid overheating. The resulting homogenates were centrifuged for 30 min at 9000 g and 4 °C. Subsequently, the lipid layer was discarded, the supernatants (S9-fraction) were removed and subjected to centrifugation at 105000 g for 1 h at 4 °C. Each resulting microsome pellet was suspended in 880 µl 0.15 M phosphate buffer (pH 7.4) containing 17 mM KCl and stored in aliquots á 100 µl at -78 °C. The amount of microsomal protein was determined according to the method of Bradford to 80 mg protein/ml.

6.6.3.2 *In vitro* microsomal incubation conditions

In vitro incubations of test compounds contained the following: 5 mM GSH or dGSH (**6.5**) (stock: 50 mM in phosphate buffer), 2 mg protein/ml phenobarbital-induced rat liver microsomes (stock: 4 mg protein/ml in phosphate buffer) and 50 µM test compound (stock: 5 mM in phosphate buffer (diclofenac) or 10 mM in 70 % ethanol (**6.1**-**6.4**). This mixture was pre-incubated at 37 °C for 5 min. Then, 50 µl of NADPH regenerating system solution A and 10 µl of solution B were added to obtain a total incubation volume of 1 ml. Incubations that contained buffer instead of microsomes served as control. After incubation for 16.5 h (diclofenac) and 2 h (**6.1**-**6.4**) the reaction was quenched by addition of 3 ml of ice-cold MeCN. The mixture was vortex mixed, allowed to stand in the refrigerator for approximately 30 min, again vortex mixed and centrifuged for 5 min at 13000 rpm (13000 g) and 4 °C. The supernatant was collected, evaporated to dryness using a speed vac and stored at -20 °C.

6.6.3.3 Detection of GSH containing metabolites of diclofenac

Samples from microsomal incubation of diclofenac were reconstituted in 500 µl of a water-acetonitrile mixture (90/10, v/v) and aliquots of 10-20 µl were injected for LC-MS/MS analysis. A Luna C18-2 HPLC column (100 x 2.0 mm, 3 µm; Phenomenex, Aschaffenburg, Germany) was used at a flow rate of 0.3 ml/min. For LC-separation following gradient was applied (for mobile phases see 6.6.1): 0 min: A/B = 90/10, 16 min: 40/60, 17-22 min: 2/98, 23-27 min: 90/10. For MS analysis of GSH adducts full scan MS analysis in a range from 250 to 700 Da and product ion scanning over a mass range of 160 to 900 Da were performed in the positive ion electrospray mode with a collision energy of 26 eV. In the MRM mode (collision energy 26 eV) following mass transitions were monitored: *m/z* 617 → 542, 617 → 488, 583 → 508 and 583 → 454.

6.6.3.4 Detection of GSH containing metabolites of 6.1, 6.2, 6.3 and 6.4

For analysis of GSH adducts samples of microsomal incubation were reconstituted in 500 µl of a water-acetonitrile mixture (90/10, v/v) and aliquots (5-20 µl) were subjected to HPLC separation using a Synergi Hydro RP HPLC column (250 x 4.6 mm, 4 µm; Phenomenex, Aschaffenburg, Germany) at a flow rate of 0.6 ml/min. Potential GSH adducts were separated by applying following gradient: 0 min: A/B = 98/2, 15 min: 85/15, 30 min: 25/75, 31-39 min: 5/95, 40-52 min: 98/2. In the full scan MS mode a mass range from 145-1200 Da (**6.1**) and from 200-1400 Da (**6.2**, **6.3**, **6.4**) was measured. Fragmentation by CID was induced at a collision energy of 30 eV. The mass range for CNL scans of **6.1** for loss of 129 Da was set to 350-800 Da. Product ions of **6.1** and **6.2** were scanned between 100-700 Da. For identification of potential GSH adducts of **6.2** following mass transitions were monitored using the MRM mode: *m/z* 665 → 536, 665 → 590 and 665 → 392.

6.6.3.5 Detection of dGSH containing metabolites of 6.1

Samples from microsomal incubation of **6.1** with dGSH were reconstituted in 500 µl of a water-acetonitrile mixture (90/10, v/v) and aliquots of 0.5-1.0 µl were injected for LC-MS/MS analysis. For used HPLC column and flow rate see 6.6.3.3. LC-separation was achieved by applying following gradient: 0 min: A/B = 90/10, 30-35 min: 20/80, 36-40 min: 90/10. Full scan over a mass range of 200-1400 Da and product ion scanning of dGSH over a mass range of 50-600 Da (collision energy: 25 eV) were performed. Furthermore, specific mass transitions of the putative dGSH adduct of **6.1** were followed, namely: *m/z* 870 → 795 and 870 → 363.

6.7 References

1. Baillie, T. A. Future of toxicology-metabolic activation and drug design: challenges and opportunities in chemical toxicology. *Chem. Res. Toxicol.* **2006**, 19, 889-893.
2. Evans, D. C.; Watt, A. P.; Nicoll-Griffith, D. A.; Baillie, T. A. Drug-protein adducts: an industry perspective on minimizing the potential for drug bioactivation in drug discovery and development. *Chem. Res. Toxicol.* **2004**, 17, 3-16.
3. Ma, S.; Subramanian, R. Detecting and characterizing reactive metabolites by liquid chromatography/tandem mass spectrometry. *J. Mass Spectrom.* **2006**, 41, 1121-1139.
4. Argikar, U. A.; Mangold, J. B.; Harriman, S. P. Strategies and chemical design approaches to reduce the potential for formation of reactive metabolic species. *Curr. Top. Med. Chem.* **2011**, 11, 419-449.
5. Argoti, D.; Liang, L.; Conteh, A.; Chen, L.; Bershas, D.; Yu, C. P.; Vouros, P.; Yang, E. Cyanide trapping of iminium ion reactive intermediates followed by detection and structure identification using liquid chromatography-tandem mass spectrometry (LC-MS/MS). *Chem. Res. Toxicol.* **2005**, 18, 1537-1544.
6. Park, B. K.; Kitteringham, N. R.; Maggs, J. L.; Pirmohamed, M.; Williams, D. P. The role of metabolic activation in drug-induced hepatotoxicity. *Annu. Rev. Pharmacool. Toxicol.* **2005**, 45, 177-202.
7. Townsend, D. M.; Tew, K. D.; Tapiero, H. The importance of glutathione in human disease. *Biomed. Pharmacother.* **2003**, 57, 145-155.
8. Anderson, M. E. Glutathione: an overview of biosynthesis and modulation. *Chem. Biol. Interact.* **1998**, 111-112, 1-14.
9. Castro-Perez, J.; Plumb, R.; Liang, L.; Yang, E. A high-throughput liquid chromatography/tandem mass spectrometry method for screening glutathione conjugates using exact mass neutral loss acquisition. *Rapid Commun. Mass Spectrom.* **2005**, 19, 798-804.
10. Dieckhaus, C. M.; Fernandez-Metzler, C. L.; King, R.; Krolikowski, P. H.; Baillie, T. A. Negative ion tandem mass spectrometry for the detection of glutathione conjugates. *Chem. Res. Toxicol.* **2005**, 18, 630-638.
11. Yan, Z.; Caldwell, G. W. Stable-isotope trapping and high-throughput screenings of reactive metabolites using the isotope MS signature. *Anal. Chem.* **2004**, 76, 6835-6847.
12. Zhu, M.; Ma, L.; Zhang, H.; Humphreys, W. G. Detection and structural characterization of glutathione-trapped reactive metabolites using liquid chromatography-high-resolution mass spectrometry and mass defect filtering. *Anal Chem* **2007**, 79, 8333-8341.
13. Dalvie, D. K.; Kalgutkar, A. S.; Khojasteh-Bakht, S. C.; Obach, R. S.; O'Donnell, J. P. Biotransformation reactions of five-membered aromatic heterocyclic rings. *Chem. Res. Toxicol.* **2002**, 15, 269-299.
14. Ghorai, P.; Kraus, A.; Keller, M.; Gotte, C.; Igel, P.; Schneider, E.; Schnell, D.; Bernhardt, G.; Dove, S.; Zabel, M.; Elz, S.; Seifert, R.; Buschauer, A. Acylguanidines as bioisosteres of guanidines: NG-acylated imidazolylpropylguanidines, a new class of histamine H2 receptor agonists. *J. Med. Chem.* **2008**, 51, 7193-7204.
15. Kalgutkar, A. S.; Driscoll, J.; Zhao, S. X.; Walker, G. S.; Shepard, R. M.; Soglia, J. R.; Atherton, J.; Yu, L.; Mutlib, A. E.; Munchhof, M. J.; Reiter, L. A.; Jones, C. S.; Doty, J. L.; Trevena, K. A.; Shaffer, C. L.; Ripp, S. L. A rational chemical intervention strategy to circumvent bioactivation liabilities associated with a nonpeptidyl thrombopoietin receptor agonist containing a 2-amino-4-arylthiazole motif. *Chem. Res. Toxicol.* **2007**, 20, 1954-1965.
16. Yu, L. J.; Chen, Y.; Deninno, M. P.; O'Connell, T. N.; Hop, C. E. Identification of a novel glutathione adduct of diclofenac, 4'-hydroxy-2'-glutathion-deschloro-diclofenac, upon incubation with human liver microsomes. *Drug Metab. Disposition* **2005**, 33, 484-488.
17. Kalgutkar, A. S.; Gardner, I.; Obach, R. S.; Shaffer, C. L.; Callegari, E.; Henne, K. R.; Mutlib, A. E.; Dalvie, D. K.; Lee, J. S.; Nakai, Y.; O'Donnell, J. P.; Boer, J.; Harriman, S. P. A comprehensive listing of bioactivation pathways of organic functional groups. *Curr. Drug Metab.* **2005**, 6, 161-225.
18. Tang, W.; Stearns, R. A.; Bandiera, S. M.; Zhang, Y.; Raab, C.; Braun, M. P.; Dean, D. C.; Pang, J.; Leung, K. H.; Doss, G. A.; Strauss, J. R.; Kwei, G. Y.; Rushmore, T. H.; Chiu, S. H.; Baillie, T. A. Studies on cytochrome P-450-mediated bioactivation of diclofenac in rats and in human hepatocytes: identification of glutathione conjugated metabolites. *Drug Metab. Disposition* **1999**, 27, 365-372.

19. Kraus, A.; Ghorai, P.; Birnkammer, T.; Schnell, D.; Elz, S.; Seifert, R.; Dove, S.; Bernhardt, G.; Buschauer, A. N(G)-acylated aminothiazolylpropylguanidines as potent and selective histamine H(2) receptor agonists. *ChemMedChem* **2009**, 4, 232-240.
20. Subramanian, R.; Lee, M. R.; Allen, J. G.; Bourbeau, M. P.; Fotsch, C.; Hong, F. T.; Tadesse, S.; Yao, G.; Yuan, C. C.; Surapaneni, S.; Skiles, G. L.; Wang, X.; Wohlhieter, G. E.; Zeng, Q.; Zhou, Y.; Zhu, X.; Li, C. Cytochrome P450-mediated epoxidation of 2-aminothiazole-based AKT inhibitors: identification of novel GSH adducts and reduction of metabolic activation through structural changes guided by in silico and in vitro screening. *Chem. Res. Toxicol.* **2010**, 23, 653-663.
21. Kraus, A. Highly potent, selective acylguanidine-type histamine H2 receptor agonists: synthesis and structure-activity relationships. Dissertation, 2008. http://epub.uni-regensburg.de/10699/.
22. Gan, J.; Harper, T. W.; Hsueh, M. M.; Qu, Q.; Humphreys, W. G. Dansyl glutathione as a trapping agent for the quantitative estimation and identification of reactive metabolites. *Chem. Res. Toxicol.* **2005**, 18, 896-903.
23. Walker, J. M. The Dansyl-Edman method for peptide sequencing. *Methods Mol. Biol.* **1994**, 32, 329-334.
24. Walker, J. M. The dansyl method for identifying N-terminal amino acids. *Methods Mol. Biol.* **1994**, 32, 321-328.
25. El-Enany, N.; Belal, F.; Rizk, M. Spectrofluorimetric determination of oxamniquine in dosage forms and spiked human plasma through derivatization with 1-dimethylaminonaphthalene-5-sulphonyl chloride. *J. Fluoresc.* **2008**, 18, 349-355.
26. Gan, J.; Harper, T. W.; Humphreys, W. G. Fluorescently labeled thiol-containing trapping agent for the quantitation and identification of reactive metabolites in vitro. US 20050186651, 2005.
27. Murakami, T.; Fukutsu, N.; Kondo, J.; Kawasaki, T.; Kusu, F. Application of liquid chromatography-two-dimensional nuclear magnetic resonance spectroscopy using pre-concentration column trapping and liquid chromatography-mass spectrometry for the identification of degradation products in stressed commercial amlodipine maleate tablets. *J. Chromatogr. A* **2008**, 1181, 67-76.

Chapter 7
Unspecific Toxicity of N^G-Acylated Hetarylpropylguanidines

7.1 Introduction

In contrast to drug toxicity arising from enzymatic bioactivation of drugs to reactive metabolites, toxic effects can be elicited by the parent compound *per se*. As a prerequisite for application as pharmacological tools for *in vivo* or cell based *in vitro* studies, representative N^G-acylated hetarylpropylguanidines were tested with respect to their potential to induce the rupture of erythrocytes (hemolysis) and toxicity in cells (cytotoxicity). Hemolysis results in the release of hemoglobin from erythrocytes. Due to the characteristic absorption maximum of hemoglobin at 580 nm the hemolytic effect of a substance can be determined spectrophotometrically. Cytotoxicity was studied in a standard crystal violet based chemosensitivity assay with long-term exposure of test compounds on HT-29 colon carcinoma cells.[1] Furthermore, short-term cytotoxic effects were assessed in a lactate dehydrogenase (LDH) assay using HT-29 cells and cultured primary human hepatocytes (PHH). The cytotoxic effect is proportional to the release of LDH activity, which is determined spectrophotometrically, measuring the LDH-catalyzed reduction of pyruvate to lactate under consumption of NADH.[2]

Selected substances out of a set of N^G-acylated imidazolylpropylguanidines and N^G-acylated 2-aminothiazolylpropylguanidines shown in Table 7.1 were used for hemolysis and cytotoxicity studies. These compounds were synthesized in our workgroup and provided by Dr. A. Kraus and T. Birnkammer.[3-4]

Table 7.1. N^G-acylated imidazolylpropylguanidines and N^G-acylated 2-aminothiazolylpropylguanidines used for hemolysis and cytotoxicity studies.

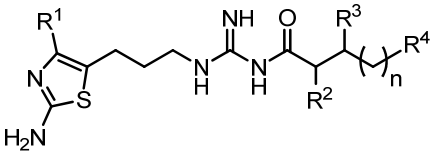

No	R^1	R^2	R^3	R^4	n
6.1	H	H	H	C_6H_5	0
6.2	H	H	CH_2CH_3	C_6H_5	0
6.3	CH_3	H	H	C_6H_5	0
6.4	CH_3	H	CH_2CH_3	C_6H_5	0
7.1	H	H	CH_3	C_6H_5	0
7.2	H	H	CH_3	cy	0
7.3	CH_3	CH_3	H	C_6H_5	0
7.4	CH_3	CH_3	H	cy	0
7.5	CH_3	H	CH_3	C_6H_5	1
7.6	CH_3	H	CH_3	cy	1
7.7	CH_3	H	CH_3	4-CH_3-C_6H_4	0
7.8	CH_3	H	CH_2CH_3	cy	0
7.9	CH_3	H	CH_3	4-OH-C_6H_4	0

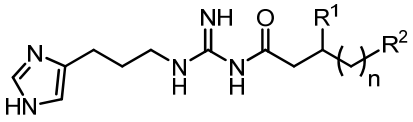

No	R^1	R^2	n
7.10	CH_3	C_6H_5	1
7.11	CH_3	cy	1
7.12	CH_3	4-CH_3-C_6H_4	0
7.13	CH_3	3-OCH_3-C_6H_4	1

7.2 Hemolytic potential of selected N^G-acylated hetarylpropylguanidines

In Figure 7.1 the percentage of hemolysis of selected N^G-acylated hetarylpropyl-guanidines (cf. Table 7.1 for structures) is shown compared to the reference compound digitonin, which is known to induce strong hemolysis.[5] At a concentration of 100 µM severe hemolysis (60-100 %) was observed for **7.4**, **7.6**, **7.8** and **7.11**. In addition, **7.2** exhibited a significant hemolytic effect (~20 %). For all other investigated compounds the hemolytic effect was rather weak. Strikingly, **7.2**, **7.4**, **7.6**, **7.8** and **7.11** have a cyclohexyl ring at the end of the acyl chain in common. It is known from literature that interactions of certain substances with the erythrocyte membrane can lead to hemolysis by inducing osmotic pressure followed by cell swelling or by partial solubilization of membrane lipids and proteins, e.g by formation of mixed micelles.[6] These mechanisms are typical for amphiphilic substances such as surfactants. Regarding the investigated N^G-acylated hetarylpropylguanidines, the introduction of a highly lipophilic cyclohexyl moiety obviously resulted in a marked increase in compromising the erythrocyte membrane. Presumably, the amphiphilic character of the compounds became more distinct, as, in contrast to the cyclohexyl moiety, the acylguanidine represents the more polar partial structure in the respective molecules due to protonation at physiological pH. Furthermore, the imidazole and 2-aminothiazole heterocyles are considered more polar as well. On the other hand, compounds bearing a less lipophilic acyl chain seemed to have a decreased tendency for solubilization of the cell membrane due to reduced amphiphilicity. At a test concentration of 30 µM the hemolytic effect especially of

compounds **7.2**, **7.4**, **7.6**, **7.8** and **7.11** was drastically decreased. Only **7.6** and **7.8** still caused weak hemolysis, whereas the effect of all other compounds was marginal (< 5 %). Probably, at 30 µM the concentration of these compounds was below the critical micellar concentration to effectively damage the erythrocyte membrane.

Taken together, in view of cellular *in vivo* experiments, concentrations higher than 30 µM of amphiphilic N^G-acylated hetarylpropylguanidines, especially those bearing lipophilic residues such as cyclohexyl, should be avoided. Less "tenside-like" compounds were found to induce only minor hemolytic effects up to a concentration of 100 µM.

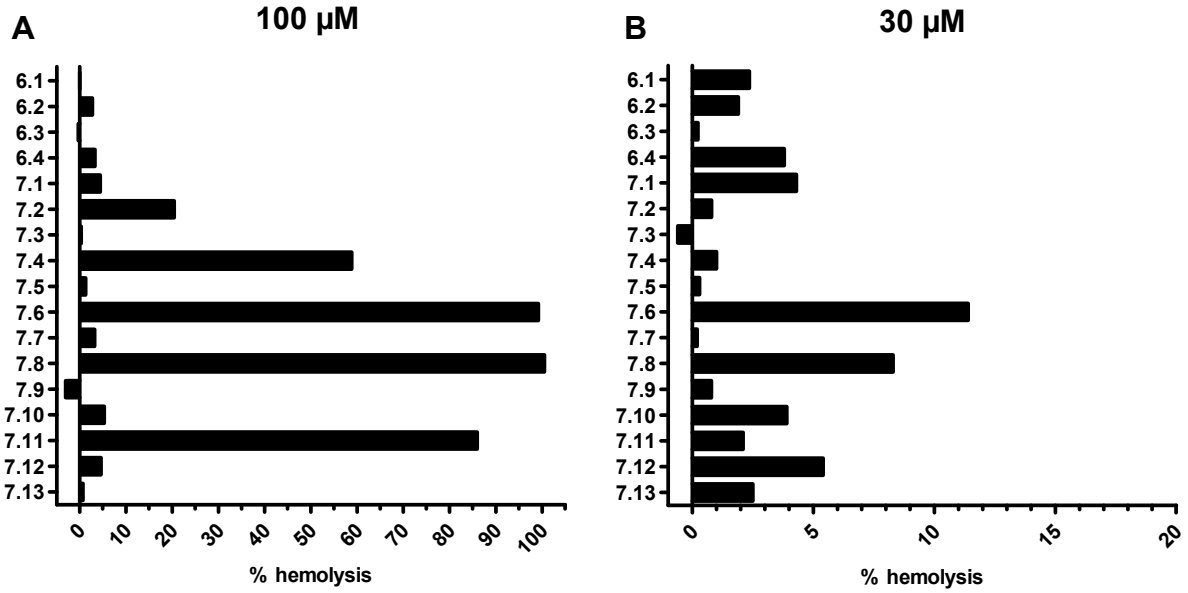

Figure 7.1. Mean percentage of hemolysis (n=2) induced by N^G-acylated hetarylpropylguanidines at 100 µM (**A**) and 30 µM (**B**).

7.3 Cytotoxicity of selected N^G-acylated hetarylpropylguanidines in the crystal violet assay

In order to investigate the potential cytotoxic effects of N^G-acylated hetarylpropylguanidines, selected compounds (**6.1**, **7.1**, **7.6**, **7.9**, **7.11**; cf. Table 7.1) were investigated in a crystal violet based chemosensitivity assay[1] on proliferating human HT-29 colon carcinoma cells over a period of approximately 200 h. Cisplatin was taken as a reference compound. The results are presented as plots of corrected T/C values (cf. Equation 7.2 in the experimental part) *vs.* time of incubation to distinguish cytotoxic (T/C_{corr} > 0 %) and cytocidal (T/C_{corr} < 0 %) drug effects (Figure 7.2 A-F).

All tested compounds showed more or less distinct cytotoxicity in the concentration range of 3-100 µM. In addition, after 200 h cytocidal effects were detected for **7.1** at 100 µM, for **7.6** at 10 µM and 100 µM and for **7.11** at 10 µM, 30 µM and 100 µM. Thus, **7.6** and **7.11** were considered the compounds with the highest cytotoxicity. This observation confirms the results from the hemolysis studies, in which the compounds, comprising a cyclohexyl moiety and assumably the highest extent of amphiphilicity, produced

the most pronounced cell-damaging effects. In conclusion, one should be aware of potential cytotoxicity of N^G-acylated hetarylpropylguanidines at micromolar concentrations with respect to cell based *in vitro* or *in vivo* studies.

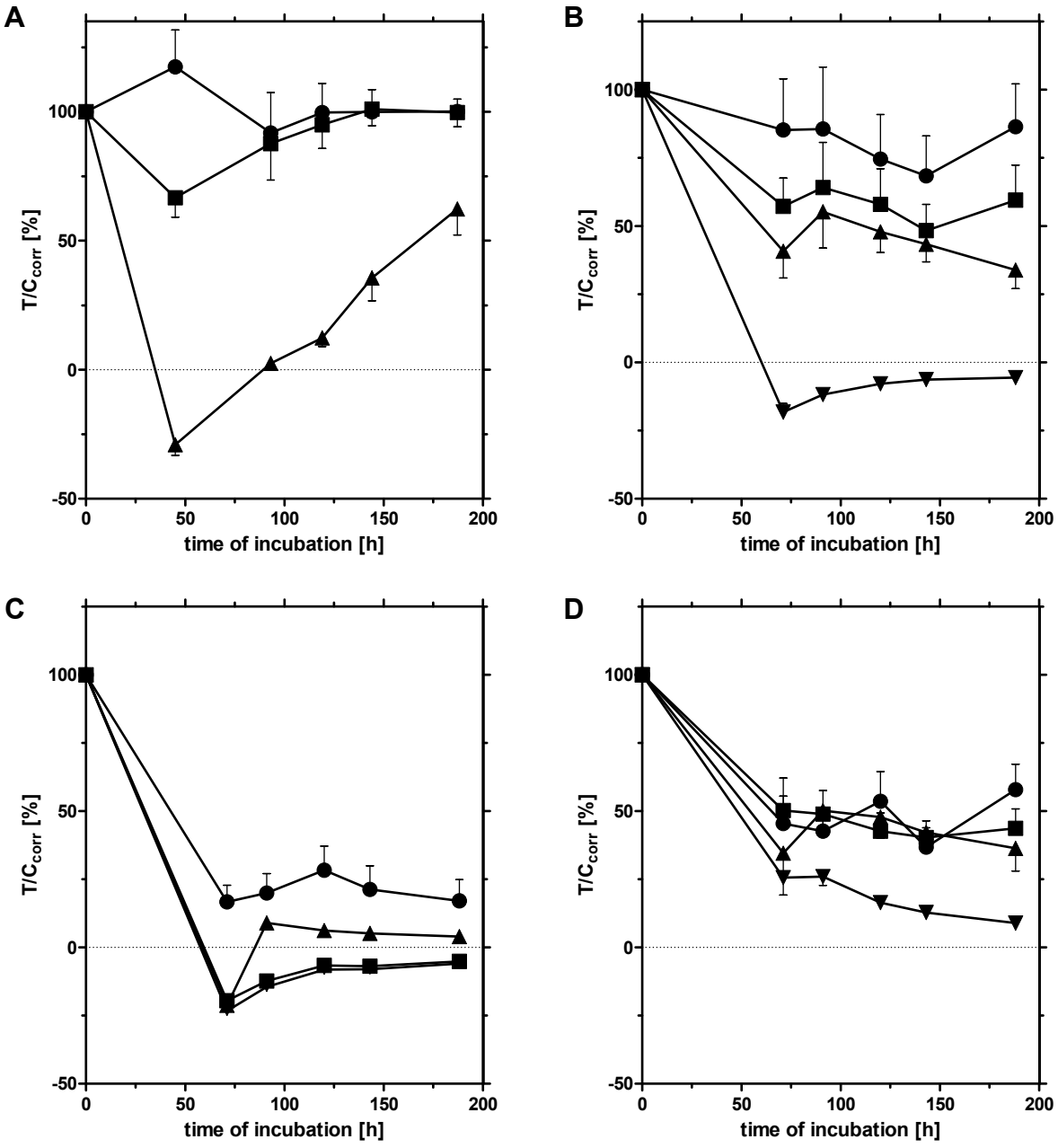

Figure 7.2 continued on page 221

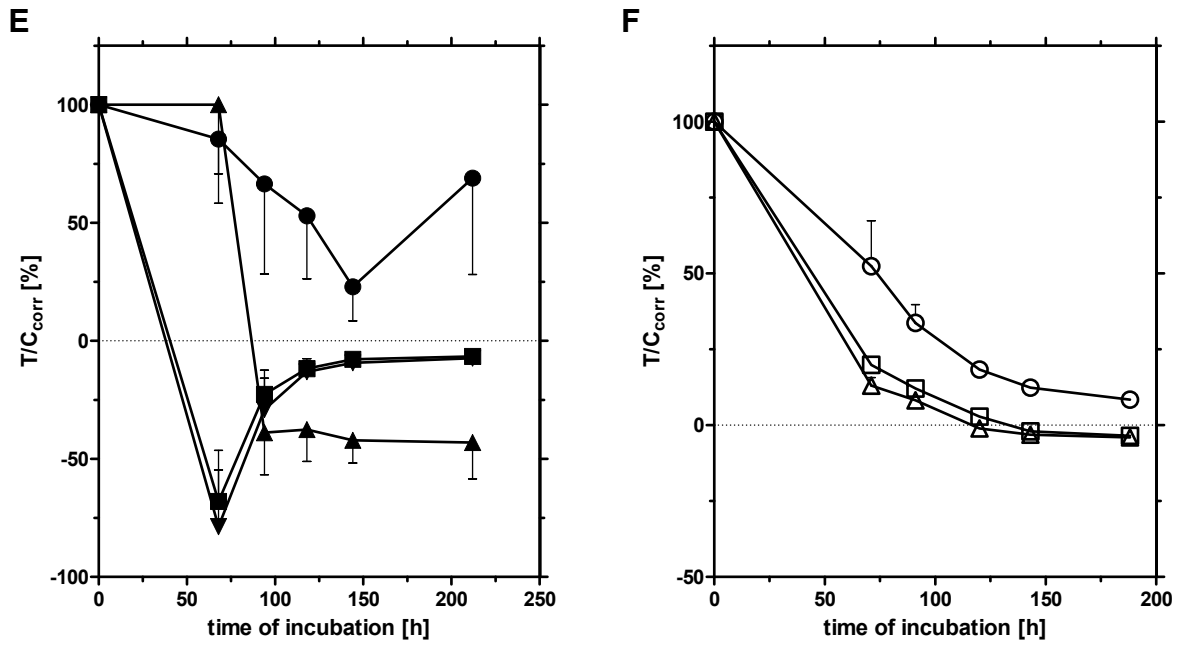

Figure 7.2. Effects of **6.1** (**A**), **7.1** (**B**), **7.6** (**C**), **7.9** (**D**) and **7.11** (**E**) on proliferating HT-29 cells upon long-term exposure. Following concentrations were used: 3 µM (●), 10 µM (■), 30 µM (▲), 100 µM (▼). Cisplatin (**F**) was used as positive control in following concentrations: 1 µM (**O**), 2.5 µM (□), 5 µM (△).

7.4 Cytotoxicity of selected N^G-acylated hetarylpropylguanidines in the lactate dehydrogenase assay

In order to assess the cytotoxicity of N^G-acylated hetarylpropylguanidines upon short-term exposure (24 h), selected compounds (cf. Table 7.1 for structures) were tested in a lactate dehydrogenase (LDH) assay on HT-29 colon carcinoma cells. To take a potential impact of metabolism on the toxification into account, the same compounds were also exposed to cultured primary human hepatocytes (PHH), as PHH generally have a higher metabolical capacity and activity.

The extent of LDH release, which positively correlates with the percentage of cell death, was determined relative to the effect of the detergent Triton X-100, which strongly induces cell lysis. In Figure 7.3 the effect of representative compounds on HT-29 cells at test concentrations of 30 µM and 100 µM, respectively (exception: **7.6**, 30 and 50 µM) are depicted. Compared to the control, all compounds except for **7.6** and **7.11** at 50 µM and 100 µM, respectively, induced no more than a slight increase in LDH release over an incubation period of 24 h. However, incubation of HT-29 cells with **7.6** at a concentration of 50 µM led to approximately 55 % cell death, and **7.11**, the most cytotoxic compound among the investigated acylguanidines, killed 100 % of the cells at a concentration of 100 µM. These findings are in accordance with the results from the crystal violet based chemosensitivity assay and from hemolysis studies. Again, **7.6** and **7.11** proved to drastically affect membrane integrity at concentrations in the upper micromolar range.

Incubation of the same set of test compounds with cultured PHHs revealed an overall higher sensitivity of PHHs compared to HT-29 cells (cf. Figure 7.4). This effect may be

caused by the absence of FCS in the culture medium. As N^G-acylated hetarylpropylguanidines are known to exhibit strong plasma protein binding, in medium devoid of FCS, the concentration of "free" compound, that can exert a cytotoxic effect, is higher. Except for **6.1**, **6.3** and **6.9**, all investigated compounds caused high percentage (up to 100 %) of cell death. Compound **7.11** even showed a relatively strong cytotoxic effect at both 30 µM and 100 µM. Obviously, lowering the lipophilicity of the acyl chain (**6.1**) or introduction of polar substituents such as a hydroxy group (**7.9**) resulted in reduced cytotoxicity. Regarding the compounds **6.1** and **6.3** as well as **6.2** and **6.4**, no significant difference in LDH release was detectable. Hence, introduction of a 4-methyl residue at the 2-aminothiazole ring does not alter the cytotoxic properties. Again, an increase in amphiphilicity by introduction of alkyl moieties at the acyl side chain, seemed to have a more distinct impact on the cytotoxic properties, presumably, by increasing the tendency for formation of micelles.

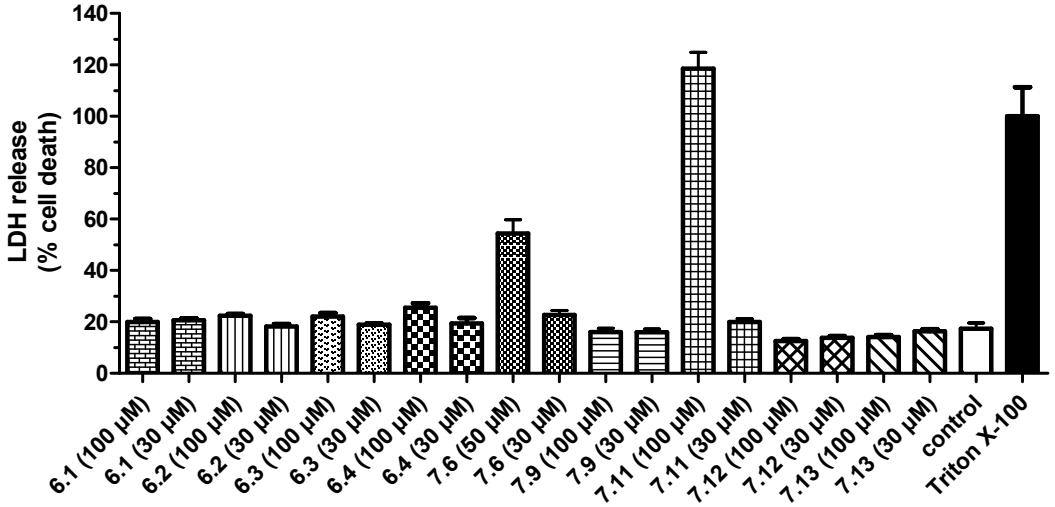

Figure 7.3. Effects of selected N^G-acylated hetarylpropylguanidines on HT-29 cells depicted as percent LDH release, respectively cell death, relative to Triton X-100 (n=3).

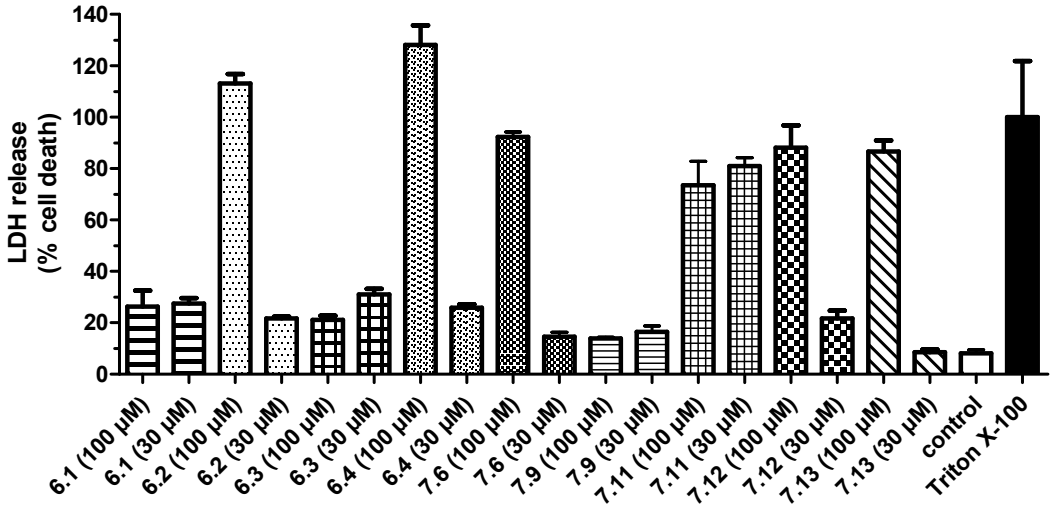

Figure 7.4. Effects of selected N^G-acylated hetarylpropylguanidines on cultured primary human hepatocytes depicted as percent LDH release, respectively cell death, relative to Triton X-100 (n=3).

7.5 Summary

With respect to their use in cell based *in vitro* studies or future *in vivo* experiments, selected N^G-acylated hetarylpropylguanidines were characterized regarding their hemolytic and cytotoxic properties. At a concentration of 30 µM only weak hemolytic effects were observed, whereas at 100 µM strong hemolysis was induced by compounds bearing a cyclohexyl residue-containing acyl chain. Obviously, the increase in acyl chain lipophilicity and overall amphiphilicity led to an enhanced damage of the erythrocyte membrane, presumably by solubilization of membrane lipids and proteins through formation of mixed micelles. In the crystal violet chemosensitivity assay all tested compounds showed a more or less distinct cytotoxic effect in the concentration range of 3-100 µM over an incubation period of 200 h. Cytocidal effects were detected for compounds containing a 4-cyclohexyl-3-methylbutanoyl chain at 10 µM to 100 µM. Furthermore, selected compounds were incubated for 24 h in a lactate dehydrogenase assay on HT-29 colon carcinoma cells and cultured primary human hepatocytes (PHH). In accordance to the results obtained from hemolysis and long-term chemosensitivity assay, compounds bearing lipophilic cyclohexyl residues, tested at a concentration of 100 µM, revealed the most pronounced compromising effect on membrane integrity. A concentration of 30 µM was generally well tolerated by HT-29 cells. However, PHHs were observed to have a higher sensitivity when incubated with N^G-acylated hetaryl-propylguanidines.

In summary, N^G-acylated hetarylpropylguanidines revealed considerable hemolytic and cytotoxic effects in the micromolar range, particularly when the acyl part of the compounds contained highly lipophilic moieties such as a cyclohexyl ring. These findings must be taken into account, when the compounds are used for cell based *in vitro* assays or in *in vivo* studies.

7.6 Experimental section

7.6.1 Determination of hemolytic properties of N^G-acylated hetarylpropyl-guanidines using mouse erythrocytes

Isotonic saline (2 ml) was added to fresh citrated mouse blood (1 ml). After centrifugation (70 g, 15 min, 4 °C) the supernatant plasma and the leukocyte-layer were removed. The resulting erythrocytes were re-suspended in isotonic saline (1 ml) and centrifuged (2000 g, 10 min, 4 °C). The supernatant was discarded and the washing procedure was repeated twice. Subsequently, the erythrocytes were stored on ice before use on the same day.

500 µl of freshly prepared erythrocytes were diluted with 9.5 ml of isotonic saline and aliquots á 50 µl were filled into each well of a microtiter plate (Greiner, Frickenhausen, Germany). Then, 1 µl of respective test compound stock solutions (1.5 mM and 5 mM, respectively in 70 % EtOH) was added to obtain the final concentration of the test

compounds (30 µM and 100 µM, respectively). For control experiments 1 µl of 70 % EtOH was added (0 % hemolysis) and 1 µl of digitonin solution (2 %, w/v) was added as a reference to induce 100 % hemolysis. Each sample was prepared in duplicate. After careful mixing, the plate was incubated for 1 h at 37 °C and shaken every 20 min. The plate was centrifuged at 2000 g for 3 min and 30 µl of each well were transferred to a new microtiter plate. After addition of 100 µl of isotonic saline into each well, the absorbance was measured at 580 nm ($\lambda_{\text{hemoglobin, max}}$) and at 485 nm ($\lambda_{\text{hemoglobin, min}}$) using a GENios Pro microplate reader (Tecan Deutschland GmbH, Crailsheim, Germany). The percentage hemolysis was calculated according to Equation 7.1.

$$\%\ \text{Hemolysis} = \left(\frac{A_{580\ \text{nm}}}{A_{485\ \text{nm}}} - \frac{A_{580\ \text{nm (0 \%)}}}{A_{485\ \text{nm (0 \%)}}}\right) \Big/ \left(\frac{A_{580\ \text{nm (100 \%)}}}{A_{485\ \text{nm (100 \%)}}} - \frac{A_{580\ \text{nm (0 \%)}}}{A_{485\ \text{nm (0 \%)}}}\right) \cdot 100$$

Equation 7.1. $A_{580\ nm}$, $A_{485\ nm}$ = measured absorbance of the sample at 580 nm and 485 nm, respectively; $A_{580\ nm\ (0\ \%)}$, $A_{485\ nm\ (0\ \%)}$ = measured absorbance of the control at 580 nm and 485 nm, respectively; $A_{580\ nm\ (100\ \%)}$, $A_{485\ nm\ (100\ \%)}$ = measured absorbance of the reference containing digitonin at 580 nm and 485 nm, respectively

7.6.2 Crystal violet chemosensitivity assay

The assay was performed according to the procedure described by Bernhardt et al.[1] In brief, tumor cells were seeded into flat-bottomed 96-well plates (Greiner, Frickenhausen, Germany) at a density of ca. 15 cells per microscopic field (magnification: 320-fold). After 48-72 h of incubation at 37 °C / 5 % CO_2, the culture medium was replaced by fresh medium containing the test compounds at various concentrations. Cells treated with medium containing the respective solvent used for the test compounds served as control. After various incubation periods, medium was discarded, the cells were fixed with 1 % glutardialdehyde solution in PBS and stored at 4 °C. At the end of the experiment the mass of viable cells was determined by simultaneous staining of all plates with 0.02 % aqueous crystal violet (Serva, Heidelberg, Germany) solution. Subsequently, excess dye was removed with water and cell-bound crystal violet was re-dissolved with 70 % ethanol. The absorbance was measured at 578 nm using a BioTek 309 Autoreader (Tecnomara, Fernwald, Germany) or at 580 nm using a GENios Pro microplate reader (Tecan Deutschland GmbH, Crailsheim, Germany).

The effects of the test compounds on the proliferating cells were presented as corrected T/C values according to Equation 7.2.

$$\text{T/C}_{\text{corr}}\ (\%) = \frac{(\text{T} - \text{C}_0)}{(\text{C} - \text{C}_0)} \cdot 100$$

Equation 7.2. T = mean absorbance of treated cells, C = mean absorbance of controls, C_0 = mean absorbance at the time when test compounds were added (t = 0).

7.6.3 Lactate dehydrogenase assay

HT-29 colon carcinoma cells were cultured in McCoy's medium supplemented with 5 % FCS. Two days prior to addition of test compounds, tumor cells were seeded into flat-bottomed 96-well plates (Greiner, Frickenhausen, Germany) at a density of ca. 60 cells per microscopic field (magnification: 320-fold) and incubated for 48 h at 37 °C / 5 % CO_2. Stock solutions (30 mM) of test compounds were prepared in 70 % EtOH. The culture medium was removed and replaced by fresh medium (200 µl per well) containing test compounds at concentrations of 30 µM and 100 µM, respectively. Cells treated with medium containing 70 % EtOH served as control. After incubation for 24 h, 2 µl each of a 10 % aqueous Triton X-100 solution were added to 8 untreated wells and were incubated for 30 min to achieve 100 % LDH release. Subsequently, the microtiter plates were centrifuged at 120 g for 3 min. 50 µl of each supernatant were transferred into fresh microtiter plates. After addition of 110 µl of 0.1 M KH_2PO_4/K_2HPO_4 buffer pH 7.00 supplemented with 1 mM EDTA and 0.1 mM DTE and 10 µl of a freshly prepared 7 mM solution of NADH (Roche Diagnostics) in buffer, the reaction was started by addition of 20 µl of a 10.5 mM solution of pyruvate in Millipore water using a GENios Pro microplate reader (Tecan Deutschland GmbH, Crailsheim, Germany). The reaction was monitored by measuring the decrease in absorbance at 340 nm caused by the oxidation of NADH over a period of ca. 9 min. The slope of the linear part of the absorbance *vs*. reaction time plot was used for determination of the LDH release, which corresponds to the percentage of cell death. Thereby, the mean slope obtained from wells treated with Triton X-100 is set to 100 % cell death.

Primary human hepatocytes were isolated and cultured as described in section 3.8.3. One day after isolation the culture medium was replaced by fresh culture medium devoid of FCS. 24 h later, the culture medium was removed and fresh medium (devoid of FCS) containing the test compounds was added. Further steps were performed according to the assay procedure described above for HT-29 cells.

7.7 References

1. Bernhardt, G.; Reile, H.; Birnbock, H.; Spruss, T.; Schonenberger, H. Standardized kinetic microassay to quantify differential chemosensitivity on the basis of proliferative activity. *J. Cancer Res. Clin. Oncol.* **1992**, 118, 35-43.
2. Bergmeyer, H. U.; Gawehn, K. *Methoden der enzymatischen Analyse*. 3., neubearb. u. erw. Aufl. ed.; Verl. Chemie: Weinheim, 1974; p XXXIX, 1150, LXXXI S.
3. Kraus, A. Highly potent, selective acylguanidine-type histamine H2 receptor agonists: synthesis and structure-activity relationships. Dissertation, 2008. http://epub.uni-regensburg.de/10699/.
4. Kraus, A.; Ghorai, P.; Birnkammer, T.; Schnell, D.; Elz, S.; Seifert, R.; Dove, S.; Bernhardt, G.; Buschauer, A. N(G)-acylated aminothiazolylpropylguanidines as potent and selective histamine H(2) receptor agonists. *ChemMedChem* **2009**, 4, 232-240.
5. Ransom, F. On the Cardiac, Haemolytic and Nervous Effects of Digitonin. *Biochem. J* **1922**, 16, 668-677.
6. Thoren, P. E.; Soderman, O.; Engstrom, S.; von Corswant, C. Interactions of novel, nonhemolytic surfactants with phospholipid vesicles. *Langmuir* **2007**, 23, 6956-6965.

Chapter 8 Summary

Figuratively, drug metabolism can be considered as two sides of the same coin; one leading to desired, beneficial effects, e.g. by activation of prodrugs, whereas the other one results in adverse side effects due to toxic metabolites. In this work both aspects were explored more closely.

Transdermal therapeutic systems (TTS) are known as drug formulations providing constant and sustained drug plasma levels at reduced application frequency. Therefore, TTS are particularly advantageous for the treatment of disorders requiring long-term pharmacotherapy as, e.g., cardiovascular diseases. By now, hypertension is recognized as one of the leading risk factors for cardiovascular morbidity and mortality. However, there is a strong discrepancy between the high incidence of hypertension and the availability of transdermally applicable antihypertensive drugs.

Thus, one part of this thesis aimed at novel derivatives of the angiotensin II AT_1 receptor antagonist candesartan and the angiotensin-converting enzyme inhibitor (ACEi) cilazapril, suitable for administration *via* a TTS. The prodrug approach was pursued to design and synthesize various ester-based candesartan and cilazapril prodrugs with physicochemical properties considered suitable to overcome the barrier function of the skin. The novel compounds were bioanalytically characterized with respect to solid-state stability, susceptibility for enzymatic hydrolysis, and stability against non-enzymatic hydrolysis. All candesartan and cilazapril prodrugs except for a simple ethyl ester of cilazapril were enzymatically hydrolyzed to release the active principle. By contrast to other ACEi, decomposition by diketopiperazine formation was not observed during synthesis and storage, due to the conformationally constrained structure of the cilazapril scaffold. Additionally, the potential candesartan prodrugs turned out to be potent angiotensin II AT_1 receptor antagonists (K_b = 0.8 – 6.4 nM) in a fura-2 Ca^{2+}-assay on rat glomerular mesangial cells.

The three most promising candidates of each group were selected for TTS development, namely candesartan 1-(isopropyloxycarbonyloxy)ethyl ester, candesartan 1-(2,2-dimethylpropanoyloxy)ethyl ester and candesartan morpholinoethyl ester as well as cilazapril 1-(ethoxycarbonyloxy)ethyl ester, cilazapril 1-(cyclohexyloxycarbonyloxy)ethyl ester and cilazapril morpholinoethyl ester. These new chemical entities were found to be comparable or even superior to the reference compounds candesartan cilexetil and cilazapril, respectively, in terms of formulate-ability, TTS quality and stability in a silicone PSA matrix.

Furthermore, the manufactured TTS containing the new prodrugs were superior to the respective candesartan cilexetil and cilazapril formulations, when investigated for transdermal permeation through animal and human skin using Franz diffusion cells.

The second part of this thesis addressed the adverse side of drug metabolism, namely toxic effects due to the formation of reactive metabolites/intermediates capable of covalent protein binding. In our workgroup highly potent N^G-acylated hetarylpropylguanidine-type H_2R agonists, comprising either an imidazole ring or a 2-aminothiazole group, were developed, which could serve as valuable pharmacological tools for *in vitro* and potential *in vivo* studies. There is strong evidence that cytochrome P450-mediated bioactivation of the 2-aminothiazole ring results in highly reactive intermediates.
Thus, the aim of this project was the detection and identification of reactive intermediates by co-incubating N^G-acylated 3-(2-aminothiazol-5-yl)propylguanidines with rat liver microsomes and glutathione (GSH) to trap putative reactive molecules. By means of liquid chromatography/tandem mass spectrometry (LC-MS) and appropriate MS/MS experiments such as full scan, constant neutral loss scanning, multiple reaction monitoring and product ion scanning, GSH adducts of reactive intermediates of N^G-acylated 3-(2-aminothiazol-5-yl)propylguanidines were detected. Benefitting from the selectivity of fluorescence detection, these results were corroborated by using dansylated GSH as a trapping agent. Interestingly, blocking of the 4-position of the 2-aminothiazole by methyl substitution seemed to be a successful strategy to prevent bioactivation of the heterocycle.

Finally, unspecific toxicity of N^G-acylated hetarylpropylguanidines was investigated, revealing considerable hemolysis and cytotoxicity in the micromolar range, particularly when the acyl part of the compounds contained highly lipophilic moieties.

In summary, the ambivalent character of drug metabolism was highlighted in this thesis. Novel synthesized prodrugs of cilazapril and candesartan turned out to be enzymatically convertible to the active drug and to be superior to the reference drugs in terms of stability, formulate-ability and skin permeability, thus representing promising compounds for transdermal antihypertensive therapy *via* TTS. By contrast, the identification of reactive intermediates of N^G-acylated hetarylpropylguanidines demonstrated that one should be aware of the potential risk of bioactivation residing in structural moieties such as aminothiazoles to avoid toxification.

Chapter 9 Appendix

9.1 Appendix 1: Abbreviations

ACE	angiotensin-converting enzyme
ACEi	angiotensin-converting enzyme inhibitor
ADR	adverse drug reaction
Ang II	angiotensin II
aq.	aqueous
ARB	angiotensin II AT_1 receptor antagonist / blocker
AT_1R, AT_2R	angiotensin II receptor subtypes
BSA	bovine serum albumine
$[Ca^{2+}]_i$	intracellular calcium ion concentration
CID	collision-induced dissociation
CNL	constant neutral loss
CPD	citrate phosphate dextrose
cy	cyclohexyl
CYP	cytochrome P450 enzyme
d	day
Da	Dalton
DCC	*N,N'*-dicyclohexylcarbodiimide
DCM	dichloromethane
DMAP	*p*-dimethylaminopyridine
DMF	dimethylformamide
DMSO	dimethyl sulfoxide
DTE	dithioerythritol
DTT	dithiothreitol
EC_{50}	agonist concentration which induces 50 % of the maximal effect
EDTA	ethylenediaminetetraacetic acid
EGTA	ethylene glycol-bis(2-aminoethylether)-*N,N,N',N'*-tetraacetic acid
EI-MS	electron impact mass spectrometry
Eq	equivalent
ESI	electrospray ionisation
EtOAc	ethyl acetate
EtOH	ethanol
$f_{50\%}$	time at which 50 % of the active principle have been formed
FCS	fetal calf serum
GI	gastrointestinal tract

GSH	reduced glutathione
GSSG	glutathione disulfide, oxidized glutathione
h	hour
HPLC	high performance liquid chromatography
HR-MS	high resolution mass spectrometry
HT-29	human colon carcinoma cell line
IC_{50}	antagonist concentration which suppresses 50 % of an agonist induced effect
^{i}Pr	isopropyl
J_{ss}	steady state flux
k	retention (capacity) factor
K_b	dissociation constant derived from a functional assay
LC-MS	liquid chromatography tandem mass spectrometry
log *P*	partition coefficient
log *D*	distribution coefficient
log $D^{5.5}$	distribution coefficient at pH 5.5
M	mol/L
MeCN	acetonitrile
MeOH	methanol
min	minute
mo	morpholine
mp	melting point
MRM	multiple reaction monitoring
m/z	mass-to-charge ratio
NADH	nicotinamide adenine dinucleotide (reduced form)
NADPH	nicotinamide adenine dinucleotide phosphate (reduced form)
n-BuLi	n-butyllithium
n.d.	not determined
NMR	nuclear magnetic resonance
PBS	phosphate buffered saline
PE	petroleum ether
PHH	primary human hepatocytes
pK_a	acid dissociation constant
PPB	plasma protein binding
ppm	parts per million
PSA	pressure-sensitive adhesive
rel. h.	relative humidity
RP-LC	reversed-phase liquid chromatography
rt	room temperature
sat.	saturated
SEM	standard error of the mean

$t_{1/2}$	half-live
^{t}Bu	*tert*-butyl
TFA	trifluoroacetic acid
THF	tetrahydrofuran
t_i	incubation period
t_{lag}	lag time
t_R	retention time
TQ	triple quadrupole
TTS	transdermal therapeutic system
UV	ultraviolet

9.2 Appendix 2: Bioanalytical studies

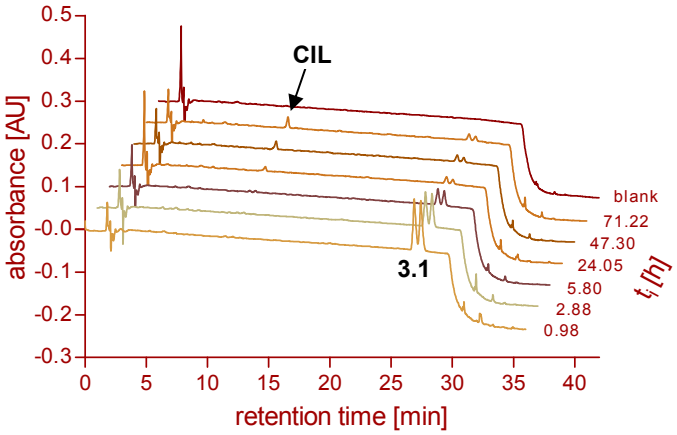

Figure 9.1. Kinetics of hydrolysis of **3.1** (two diasteromers) in phosphate buffer.

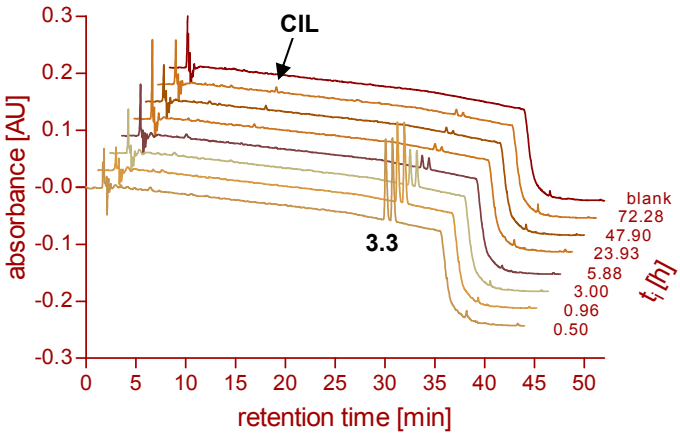

Figure 9.2. Kinetics of hydrolysis of **3.3** (two diasteromers) in phosphate buffer.

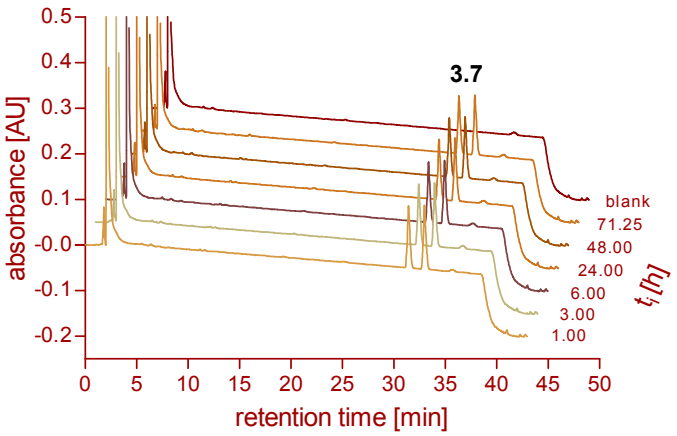

Figure 9.3. Kinetics of hydrolysis of **3.7** (two diasteromers) in phosphate buffer.

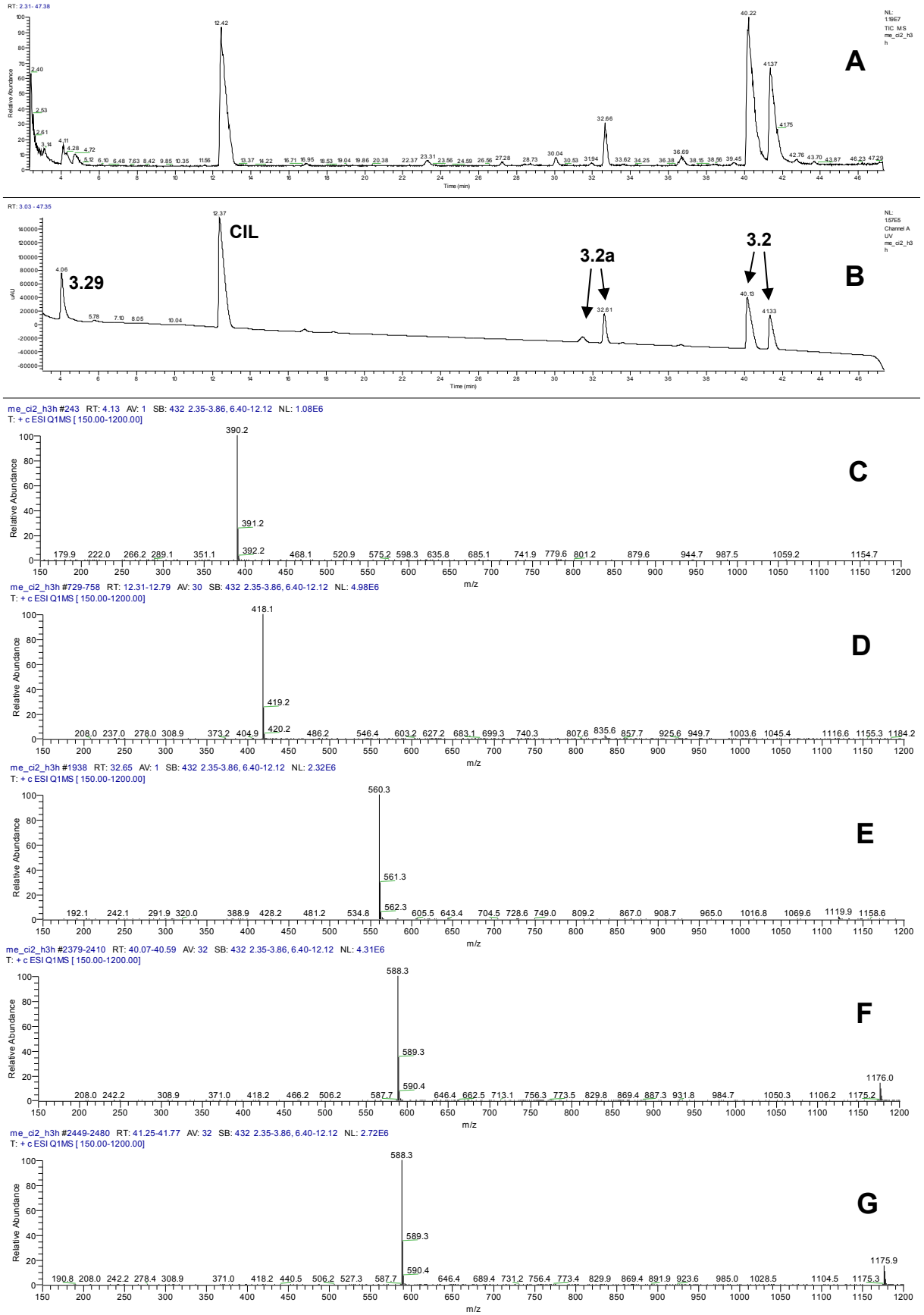

Figure 9.4. LC-MS analysis of a sample of **3.2** incubated for 3 h in porcine skin homogenate. **A**: TIC, **B**: UV, **C**: ESI-MS spectrum of **3.29**, **D**: ESI-MS spectrum of **CIL**, **E**: ESI-MS spectrum of one diastereomer of **3.2a**, **F**+**G**: ESI-MS spectra of the two diastereomers of **3.2**.

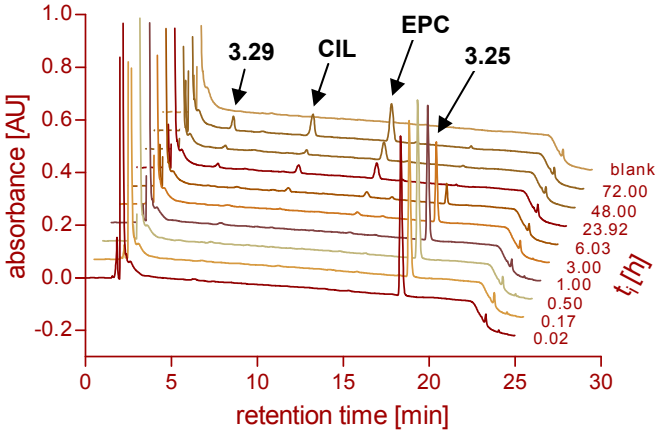

Figure 9.5. Kinetics of hydrolysis of **3.25** in the presence of porcine liver esterase.

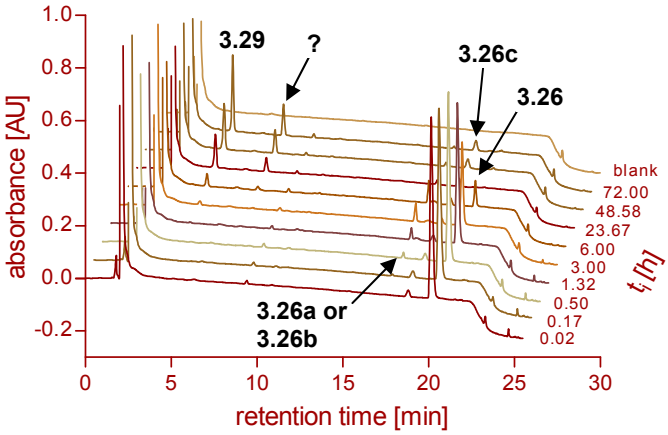

Figure 9.6. Kinetics of hydrolysis of **3.26** in the presence of porcine liver esterase.

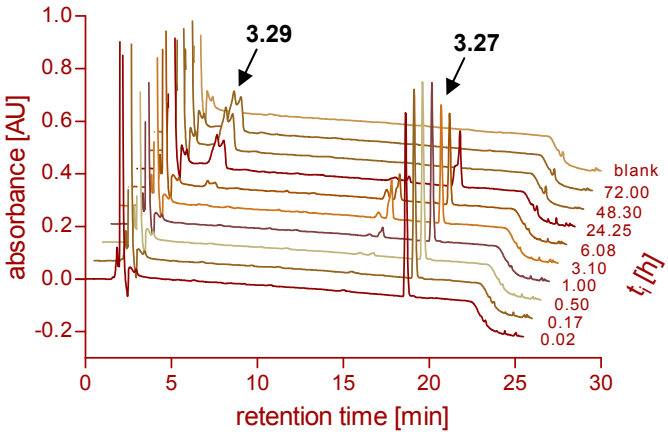

Figure 9.7. Kinetics of hydrolysis of **3.27** in porcine skin homogenate.

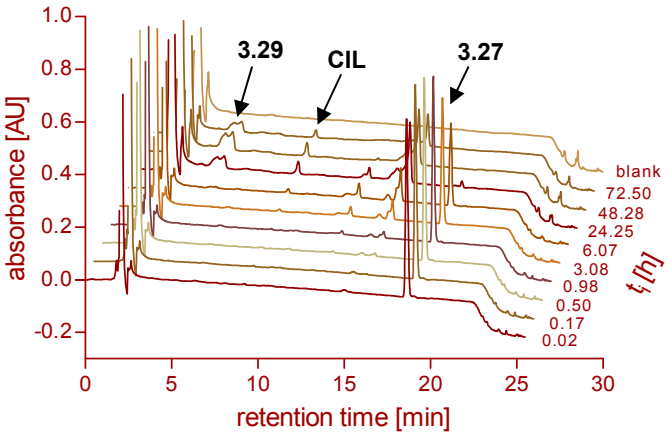

Figure 9.8. Kinetics of hydrolysis of **3.27** in human plasma.

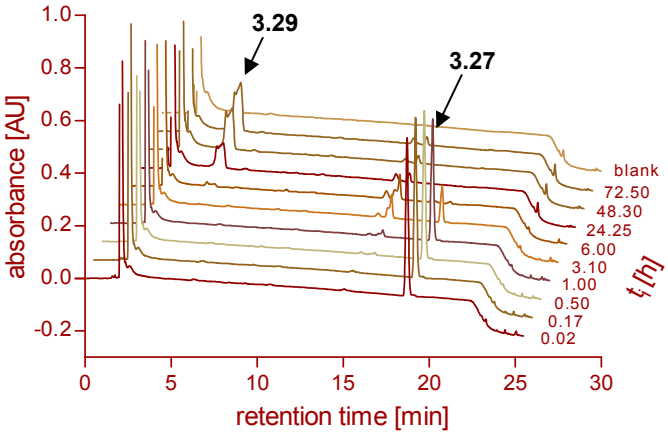

Figure 9.9. Kinetics of hydrolysis of **3.27** in the presence of porcine liver esterase.

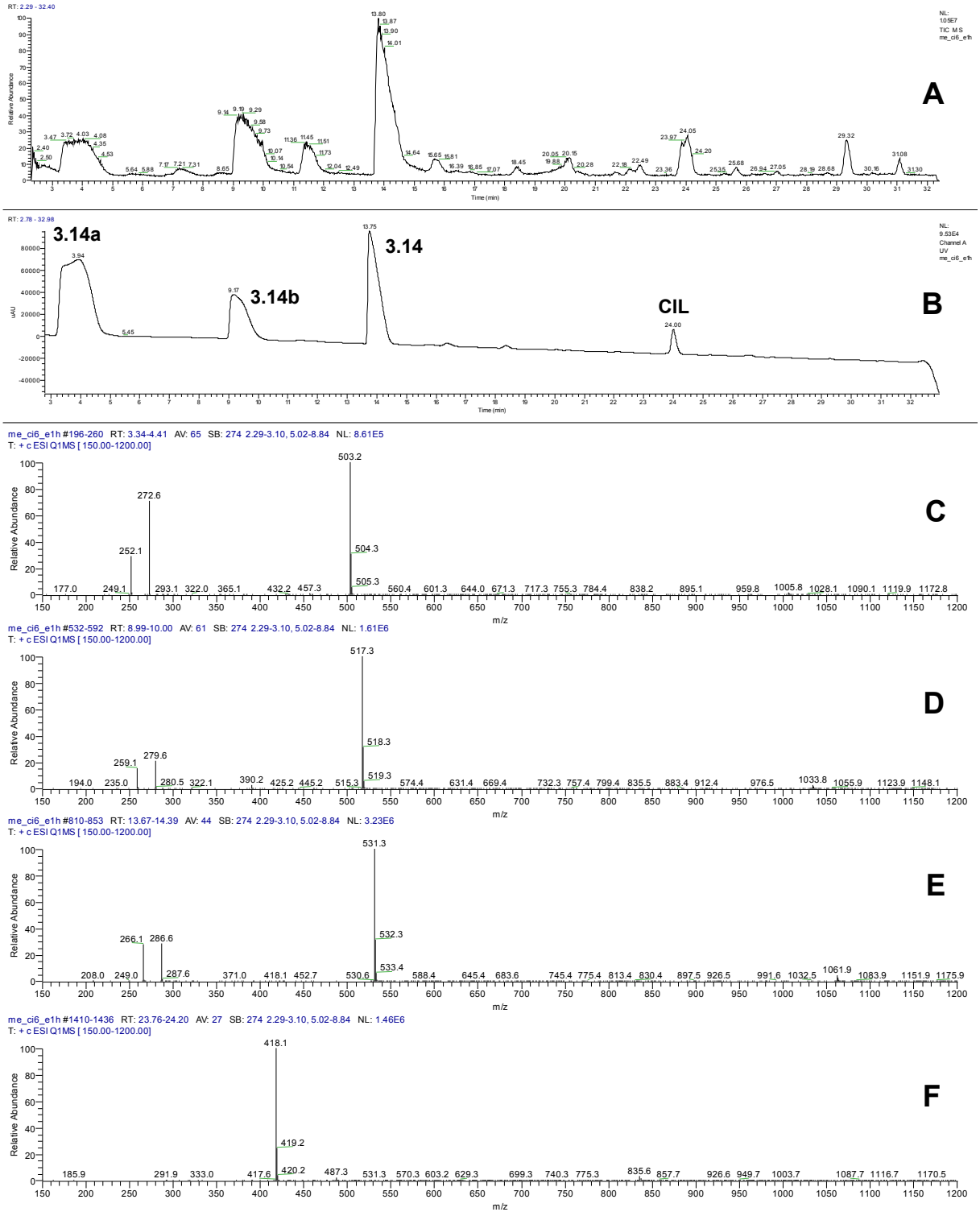

Figure 9.10. LC-MS analysis of a sample of **3.14** incubated for 1 h with buffered porcine liver esterase. **A**: TIC, **B**: UV, **C**: ESI-MS spectrum of **3.14a**, **D**: ESI-MS spectrum of **3.14b**, **E**: ESI-MS spectrum of **3.14**, **F**: ESI-MS spectrum of cilazapril (**CIL**).

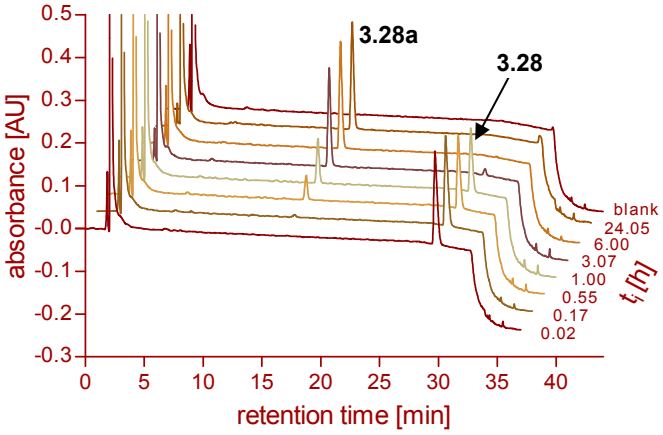

Figure 9.11. Kinetics of hydrolysis of **3.28** in the presence of porcine liver esterase.

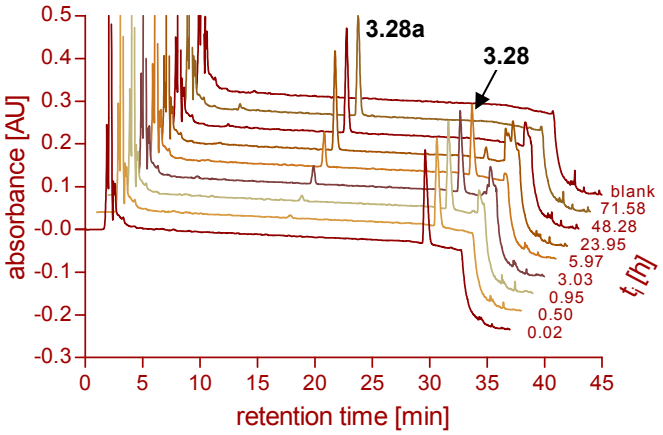

Figure 9.12. Kinetics of hydrolysis of **3.28** in human plasma.

9.3 Appendix 3: Publications and scientific presentations

Ertel, M., Bernhardt, G., Nink, J., Buschauer, A., Novel prodrugs of (1*S*,9*S*)-9-[[(1*S*)-1-carboxy-3-phenylpropyl]amino]octahydro-10-oxo-6*H*-pyridazino[1,2-a][1,2]diazepine-1-carboxylic acid and their use in transdermal therapeutic systems. European Patent application, EP11171006.7, 2011

Scientific presentations:

- **5th Summer School "Medicinal Chemistry", organized by the DFG Research Training Group Medicinal Chemistry (GRK 760), Regensburg (Germany), September 2010**
  Oral poster presentation: *Reactive intermediates in the biotransformation of aminothiazole-type histamine H_2 receptor agonists: Detection by glutathione trapping using LC-MS.* Abstract no. P11. Book of Abstracts p. 207-208.

- **XXIst International Symposium on Medicinal Chemistry, organized by the European Federation for Medicinal Chemistry (EFMC), Brussels (Belgium), September 2010**
  Poster presentation: Ertel, M., Bernhardt, G. and Buschauer, A., *Reactive intermediates in the biotransformation of aminothiazole-type histamine H_2 receptor agonists: Detection by glutathione trapping using LC-MS.* Abstract no. PC.179, *Drugs of the Future* 35 Suppl. A, 135 (2010).

- **Annual Meeting "Frontiers in Medicinal Chemistry", organized by the division Medicinal Chemistry of the GDCh and the division Pharmaceutical/Medicinal Chemistry of the DPhG, Regensburg (Germany), March 2008**
  Poster presentation: Ertel, M., Bernhardt, G. and Buschauer, A., *Synthesis and (bio)analytical studies of potential transdermally applicable prodrugs of the angiotensin II AT_1 receptor antagonist candesartan.* Abstract no. CAR11, Book of Abstracts, page 97.

- **Annual Meeting of the German Pharmaceutical Society (DPhG), Erlangen (Germany), October 2007**
  Poster presentation: Ertel, M., Bernhardt, G. and Buschauer, A., *Potential candesartan prodrugs for transdermal application: Synthesis and (bio)analytical studies.* Abstract no. G10, Book of Abstracts, page 121.

Ich erkläre hiermit an Eides statt, dass ich die vorliegende Arbeit ohne unzulässige Hilfe Dritter und ohne Benutzung anderer als der angegebenen Hilfsmittel angefertigt habe; die aus anderen Quellen direkt oder indirekt übernommenen Daten und Konzepte sind unter Angabe des Literaturzitats gekennzeichnet.

Regensburg, im Juni 2011

(Miriam Ertel)